



Khan, Aneesah M. (2022) *Developing physiological 3D in vitro tissue models for rheumatology research*. PhD thesis.

<https://theses.gla.ac.uk/82838/>

Copyright and moral rights for this work are retained by the author

A copy can be downloaded for personal non-commercial research or study, without prior permission or charge

This work cannot be reproduced or quoted extensively from without first obtaining permission in writing from the author

The content must not be changed in any way or sold commercially in any format or medium without the formal permission of the author

When referring to this work, full bibliographic details including the author, title, awarding institution and date of the thesis must be given

Enlighten: Theses

<https://theses.gla.ac.uk/>  
[research-enlighten@glasgow.ac.uk](mailto:research-enlighten@glasgow.ac.uk)



University  
of Glasgow

**Developing physiological 3D *in vitro*  
tissue models for rheumatology  
research**

**Aneesah M. Khan**  
BSc (Hons), MRes

Submitted in the fulfilment of the requirements of the Degree of  
Doctor of Philosophy  
College of Medical, Veterinary and Life sciences  
Institute of Infection, Immunity and Inflammation  
University of Glasgow

**April 2022**

## Abstract

Rheumatoid arthritis is an inflammatory disease in which synovial fibroblasts maintain the persistence of inflammation within the joint, dependent on a unique pathological phenotype induced by numerous epigenetic modifications. However, knowledge of the role of these stromal cells is not completely understood. All treatments for rheumatoid arthritis are immunosuppressive drugs that target the entire immune system, resulting in many severe side effects for patients. Conventional culturing systems in 2D flat surfaces have been useful in the investigation of synovial fibroblast-dependent inflammation in rheumatoid arthritis, but inevitably lead to cellular adaptation to non-physiological plastic surfaces, that do not recapitulate the complex polarised 3D matrix where synovial fibroblasts sit in the joints. Thus, better 3D physiological models would provide a better and less artefactual understanding of the role these cells in inflammation to advance more translational research. Furthermore, understanding mechanisms through which synovial fibroblasts mediate this persistence as well as the discovery of new stromal markers in order to identify specific functional subsists of synovial fibroblasts that may be promising as disease specific therapeutic targets. This study will look at the influence of two specific 3D culture systems - polystyrene scaffold (Alvetex®) and Fibronectin pegylated hydrogels - on synovial fibroblast-dependent inflammation and their biological responses as well as the effect of the presence of matrix components on synovial fibroblast biology. The final aim of this project is to develop better physiological 3D culture systems, to obtain a better understanding of the role of fibroblasts in rheumatoid arthritis, using animal models prior to translation of these platforms to human disease.

These studies revealed that synovial fibroblasts cultured in 3D microenvironments such as Alvetex® after initially being grown in 2D, could potentially recapitulate the *in vivo* environment better than conventional 2D cultures, whilst collagen induced arthritis-synovial fibroblasts still present a pro-inflammatory phenotype. However interestingly, culture of the latter synovial fibroblasts in FNPEG hydrogels resulted in the cells expressing a more “remission’ like phenotype, exhibiting a less pro-inflammatory transcriptional programming. This not only provides rationale for the use of hydrogels and other 3D platforms in the study of

the role of synovial fibroblasts in rheumatoid arthritis but also presents as a potential therapeutic to target synovial fibroblasts specifically.

# Table of Contents

Abstract .....	ii
Table of Contents.....	iv
List of Tables .....	viii
List of Figures .....	ix
Acknowledgements.....	xi
Impact of the COVID-19 pandemic .....	xiv
Author’s Declaration.....	xv
Abbreviations.....	xvi
<b>Chapter 1 General Introduction .....</b>	<b>1</b>
1.1 Rheumatoid Arthritis.....	1
1.2 Factors involved in RA and diagnosis of the disease .....	1
1.2.1 Genetic and environmental factors .....	1
1.2.2 ‘Pre-clinical’ elements in the diagnosis of RA .....	2
1.2.3 Medications and treatments.....	4
1.3 Synovial joint and RA.....	5
1.3.1 Synovial joint .....	5
1.3.2 Synovial membrane .....	6
1.3.3 Why does inflammation persist in RA? .....	7
1.3.4 Autoimmune Synovitis.....	8
1.3.5 Inflammatory cytokines and their role in RA.....	9
1.4 Synovial fibroblasts (SFs).....	12
1.4.1 Synovial fibroblasts in RA .....	13
1.4.2 Epigenetic remodelling of RA-SFs.....	17
1.5 Hypothesis and aims .....	19
<b>Chapter 2 Materials and Methods.....</b>	<b>27</b>
2.1 Mice .....	27
2.2 Collagen induced arthritis (CIA) model .....	27
2.3 Isolation and culture of SFs.....	27
2.3.1 Isolation of primary SFs from murine joints for ex vivo cell culture ..	27
2.3.2 Routine cell maintenance and culture .....	28
2.3.3 Flow Cytometric analysis and cell sorting .....	29
2.3.4 Magnetic bead separation .....	30

2.4 Preparation of Alvetex® scaffolds and cell seeding .....	31
2.4.1 Culture of SFs in Alvetex® inserts in a 6-well plate .....	31
2.5 Preparation of FNPEG hydrogels .....	31
2.5.1 PEGylation of fibronectin (FN) .....	31
2.5.2 Hydrogel formation .....	32
2.6 Nanoindentation.....	33
2.7 Histology.....	33
2.7.1 Preparation of joint wax blocks.....	33
2.7.2 Preparation of Alvetex® wax blocks .....	34
2.7.3 Microtome sectioning: joint and Alvetex®.....	34
2.7.4 Cryostat sectioning: hydrogel .....	34
2.7.5 Histology: Haematoxylin and Eosin (H&E) staining.....	35
2.8 Immunohistochemistry and fluorescent microscopy .....	35
2.8.1 Alvetex® and joint sections .....	35
2.8.2 Imaging of full hydrogels.....	36
2.9 ELISA .....	37
2.10 RT-PCR .....	37
2.10.1 RNA extraction .....	37
2.10.2 cDNA synthesis .....	39
2.10.3 PCR .....	40
2.10.4 RNA-Seq analysis.....	40
2.11 Statistical analysis.....	41
<b>Chapter 3 Characterisation of Naïve SFs and pathogenic SFs from CIA mice using conventional 2D cell cultures .....</b>	<b>51</b>
3.1 Introduction.....	51
3.1.1 Collagen Induced Arthritis (CIA) .....	51
3.1.2 Conventional 2D culture of expanded SFs ex vivo.....	53
3.1.3 Integrins and Fibronectin in synovial tissue.....	54
3.2 Aims and Objectives .....	55
3.3 Results .....	56
3.3.1 Histological characterisation of CIA and visualisation of SFs within the synovial joint .....	56
3.3.2 SF viability and pro-inflammatory responses of CIA-SFs.....	56
3.3.3 Fibronectin induced expression of MMP and pro-inflammatory cytokines in Naïve and CIA-SFs.....	58
3.3.4 SF subset differentiation is lost in Naïve- and CIA-SF 2D cultures .....	59
3.4 Concluding remarks .....	60

<b>Chapter 4 Characterisation of explant Naïve- and CIA-SF responses following transfer to 3D polystyrene scaffolds.....</b>	<b>67</b>
4.1 Introduction.....	67
4.1.1 Alvetex®: Three-dimensional polystyrene scaffold.....	69
4.1.2 Culture environment impacts on cell behaviour .....	69
4.2 Aims and Objectives .....	71
4.3 Results .....	72
4.3.1 Microenvironment and fibronectin effect morphology and pro-inflammatory gene expression in Naïve SFs .....	72
4.3.2 Organisation, migration, proliferation and pro-inflammatory phenotype of Naïve- and CIA-SFs cultured on 3D polystyrene scaffolds .....	75
4.3.3 The effect of FN and 3D microenvironment on SF subset differentiation in Naïve and CIA-SFs .....	78
4.4 Concluding remarks.....	79
<b>Chapter 5 Use of fibronectin pegylated hydrogels to study the responses of Naïve and CIA-SFs to determine if this platform supports recovery of functional specialization.....</b>	<b>93</b>
5.1 Introduction.....	93
5.1.1 Fibronectin Pegylated hydrogels.....	95
5.2 Aims .....	97
5.3 Results .....	98
5.3.1 Fibronectin pegylated hydrogels provide a viable culture system for studying SF biology .....	98
5.3.2 Organisation and properties of SFs in FNPEG hydrogels .....	99
5.3.3 Organisation of SF subsets in FNPEG hydrogels.....	101
5.3.4 Synovial fibroblast responses in degradable and non-degradable FNPEG hydrogels .....	102
5.3.5 The impact of cells and media on the stiffness of degradable FNPEG hydrogels over time.....	104
5.3.6 Stiffness influences SF function in degradable FNPEG hydrogels .....	106
5.4 Concluding remarks .....	107
<b>Chapter 6 SFs exhibit differential gene expression when cultured in different microenvironments .....</b>	<b>126</b>
6.1 Introduction.....	126
6.2 Aims and objectives .....	127
6.3 Results .....	128
6.3.1 RNA-Seq identifies that the microenvironment influences gene expression of inflammatory SFs .....	128

6.3.2 Stimulation with IL-1 $\beta$ influences differential gene expression in inflammatory SFs in different microenvironments .....	135
6.4 Concluding remarks .....	137
<b>Chapter 7 Discussion.....</b>	<b>157</b>
7.1 Summary.....	157
7.2 Towards developing platforms for more effective pre-clinical testing of therapies for RA.....	158
7.3 Hydrogels - culture systems to study SF biology and/or therapeutic delivery tools for RA.....	161
<b>List of References .....</b>	<b>166</b>
<b>Appendix .....</b>	<b>189</b>

## List of Tables

Table 1-1: Types of biologic treatments for RA patients, their targets, examples, and mechanisms.....	24
Table 2-1: Antibodies to determine SFs (1:100 FACs buffer) Antibodies to determine SFs (1:100 FACs buffer) .....	42
Table 2-2: Components and volumes for the PEGylation of Fibronectin for hydrogel formation .....	45
Table 2-3: Components and volumes required for the formation of non-degradable Fibronectin PEGylated hydrogels .....	46
Table 2-4: Components and volumes required for degradable Fibronectin PEGylated hydrogel synthesis. Different weights (wt %) were used to obtain hydrogels of different stiffnesses. ....	47
Table 2-5: Primary, secondary antibodies and isotypes with dilutions .....	50
Table 3-1: Animal models used in RA research and their characteristics .....	61

## List of Figures

Figure 1-1: Anatomy and pathophysiology of healthy and arthritic synovial joints. ....	22
Figure 1-2: Risk factors associated with RA. ....	23
Figure 1-3: RA pathophysiology.....	25
Figure 1-4: Distinct fibroblast subsets perform different functions in RA. ....	26
Figure 2-1: Identifying SF population using FACs. ....	43
Figure 2-2: Schematic of Alvetex® inserts and seeding. ....	44
Figure 2-3: Schematic view of the ferrule-top nanoindenter setup.....	48
Figure 2-4: Schematic representation of load vs depth graph from nanoindentation. ....	49
Figure 3-1: Pathophysiology of Naïve and CIA joints in mice. ....	62
Figure 3-2: SFs from CIA mice exhibit increased production of pro-inflammatory mediators. ....	63
Figure 3-3: Viability and morphology of cells cultured in 2D. ....	64
Figure 3-4: Effect of FN on MMP3 and IL-6 secretion in SFs in 2D.....	65
Figure 3-5: Expression of SF subset markers - VCAM1 and CD90 - in the presence and absence of FN. ....	66
Figure 4-1: Cell morphology in <i>in vivo</i> environments and in 2D <i>in vitro</i> environments. ....	81
Figure 4-2: Alvetex® can be treated with differing ECM components.....	82
Figure 4-3: Morphology of Naïve SF in a 3D polystyrene scaffold. ....	83
Figure 4-4: Differential expression of Ccl2, Mmp9, Mmp13, Mmp13, Tgf-b1 and ST6Gal in SFs cultured in 2D and Alvetex® and the effect of the presence of FN. ....	84
Figure 4-5: Effect of the presence of FN on expression of Mmp3 and IL-6 in SFs cultured in a 3D polystyrene scaffold. ....	85
Figure 4-6: Expression of inflammatory cytokines in Naïve SFs released by cells cultured in 2D and 3D culture systems.....	86
Figure 4-7: Migration and organisation of SFs in Alvetex®. ....	88
Figure 4-8: The effect of FN on the proliferation of SFs. ....	89
Figure 4-9: Effects of FN and IL-1 $\beta$ stimulation on MMP3 and IL-6 secretion in SFs in Alvetex®. ....	90
Figure 4-10: Expression of stromal marker vimentin and by SF subset markers - VCAM1 and CD90 - in the presence and absence of FN. ....	92
Figure 5-1: Schematic diagram of hydrogel formation.....	109
Figure 5-2: Cell viability is not compromised by 3D culture in non-degradable 5 wt % FNPEG hydrogels. ....	111
Figure 5-3: 3D reconstruction of Naïve and CIA SFs cultured in non-degradable 5 wt % FNPEG hydrogels. ....	112
Figure 5-4: Morphologies and physical cell properties of SFs in 5 wt % FNPEG hydrogels. ....	113
Figure 5-5: Naïve and CIA SFs display a distinct distribution within 5 wt % FNPEG hydrogels. ....	114
Figure 5-6: 3D reconstruction of SFs subsets VCAM1 and CD90 cultured in non-degradable 5 wt % FNPEG hydrogels. ....	116
Figure 5-7: Naïve and CIA SFs display differences in subset marker intensities. ....	117
Figure 5-8: An increase in SF lining subset (VCAM1) expression is observed when CIA-SFs are cultured in FNPEG hydrogels. ....	118

Figure 5-9: SF cytokine expression of MMP3, CCL2 and IL-6 in degradable and non-degradable gels. ....	119
Figure 5-10: Stiffness over time of different wt % degradable FNPEG hydrogels. ....	121
Figure 5-11: The effect of Naïve SFs on the “stiffness” of different degradable wt % FNPEG hydrogels over 7 days. ....	123
Figure 5-12: The effect of different wt % FNPEG hydrogels containing CIA SFs on stiffness over 7 days. ....	124
Figure 5-13: Stiffness affects cell function. ....	125
Figure 6-1: RNA-Seq analysis of sorted SFs. ....	139
Figure 6-2: Up and downregulated pathways in CIA sorted SFs compared to Naïve. ....	140
Figure 6-3: RNA-Seq analysis of SFs cultured in 2D. ....	141
Figure 6-4: Up and downregulated gene expression in Naïve and CIA SFs cultured in 2D with FN for 7 days. ....	142
Figure 6-5: 2D RNA-Seq validation. ....	143
Figure 6-6: RNA-Seq analysis of SFs cultured in Alvetex®. ....	144
Figure 6-7: Up and downregulated gene expression in Naïve and CIA SFs cultured in Alvetex® with FN for 7 days. ....	145
Figure 6-8: Alvetex® RNA-Seq validation. ....	146
Figure 6-9: RNA-Seq analysis of SFs cultured in FNPEG hydrogels. ....	147
Figure 6-10: Up and downregulated gene expression in Naïve and CIA SFs cultured in FNPEG hydrogels for 3 days. ....	148
Figure 6-11: FNPEG RNA-Seq validation. ....	149
Figure 6-12: The functional consequences of SFs cultured in differing culture systems. ....	151
Figure 6-13: PCA and differential gene expression comparison of SFs cultured in different microenvironments. ....	152
Figure 6-14: RNAseq analysis of SFs Naïve cultured in 2D with FN in the presence and absence of IL-1 $\beta$ : stimulation. ....	153
Figure 6-15: RNA-Seq analysis of SFs Naïve cultured in Alvetex® with FN in the presence and absence of IL-1 $\beta$ : stimulation. ....	154
Figure 6-16: RNA-Seq analysis of SFs Naïve cultured in FNPEG hydrogels with FN in the presence and absence of IL-1 $\beta$ : stimulation. ....	155
Figure 6-17: Up regulated gene expression in Naïve SFs in the presence of overnight IL-1 $\beta$ stimulation cultured with FN for 7 days (2D and Alvetex®) or 3 days (FNPEG hydrogels), in differing culture systems. ....	156

## Acknowledgements

First, I would like to express my sincere gratitude to my supervisors, Margaret Harnett, Miguel Pineda and Manuel Salmeron-Sanchez for their invaluable guidance, continuous support and patience throughout my PhD. Thank you, Maggie, for always being there to lend an ear and for sharing with me your advice and experiences. You have been a great friend to me as well as an inspiration and I am really lucky to have worked with you.

I cannot begin to express my thanks to my supervisor Miguel, who's enthusiasm, motivation and immense knowledge has deeply inspired me. I have faced many challenges throughout the course of my PhD, and I honestly could not have got through it if it weren't for your kindness and encouragement. I really appreciate it and will be forever grateful. It has been a privilege. I would also like to thank Oana Dobre for being an exceptional post doc to work alongside. You opened my eyes to the world of bioengineering and your invaluable suggestions and advice helped immensely during this project. You taught me everything I needed to know about hydrogels, and I now have a deeper appreciation for the work you do. Stressful moments in the lab (specifically getting RNA from the hydrogels) were made enjoyable with your sense of humour and positive outlook. It has been a long struggle, but we got there eventually!

Thanks to all who helped me during this PhD at the SGDB, Rankine and CVR, without your expertise I would have been lost. Thank you, Sara, for helping me with the protocol for hydrogel formation. Fiona, for being an amazing histology teacher, for without your guidance I wouldn't have been able to master the dreaded microtome. Colin, Leandro and Susan, for enhancing my microscope knowledge and teaching me all about IMARIS. Special thanks to Yilin, I have enjoyed working with you in the lab, thank you for helping me with all the animal models (especially the jumping mice), and for being there to lift my spirits when experiments weren't working out, with funny videos of your cats. Thank you for your friendship, I will look back at our time in the lab with great fondness.

Finally, I would like to thank my parents, my family and my husband for their continued love, support and encouragement, without which I wouldn't be where I am today.

I would like to dedicate this thesis to my mum and dad.

## Impact of the COVID-19 pandemic

The sudden closure of labs in March 2020 due to the Covid-19 pandemic, significantly impacted my PhD and in turn my thesis. As I was one of those in the shielding clinically vulnerable category, I lost even more time in the lab than most of my peers, which was then exacerbated when the second lockdown occurred. During this period, I was in my final year of my PhD and so lab time was crucial as I had spent the previous year's optimising my hydrogel formulation and protocols. I had planned on furthering my research using the formulated fibronectin pegylated gels, investigating the impact of hydrogel stiffness on specific synovial fibroblast responses as well as creating a co-culture environment using different extracellular matrix components within the hydrogels to mimic a more joint-like microenvironment. I was not able to perform the latter, which was planned to further my translational project aims. Rather, in the time available, I focused the Chapter on the mechanical properties of hydrogels, looking at how stiffness affected cell function as this more clearly complemented the existing body of work. This involved furthering the collaboration with bioengineers from Professor Manuel Salmeron-Sanchez' lab, where I had been mentored by a post doc, Oana during all the experiments presented in the hydrogel chapter. However, as I couldn't receive training that enabled me to perform certain experiments on my own due to the government guidelines on the number of people within the lab at a certain time, and only limited individuals could use the lab at any given time, I could not carry out repetitions of the nanoindentation experiments in Chapter 5, resulting in some incomplete preliminary data for the arthritic synovial fibroblasts.

As my project was wet lab based, I found working from home during the Covid-19 pandemic very difficult. However, despite this I feel I have done my best to mitigate these circumstances and make the most of the time I had at home, by receiving training in bioinformatics analysis of RNA-Seq data that has allowed me to directly analyse my raw data from sequence alignment through to pathway analysis (as opposed to using an established pipeline) and hence has expanded my skills portfolio and furthering my PhD.

## Author's Declaration

I declare that, except where explicit reference is made to the contribution of others, that this dissertation is the result of my own work and has not been submitted for any other degree at the University of Glasgow or any other institution.

Printed Name: Aneesah M. Khan

Signature: \_\_\_\_\_

## Abbreviations

ACPAs	Anti-citrullinated protein antibody
AF488	Alexa Fluor 488
AF647	Alexa Fluor 647
AIA	Antigen-Induced Arthritis
BSA	Bovine serum albumin
CAIA	Collagen Antibody Induced Arthritis
CCL2	Chemokine ligand 2
CDH11	Cadherin 11
CD90	Cluster of Differentiation 90 (also known as Thy-1)
CIA	Collagen-induced arthritis
CTGF	Connective tissue growth factor
DAPI	4', 6-diamidino-2-phenylindole
DAS	Disease activity score
DC	Dendritic cells
DMARD	Disease modifying anti-rheumatic drug
DMEM	Dulbecco's Modified Eagle Medium
DNA	Deoxyribonucleic acid
ECM	Extracellular Matrix
ELISA	Enzyme-linked immunosorbance assay
FACS	Fluorescence-activated cell sorting
FAP	Fibroblast-activation protein
FBS	Foetal bovine serum
FCA	Freund's Complete Adjuvant
FGF	Fibroblast Growth Factor
FN	Fibronectin
FNPEG	Fibronectin pegylated
FSC	Forward scatter
H & E	Haematoxylin and eosin
ICAM-1	Intracellular adhesion molecule 1
IF	Immuno-fluorescence
IFN- $\gamma$	Interferon gamma
IHC	immunohistochemistry
IL	interleukin
i.p	Intra-peritoneal
i.v	Intra-venous
JIA	Juvenile Idiopathic Arthritis
KO	Knock out
LPS	Lipopolysaccharide

M-CSF	macrophage-colony stimulating factor
MFI	mean fluorescence intensity
mRNA	messenger RNA
MMP:	Matrix metalloproteinase
MTX	methotrexate
NfκB	nuclear kappa B
NSAIDs	non-steroidal anti-inflammatory drugs
OA	osteoarthritis
OB	osteoblast
OC	osteoclast
OCP	osteoclast precursor
PBS	Phosphate buffered saline
PBS-T	Phosphate buffered saline + Tween
PC	Phosphorylcholine
PCR	polymerase chain reaction
PEGSH	Peg dithiol
Peg	4-Arm-Pegmal
RA	Rheumatoid Arthritis
RANK	Receptor activator of nuclear factor kappa-B
RANK-L	Receptor activator of nuclear factor kappa-B ligand
RASF	Rheumatoid arthritis synovial fibroblasts
RF	Rheumatoid Factor
RNA	Ribonucleic acid
ROS	reactive oxygen species
RT-PCR	Reverse transcriptase polymerase chain reaction
SF	Synovial fibroblasts
SPARC	Secreted Protein Acidic And Cysteine Rich
SSC	side scatter
TGF-β	transforming growth factor beta
THBS4	Thrombospondin 4
TIMP1	Tissue inhibitor matrix metalloproteinase 1
TINAGL1	Tubulointerstitial Nephritis Antigen Like 1
TNC	Tenascin C
TNF-α	Tumour necrotic factor alpha
VCAM-1	Vascular cell adhesion protein 1
VEGF	Vascular endothelial growth factor
WT %	Weight
ZIA	Zymosan Induced Arthritis

# Chapter 1 General Introduction

## 1.1 Rheumatoid Arthritis

Rheumatoid arthritis (RA) is a chronic inflammatory autoimmune disease that causes progressive articular damage, mainly to the synovial joints. RA is the second most common form of arthritis within the UK, with more than 400,000 people affected by the disease. It has been found to affect women more than men, with approximately 2-3 times more women developing the disease compared to men (NRAS | Rheumatoid arthritis charity, 2022). The chronic stage of the disease is characterised by the hyperproliferation of synovial tissue and inflammatory cell infiltration leading to the formation of a thickened synovium, termed the pannus. This pannus formation (Figure 1-1) leads to erosion of the cartilage and bone within the joint (Armaka, Gkretsi, Kontoyiannis and Kollias, 2009). Joints commonly affected include small joints like fingers, feet and wrists and larger joints such as knees and hips, with clinical symptoms of swollen, red, inflamed, and painful joints that can eventually lead to loss of joint function in the absence of treatment (Hudson and Whittum-Hudson, 2009). There are various risk factors thought to be associated with RA such as smoking, genetics and environment, however the aetiology of RA remains uncertain and despite there being various treatments available to help slow the progression of disease, RA remains incurable. Moreover, current front-line treatments do not work for all patients and lead to immunosuppression which can potentially lead to substantial adverse effects in patients ranging from mild discomfort to severe pain as well as increased risk rate of infections and disease (Guo et al., 2018). Therefore, an improved understanding of the development of joint disease would provide insights into pathogenesis that could ultimately lead to more effective treatments and/or novel preventive strategies in RA.

## 1.2 Factors involved in RA and diagnosis of the disease

### 1.2.1 Genetic and environmental factors

Various risk factors have been found to be associated with RA (Figure 1-2), with studies showing that roughly 50% of RA cases can be attributed to genetic factors (Kurkó et al., 2013). Multiple genes have been associated with RA, with two gene

loci specifically shown to be involved in RA progression and development. Thus, a major genetic contribution to disease predisposition lies within the Major Histocompatibility Complex HLA class II region, with more than 80% of patients that have RA carrying at least one of the disease-associated, Class II, DR Beta1 (HLA-DRB1) alleles: DRB1\*0101, DRB1\*0401, DRB1\*0404 and DRB1\*0405. Another genetic factor strongly associated with RA is the protein tyrosine phosphatase 22 gene (PTPN22), which is also involved in juvenile idiopathic arthritis (JIA) (Kerlan-Candon et al., 2001). Environmental factors may also play a role in RA, with factors such as obesity, infections, stress, exposure to insecticides having all been extensively studied to try and understand better how the disease comes about as well as their impact on susceptibility to developing RA. However, the most well-known environmental factor in RA has been shown to be smoking, which can increase the risk of RA by up to 40-fold (Edwards and Cooper, 2006). Despite these known genetic and environmental factors, how their cues are integrated with disrupted immune system networks to drive initiation of the development of RA is still not completely understood, and thus a better understanding on how the disease progresses is needed to ensure earlier diagnosis and treatment to provide patients with the possibility of remission and prevent joint damage that otherwise becomes irreversible.

### ***1.2.2 'Pre-clinical' elements in the diagnosis of RA***

It is well-established that there is a stage in RA development in most patients that has been characterised by expression of autoantibodies (as well as other biomarkers) in the absence of the clinically evident chronic inflammation that is symptomatic of RA. This 'preclinical' stage of RA is characterised by increased production of two important classes of autoantibodies, namely rheumatoid factor (RF) and antibodies to citrullinated protein antigens (ACPAs) (Demoruelle and Deane, 2011). Although, the most common assay (anti-cyclic citrullinated peptide [CCP] detection) of ACPAs does not allow recognition of definitive citrullinated antigen targets, newer technological advancements such as multiplex arrays are ensuring a deeper understanding of the reactivities of antibodies in response to individual citrullinated peptides and epitopes. RFs are a class of immunoglobulins (Igs), containing varying isotypes as well as affinities, that react against the Fc (fragment crystallisable) region of Immunoglobulin G (IgG): this results in the

production and deposition of immune complexes that promote inflammation and are thus thought to be involved in the initiation of RA and its development. They most likely arise because of the immune response to infection (a risk factor for RA) as low affinity RFs have been shown to play a crucial role in immune responses to various infectious organisms whilst high affinity RFs demonstrate a higher degree of severity and persistence in disease in patients with RA. However, this is heavily dependent on genetics, and they may also regulate effects of the production of Ig via regulation of activation of B cells. Clinically, it is best that RFs and ACPAs are measured together as both markers enhance the accuracy of diagnosis, particularly in cases of early RA diagnosis (Ingegnoli, Castelli and Gualtierotti, 2013). Moreover, determination of RF isotypes, individually or combined, can aid in guiding and handling patients, from diagnosis until treatment. However, the autoimmunity most specifically linked to RA has been associated with production of ACPA, with most RA patients generating these “auto”-antibodies. Indeed, anti-CCP antibodies can be identified in the sera of 60-80% of RA patients with a specificity of 85-99% (Aggarwal et al., 2009). These target a protein modification (citrullination), rather than the native protein, and are found in many matrix proteins such as vimentin or fibrinogen. Citrulline itself is produced through posttranslational modification of arginine that is catalysed via intracellular enzymes known as peptidylarginine deiminases (PADs) (Alghamdi et al., 2019) and citrullination can lead to alterations of the properties of self-peptides resulting in their immunogenicity. Studies have therefore shown that this marker is far more advantageous to look at compared to RF (Kurowska, Kucawarnawin, Radzikowska and Maśliński, 2017). Although they may play a role in initiation and development of RA, they are most likely not the main reason or initiator in the disease and many fundamental questions still need to be answered, specifically for identifying individuals who are at a greater risk, that would benefit significantly from early clinical care, as well as for development and enhancement of novel treatments and preventative measures for RA.

Thus, over the last decade, a combination of genetic and environmental factors (as mentioned previously) has been shown to contribute to rendering the host susceptible to autoimmunity and the consequent appearance of joint inflammation. Various immune system cells such as macrophages, dendritic cells,

mast cells, B cells, neutrophils and T cells have all been found to be involved in disease progression and make a pathogenic contribution to the early loss of self-tolerance. Moreover, they promote progression of inflammation in the joint and the collective action of the immune system cells and stromal cells results in joint damage (McInnes and Schett, 2017; Weyand and Goronzy, 2020).

### ***1.2.3 Medications and treatments***

The goal of present-day RA therapies is to either lessen or alleviate the pain patients experience or to slow the progression of the disease itself (Ishchenko and Lories, 2016). To reduce pain, patients are given drug combinations of paracetamol and codeine such as co-codamol. However, this simply alleviates the pain and does not treat the arthritis itself or aid in lessening the symptomatic inflammation present in the joints. Therefore, patients are generally prescribed non-steroidal anti-inflammatory drugs (NSAIDs) to reduce the inflammation that plays a role in controlling the symptoms of RA as well as helping with the pain: examples include ibuprofen, naproxen and diclofenac. Another therapeutic approach for RA involves glucocorticoids, which are generally used to treat sudden flares of joint pain. However, despite the success of glucocorticoids, they are known to be associated with adverse side-effects such as increasing blood pressure, anxiety, and risk of cataracts, sparking debates on the best way to use these drugs to treat RA: thus, gaps in knowledge of this class of treatment need to be further investigated. Despite these medications being employed to reduce inflammation, they are not used to prevent the progression of the disease and are generally used in combination with other therapies to prevent or slow down the progression of joint damage. There are a variety of such medications available, and these are separated into categories, the first being Disease Modifying Anti-Rheumatic Drugs (DMARDs) and the second being, Biologics (Curtis and Singh, 2011). The latter suppress the inflammatory response slowing down the progression of RA, either alone or in combination with other drugs, and in turn allowing many patients a better quality of life, with some patients even achieving remission. For many, disease activity continues however, but the use of DMARDs slow the activity and intensity of the disease with patients generally experiencing symptom-free periods or less intense flare-ups while taking these medications. DMARDs are generally steroids such as leflunomide and methotrexate, the latter

being one of the most common DMARDs that is effective for the majority of RA patients and can even be taken by children. Nevertheless, they can exhibit serious side-effects such as birth defects, shortness of breath, appearance of rashes as well as toxicity to the liver and bone marrow (the latter specific to methotrexate).

Biologics are essentially “modern” DMARDs, being engineered immunomodulatory proteins designed to target specific cells or inflammatory mediators such as cytokines that incite inflammation as well as destruction of cartilage and bone (Table 1-1). Many of the drugs used to treat RA selectively target and inhibit cytokines highly expressed in the joint of RA patients such as IL-6, TNF- $\alpha$ , IL-17, IL-1 $\beta$ , but result in patients being immunocompromised as these cytokines are needed to fight infections (Wilsdon and Hill, 2017; Strand, 1999). Clinical trials have shown that TNF- $\alpha$  blocking agents, such as etanercept (ETN) infliximab (IFX) and adalimumab (ADA), relieve joint inflammations and slow the radiographic progression of joint damage and improve physical function in advanced RA (MA and XU, 2012).

Even though the use of biologics alone or in combination with other drugs have shown to help against inflammation, many patients exhibit, at least to some extent, disease persistence or further immunosuppression, in turn increasing the patient’s risk of infection. Therefore, further treatments need to be developed to target affected joints (Filer, 2013), rather than the entire immune system, to ensure that the body is not compromised and is still able to fight effectively against infection whilst the inflammation is being treated specifically, allowing patients a better quality of life.

## **1.3 Synovial joint and RA**

### ***1.3.1 Synovial joint***

RA predominantly affects the synovial joints, in which pain and swelling due to infiltrated cells and increased synovial fluid, as well as cartilage and bone damage is present. Synovial joints are the most common type of joint in the body and are articular joints found in between bones that move against each other, such as in

the knees and wrists, to provide fluid movement and mechanical support (Sweeney and Firestein, 2004).

Synovial joints contain a joint cavity, with the walls of the area being formed by the articular capsule, which is a fibrous connective tissue structure attached to the bones outwith the articulating surface of the bone. Within the joint cavity, friction between bones of the synovial joint is minimised by the articular cartilage. The latter is a fine layer of hyaline cartilage that coats the complete connecting surface of the bones, ensuring they move fluidly and easily against one another without causing damage to the tissues on the bones. The synovial membrane (also known as the synovium) is soft tissue lining the inner surface of the articular capsule and the cells that make up this lining produce and secrete synovial fluid, which is a thick, clear, viscous fluid that acts as a lubricant between the bones of the joint, further enhancing the smoothness of motion as well as supplying the articular cartilage with nourishment and is another major feature that makes synovial joints different to other joints. Outwith the articulating surfaces, the bones are joined by ligaments that are strings of connective tissue used to strengthen and support the joint by holding the bones together and stopping them from detaching (Tarafder and Lee, 2016) (Figure 1-1).

### ***1.3.2 Synovial membrane***

The synovial membrane consists of two layers, the outer sublining layer (subintima or subintimal) and the inner lining layer (intima or intimal). There are two main types of synoviocytes: macrophagic (type A synoviocytes) or fibroblastic (type B synoviocytes) (Frisbie, 2012). Type A synoviocytes are resident cells derived from bone marrow monocytes (Tu et al., 2020) and which strongly express markers common to other macrophages such as MHC Class II, CD163, CD68, CD14 and Fc $\gamma$ R. They are located within the stromal cell network and play a role in the resolution of inflammation/tissue damage in the joint cavity as well as in antigen presentation (Bartok and Firestein, 2010). On the other hand, type B synoviocytes - also known as fibroblast like synoviocytes (FLS) or synovial fibroblasts (SFs) - are mesenchymal cells found in both the intimal and subintimal layers of the synovial membrane (Li et al., 2019). They are organised as 2-3 layers of cells that make up 75-80% of all synoviocytes in a normal human synovium. They interact with each

other as well as with the extracellular matrix (ECM) through various molecules such as  $\alpha1\beta1$  integrin  $\alpha2\beta1$  integrin and cadherin-11 (CDH11). SFs have been shown to play a crucial role in the organisation of the synovial lining as they have an intrinsic ability to generate a three-dimensional complex synovial lining structure from the tightly packed synovial lining cells, as well as being responsible for the production of synovial fluid components and the ECM (Mathiessen and Conaghan, 2017; Müller-Ladner et al., 2007). They exhibit markers of other fibroblast population such as vimentin, Thy1/CD90 and type IV and V collagen, CD44 and vascular cell adhesion molecule 1 (VCAM-1), the latter of which is not expressed by most other populations of fibroblasts being rarely seen on non-intimal mesenchymal cells. Moreover, integrins such as  $\alpha4\beta1$ , as well as intracellular adhesion molecule-1 (ICAM-1) and integrin receptor are also expressed by type B synoviocytes (Bartok and Firestein, 2010).

### ***1.3.3 Why does inflammation persist in RA?***

Inflammation is a normal physiological response to tissue damage and pathogen infection, that resolves relatively quickly in normal circumstances. Yet, in many chronic conditions such as RA, this inflammatory response persists resulting in significant tissue, joint and organ damage. However, despite the importance of inflammatory dysregulation in chronic conditions being established, the underpinning pathogenic mechanisms remain ambiguous.

As a chronic, systemic autoimmune disorder, immune system cells such as B cells, T cells and macrophages play important roles in the pathogenesis of RA. These cells circulate in peripheral blood and infiltrate the synovial membrane, inducing SFs to hyper-proliferate and destroy bone and cartilage (Bustamante, Garcia-Carbonell, Whisenant and Guma, 2017). For example, in RA, the main role of T cells is to activate macrophages and fibroblasts, transforming the latter into cells destructive to the tissue and in turn, the joint. Similarly, B cells activate macrophages resulting in the production of an array of cytokines and chemokines that support joint inflammation. Activated RA-SFs play essential roles in determining the site at which inflammation occurs: in the subsequent maintenance of persistent inflammation in the joint microenvironment, as reflected in hyperplasia of resident stromal cells and the organisation of T and B

cell infiltration, SFs promote inflammatory cell survival as well as the development of ectopic lymph nodes within the joint, resulting in disease perpetuation (Juarez, Filer and Buckley, 2012). SFs are not only structural cells as initially thought but are also key to the consolidation of joint inflammation that leads to chronic disease. Considering the latter, targeting the SFs, could provide a new, better therapeutic approach as opposed to one involving suppression of global immune mechanisms.

#### **1.3.4 Autoimmune Synovitis**

In RA, the synovial tissue becomes noticeably thicker, with an increase in the infiltration of inflammatory cells leading to the joint damage (cartilage and bone destruction), characteristic of RA. The inflammation, known as synovitis, also features hyperplasia of the synovial membrane resulting from SF hyperproliferation and increased SF migration to, and infiltration of, the inflamed region. The intimal layer also undergoes an escalation in cellularity, with the lining of the cells extending from 1-2 cells thick to that of 10-20 cells thick, with an increased number of both type A and type B synoviocytes, as well as infiltration of immune system cells specifically macrophages, B and T lymphocytes, dendritic cells, mast cells and plasma cells (Sitt, Griffith and Wong, 2016) (Figure 1-3). The aberrant recruitment and retention of inflammatory cells is an important part of synovitis and involves the generation of chemoattractant proteins at the inflamed area and the upregulation of adhesion molecules by endothelial tissue in synovial micro-vessels. These chemoattractants are found to be significantly elevated in the synovium of RA patients and they can be made by both types of synoviocytes in the intimal layer of the synovium (Ospelt et al., 2009). Along with infiltration of cells, in the RA synovium there is also an increase in the expression of pro-inflammatory cytokines such as IL-1 $\beta$ , IL-6, IL-17, and TNF- $\alpha$ , as well as production of MMPs (Smeets, Kraan and Tak, 2003). These factors play a crucial role in the induction and maintenance of the inflammation of the synovial joint as well as the progression and development of RA.

### **1.3.5 Inflammatory cytokines and their role in RA**

In a normal healthy synovium, the presence of cytokines such as tumour necrosis factor  $\alpha$  (TNF- $\alpha$ ), interleukin-1 $\beta$  (IL-1 $\beta$ ), interleukin-17 (IL-17) and interleukin-6 (IL-6) have the potential to become pro-inflammatory (Lubberts and van den Berg, 2003) and consistent with this, their expression has been found to be elevated in patients with RA, indicating to their importance in RA pathophysiology (Figure 1-3).

#### **1.3.5.1 The role of IL-1 $\beta$ in**

The inflammatory cytokine IL-1 $\beta$  has been shown to be a key mediator in autoimmune diseases such as RA, with its signalling resulting in the production of other cytokines like IL-6 and TNF- $\alpha$  and activation of pathogenic signalling networks (Arend, Malyak, Guthridge and Gabay, 1998). It also has a greater capacity (as opposed to TNF- $\alpha$ ) of increasing matrix degradation through the induction of MMPs and PGE2 production in synovial cells, as well as playing a role as a mediator of bone and cartilage destruction. Moreover, the cytokine has been shown to decrease the process of repair through matrix synthesis suppression (Cutolo, 2011). Studies have shown that IL-1 $\beta$  and Interleukin-1 receptor antagonist (IL-1Ra) are elevated within the synovium of RA patients with inflamed joints (Hopkins, Humphreys and Jayson, 1988). Whilst IL-1 $\beta$  has been shown to cause the migration of inflammatory cells into the structures of joints and the synovium of RA patients, IL-1Ra non-productively binds to IL-1R, preventing IL-1 $\beta$  signalling to the cell, conclusively blocking its effects (Cutolo, 2011). IL-1Ra has been shown to suppress cytokine-induced catabolism in the cartilage in the synovium and has been investigated in the form of a potential therapeutic injection to treat inflammation in arthritic patients (Mehta et al., 2019).

There are two key mechanisms through which RA synovial tissue aids in cartilage loss. The first being a direct mechanism which involves the production of MMPs and cathepsins by the RA synovium, the second involves the remodelling of the joint cartilage via chondrocyte function deregulation through the release of cytokines such as IL-1 $\beta$  - which induces the expression of proteinases, SFs and chondrocytes - as well as other mediators from the synovium. Moreover, RA-SFs have been shown to display increased MMP production (MMP-1,3,13,14 and 15) and

significantly contribute the joint destruction commonly seen in RA. The elevated MMP expression by SFs is not only upregulated by increased expression of IL-1 $\beta$  and TNF- $\alpha$  but is also sustained intrinsically by RA-SFs, which exhibit a transformed phenotype (Rengel, Ospelt and Gay, 2007). The cartilage has the potential to be further destroyed by destructive enzymes leading to degradation and erosion of the bone. Therefore, specifically, and selectively blockading IL-1 is a targeted, rational treatment against the destructive effects of this cytokine on those with RA (Schiff, 2000). Indeed, in experimental models IL-1 blockers and IL-1Ra have significantly reduced clinical and histological disease parameters in RA patients (Kay, 2004).

Reflecting this, there are a number of IL-1 blockers commercially available to treat patients with RA such as Anakinra, Canakinumab, and Riloncept. A study investigating the effect of Anakinra in RA patients showed that treatment reduced the migration of inflammatory cells into the joint, as well as considerably reducing the joint damage seen after 48 weeks, as opposed to the progressive loss of cartilage and increased pain that would have been present if patients had not been treated. The latter is due to IL-1 $\beta$  inhibiting osteoclasts in RA (Dinarello, Simon and van der Meer, 2012).

#### **1.3.5.2 The role of TNF- $\alpha$ in RA**

TNF- $\alpha$  is both an autocrine simulator and paracrine inducer of other pro-inflammatory cytokines by coordinating innate and adaptive immune responses and has also been shown to stimulate the expression of adhesion molecules (e.g., I-CAM) (Vasanthi et al., 2007) by SFs. It is an important cytokine involved in promoting normal immune responses, however high levels of this cytokine have been found in the serum and synovial fluid of patients with RA with the consequent unresolved inflammation playing a crucial role in joint pathology. Activated CD4+ T cells can stimulate macrophages, monocytes and SFs to produce IL-1 $\beta$ , IL-6, and TNF- $\alpha$  (Yap et al., 2018). As these T cells also express receptor activator of nuclear factor kappa-B ligand (RANK-L), they can also stimulate differentiation of osteoclasts resulting in cartilage destruction (Kong et al., 1999). As TNF- $\alpha$  can regulate IL-6 production (Matsuno et al., 2002), in cultures of synovial cells from

RA patients, inhibiting TNF- $\alpha$  significantly reduced the production of IL-1, IL-6, IL-8 and GM-CSF. Therefore, inhibition of TNF- $\alpha$  may have a wider effect on inflammation compared to inhibition of other less pleiotropic cytokines found at elevated levels in synovial fluids such as IL-1 (Vasanthi et al., 2007). Indeed, it is easy to see why anti-TNF- $\alpha$  therapeutics are widely used as a treatment, however like all immunosuppressants they come with many side effects, dictating that more cell specific targeted treatments of RA are required (Farrugia and Baron, 2016).

#### **1.3.5.3 The role of IL-17 in RA**

Studies have shown that IL-17 is involved in mediating the joint destruction characteristic of RA, with immunostaining of the synovial tissue of RA patients showing that a subset of CD4+CD45RO+ memory T cells produce this cytokine, whilst these are not found in synovial tissue samples from patients with osteoarthritis (OA). Furthermore, it was found that the level of IL-17 in the synovial fluid of RA patients was significantly higher than that of OA patients (Kotake et al., 1999). The high secretion of this cytokine occurs through interactions with the molecule podoplanin, secreted by monocytes and SFs in the lining layer (Croft et al., 2016; Noack, Ndongo-Thiam and Miossec, 2016A; Noack, Ndongo-Thiam and Miossec, 2016B) and cartilage damage is, to an extent, induced by synovial cytokines like IL-17. Certainly, addition of anti-IL-17 antibodies to RA synovial cultures resulted in a decrease in MMP-1 production and collagenase activity but did not affect TIMP1 production, supporting a role for IL-17 in joint damage (Chabaud et al., 2000). This was further supported by studies in which mice were given IL-17 intra-articularly, resulting in cartilage degradation (Chabaud et al., 2001). Moreover, this cytokine has been found to trigger the migration of SFs and promote the invasiveness of inflammatory cells (Hot, Zrioual, Lenief and Miossec, 2012) to induce destruction of tissue within the synovial joint (Bottini and Firestein, 2012), specifically the destruction of the cartilage matrix and erosion of bone.

#### **1.3.5.4 The role of IL-6 in RA**

Another important cytokine involved in the pathogenesis of inflammation in RA is IL-6, with RA patients being found to have increased levels of this cytokine in their

serum and synovial fluid and the levels correlating with disease activity and joint destruction. It appears to play a role in local inflammation resulting in joint damage via instigation of IL-8 and monocyte chemoattractant protein-1 (MCP-1) production by endothelial cells as well as bringing about activation of adhesion molecule expression and consequent recruitment of leucocytes into the joints affected (Suzuki, Hashizume, Yoshida and Mihara, 2009). This cytokine also promotes synovitis and joint destruction through the stimulation of neutrophil migration, osteoclast maturation and vascular endothelial growth factor (VEGF)-stimulated pannus formation (Srirangan and Choy, 2010; Nakahara et al., 2003). Furthermore, the production of IL-6 by synoviocytes leads to proliferation and differentiation of osteoclasts (Srirangan and Choy, 2010), thus linking the production of this cytokine to bone erosion. Its causal role in RA has also been studied using various animal models: for example, in antigen-induced arthritis (AIA), blocking of IL-6 activity results in the severity of RA in this mouse model being decreased (Ohshima et al., 1998). All the above makes blocking IL-6 another potential therapeutic target for RA treatment.

#### **1.4 Synovial fibroblasts (SFs)**

Despite RA being an autoimmune disease, other cells of non-immune origin such as SF, have been shown to be involved in pathogenesis, playing a crucial role in the perpetuation of joint inflammation in RA (Lefevre, Meier, Neumann and Muller-Ladner, 2014). SFs are the major type of stromal cells found in the synovium. In health, SFs provide the joint cavity and cartilage with nutritional support and lubricating molecules such as hyaluronic acid. They also play a role in continuous matrix remodelling through production of a range of matrix components such as collagen as well as matrix degrading enzymes (Müller-Ladner et al., 2007). Moreover, in RA, SFs are “transformed” into pro-inflammatory cells that produce a range of cytokines such as IL-1, IL-6 and TNF- $\alpha$  that perpetuate inflammation as well as releasing proteases that aid in cartilage degradation (Bartok and Firestein, 2010; Szekanecz, Kim and Koch, 2003).

### **1.4.1 Synovial fibroblasts in RA**

Morphologically, activated RA synovial fibroblasts (RA-SFs) look more rounded in shape, with a pale and prominent nucleus, compared to their usual spindle-like shape (Lefevre, Meier, Neumann and Muller-Ladner, 2014). RA-SFs also change their functional phenotype (Fassbender and Simmling-Annefeld, 1983) with those in the inner lining exhibiting alterations in their signalling and epigenetic networks and expression of matrix degrading enzymes. These alterations are reminiscent of those associated with tumours, as the SFs become invasive and aggressive towards the bone and cartilage (Huber et al., 2006) and display characteristics similar to that of tumour-like mesenchymal cells (Yuan et al., 2004). For example, the pannus appears to behave almost like an invasive tumour, with SFs showing the ability to migrate and attach to it, resulting in bone and cartilage invasion (Pap, Müller-Ladner, Gay and Gay, 2000).

Destruction of the bone and cartilage is in effect the end stage of RA pathogenesis and it has been found that RA-SFs promote this cartilage degradation. RA-SFs initially cause bone erosion and cartilage damage directly via secretions of cathepsins and MMPs, specifically MMP1 and MMP13, as well as the stromelysin, MMP3 and the gelatinases, MMP2 and MMP9 (Pap et al., 2000). The production of these MMPs is greatly increased through RA-SF and T cell interaction (Burger et al., 1998). In addition, they can also indirectly initiate damage to the bone and cartilage through inducing osteoclastogenesis via RANK-L secretion along with that of VEGF that can act as an alternative to M-CSF (Danks et al., 2015). This idea that the cartilaginous structure within the joint may in fact be destroyed by RA-SFs is further supported by a study using CDH11 knockout mice. These mice, which do not exhibit a synovial intimal layer and are therefore SF deficient, were protected from cartilage damage induced by arthritis, despite continuous progression of inflammation and bone damage (Lee et al., 2007).

#### **1.4.1.1 RA-SF and ECM**

In health, SFs produce the extracellular matrix (ECM) components of synovial fluid and are therefore important for joint lubrication (Ospelt, 2017). The ECM in the synovial joint is composed of substances such as water, collagen (type II constituting 90% of synovial collagen), as well as non-collagenous proteins,

glycoproteins and extracellular glycosaminoglycans. In healthy joints the synovium acts as a leaky, restricting membrane that has enough resistance to maintain the synovial fluid within the joint, yet has sizeable (micrometre) intracellular gaps through which the ECM most likely plays an important role in the resistance of the lining to synovial fluid escape (Sabaratnam, Coleman, Mason and Levick, 2006). The hydraulic resistance of ECM is based on the concentration of glycosaminoglycans, glycoproteins and proteoglycans in collagen fibrils (Tarafder et al., 2016), as fluid passes through the narrow spaces between the polymer chains (Levick, 1987). Due to the high hydraulic resistance, the synovial matrix displays a high concentration of glycosaminogen, which when depleted results in an increase in synovial hydraulic permeability (Scott et al. 1998).

In RA, the RA-SFs upregulate adhesion molecules, causing a significant interaction between the RA-SFs and the ECM that triggers the processes resulting in bone and cartilage degradation. For example, RA-SF attachment to the articular cartilage is the initial stage required for invasion of the synovium, and this is mediated by upregulation of adhesion molecules on the surface of RA-SFs. These adhesion molecules ensure that fibroblasts are secured to the ECM of the cartilage, mainly via collagen type II and glycosaminoglycans (Huber et al., 2006). Fibroblasts appear to be dynamic cells that can develop distinct phenotypes dependent on differences in their environment (Saxena et al., 2013). In environments that are inflammatory, fibroblasts acquire a pro-inflammatory and matrix degrading phenotype as, for example, pro-inflammatory cytokines, such as IL-1 $\beta$  delay myofibroblast conversion and induce chemokine and MMP synthesis by tissue fibroblasts. Inflammatory activation of fibroblasts may play a role in ECM changes, with inflammation being associated with protease activation and generation of matrix fragments with pro-inflammatory properties (Frangogiannis, 2016).

#### **1.4.1.2 Synovial fibroblast subsets and their markers**

Studies using SCID human-mouse models showed implanted RA-SFs to be differentiated into two main distinct fibroblast subsets located within different anatomical compartments of the inflamed synovial membrane (Croft et al., 2016). Lining synovial fibroblasts are those found proximal to the cartilage (Figure 1-4) in a layer a couple of cells thick that produces synovial fluid. Consistent with them

having been found to be associated with increased cartilage degradation *in vitro* (Croft et al., 2013), they are involved in the attachment, invasion and degradation of cartilage (Croft, Naylor, Filer and Buckley, 2014). Although these cells have been found to produce pro-inflammatory cytokines during inflammation, this is at a decreased level compared to SFs in the sublining area. They have also been found to produce small quantities of RANK-L, which is required for the induction of osteoclastogenesis but, interestingly, when there is no inflammation present, there is an increased production of osteoprotegerin (OPG), which counteracts the effects of RANK-L inflammation, thereby acting as a homeostatic control mechanism for repair (Smith, 2003). Bone loss is a significant problem that goes hand in hand with chronic inflammation, highlighting the relationship between bone erosion and inflammation as the effects of pro-inflammatory factors play a crucial role in osteoclastogenesis which leads to bone resorption. Specifically, loss of homeostatic regulation is due to interference of the balance between RANK-L and OPG, which is key to regulating the remodelling and repair of bone. Thus, OPG is secreted by osteoblasts and protects against excessive bone resorption by blocking RANK-L interacting with RANK, by binding to it (Kapasa et al., 2017). By contrast, sublining SFs are found distal to the cartilage and express phenotypic markers such as CD248 and CD90 [also known as Thy1]. Cells expressing both of these markers are never found in the lining layer or invade the cartilage, being more associated with promoting inflammation. The development of such stromal architecture in these SCID mice was very similar to that observed *in vivo* in the inflamed synovial membrane (Croft, Naylor, Filer and Buckley, 2014), suggesting the latter is not dependent on immune system cell actions.

Biomarkers in diseases like RA are important as they allow a better understanding as well as identification of specific subsets or cell types facilitating investigation of their role in the progression and initiation of disease. Recent interest has focused on the stromal markers differentially expressed in the lining and sublining layers as both types play different roles in RA and understanding and identifying these subpopulations of SFs could prove useful in developing better treatments of RA. The cells proximal to cartilage (lining) have recently been shown to express markers identifying a lining layer phenotype (Fibroblast activation protein  $\alpha$  [FAP $\alpha$ ], VCAM-1, CDH11, CD90). FAP is a membrane antigen that is expressed

dynamically by fibroblasts in both lining layers in patients with RA, with baseline expression levels higher in those individuals with early synovitis who progressed to RA over time (Choi et al., 2017). Indeed, three types of stromal cells express FAP: pericytes, lining layer and sublining layer SFs (Tchou et al., 2013) and deletion of FAP-expressing cells attenuates leukocyte infiltration, and therefore there is a decrease in chemokine and cytokine production. Furthermore, such deletion also protects the joint from bone erosion (Ospelt et al., 2010; Bauer et al., 2006).

RA is characterised by hyperplasia of the synovial lining and invasion of cartilage and bone by the lining subset of SFs. These SFs have been shown to have elevated expression of VCAM1, with the intensity of VCAM1 expression correlating with the degree of severity of inflammation of the synovial lining (Croft, McIntyre, Wibulswas and Kramer, 1999; Carter and Wicks, 2001). Adhesion molecule cadherin-11 (CDH11), which is selectively expressed on fibroblasts, has also been implicated as an important mediator of inflammation with an apparent important role in SF activation and inflammation via MAPK and NF- $\kappa$ B signalling (Warde, 2011). However CD90, a marker which differentiates inflammatory fibroblasts in the lining layer from those in the sublining layer, appears to be more specifically involved in cartilage destruction. As this marker allows SF subsets to be distinguished, a better understanding of the differential roles of these SF subtypes in RA can be investigated. For example, studies showed that sublining FAP $\alpha^+$ CD90 $^-$  cells were found to migrate to the bone and cartilage to cause destruction whilst FAP $\alpha^+$ CD90 $^-$  fibroblasts, even when restricted to the synovial lining layer, selectively mediate bone and cartilage damage with little effect on inflammation (Figure 1-4). However, FAP $\alpha^+$ CD90 $^+$  cells are also found in the synovial membrane sublining layer and these SFs are associated with the inflammation observed in disease; for example, they express cytokines that can attract inflammatory cells resulting in a more severe and persistent inflammatory arthritis, with minimal effect on bone and cartilage (Croft et al., 2019).

Characterisation of SFs in the synovium by single cell RNA sequence analysis actually identified the presence of additional fibroblast subtypes in RA joints, a situation which differed from that of osteoarthritis (OA) controls and facilitated

subsetting of lining and sublining SFs and their functions. Three functional subsets were characterised as being CD34<sup>-</sup>CD90<sup>-</sup>, CD34<sup>-</sup>CD90<sup>+</sup> and CD34<sup>+</sup> SFs in RA synovial tissue, with the subsets differing in their cytokines and matrix metalloproteinases expressed in response to TNF- $\alpha$  stimulation (Mizoguchi et al., 2017). The marker CD34 can be used to identify sublining SFs as CD34<sup>-</sup>CD90<sup>+</sup> SFs are enriched around blood vessels in the deep sublining area of the synovium (Abuwarwar, Knoblich and Fletcher, 2018) and elevated levels of them are involved in increased bone destruction in RA (McHugh, 2019). Nevertheless, the transcriptomic profile of CD34<sup>-</sup>CD90<sup>+</sup> fibroblasts correlated with invasion and migratory behaviour and secretion of pro-inflammatory cytokines and proliferation (Onuora, 2018).

Overall, SFs from the lining and sublining layers differ in phenotype and therefore represent distinct subtypes of the SF population (Ospelt, 2017), with SFs from differing anatomical sites carrying out specific specialised functions. SF in the lining layer of the joint express the adhesion molecules VCAM1 and CDH11 and the enzyme phosphodiesterase 4 (PDE4), whilst those in the sublining layer express CD248 and CD90 (Croft et al., 2016; Maia et al., 2010). As they differ in terms of gene expression patterns and functions, this could explain why certain joints are much more susceptible to developing certain types of arthritis compared to others, as the sublining subset is more inflammatory whilst the lining subset is more involved in erosion and degradation of the joint (Frank-Bertoncelj et al., 2017).

#### ***1.4.2 Epigenetic remodelling of RA-SFs***

SFs perpetuate disease and do not lose their inflammatory phenotype as they become epigenetically modified to an aggressive phenotype. Epigenetic modifications are chemical alternations on DNA molecules and histones that regulate the responsiveness of genes in terms of transcription, with chromatin remodelling and noncoding RNAs thought to be key epigenetic regulatory mechanisms determining the gene expression signature of the cell. Accordingly, they shape the formation of cell and tissue specific phenotypes. Despite the high stability of epigenetic modifications, they can be reversed and/or modified via environmental factors and therefore act as a vital mechanism for cell survival and adaptation to new environments or diseases. Certainly, epigenetic mechanisms are

crucial to RA pathophysiology, contributing to disease aetiology as well as providing strong biomarkers of disease activity and progression (Karami et al., 2020).

Activated RA-SFs are key effectors in RA pathogenesis, with the activation occurring through interactions between RA-SFs and other cells present within the synovial microenvironment early in disease progression. Pro-inflammatory cytokines such as TNF- $\alpha$ , IL-1 $\beta$  and IL-6 all play a fundamental role in the activation of RA-SFs (Pap, Müller-Ladner, Gay and Gay, 2000). Following activation, RA-SFs also produce these cytokines, resulting in maintenance of regulatory feedback loops as well as promote the production of MMPs, cathepsins, aggrecans and their inhibitors (McInnes and Schett, 2007). However, other cell intrinsic mechanisms must result in their activation, as the persistence of the activated phenotype of RA-SFs is independent of these cytokines (Müller-Ladner, et al 1996) and individuals who are treated for RA with anti-cytokine therapies, still experience symptoms and are not cured (Firestein, 2003).

Studies have shown that SF responses to pro-inflammatory stimuli are caused through continuous changes in the transcription levels of genes pertinent to disease, with RA-SFs showing an upregulation in expression of proto-oncogenes, adhesion molecules and MMPs, as well as decreased expression of tumour suppressor genes. These continuous gene transcription changes account for the “aggressive” behaviour exhibited by RA-SFs, with patterns of differential gene expression apparent in both disease and health displayed in differing anatomical locations (Juarez, Filer and Buckley, 2012). Certainly, RA-SFs have been found to exhibit global genomic DNA hypomethylation (an epigenetic change in promoter regions correlating with gene expression upregulation) resulting in upregulation of disease-relevant genes (Karouzakis et al., 2009). Specifically, RA-SFs are subject to an epithelial-mesenchymal transition (EMT)-like mechanism, embracing a mesenchymal-fibrotic phenotype (Haniffa, Collin, Buckley and Dazzi, 2008; Zvaifler, 2006) that is epigenetically rewired to over-produce pathogenic mediators such as proinflammatory cytokines that prompt joint damage, the secretion of MMPs, that facilitate cartilage destruction and bone erosion, and RANK-L, which affects osteoclastogenesis (Nygaard and Firestein, 2020). These

epigenetically rewired aggressive SFs demonstrate a hyperplastic, invasive and aberrantly inflammatory phenotype as well as dysregulation of their functional outcomes (Collins and Wann, 2020; Teves et al., 2019).

Murine studies carried out by Corbet et al, using a Collagen-Induced Arthritis (CIA) mouse model also showed that CIA-SFs displayed hypomethylated global DNA compared to naïve SFs and that this could be recapitulated *in vitro* through cytokine stimulation (IL-17 and IL-1 $\beta$ ). Such global DNA hypomethylation correlated with a reduction of DNA methyltransferase-1 (DNMT1) expression and the cells were found to display increased levels of IL-6, CCL2, MMP9 and MMP13 in the presence and absence of IL-17 stimulation. Moreover, the resulting joint destruction observed in the CIA mice was found to be associated with elevated levels of hypoxia in cells in the joint, as well as induction of vascular leakage (Corbet et al., 2020).

Intriguingly, epigenetic imprinting conveys site specificity, driving RA-SF to adjust their gene expression in response to the microenvironment of the RA synovium (Bird, 2007). It can be concluded that the SF population is heterogeneous and in RA, SFs are epigenetically rewired to aggressive phenotypes.

## 1.5 Hypothesis and aims

Thus, as it has now been established that SFs play a significant role in the perpetuation of inflammation and joint damage in RA, they are an interesting therapeutic target which may avoid the side effects associated with generalised immunosuppression. However, as SFs appear to lose their aggressive physiological characteristics under traditional culture conditions (Sung et al., 2013), the role that SFs play is not completely understood, and may prevent identification of potential drug targets. Although currently there are no “gold standard” *in vitro/ex vivo* models that ‘mimic’ the 3D architecture of the synovial joint and its inflammatory environment, it appears that fibroblasts in 3D cultures display more “*in vivo*” behaviours compared to stromal fibroblasts cultured in 2D systems. Thus, if a better understanding of these cells function could be established by optimising *ex vivo/in vitro* culture systems to more fully recapitulate *in vivo* responses, this

could promote development of drugs selectively blocking the pathogenic effects of SFs in the joint and hence provide RA treatments without immunosuppression, resulting not only in less risk for patients but also a more direct therapy. Therefore, developing more appropriate *in vitro* platforms for testing SFs may facilitate translation of recent *in vivo* biological and pathological findings to the clinic and provide an opportunity to develop non-immunosuppressive therapies. The treatment goal of RA is to achieve low disease activity and remission; however, a strong unmet medical need still exists as not all RA patients have met clinical remission, with 25% of patients still suffering from moderate to high disease activity characterised by systemic inflammation, synovitis, bone and cartilage erosion as well as pannus formation in the later stages. Thus, despite, animal and 2D culture models and the potential therapies through clinical trials from the latter, newer medications still need to be developed, indicating the failures of current models.

Although they are not immune system cells, SFs are able to create a microenvironment that perpetuates inflammation in the joints of patients with RA. Therefore, as outlined above, by targeting these cells it may be possible to provide new therapeutic alternatives to current immunosuppressive drugs, circumventing their inherent attendant and severe side effects. However, there are no drugs currently available that specifically target the fibroblast compartment in RA. My hypothesis is that this may be due to the failure of traditional *in vitro* 2D culture experiments to recapitulate the physiological signalling of cells found within the joint preventing understanding of relevant pathogenic SF functional responses. Importantly, 3D culture systems are constantly being developed to mimic tissue-specific physiological or pathophysiological disease-specific microenvironments, where cells are not only able to proliferate and differentiate but also participate in cell-to cell and cell-to ECM interactions. Popular types of 3D scaffolds include hydrogels/matrigels (polymeric material containing a network of crosslinked polymer chains) and inert matrices (sponge-like membrane made of polystyrene, containing pores to allow for cell proliferation and growth). Interestingly, hydrogels have been used to develop ECM-based RA treatments with the development of injectable tyramine modified hyaluronic acid (HA-Tyr) hydrogels that act to reduce interleukin-6 (IL-

6), prostaglandin E2 levels in collagen-induced arthritis (CIA) animal models (Kim et al., 2011).

The core aim of this project is therefore, by comparing *in vitro* SF responses in classical 2D cultures with those in both polystyrene scaffold (Alvetex®) and hydrogel 3D cultures, to determine whether SFs grown in 3D culture systems exhibit functional phenotypes more characteristic of those observed *in vivo* and also whether these platforms provide a better understanding of the spatially dynamic and ECM-interacting role of SFs in the joint and during pathogenic transformation in CIA. The information gained could contribute to the development of more pathophysiologically relevant models of the joint in RA and hence ultimately, translation of these platforms for drug development targeting the human disease.

The specific objectives of the project are:

- to characterise the inflammatory responses of Naïve and CIA SFs cultured in 2D and 3D (Alvetex® scaffolds and FibronectinPEG (FNPEG) hydrogels) microenvironments
- to explore the ability of activated SFs to migrate and organise throughout Alvetex® and FNPEG hydrogels
- to evaluate whether SF subpopulations can be identified and maintained in any of these culture systems
- to investigate the (differential) impact of *ex vivo* culture in each of these systems on the pro-inflammatory gene expression of Naïve and CIA-SF and how these are modulated by the incorporation of ECM components like Fibronectin (FN) in the culture platforms.

These combined approaches should increase our fundamental understanding of SF biology, particularly with respect to their functional plasticity under conditions of chronic inflammation. In addition, they should provide information critical to the design of better 3D *in vitro* models of the arthritic joint will facilitate exploring the role of fibroblasts in perpetuating joint inflammation in RA as well as a better understanding of potential sites of intervention for human disease.

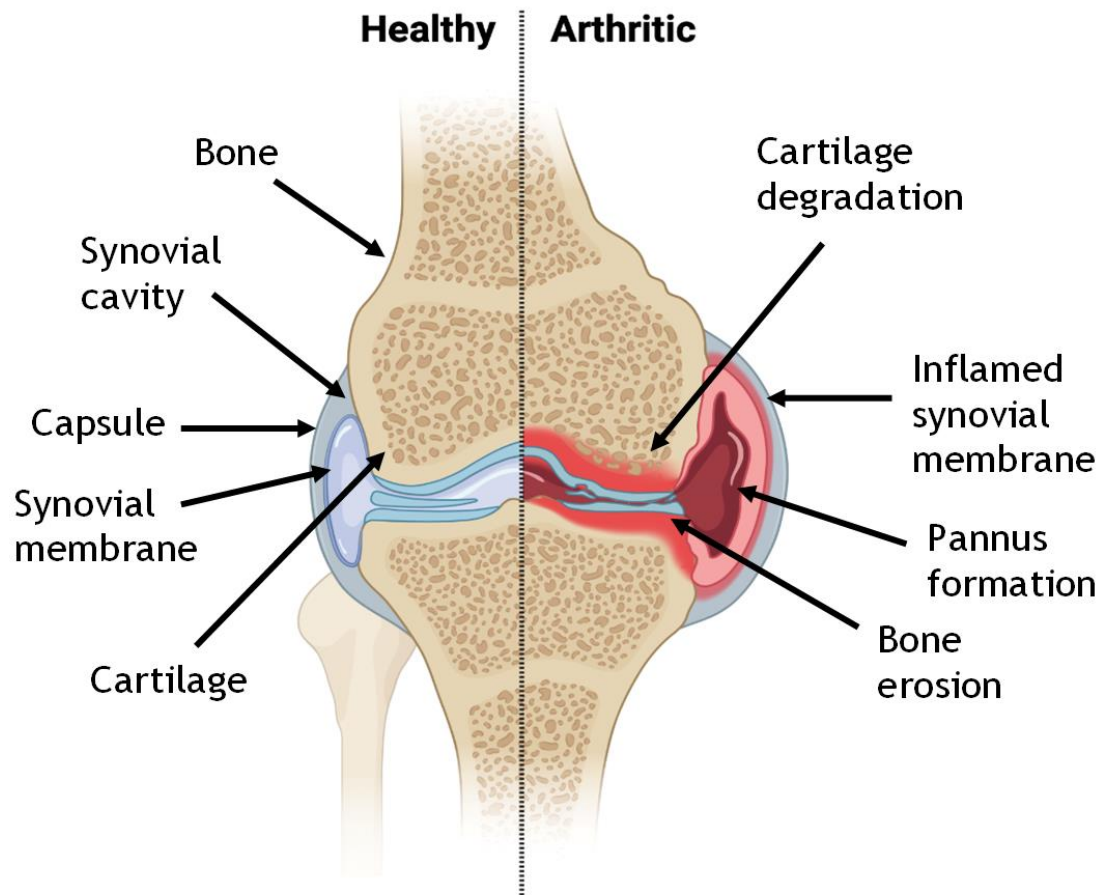


**Figure 1-1: Anatomy and pathophysiology of healthy and arthritic synovial joints.** In a healthy joint (left), there is no swelling in the synovial joint capsule, cartilage and bone are intact. The synovium membrane is a thin layer of cells that provides structural and nutritional support to the joint. During RA (right), the tissue architecture changes to show characteristic disease symptoms of chronic joint inflammation. There is swelling, and an inflamed synovial membrane that becomes a critical mediator of disease chronicity. The arthritic joint develops a pathogenic pannus, and eventually, cartilage and bone erosion (Created with BioRender.com).

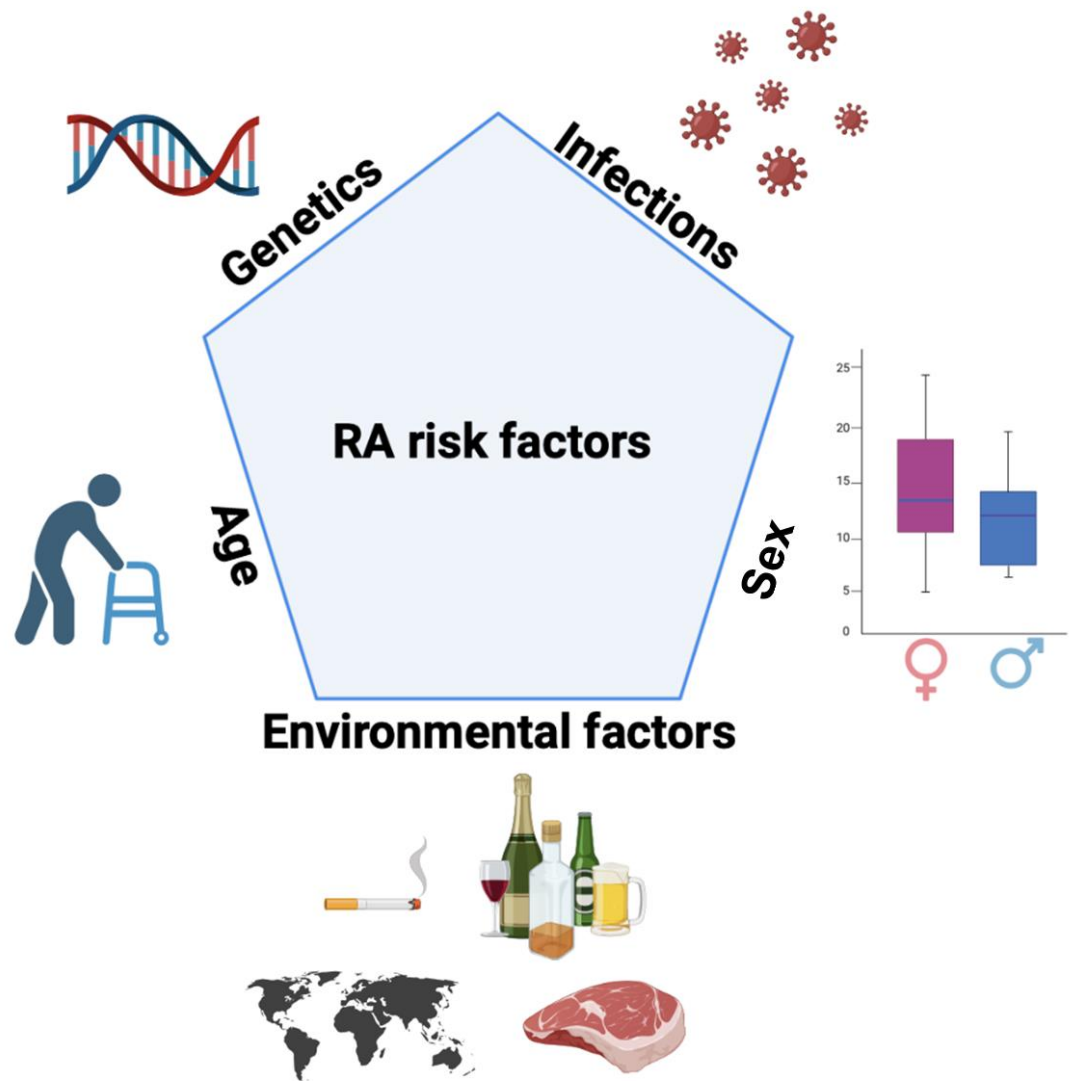


**Figure 1-2: Risk factors associated with RA.**

Several factors have been described to affect RA initiation, including age, infections, genetics and sex, with women more likely to develop RA than men. Environmental factors may also play a role, like diet, alcohol or smoking, being smoking the highest risk factor. Geographical location also plays a role in increased risk, perhaps as a consequence of distinct environmental changes (created with BioRender.com)

**Table 1-1: Types of biologic treatments for RA patients, their targets, examples, and mechanisms**

Type of biologic	Example(s)	How it works
B- cell depleter	Rituximab (monoclonal antibody)	CD20-induced apoptosis, complement dependent cytotoxicity, antibody dependent cell-mediated cytotoxicity, and selective targeting and depletion of B cell subsets.
IL-1 $\beta$ blocker	Anakinra (Interleukin antagonist)	Blocks IL-1 in turn reducing the migration of inflammatory cells into the joint.
IL-6 blocker	Tocilizumab (Monoclonal antibody)	Targeting of the IL-6 pathway by blocking IL-6 receptor.
TNF- $\alpha$ blocker	Etanercept Certolizumab pegol (Monoclonal antibodies)	Reduces inflammatory reaction of the body by blocking TNF- $\alpha$ (which induces bone loss), hence preventing it to bind on its receptor (TNFR1 or TNFR2).
Janus kinase (JAK) inhibitor	Tofacitinib Baricitinib Upadacitinib	Inhibiting the activity of one or more of the Janus kinase family of enzymes (JAK1, JAK2, JAK3, TYK2), thereby interfering with the JAK-STAT signalling pathway.
T-cell inhibitor	leflunomide	Prevent autoimmunity by dampening autoreactive T-cell proliferation directly or indirectly via regulatory T cells (Tregs).
PDE inhibitor	Apremilast (Phosphodiesterase inhibitors)	Inhibits TNF- $\alpha$ production from human synovial cells

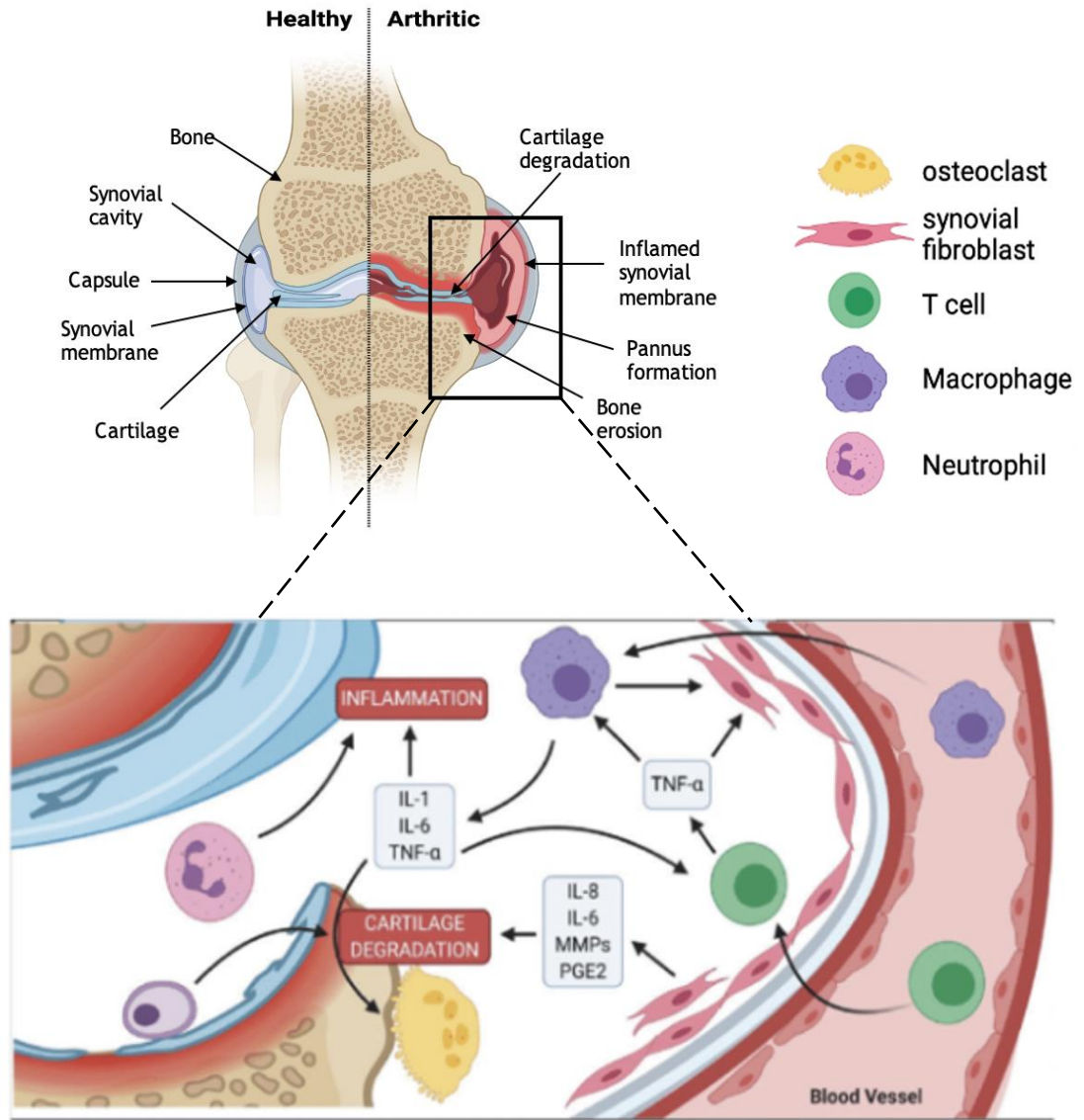


**Figure 1-3: RA pathophysiology.**

Multiple immune networks have been described in RA pathophysiology. TNF-alpha is one of the key players in disease progression, it activates multiple immune system cells, like macrophages, monocytes, and non-immune system cells, such as osteoclasts and synovial fibroblasts (SFs). As a result, T-cells infiltrate the synovial membrane, initiating inflammation. Joint degradation occurs via recruitment of macrophages and secretion of inflammatory cytokines. The pro-inflammatory cytokines shown promote osteoclast-mediated bone erosion by up-regulating local RANK-L production (Adapted from Akram et al., 2021 with Biorender.com).

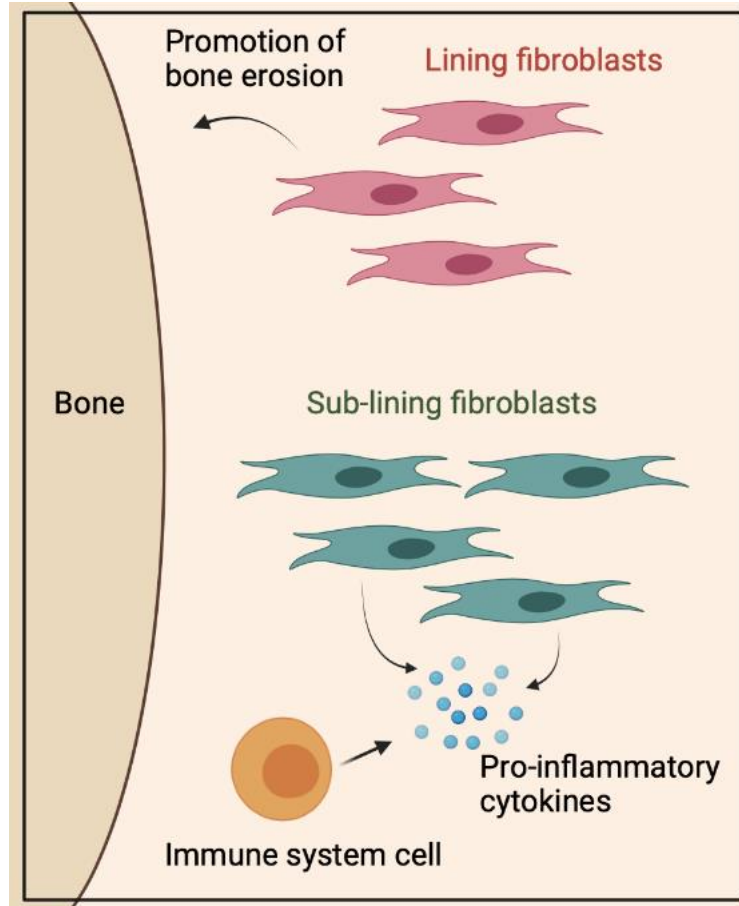


**Figure 1-4: Distinct fibroblast subsets perform different functions in RA.**

Joint showing location of two different subpopulations of synovial fibroblasts - lining and sublining - and their different functions in RA. Lining SFs are predominantly involved in bone and cartilage erosion, whilst sublining SFs are more involved with inflammatory nature of RA (created with Biorender.com).

## Chapter 2 Materials and Methods

### 2.1 Mice

Male DBA/1 mice were purchased at 6-8 weeks of age (Envigo; Bicester, UK) and then housed and maintained at the Central Research Facility in the University of Glasgow. All experiments were approved by and carried out in accordance with the Animal Welfare and Ethical Review Board of the University of Glasgow, UK Home Office Regulation and Licenses PPL P8C60C865 and PIL ID5D5F18C.

### 2.2 Collagen induced arthritis (CIA) model

CIA was induced as described using bovine Collagen type II (CII-100 µg) emulsified with complete Freud's adjuvant (MD Biosciences) and injected intradermally on day 0. On day 21, mice were injected intraperitoneally with a further 200 µg of CII in PBS. Inflammation of paws was assessed every 2 days following the booster injection, through articular scoring and the use of a callipers to quantitatively assess changes in paw size. Joint pathology was scored as follows: 0 = No evidence of erythema or swelling, 1 = Erythema and mild swelling confined to tarsals or ankle joints, 2 = Erythema and mild swelling extending from the ankle to the tarsals, 3 = Erythema and moderate joint swelling extending from the ankle to metatarsal joints, 4 = Erythema and severe swelling encompassing ankle, foot and digits or ankyloses of the limb. Mice were continually observed for any inflammation and culled once stable pathology was established, typically between day 31 to day 42. However, if the severity threshold was breached such that the total articular index exceeded 10 or more than three paw joints were inflamed, ulceration of the IP injection site extended  $\geq 5$  mm, paw thickness exceeded 4.5 mm or weight loss exceeded 20% of controls, affected mice were culled immediately.

### 2.3 Isolation and culture of SFs

#### *2.3.1 Isolation of primary SFs from murine joints for ex vivo cell culture*

Mice were euthanized using carbon dioxide, according to guidelines for the Institutional Animal Care. The mouse was then placed in a face-up position and

rinsed with 100% ethanol. The skin was peeled back, and soft tissue removed from hind and front paws using scissors and forceps, ensuring no skin remains on the limbs. Using scissors, a cut was made above the knee joint and then the limb was sprayed with 100% ethanol and placed in a tube filled with HBSS medium containing antibiotics (pen/strep and nystatin) at 50 units/ml. This was repeated with the rest of the joints. The cut joints were rinsed into a tissue culture plate containing 70% ethanol and then transferred to a dish containing HBSS. All of the fat and muscle was removed leaving the bones using forceps and scissors, taking care to avoid breaking the bones and prevent bone marrow cell contamination. A HBSS-based digestion solution containing fresh collagenase IV (10 mg/ml) and antibiotics was prepared and diluted to obtain a concentration of 5 mg/ml using DMEM medium containing 10% FCS and the solution was filtered using a strainer. The stripped bones (dislocated and cut at the joints) were placed in bijoux tubes with 3 ml DMEM medium containing 10% FCS (1 mouse per bijoux) and 3 ml of the freshly made and filtered digestion solution added to make the final concentration of 1 mg/ml in complete DMEM (10% FBS 1% L-Glutamine and 1% Pen/Strep). The joint samples were incubated in a shaking cupboard at 37°C for 40 min at maximum shaking speed of 100 rpm. The tubes were then vortexed vigorously to release cells, and the contents placed in a 50 ml tube containing 5 ml DMEM medium containing 10% FCS. The samples were rinsed and vortexed with 3 ml of DMEM solution three times with the contents transferred to fresh 50 ml tubes each time to ensure all the cells have been released and transferred. The 50ml tubes were then centrifuged at 500 g for 10 min at room temperature. The cells were resuspended in 12 ml DMEM and seeded into 75cm<sup>2</sup> flasks (each flask containing tissue from individual mice) and placed in the incubator.

### ***2.3.2 Routine cell maintenance and culture***

One day after the first seeding, without removing the small pieces of tissue that provide a platform for SFs to grow around, the medium (DMEM [VWR International, UK] cell growth medium, supplemented with 10% (v/v) foetal bovine serum (FBS) and 5% (v/v) 200 mmol/L L-Glutamine (Invitrogen, Paisley, UK), Non-essential amino acids (NEAA) and antibiotics) was changed. The cells were then monitored daily, and the medium changed every 3 days, with the cells maintained at 37°C in a 5% CO<sub>2</sub> environment. To change the medium, 2-3 ml of the original medium in

the flask was left and 9-10 ml of fresh DMEM (+Pen/Strep) medium was added. When groups of cells were observed under the microscope, the pieces of tissue were removed. Passaging of cells was carried out when the cells reached confluency over 90% of the flask (typically up to 10 days after isolation). Passaging required cell trypsinisation that was carried out by removing the medium from the flask and washing the cells with PBS, after which 4 ml warm 0.05% (v/v) trypsin-ethylenediaminetetracetic acid (EDTA; Life Technologies, Paisley, UK) solution was added to the flask and the flask placed in the incubator for 3 min, after which the solution containing the released cells was removed from the flask and added to a tube containing 5 ml complete DMEM medium. Cells were centrifuged at 500 g for 10 min at room temperature, the resulting supernatant discarded and 12 ml complete DMEM medium was added to resuspend the cell pellet at  $2.25\text{-}3.75 \times 10^6$  per ml and seeded into new 75 cm<sup>2</sup> flasks, typically being “split” 1:2 or 1:3 depending on the cell numbers. At passage 3, cells were stained with antibodies specific for CD11b, CD54, CD90.2 and CD106 to check their purity using flow cytometry as the expanded explant SF cultures should be >80-90% CD90.2+, >85% CD56+, >80% CD106+ and <1-2% CD11b+. The expected number of expanded cells from one mouse are  $\sim 5\text{-}10 \times 10^6$  cells. If more cells and/or higher levels of CD11b+ cells are observed, then the SFS were purified using magnetic beads to remove any macrophages and the resultant purity confirmed using FACs.

### ***2.3.3 Flow Cytometric analysis and cell sorting***

Single cell suspensions freshly isolated from the joints or SF populations obtained by explant culture were stained at 4°C with Zombie Violet (1:500 dilution BioLegend, 423113) and incubated at room temperature for 15 min to discriminate live and dead cells. FACs buffer (PBS + 0.5% FCS + 2mM EDTA) was then added to the suspension and the cells centrifuged for 5 min at 500 g. The pelleted cells were then washed three times with FACs buffer, centrifuged and resuspended at  $1 \times 10^5\text{-}10^6$  in 100µl of Fc block (Invitrogen, MFCR00-4) containing CD16/CD32-specific antibodies added to block cell-surface Fcγ receptors by incubation for 10 min at room temperature. The relevant directly conjugated primary antibodies or their corresponding isotypes (Table 2-1) were added to the FACs tubes and incubated for 30 min at 4°C, whilst being protected from the light. Cells were then washed with FACs buffer three times before being treated with the

appropriate secondary antibody/streptavidin-conjugated fluorophores. Non-stained control cells were also prepared. Again, cells were washed with FACs buffer (three times) and resuspended in 1 ml FACs buffer and their staining analysed using a BD LSR II flow cytometer (Flow core facility). Data were analysed via the software programme, FlowJo (version 10.8).

Single-cell synovial suspensions for sorting were obtained as described above (section 1.3.3) and SFs were purified using antibodies specific for stromal cells/SF markers such as CD45 (Biolegend, 103106), CD90 (Biolegend, 103106), podoplanin (PDPN) (Biolegend, 105316) and CD31 (Invitrogen, 12-0311-81) (Croft et al., 2019; Mizoguchi et al., 2018) with cell sorting being performed immediately after staining, using a FACS Aria III machine (GBRC Flow core facility). For sorted populations, purity was determined by reanalysis immediately post sorting and purity was found to be >99% for the SF target population (CD31<sup>-</sup>, CD45<sup>-</sup>, PDPN<sup>+</sup> (Figure 2-1). CD31 acted as a dump channel, whilst CD45 was used to eliminate both endothelial and immune populations from the gate in order to sort out the stromal cells. All antibodies were used at 1:100 dilution.

#### **2.3.4 Magnetic bead separation**

To remove contaminating myeloid cells (CD11b<sup>+</sup>) from *ex vivo* cultures, antibody-conjugated magnetic bead depletion was performed using Miltenyi Biotech bead technology. Cells were labelled with a CD11b-specific biotinylated antibody (BioLegend, B259438; 1-2  $\mu$ ls per  $1 \times 10^6$  cells) for 10 min, washed to remove unbound primary antibody by adding 1-2 mls of labelling buffer per  $10^7$  cells, centrifuged and the supernatant aspirated. The cell pellet was then resuspended in Miltenyi Biotech Labelling buffer ( $90 \mu$ l /  $10^7$ ) cells and 10  $\mu$ ls of Streptavidin-conjugated Microbeads added per  $10^7$  cells. The solution was mixed well and incubated for 15 min at 4°C. Cells were washed with 1-2 ml of FACs buffer per  $10^7$  cells, centrifuged, the supernatant aspirated, and cells resuspended in 500  $\mu$ l Miltenyi Biotech separation buffer. The later was then passed through magnetic separation columns which were then placed in the magnetic field of the suitable MACS separator (chosen based on number of total cells). The columns were initially rinsed with FACs buffer after which the cell suspension was added to the column, with the resulting magnetic retention of the macrophages allowing

collection of unlabelled, purified SF cells which were obtained by washing the columns three times with separation buffer. FACs analysis was carried out to ensure the collected cells were SFs, with purity typically >90%.

## **2.4 Preparation of Alvetex<sup>®</sup> scaffolds and cell seeding**

### ***2.4.1 Culture of SFs in Alvetex<sup>®</sup> inserts in a 6-well plate***

Alvetex<sup>®</sup> scaffolds (AMS Biotechnology (Europe) Lt, Abingdon) were rendered hydrophilic with 70% ethanol, by ensuring the entire surface of the scaffolds were washed. The ethanol was removed, and the scaffolds washed with PBS twice (for ~1 min) and aspirated. The scaffolds were then coated with fibronectin (RD System, 1030-FN) in PBS at a concentration of (0.5 mg/ml) and incubated at room temperature for 1 h in a well plate. The FN solution was then aspirated and replaced with complete DMEM medium. Scaffolds were then seeded with cells ( $1 \times 10^6$  cells per scaffold), with the cells dispensed at the centre of the scaffold and then incubated at 37°C with 5% CO<sub>2</sub> for 1-2 h to facilitate cell attachment (Figure 2-2). The cells were then gently flooded with medium to the desired level as well as in the well plate below and cells were then grown on the scaffold for 7 to 9 days, with the medium being changed every second day.

## **2.5 Preparation of FNPEG hydrogels**

### ***2.5.1 PEGylation of fibronectin (FN)***

#### **2.5.1.1 Denaturation of FN**

The required amount of Fibronectin (FN, YoProteins, 3 mg mL<sup>-1</sup>; usually 50 µg per 50 µl hydrogel) was pegylated. FN was denatured in 100 µl denaturing buffer (5 mM Tris(2-carboxyethyl)phosphine hydrochloride [TCEP, pH 7, Sigma] and 8 M urea [Fisher, 18 M stock] in phosphate buffer saline [PBS, Gibco, pH 7.4]) for 15 min at room temperature (Table 2-2).

#### **2.5.1.2 Protein PEGylation**

An appropriate amount of 4-arm-PEG-Maleimide (PEGMAL, 20 kDa, LaysanBio) was incubated for 30 min at room temperature at a molar ratio FN:PEGMAL 1:4 (usually 9 µg/50 µg FN). The tubes were then placed on a rotating platform (100 rpm) at

room temperature for 30 min. The reaction was stopped with 0.5  $\mu\text{l}$  NaOH (1M stock).

### **2.5.1.3 Protein alkylation**

After PEGylation, remaining non-reacted cysteine residues were blocked by alkylation using 14 mM iodoacetamide (IAA, Sigma) in PBS at pH 8 (on a rotating platform (100 rpm)) for 2 h at room temperature. The product of the reaction was dialysed using (Mini-A-Lyzer, MWCO 10 kDa, ThermoFisher) against PBS for 1 h at room temperature.

### **2.5.1.4 Protein Precipitation**

The protein solution was then precipitated using cold ethanol. Briefly, nine volumes of cold absolute ethanol were added to the protein solution and mixed well using a vortex mixer. The mixture was then incubated at  $-20^{\circ}\text{C}$  overnight and centrifuged at 15,000 g and  $4^{\circ}\text{C}$  for 15 min. The supernatant was discarded, and the protein pellet was further washed with 90% cold ethanol and centrifuged again at 15,000 g and  $4^{\circ}\text{C}$  for 5 min. Pellets were dried and solubilised using 8 M urea at a final protein concentration of  $2.5\text{ mg mL}^{-1}$ . Once the protein was dissolved, the solution was dialysed against PBS for 1 h and stored in the freezer.

## **2.5.2 Hydrogel formation**

PEG hydrogels were formed using the Michael-type addition reaction under physiological pH and temperature. Briefly, a final concentration of  $1\text{ mg mL}^{-1}$  of PEGylated FN was added to different amounts of PEGMAL weights (wt %) (3 wt %, 5 wt % or 10 wt %) to obtain the relevant stiffness of hydrogel required. Following this, the thiolated crosslinker was added, at a molar ratio 1:1 maleimide:thiol to ensure full crosslinking. The crosslinkers used were either PEG-dithiol (PEGSH, 2 kDa, Creative PEGWorks; for non-degradable gels) (Table 2-3) or mixtures of PEGSH and protease-degradable peptide, flanked by two cysteine residues (VPM peptide, GCRDVPMSMRGGDRCG, purity 96.9%, Mw 1696.96 Da, GenScript; for degradable gels) (Table 2-4). Once the crosslinker was added, samples were incubated for 1 h at  $37^{\circ}\text{C}$  to allow the gels to “cure”. All non-degradable gels

used in imaging experiments were 5 wt % PEGMAL as this is estimated to be close to the stiffness of a healthy synovium.

Although hydrogels containing PEGSH eventually degrade, in this thesis they will be referred to as non-degradable as they take many months to degrade, and the gels are used for cell studies no longer than 2 weeks. It is this stability that makes their use an appealing choice for kinetic studies. On the other hand, the addition of VPN in combination with PEGSH, significantly increases the hydrogel degradation time frame. Depending on the volume of VPM:PEGSH used the time for degradation can vary from 3 - 10 days, with the higher volume of VPM used, the quicker the hydrogel degrades.

## **2.6 Nanoindentation**

Hydrogels were prepared using different volumes of 4-Arm PEGmal, PEGdithiol and VPM (peptide) as shown in Table 2-3 to create hydrogels of differing stiffness. The gels were either cultured in media, with cells or PBS (without cells) with the stiffness of the gels measured at days 0, 3 and 7. Young's moduli of hydrogels were measured using a Chiaro Nanoindenter (Optics 11) and a probe with a spherical indenter tip with a radius of 2200 nm (Figure 2-3). The Chiaro nanoindenter uses this optical fiber sensor to gently push a spherical glass tip on the surface of the gel allowing a measurement of Young's moduli (Figure 2-4). Young's modulus was derived using the Hertz model to an indentation depth of 10% of the tip radius. Values are given as the mean of ~ 20 indentations and the standard deviation (SD).

## **2.7 Histology**

### ***2.7.1 Preparation of joint wax blocks***

Whole paws were harvested and fixed with 4% paraformaldehyde. They were then sent to the GBRC Histology Research Service (Veterinary Diagnostic services) to be processed to paraffin blocks and sent back, ready to be sectioned using a microtome.

### **2.7.2 Preparation of Alvetex<sup>®</sup> wax blocks**

After cells were cultured in the scaffold for the indicated time, the medium was aspirated from the scaffolds which were then washed carefully with PBS twice. The scaffolds were then removed from their inserts (using scissors or scalpel) and fixed using 4% PFA at 4°C for 12-24 h. The fixative was aspirated, and the scaffolds were washed three times with PBS and then the scaffolds were progressively dehydrated using a series 30%, 50%, 70%, 80%, 90% and 95% solutions of ethanol, each of which being incubated at room temperature for 15 min, and finally stored in 95% ethanol. Fully dehydrated scaffolds were achieved by placing them in 100% absolute ethanol for 30 min. The ethanol was then aspirated, and the scaffolds were inserted into labelled cassettes and into the paraffin processor (Leica Asap 300), where they were treated with HistoClear for 30 min, then a 50:50 solution of HistoClear and molten paraffin wax (60 °C) for 30 min and then with HistoClear:wax mix and incubated at 60°C for a further 60 min. The scaffolds were transferred to plastic embedding moulds and orientated into the required position and embedded in wax using the Thermo scientific Histostar. The wax was left to cool and set at room temperature for 1-2 h. Once hardened, the wax embedded block was removed from the plastic mould ready for sectioning.

### **2.7.3 Microtome sectioning: joint and Alvetex<sup>®</sup>**

Sections of 5 µm (Alvetex<sup>®</sup>) and 7 µm (paw) were cut using a microtome (Leica RM2125). The sections were then transferred to a slide water bath (40°C), floating them on the surface of the water to enable them to flatten out. Sections were then transferred to Superfrost Plus slides (Thermo, 4951PLUS4). They were left to dry overnight to ensure no water remained under the samples.

### **2.7.4 Cryostat sectioning: hydrogel**

After cells were cultured in the hydrogel for the indicated time, the hydrogels were fixed with 2 ml of 4% PFA for 30 min. The hydrogels were then dehydrated in 30% sucrose solution (3 g sucrose + 10 ml PBS) overnight at 4°C. They were then placed in moulds filled with OCT, ensuring the entire gel was covered and there were no bubbles visible. The moulds were then placed immediately at -80°C

overnight prior to cutting sections at 20 µm on the cryostat, which following slide attachment were stored at -20°C.

### ***2.7.5 Histology: Haematoxylin and Eosin (H&E) staining***

For staining of frozen section such as hydrogels, the slides were removed from the freezer and wrapped in foil for 20 min at room temperature, then left unwrapped for a further 10 min. The samples were fixed in ice-cold acetone/ethanol (75%/25%) for 10 min, then left to air dry for a further 10 min. The slides were washed under running water prior to staining. Paraffin sections (joint and Alvetex®) were heated in an oven for 35 min at 60°C, after which they were placed in xylene to dewax and hydrated through a graded series of ethanol (100%, 90%, 70%; 6 min incubations of each) solution and then washed under running water.

The sections/slides were then placed in Harris Haematoxylin for 3 min (twice) and then washed under running water to remove excess staining. Haematoxylin is a violet/purple stain that binds to basophilic substances such as DNA, allowing nuclei to be seen under the microscope in purple. To reduce background colour, the sections were dipped in 1% Acid/Alcohol for a few seconds, quickly rinsed under running water, dipped in Scott's Tap Water Substitute and then again quickly rinsed under running water. Following this, counter-staining was carried out in which the sections were placed in 70% ethanol and then 1% Eosin for a few min. Eosin is a red stain that binds to acidophilic substances such as cytoplasm, red blood cells and collagen. Sections were then dehydrated in 90% and 100% ethanol and 100% xylene. Coverslips were mounted over tissue sections with DPX mountant and left to dry overnight. Imaging of hydrogel cryosections and/or joints/Alvetex® microtome sections was performed on an EVOS brightfield microscope at x10 magnification.

## **2.8 Immunohistochemistry and fluorescent microscopy**

### ***2.8.1 Alvetex® and joint sections***

The paraffin embedded sections were heated for 35 min at 60°C, after which they were placed in xylene to dewax and hydrated through a graded series of ethanol (100%, 90%, 70%, with 6-min incubations of each) solutions. Slides were placed in

antigen retrieval buffer (pH 6) and microwaved at 800 W, covered in tinfoil and incubated at room temperature for 20 min. The sections were then washed with 0.05% PBS Tween (PBS-T) twice and then blocked using PBS 10% FBS for 30 min at room temperature. Sections to be stained using biotinylated antibodies were treated by blocking endogenous biotin (Molecular probes kit, Cat: SP-2002) prior to staining with the relevant antibodies (Table 2-5). For blocking, sections were incubated with streptavidin solution for 15 min at room temperature, then briefly rinsed with PBS-T before being incubated for 15 min at room temperature with biotin solution. Primary antibodies (in PBS 0.3% Triton x-100 with 1% BSA) were added overnight at 4°C. Samples were washed and then incubated with the appropriate secondary antibody/streptavidin-conjugated fluorophores or relevant control antibody isotypes for 1 h at room temperature in the dark. They were then rinsed three times with PBS and samples were mounted with Slow-Fade diamond mounting media with DAPI (Vectashield). Images of Alvetex<sup>®</sup> and joint sections were obtained on the EVOS brightfield microscope. Quantification of cells within the Alvetex<sup>®</sup> scaffold and the intensities of fluorescent subset markers (VCAM1 (lining) and CD90 (sublining)) of SFs were determined manually.

### ***2.8.2 Imaging of full hydrogels***

For imaging of whole hydrogels (as opposed to cryosections), the hydrogels were removed from their inserts and fixed with 4% PFA for 30 min at room temperature prior to staining. Permeabilisation of the cells (for both cryosections and whole hydrogels) was carried out for 15 min at room temperature using 0.1% Triton. followed by washing once with PBS. The hydrogels were then treated with PBS containing 1% BSA for 30-60 min at room temperature, after which the primary antibody was added (Table 2-5) and left overnight at 4°C. The following day the samples were treated with the appropriate secondary antibody (Table 2-5) or streptavidin-conjugated fluorophores for 1 h at room temperature. The samples were washed with PBS containing 0.5% Tween20 and mounted onto a glass bottom petri dishes using Vectashield slow fade mounting media containing DAPI (VectorLabs). Scanning and imaging of entire hydrogels was carried out on a Leica DM8 widefield microscope using LAS X Life Science software at a magnification of x10. The hydrogels were imaged in a tilescan format with z-steps of ~10 µm to

obtain stacked images, which were then merged together to form a detailed representative image of the cells within the hydrogel. The image was then deconvoluted using Huygens essential after which it was processed using IMARIS (“Cell biologist package”) to obtain 3D reconstructions of the gel and investigate parameters such as volume, area, sphericity, intensity and location of each cell.

## 2.9 ELISA

Cytokine secretion was measured using the relevant ELISA kits as instructed by the manufacturers. Typically, cells were seeded in 96-well plates (Corning) at  $1 \times 10^4$  cells per well in DMEM medium containing 10% FCS, incubated overnight and then stimulated for 24 h with IL-1 $\beta$  (10 ng/ml, Immunotools) or IL-17 (25 ng/ml, Immunotools). The supernatants were collected and analysed for secretion of Interleukin 6 (IL-6) and Monocyte Chemoattractant Protein-1 (MCP-1/CCL2) (Ready- SET-GO!® from eBioScience). Briefly, the plates were coated overnight at 4°C with the relevant capture antibody. Following blocking for 1 h, the samples or standards were added, and plates incubated overnight at 4°C. The samples were then washed and incubated with detection antibody for a further hour and then streptavidin-conjugated horseradish peroxidase was added for 30 min at room temperature. The 96-well plates were then washed for a final time with PBS-T, before being incubated with TMB substrate. After the colour developed from blue to yellow, the stop solution (1M H<sub>2</sub>SO<sub>4</sub>) was added. Absorbance for each well was read at 450 nm using a Tecan Sunrise plate reader.

## 2.10 RT-PCR

### 2.10.1 RNA extraction

#### 2.10.1.1 RNA extraction from SFs freshly isolated from the joint or cultured in 2D

Cells taken directly from the paws of Naïve and CIA mice were sorted using FACS (section 1.3.4) to isolate a purified population of SFs prior to RNA extraction whilst for 2D cultures, following checking of purity, the required SFs were harvested. RNA lysis (RLT) Buffer (350  $\mu$ l) was added to pelleted SFs (maximum of  $5 \times 10^5$  cells/sample). The lysate was homogenised by passing the solution through a 20-gauge needle 10 times using a sterile plastic syringe. Equal volumes of 70% ethanol

were added to the homogenised lysates and pipetted up and down 10 times to ensure the solution was completely mixed. Samples were transferred to RNeasy MinElute spin columns in 2 ml collection tubes, then centrifuged for 15 sec at 8000 g. Following discarding of the flow-throughs, Buffer RW1 (350 $\mu$ l) was added and the samples were centrifuged for 15 sec at 8000 g to wash membrane bound RNA. The flow-throughs were again discarded and DNase I reagent (10  $\mu$ l DNase I stock solution mixed with 70  $\mu$ l Buffer RDD) was added to the column membranes and incubated at room temperature for 15 min. The Buffer RDD not only ensures that RNA remains bound to the column but also provides an efficient on-column digestion of DNA. Buffer RW1 (350  $\mu$ l) was then added to the columns, and the tubes micro-centrifuged for 15 sec at 8000 g and the flow throughs discarded. The RNeasy MinElute spin columns were then placed in fresh 2 ml collection tubes and Buffer RPE (500  $\mu$ l) added (ensuring it was diluted with ethanol according to manufacturer's instructions) to wash the membrane bound RNA, after which the tubes were micro-centrifuged for 15 sec at 8000 g and the flow-throughs discarded. Ethanol (80%; 500  $\mu$ l) was then added to the RNeasy MinElute spin columns and following micro-centrifugation for 2 min at 8000 g, the collection tube was discarded. The RNeasy MinElute spin columns were again placed in fresh 2 ml collection tubes, the caps were left open, and centrifuged at full speed (>10000 g) for 5 min to dry the membrane. The flow-throughs and the collection tubes were discarded, and the RNeasy MinElute spin columns placed in fresh 1.5 ml collection tubes and 14  $\mu$ l of RNase-free water added directly to the centre of the spin column membrane. The lid was closed gently, and the tubes centrifuged for 1 min at full speed to elute the RNA. RNA concentrations were determined by nanodrop, with a typical reading of 100-140 ng/ $\mu$ l.

#### **2.10.1.2 RNA extraction from cells cultured in Alvetex<sup>®</sup>**

The Alvetex<sup>®</sup> scaffold cultures were gently washed in PBS and transferred to clean plates. Cells were lysed by adding 600  $\mu$ l Qiagen RNeasy<sup>®</sup> kit lysis buffer RLT per well, and then the plates were placed on a rotating platform (100 rpm) for 10 min at room temperature. The lysate was homogenised by passing the solution through a 20-gauge needle 10 times using a sterile plastic syringe. RNA was extracted using Qiagen kit, as per manufacture instructions as mentioned previously (1.10.1.1).

RNA concentrations were determined using nanodrop, with a typical reading of 20-30 ng/ $\mu$ l.

### **2.10.1.3 RNA extraction from cells cultured in Hydrogels**

Initially the hydrogels were made with 1:1 VPM:PEGSH, to allow the hydrogels to degrade over the period of 1 week, after which RNA would be extracted. However, this resulted in poor quality RNA that was not suitable for RNA-Seq. Following comprehensive optimisation trials, this was found to be due to the addition of the PEGSH, which interfered with the degradation of the gel for RNA extraction. Therefore, the degradable hydrogels were made with 100% VPM resulting in the degradation of the gel after 3 days and a better quality of extracted RNA.

The hydrogels were removed from their inserts and placed in tubes with an equal volume of 2.5 mg/ml collagenase in PBS and incubated at 37°C for 90 min, gently pipetting samples slowly every 30 min to help release cells from the degrading gel. Following incubation, the samples were pipetted vigorously and passed through 100  $\mu$ m cell strainers into tubes and then centrifuged at 500 g for 10 min at 4°C, to obtain cell pellets and ensure that any pieces of non-degraded gel were removed. RNA was extracted using Qiagen kit, as per manufacture instructions as mentioned previously (1.10.1.1). RNA concentrations were determined using nanodrop, with a typical reading of 5-10 ng/ $\mu$ l.

### **2.10.2 cDNA synthesis**

cDNA was synthesized using the High-Capacity cDNA reverse transcription kit (Applied Bio- systems, Life Technology, UK) and KiCqStart® qPCR Ready Mix (Sigma-Aldrich), converting 100 ng RNA per reaction and assuming the reaction achieved completion, creating 100 ng cDNA. Briefly, RNA samples were diluted to 10 ng/ $\mu$ l and 10  $\mu$ l added to a reaction mix containing reverse transcriptase, dNTPs, RNase inhibitor and random primers as per manufacturer's instructions. Samples were incubated at 25°C for 10 min, followed by 37°C for 2 h and then 95°C for 5 min to inactivate the enzyme. cDNA was diluted to 2 ng/ $\mu$ l using nuclease free water and the cDNA samples were stored at -20°C, prior to quantitative PCR.

### **2.10.3 PCR**

Transcripts were analysed by qPCR in duplicate in either 96- or 384- well plate formats. Depending on the plate used, a master mix was made of the following: Taqman probes 20x (0.5/0.25  $\mu$ l), 2x reaction buffer (5/2.5  $\mu$ l), cDNA (enough for 10 ng) and dH<sub>2</sub>O (enough for 10/5  $\mu$ l total). Plates were run on Applied Biosystems StepOne Plus™ real-time PCR system. Cycling conditions were as follows: 20 seconds at 95°C, then 40 cycles of denaturation at 95°C for 3 seconds and annealing at 60°C for 20-30 seconds. Data were normalised to the reference gene  $\beta$ -actin to obtain the  $\Delta$ CT values that were used to calculate the fold change from the  $\Delta\Delta$ CT values following normalisation to biological control group.

### **2.10.4 RNA-Seq analysis**

RNA integrity was checked using the Agilent 2100 Bioanalyzer System and all purified RNA samples had a RIN value >9. For 2D and Alvetex® samples the libraries were prepared using the TruSeq mRNA stranded library preparation method, this kit prepares a library that when sequenced represents the reverse/negative strand, furthermore it uses the standard TruSeq adapters for the library. However, for FNPEG hydrogels the libraries were prepared using the NEBNext Single Cell-Low Input RNA Library Prep Kit for Illumina. Samples were sequenced 2  $\times$  75 bp to an average of more than 30 million reads. All RNA-Seq reads were then aligned to the mouse reference genome (GRCM38) using Hisat2 version 2.1.0, and featurecounts version 1.4.6 was used to quantify reads counts using the [Galaxy portal](#) at the University of Glasgow. Data quality control, non-expressed gene filtering, median ratio normalization (MRN) implemented in DESeq2 package, and identification of differentially expressed (DE) genes was done using the R Bioconductor project [DEbrowser](#) (Kucukural et al., 2019). Genes that passed a threshold of  $p_{adj} < 0.01$  and  $\log_2$ foldChange > 2 in DE analysis were considered for further analysis. Gene Ontology (GO) enrichment, KEGG pathway enrichment, and UniProt Keywords enrichment were performed in String version 11.0 (<https://string-db.org>) based on statistically significant DE genes.

## 2.11 Statistical analysis

All statistical analyses performed were carried out using GraphPad Prism software (version 8.9). Normalisation and standardisation of data was carried out when applicable using GraphPad Prism software. For graphs in which normal distribution of data was assumed 'robust estimation' was used to draw random repeated samples from the data, using the mean to obtain the estimate of variance, allowing for the using of parametric statistics. Data represented as mean  $\pm$  standard deviation (SD) of technical replicates, or biological replicates when indicated and SEM for individual mice/pooled experiments. For comparing 2 groups, a variable for more than 2 groups and two variables for more than 2 groups the parametric statistics Student t test, one-way ANOVA and two-way ANOVA with Tukey's multiple comparison correction were performed, respectively. P values shown as:

\* $p < 0.05$  or #  $p < 0.05$  or <sup>â</sup>  $p < 0.05$

\*\*  $p < 0.01$  or ##  $p < 0.01$  or <sup>ââ</sup>  $p < 0.01$

\*\*\*  $p < 0.001$  or ###  $p < 0.001$  or ####  $p < 0.0001$

\*\*\*\*  $p < 0.0001$  or <sup>âââ</sup>  $p < 0.001$  or <sup>ââââ</sup>  $p < 0.0001$

Differing symbols were used when multiple comparisons were made in an individual experiment.

**Table 2-1: Antibodies to determine SFs (1:100 FACs buffer) Antibodies to determine SFs (1:100 FACs buffer)**

<b>Antibody</b>	<b>Ref</b>
CD45	BioLegend: 103106
CD90	BioLegend: 328109
Podoplanin	BioLegend: 105316
CD31	Invitrogen, 12-0311-81

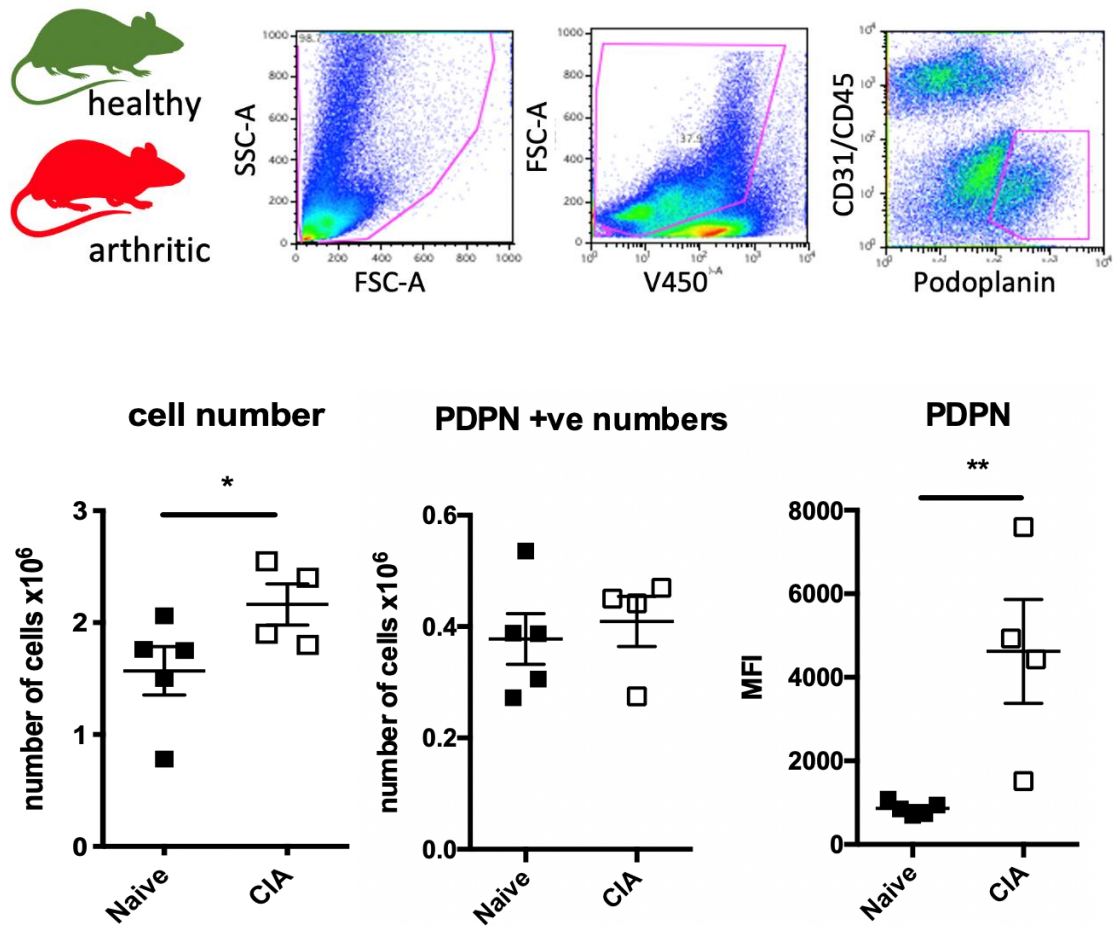


**Figure 2-1: Identifying SF population using FACs.**

Cells were isolated from the synovium of healthy and CIA mice following collagen digestion of the tissue. Live synovial fibroblasts were sorted based on the expression of surface markers (Podoplanin<sup>+</sup>, CD45<sup>-</sup>, CD31<sup>-</sup>) detected by specific antibody staining as shown in dot plots. SFs were subsequently isolated by Flow cytometry sorting. The number of isolated cells, PDPN<sup>+</sup>, and expression of PDPN are shown. Data are presented as mean  $\pm$  SEM. Naive  $n = 5$ , arthritic  $n = 4$ . Statistical significance was calculated using a one-tail unpaired  $t$ -test, \* $p < 0.05$  and \*\* $p < 0.01$ .

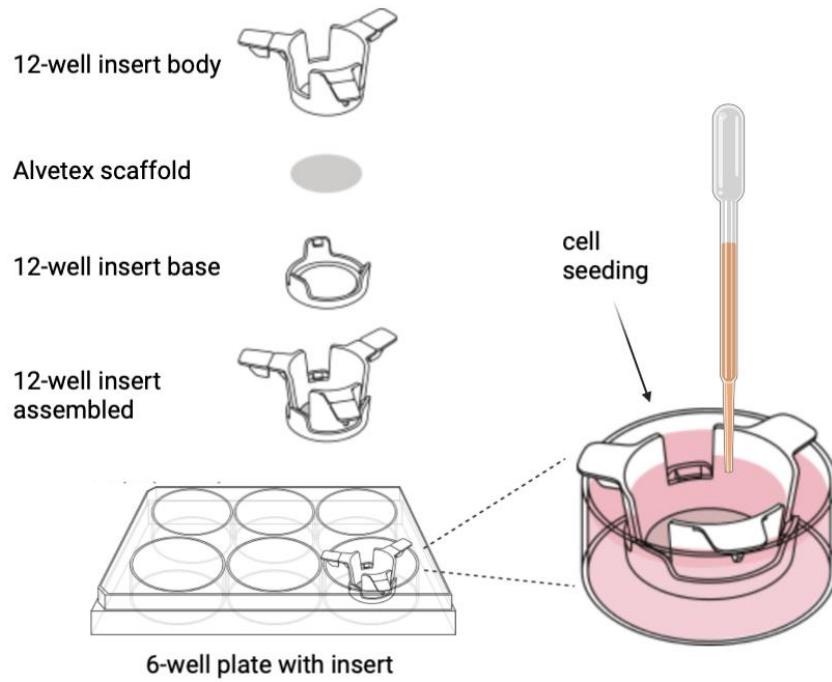


**Figure 2-2: Schematic of Alvetex® inserts and seeding.**

Alvetex® (Reprocell Code: AVP004/AVP005) supports are made of two main components, the polystyrene 3D scaffold where cells grow and a plastic insert to hold the disc into plate wells. SFs are first seeded onto the insert that is placed into a well-plate prior, allowing cells to attach to the scaffold for 90 minutes. Media is subsequently added to the well covering the scaffold containing the cells. Adapted from (Alvetex® Strata Biortrend, 2021) with BioRender.com

**Table 2-2: Components and volumes for the PEGylation of Fibronectin for hydrogel formation**

<b>Component</b>	<b>Volume</b>
Fibronectin (3 mg/ml)	16.6 $\mu$ l
0.5 M tris(2-carboxyethyl)phosphine (TCEP)	1 $\mu$ l
8 M urea	44.4 $\mu$ l
PBS	38 $\mu$ l
<b>Total</b>	<b>100 <math>\mu</math>l</b>

**Table 2-3: Components and volumes required for the formation of non-degradable Fibronectin PEGylated hydrogels**

<b>Component</b>	<b>Volume Per gel</b>
Fibronectin (made in PEGylation of fibronectin mentioned in Table 2-2)	20 $\mu$ l of 2.5 mg/ml
4-arm Peg maleimide (4-PEG-MAL)	8 $\mu$ l of 250 mg/ml
Poly (ethylene glycol)dithiol (PEGdithiol)	4.1 $\mu$ l of 100 mg/ml
Cells in PBS or media without cysteines	17.9 $\mu$ l (50,000 cells per gel)
<b>Total</b>	<b>50 <math>\mu</math>l</b>

**Table 2-4: Components and volumes required for degradable Fibronectin PEGylated hydrogel synthesis. Different weights (wt %) were used to obtain hydrogels of different stiffnesses.**

Component	Stock conc.	3 wt %	5 wt %	10 wt %
FN	2.5 mg/ml	20 $\mu$ l	20 $\mu$ l	20 $\mu$ l
4-arm Peg maleimide (4-PEG-MAL)	250 mg/ml	5 $\mu$ l	8 $\mu$ l	16.6 $\mu$ l
Poly (ethylene glycol)dithiol (PEGdithiol)	100 mg/ml	1.25 $\mu$ l	2.05 $\mu$ l	4 $\mu$ l
VPM crosslinking peptide	100 mg/ml	1.25 $\mu$ l	2.0 5 $\mu$ l	4 $\mu$ l
Cells in PBS	N/A	5.4 $\mu$ l	5.4 $\mu$ l	5.4 $\mu$ l
PBS	1XPBS	17.1 $\mu$ l	12.5 $\mu$ l	N/A

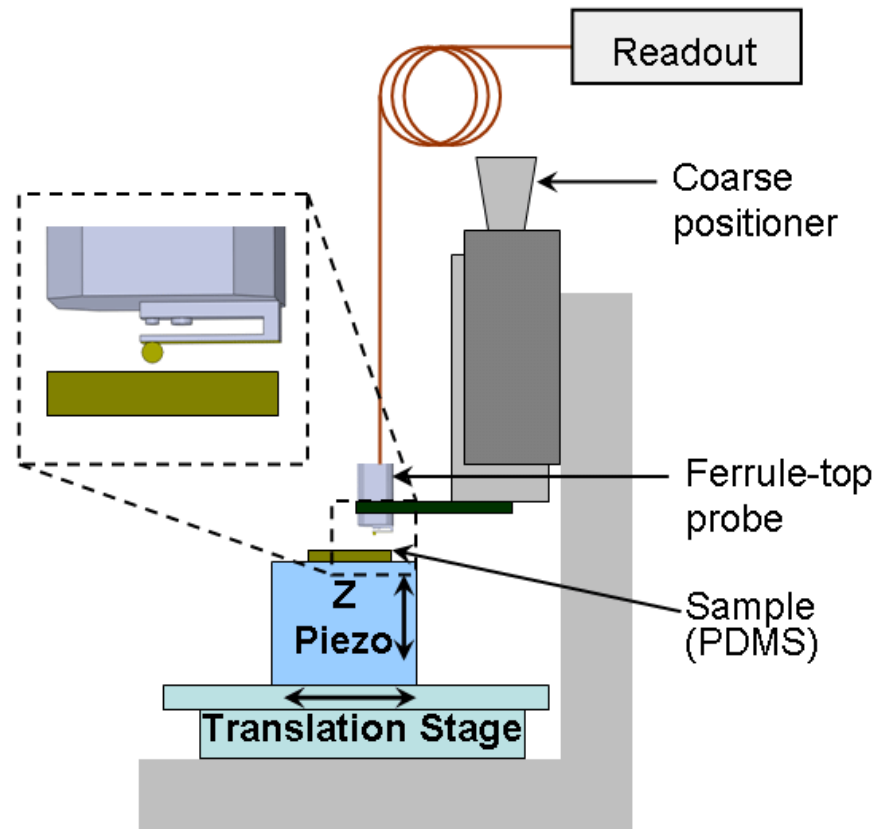
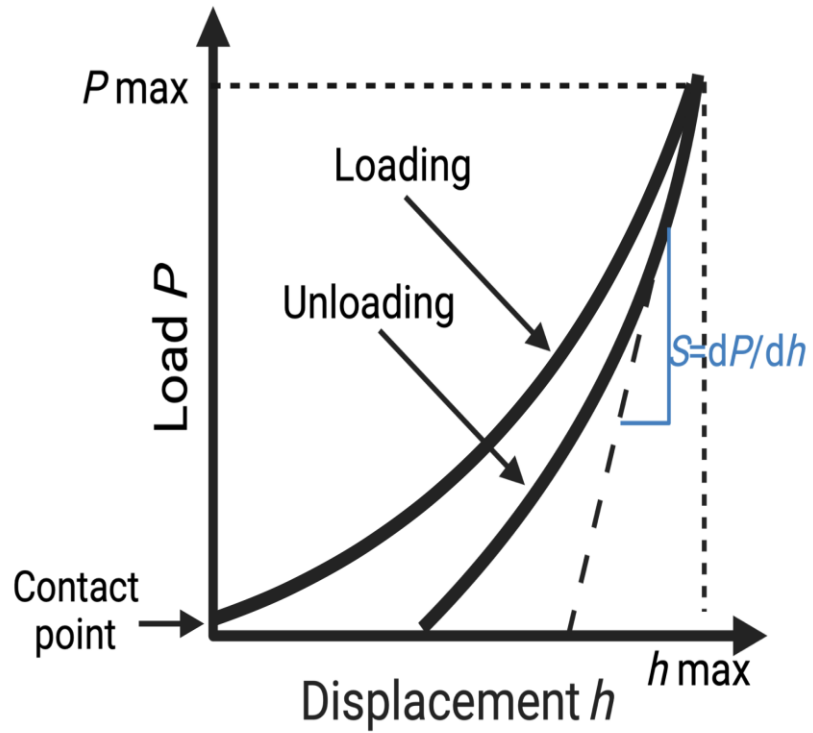


Figure 2-3: Schematic view of the ferrule-top nanoindenter setup (Chavan et al., 2012)



**Figure 2-4: Schematic representation of load vs depth graph from nanoindentation.**  
Adapted from (Hu, Farahikia and Delfanian, 2014) and created with BioRender.com

Table 2-5: Primary, secondary antibodies and isotypes with dilutions

Primary Antibody	Dilution	Ref
Vimentin	1:200	Sigma 058M4885V
VCAM1	1:50	Affbiotech: 25W0785
Biotin anti-mouse CD90.2	1:50	BioLegend: B147729
Secondary Antibody	Dilution	Ref
Chicken anti-goat AF647 IgG(H+L)	1:200	Invitrogen: 1882197
Goat anti-rabbit AF647 IgG(H+L)	1:200	Invitrogen: A27040
Streptavidin 647	1:200	Invitrogen: 1893503
Isotype	Dilution	Ref
Goat Isotype Ctrl	1:200	ThermoFisher: 31245
Normal rabbit IgG non-conjugated	1:100	Santa cruz biotech: J1609
Biotin rat IgG2a k Iso Ctrl	1:100	BioLegend: B196171

# Chapter 3 Characterisation of Naïve SFs and pathogenic SFs from CIA mice using conventional 2D cell cultures

## 3.1 Introduction

### 3.1.1 *Collagen Induced Arthritis (CIA)*

In human studies, the required tissues may not always be available or ethically obtainable and therefore, experimental animal models are crucial for investigating the pathways and mechanisms leading to disease as well as those contributing to its perpetuation. While no animal model can perfectly recapitulate the human condition, a range of generally easily reproducible animal models of RA have been developed to advance our understanding of this disease and also provide pre-clinical experimental models for potential therapeutic and diagnostic targets to be identified and validated, particularly following the availability of genetically modified animals (Kannan, Ortmann and Kimpel, 2005).

Thus, as for many other conditions, animal models act as an alternative to recapitulate various aspects of RA disease (Asquith, Miller, McInnes and Liew, 2009; Caplazi et al., 2015) but of the various animal models used in RA research (Table 3-1) the collagen-induced arthritis (CIA) model used in this thesis is one of the most commonly used and is considered the gold standard as it mirrors various autoimmune and inflammatory arthritis aspects of RA. CIA is associated with the production of collagen-specific autoantibodies as well as chronic inflammation leading to the development of an acute asymmetric polyarthritis, characterised by the synovial hyperplasia and infiltration, cartilage degradation as well as bone erosion that is seen in human RA (Williams, 2004). Autoimmune arthritis is induced in this model by immunization with an emulsion of complete Freund's adjuvant and type II collagen (CII), with the anti-type II collagen IgG antibodies generated mimicking the autoantibody production against self-type II collagen, as well as reacting to citrullinated proteins and IgG such as rheumatoid factor (RF), seen in RA patients. Also as seen in RA, pro-inflammatory cytokines such as TNF- $\alpha$  and IL-1 $\beta$  are highly expressed in arthritic joints of CIA mice and inhibition of these cytokines leads to a reduction in the severity of RA, giving further weight to the

importance of this specific model (Brand, Latham and Rosloniec, 2007). The most commonly used mouse strain used for the CIA model is DBA/1, as they exhibit a high incidence/high severity of pathology especially when compared to C57BL/6 mice, which are generally considered resistant to CIA and display low severity of disease. However, to study the effect of genetic modification on the development of RA, C57BL/6 mice are generally used as targeted gene deletion has been problematic in DBA/1 mice (Rajaiah and Moudgil, 2009; Luross and William, 2011).

The CIA model has not only aided in our understanding of RA pathogenesis but has proven to be a suitable model for testing not only anti-inflammatory but also analgesic drugs for potential use in RA (Inglis et al., 2007). CIA models have allowed analysis of articular tissues at earlier disease stages, showing irregularities within the synovium, including the deposition of fibrin in the joints as well as hyperplasia of the synovial lining observed prior to clinical arthritis. Moreover, exploration of the synovial tissue of mice immunised with type II collagen and CFA 10 days prior to clinical proof of joint swelling or tenderness appeared to show hyperplasia of the lining, mesenchymal-appearing cells as well as vasodilation. However, no infiltration of lymphocytes or leukocytes was observed. Supporting cellular activation in the earliest stage of murine CIA model, the activated form of NF- $\kappa$ B was detected in the synovial lining cells 10 days prior to joint swelling (Bustamante, Garcia-Carbonell, Whisenant and Guma, 2017). Furthermore, the CIA murine models have also shown similar SF hyper-responses akin to those observed in RA, with CIA-SFs displaying enhanced cytokine production relative to their Naïve counterparts, *ex vivo* (Pineda et al. 2014), suggesting they can be exploited for dissection of SF pathogenesis. For example, administration of rIL-22 to mouse paws during the initial stages of CIA leads to an enhanced basal and IL-17-stimulated IL-6 response by the SFs *ex vivo* (Pineda et al., 2014), suggesting that the responses seen in RA-SFs can be experimentally mimicked, at least in part by CIA-SFs. Consistent with this idea, another study showed that IL-22 promotes osteoclast differentiation from human monocytes through RANKL production by SFs *in vitro*, findings consistent with the RA literature (Miyazaki et al., 2018). Moreover, and consistent with the induction of a stable hyper-responsive SF phenotype in RA, murine studies carried out by Corbet et al, showed that CIA-SFs cultured for 3-4 passages *ex vivo* displayed

hypomethylated global DNA compared to Naïve SFs, and this could be mimicked *in vitro* through chronic cytokine (IL-17 and IL-1 $\beta$ ) stimulation of Naïve SFs for 14 days. The Global DNA hypomethylation correlated with a reduction of DNA methyltransferase-1 (DNMT1) expression, which was also found to be down regulated in CIA-SFs. These “rewired” cells have been found to display increased levels of MMP9 and MMP13 in the presence and absence of IL-17 stimulation and the joint destruction observed in the CIA mice was found to be associated with elevated levels of hypoxia in cells in the joint, as well as induction of vascular leakage (Corbet et al., 2020). The latter knowledge has been gained using 2D culture systems and have proved valuable in developing our understanding of RA-SF responses, including that of their epigenetic rewiring to a “transformed” pathogenic phenotype.

### ***3.1.2 Conventional 2D culture of expanded SFs ex vivo***

Understanding the mechanisms underlying the function and pathology of cells, tissue and organs as well as disease mechanisms and drug discovery (Greenman et al., 2007) became increasingly feasible due to the development of animal models and culture systems (Yamada and Cukierman, 2007; W Jacoby, I Pasten, 1979). However, rather than a “one-size fits all” approach, choosing the best and most appropriate cell culture methods for modelling particular diseases may allow a better understanding of their biology and, in turn, aid in the development of better treatment options (Aggarwal, Danda, Gupta and Gehlot, 2009).

Until recently, cell culture of mammalian adherent cells generally involved growing monolayers of cells attached to a flat and rigid two-dimensional (2D) substrate such as glass or plastic (polystyrene). It is important to note that despite the cells being described as grown on ‘plastic’ 2D culture systems, the cell themselves do not have receptors for polymers such as plastic. Therefore, they are unable to interact with the synthetic substrate unless coated with an adhesive protein/peptide (Lerman et al., 2018). Conventional 2D culture systems are generally treated with a polymeric protein/polypeptide allowing a positive charge, causing the negatively charged cells to be attracted. Furthermore, cells also secrete ECM to allow for better adhesion to the culture surfaces *in vitro* (Cooke et al., 2008). Such cultures have provided a commonly used and easy

way to conduct *in vitro* research as they allow for high performance, reproducibility, long term culture and the performance of functional tests. Furthermore, the assay components are (relatively) cheap and commercially available. However, 2D adherent cell cultures may not recapitulate the key conditions of *in vivo* responses as they introduce artificial pressures and tensions, which may subsequently alter cellular processes that are dependent on spatiality, e.g., invasion and replication, as well as affecting how they respond to different stimulus and treatments (Danielson, Perez, Romano and Coppens, 2018). However, even with 2D systems, modifications that attempt to address the physiological microenvironment can be made, for example, through the addition and coating of ECM component(s) in order to develop a better understanding of the cell-ECM interactions.

### ***3.1.3 Integrins and Fibronectin in synovial tissue***

Synovial fibroblasts show elevated expression of integrins in RA, as well as upregulated levels of ligands such as Fibronectin (FN) and collagen. The resulting overstimulation of cells via integrin mediated signals results in the increased basal secretion of pro-inflammatory cytokines such as IL-6 and IL-8 as well as MMPs. All cells within the synovial tissue express a specific subset of integrins dependent on their origin and lineage. Thus, SFs, lymphocytes, macrophages and endothelial cells all express the integrin subunit  $\beta 1$  (Lowin et al., 2009). The FN receptor  $\alpha 5\beta 1$  and laminin receptor  $\alpha 3\beta 1$  is expressed on all synovial cells, whilst  $\alpha 4\beta 1$ , which aside from FN also binds VCAM1, was found to be expressed by lymphocytes. Regarding the synovial tissue, integrin expression is also dependent on the anatomical location of the cell in question, with the expression of the majority of integrins similar throughout the synovial tissue apart from in the synovial lining layer where activated SFs and macrophages degrade the ECM and invade the cartilage. Interestingly, therefore, the laminin receptor  $\alpha 6\beta 1$  is expressed by SFs, but not macrophages, in the lining layer and these cells also generally express upregulated levels of  $\alpha 5$  and  $\beta 1$  integrins when compared to SFs of the sublining area, suggesting that increased integrin expression is associated with a more “aggressive” phenotype of SFs (Lowin and Straub, 2011).

FN is an ECM component that plays a key role in communication between intracellular and extracellular environments as evidenced by its significant effect on cell behaviour following binding of integrin receptors on the surface of cells (Pearson, Klebe, Boyan and Moskowicz, 1988). It is an adhesive glycoprotein, widely distributed in ECM that acts to regulate adhesion, migration, differentiation as well as morphogenesis and wound healing as it is a crucial cell-adhesive ECM protein, found in injured tissues undergoing regeneration (Pankov and Yamada, 2002). SFs express  $\alpha_5\beta_1$  and  $\alpha_v\beta_3$  and these integrins are vital for the binding of FN (Parisi, 2007; Bachman, Nicosia, Dysart and Barker, 2015; Lowin et al., 2009) that plays a role in guiding fibroblast migration to the pannus (Shiozawa, Shiozawa, Shimizu and Fujita, 1984; Toffoli et al., 2020). These SF-ECM interactions also modulate MMP production (Nuttelman, Mortisen, Henry and Anseth, 2001) as well as mediating the SF adhesion to cartilage and stabilisation of invadopodia, dynamic actin-rich membrane protrusions that degrade the ECM via local deposition of proteases and are involved in cell invasion (Jin, Xu and Hereld, 2008). ECM components such as FN also bind growth factors, actively increasing RA-SF attraction and adhesion to the cartilage (Schultz, 2018).

### 3.2 Aims and Objectives

The core aim of this chapter was to characterise the responses of Naïve and pathogenic SFs derived from the mouse CIA model of RA, not only to confirm the reported hyper-responsiveness of CIA SFs, but also to further explore the stability of this transformed phenotype and provide a “reference” profile of responses for comparison with those obtained following subsequent culture in 3D (Alvetex® and hydrogel) platforms. The key specific aims of this chapter are to:

- Characterise the inflammatory cytokine responses of Naïve and CIA SFs and hence further explore the stability of the hyper-responsive phenotype of CIA-SFs in 2D cultures
- Test the effects of FN on these responses to determine whether incorporation of features associated with SF interaction with the ECM modulates the nature/stability of the responses of Naïve and CIA-SFs
- To investigate whether SF subpopulations can be identified and maintained in 2D cultures

### **3.3 Results**

#### ***3.3.1 Histological characterisation of CIA and visualisation of SFs within the synovial joint***

To validate the characterisation of healthy and pathogenic SFs, paws from Naïve and CIA mice were harvested, sectioned and histopathological (H&E staining) was carried out (Figure 3-1A). Analysis showed cell infiltration and pannus formation in CIA, but not Naïve, joints with increasing numbers of cells in the synovial membrane encroaching into the joint space as well as the cartilage destruction also characteristic of RA (Sudoł-Szopińska et al., 2012).

Following histopathological analysis of joint disease in CIA, SFs were visualised within the synovial joint (Figure 3-1B), by immunofluorescence staining for the stromal cell marker, vimentin [also known as a fibroblast intermediate filament] as this is the major intermediate filament found in non-muscle cells, and generation of vimentin fragments are upregulated in RA-SFs (Vasko et al., 2016). Thus, this marker has been used throughout the thesis to show that cultured cells are from stromal origin, and that only the SFs have expanded as there is no direct marker for SFs.

Sections of Naïve and CIA mice knee joints were therefore stained with an antibody specific for vimentin (or an isotype control), counterstained with the nuclear stain, DAPI) and imaged using a confocal microscope. It can be seen from Figure 3-1B that the synovial cells are clearly stained with the marker within the synovial lining of the synovium, while cells in the sections treated by the isotype control antibody are not. Consistent with the onset of joint pathology, the layer of synovial lining cells in the CIA sample appears to be thicker indicating pannus development.

#### ***3.3.2 SF viability and pro-inflammatory responses of CIA-SFs***

Having established that the SFs within the CIA joint exhibit characteristics observed in RA, it was next investigated whether explant cultures of these cells from CIA mice retained a hyper-responsive “pathogenic” phenotype relative to those from naïve mice, when cultured on traditional 2D platforms, as a

consequence of epigenetic changes occurred *in vivo*. Firstly, as patients with RA exhibit elevated levels of pro-inflammatory cytokines present within the synovial joint, the spontaneous release of two proinflammatory mediators found to be present in the RA synovium (Caiello et al., 2014) namely, CCL2 (Figure 3-2A) and IL-6 (Figure 3-2B) was determined. In addition, their responsiveness to further inflammatory cues was investigated by stimulation of the SFs by the pathogenic cytokine, IL-17 (Robert and Miossec, 2019), which promotes IL-6 and IL-8 release by RA-SFs (Hwang et al., 2004). This revealed that the CIA-SFs exhibited more pro-inflammatory responses than their Naïve counterparts, both in terms of basal and IL-17-stimulated release. Importantly, these data confirmed that the hyper-responsive CIA phenotype is stable and maintained for 4 passages of culture in 2D platforms.

Having established that CIA-SFs cultured in 2D exhibit enhanced pro-inflammatory responses relative to Naïve SFs, the viability of SFs cultured in 2D was then investigated using Live and Dead staining and imaged using fluorescence microscopy (Figure 3-3A). Following culture for 4 passages both Naïve and CIA SFs exhibited ~90% live cells. This indicates the cells can grow and survive effectively in culture even after being removed from their physiological joint environment. Next, the morphology of the SFs was examined, using H&E staining to observe cell shape (Figure 3-3B) and this was examined in the presence and absence of FN to examine the impact of SF interaction with the ECM on such cultures. It appears that the presence of FN promotes clustering of both Naïve and particularly, CIA SFs, presumably reflecting the proposal that FN aids fibroblast migration. Cooperation amongst multiple integrin and non-integrin receptors is required for fibroblast migration on FN, with this stringency affecting cell mobility (Clark et al., 2003). As FN-binding  $\alpha 5\beta 1$  integrins are upregulated in RA synovium and synovial fluid, arthritic SFs are more likely, than Naïve SFs to recognise and interact with FN and hence potentially receive at least quantitatively differential signals that may impact on their functional responses. This may be reflected here in the enhanced clustering of CIA, relative to Naïve, SFs observed.

### 3.3.3 Fibronectin induced expression of MMP and pro-inflammatory cytokines in Naïve and CIA-SFs

Following on from the findings of the enhanced pro-inflammatory responses of CIA-, relative to Naïve-, SFs, the effect of FN on their IL-6 and MMP3 secretion was investigated to explore whether these SFs phenotypes differentially interact with this component of the ECM. In addition, it was also investigated how FN interactions impacted on their responses to fresh pro-inflammatory cues *ex vivo*, such as IL-1 $\beta$  stimulation.

Firstly, crystal violet staining, carried out to determine the number of Naïve and CIA SFs pertaining in the cultures in the absence and presence of FN (Figure 3-4A) and/or IL-1 $\beta$  stimulation (Figure 3-4B), showed that the number of CIA, compared to Naïve, SFs was significantly greater, presumably due to the 'aggressive' proliferative nature of activated SFs. However, culture on FN does not further significantly affect the cell numbers of either phenotype. Due to the hyperplasia of the CIA SFs, the crystal violet staining was then used to normalise the cytokine release detected in cell culture supernatants on a per cell basis.

The cells were treated with medium  $\pm$  IL-1 $\beta$  overnight before the release of IL-6 and MMP3, the latter of which has also been found to be elevated in the synovial fluid of RA patients (Sun et al., 2014; Srirangan and Choy, 2010), was determined. In these experiments, IL-6 (Figure 3-4C) secretion appear consistent whilst MMP3 (Figure 3-4E) showed increased basal (steady-state) by CIA-SFs, compared to Naïve SFs. Although there was an increase in the steady-state IL-6 and MMP3 cytokine production by both Naïve and CIA SFs when grown on FN, that exhibited by CIA-SFs was more significantly upregulated. This is likely due to the upregulation of integrin  $\alpha$ 5 $\beta$ 1 [also known as the FN receptor], contributing to the aggressive behaviour of the CIA-SFs through the induction of pro-inflammatory cytokine (IL-6) and cartilage degrading enzyme (MMP3) release (Zeisel, Druet, Wachsmann and Sibilis, 2005).

As IL-1 $\beta$  is a key initiator of RA pathogenesis, its addition is useful for mimicking the inflammation in the arthritic joint environment in *in vitro* cultures. Consistent

with this, the expression of both IL-6 (Figure 3-4D) and MMP3 (Figure 3-4F) in the conditioned medium was increased significantly above steady-state levels when SFs were stimulated with IL-1 $\beta$  in both Naïve and CIA cultures. However, CIA-SFs released more of the pro-inflammatory cytokine and MMP compared to Naïve SFs and when stimulated, CIA-SFs showed an increase in expression of both cytokines when cultured in the presence of FN. This could be due to FN signals cooperating with those of IL-1 $\beta$  to recapitulate a more pro-inflammatory environment.

### ***3.3.4 SF subset differentiation is lost in Naïve- and CIA-SF 2D cultures***

It has been established that SFs in the lining and sublining layers of the synovial membrane differ not only anatomical location but in function. Thus, lining SFs have been found to be involved in the bone and cartilage degradation characteristic of RA, whilst the sublining SFs have been found to be more involved in the pro-inflammatory signalling associated with the disease (Croft et al., 2016). Various markers have been used to identify SF subsets (Nygaard and Firestein, 2020) and increasingly, through the use of such markers the role of SF subsets in the pathogenesis of RA has been better understood, ultimately potentially allowing for better therapeutics to be developed.

To explore the stability/maintenance of SF subset phenotypes in explant 2D cultures, immunofluorescence staining was carried out after 4 passages targeting vimentin to validate cells as SF and exploiting differential VCAM1 (lining marker) and CD90 (sublining marker) expression to identify the SF subsets (Figure 3-5). Prior to staining, Naïve and CIA SFs were cultured in the presence and absence of FN to also allow assessment of the impact of ECM interactions on subset maintenance. The cells from all cohorts strongly express vimentin confirming they are all SFs. However, unlike the 30/70% (Naïve) and 40%/60% (CIA) distribution of lining to sublining phenotypes found in freshly isolated SF populations (Wang et al. unpublished), all of these SFs also appeared to be positively stained for the markers of lining and sublining SFs in both the Naïve and CIA cohorts, essentially showing no segregation into subpopulations and corroborating previous studies from this lab showing generation of a homogeneous population of SFs during ex

*vivo* growth in monolayer cultures, as evidenced by their uniform expression of CD90 and VCAM1 (Pineda et al., 2014). Thus, the capacity to maintain the distinct subpopulation phenotypes of lining and sublining SFs appears to be lost in 2D culture. Although this loss cannot be prevented by culture on FN, the cells expressing VCAM1 and CD90 appear brighter when grown in the presence of this ECM component: this could reflect that FN being richly expressed within the synovial joint, may be a source of activation and acquisition of invasiveness of SFs via upregulation of these cell surface receptors (Sanchez-Pernaute, 2003).

### 3.4 Concluding remarks

The characteristics of Naïve and CIA-SFs determined above are consistent with those of their counterparts in various animal models and human disease using similar 2D platforms, reported in the literature (Ruelas et al., 2020). Importantly for their use as a reference profile, the presented data recapitulate SF signalling, in terms of the hyper pro-inflammatory nature of the CIA-SFs, when compared to Naïve SFs *in vivo* or freshly isolated *ex vivo* (Kemble and Croft, 2021). However, despite the many studies of such hyper-responsive RA/CIA-SFs, no SF-targeted therapeutic has been developed to date perhaps suggesting models that sustain differentiated SF lining and sublining phenotypes and/or allow more optimal physiological interactions and signalling between cells are required to provide a better insight into potential therapeutic interventions. It is therefore the aim of the following chapters to determine the characteristics of explant SFs transferred to different types of 3D cultures, Alvetex® scaffolds and hydrogels, to explore whether the more physiological architecture provided supports (re)differentiation of the SFs to phenotypes that display characteristics more physiologically related to freshly isolated Naïve and CIA SFs.

**Table 3-1: Animal models used in RA research and their characteristics**  
(Asquith, Miller, McInnes and Liew, 2009)

Animal model	Characteristics
Collagen Induced Arthritis (CIA)	Polyarthritis, antibody and T-cell response. Inoculation with type II collagen induces relapsing/remitting arthritis but is self-limiting. Only inducible in susceptible strains of rodents
Collagen Antibody Induced Arthritis (CAIA)	Self-limiting polyarthritis in all animals, onset within 2 d, macrophage and polymorphonuclear cell involvement, no T- and B-cell involvement. Can be induced in most strains of mice.
Zymosan Induced Arthritis (ZIA)	Monoarthritis, develops 3 days after inoculation and subsides by day 7, but has shown to relapse after day 25. TLR 2 dependent and can be induced in multiple strains of mice.
Antigen Induced Arthritis (AIA)	Inoculation with antigen by intra-articular injection and precludes analysis of the systemic component of disease.
Spontaneous transgenic models of arthritis	Spontaneous chronic and progressive polyarthritis, onset of disease at 3-4 weeks of age. This includes the KBxN, SKG and DNase II <sup>-/-</sup> IFN-IR <sup>-/-</sup> and human TNF- $\alpha$ transgenic mice. These mutations have so far only been identified in mice.

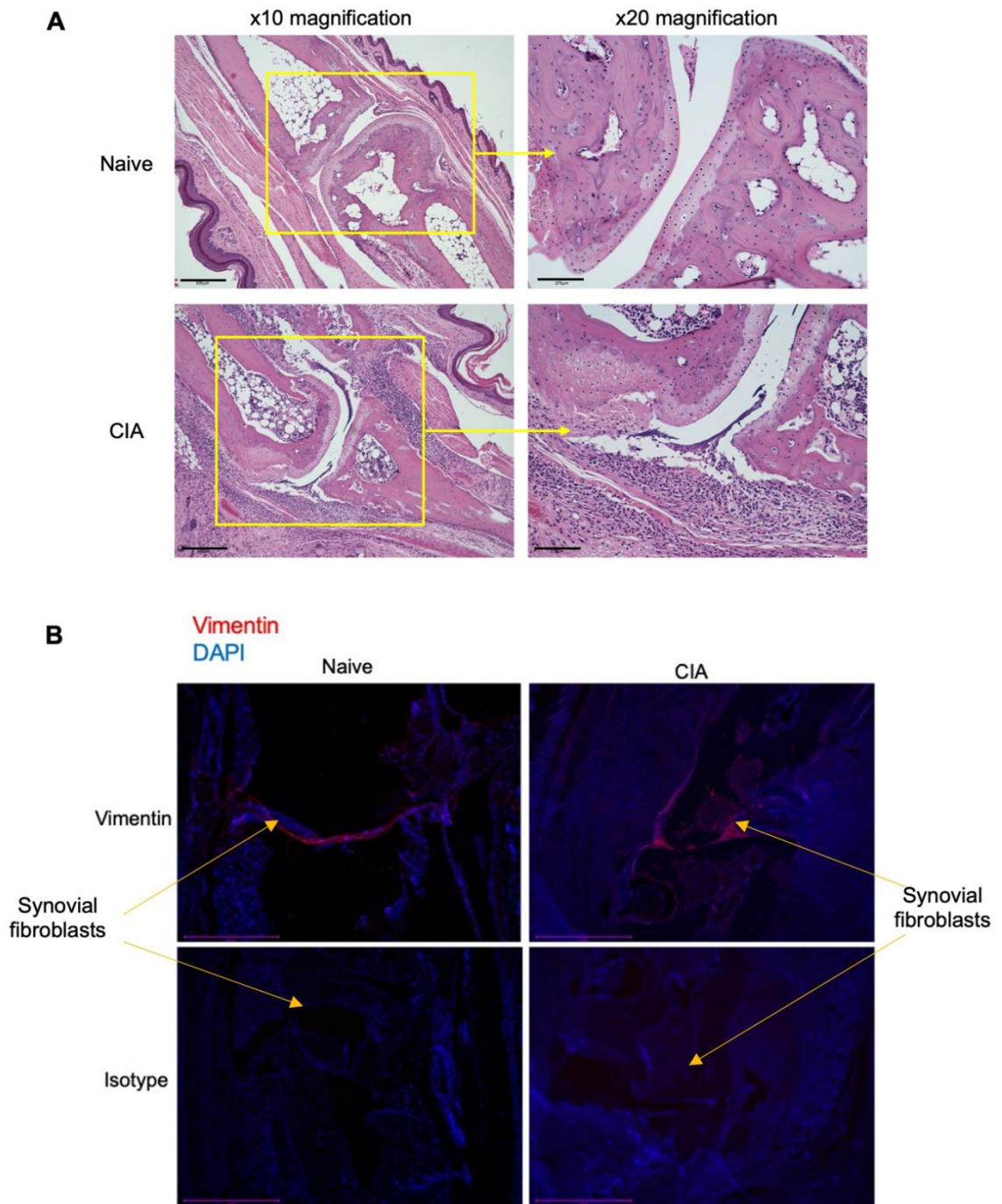


**Figure 3-1: Pathophysiology of Naïve and CIA joints in mice.**

(A) Haematoxylin and Eosin staining was carried out on representative sections of the hind left paws at x10 magnification (scale: 500  $\mu$ m) and x20 magnification (scale: 275  $\mu$ m) from Naïve (top panels) and CIA (bottom panels; score 8) mice. Images were taken on EVOS brightfield microscope. (B) Immunofluorescent staining was carried out on mouse joint sections (7  $\mu$ m). Vimentin antibody staining (red) and DAPI (blue) was carried out on Naïve section (top left) with isotype (bottom left; score 6) and on CIA sections (top right) with isotype (bottom right). Images were taken at x10 magnification (scale: 500  $\mu$ m) on a confocal microscope

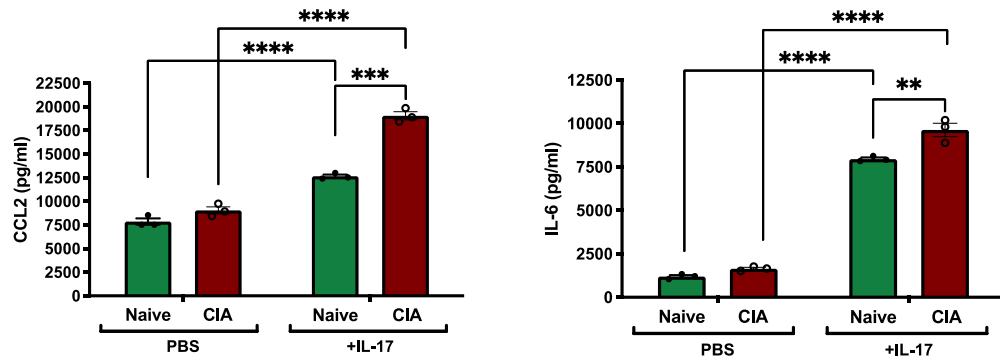


**Figure 3-2: SFs from CIA mice exhibit increased production of pro-inflammatory mediators.**

Following culture (Materials & Methods section 2.9) in the presence and absence of IL-17 stimulation for 24 h, conditioned medium was collected and release of (A) CCL2 (B) and IL-6 was determined. Data are presented as means  $\pm$  SD, where each dot represents a biological replicate (in technical triplicates). Statistical significance was determined using One-way ANOVA and Tukey's test for multiple comparisons; \*\* $p < 0.001$ , \*\*\* $p < 0.0001$  and \*\*\*\* $p < 0.0001$ .

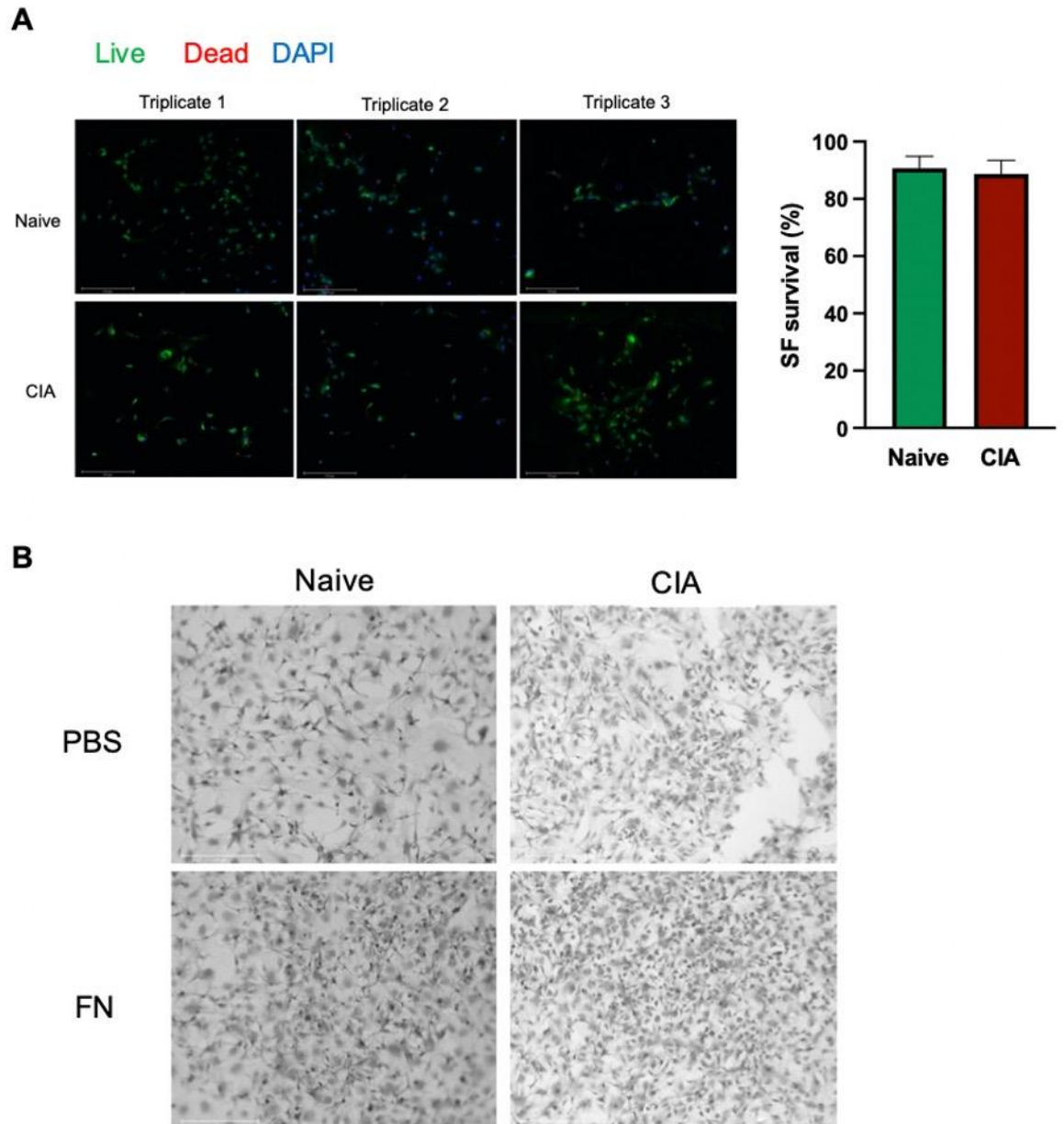


**Figure 3-3: Viability and morphology of cells cultured in 2D.**

(A) Live and dead staining of Naïve and CIA fibroblasts grown in a 2D platform, to observe fibroblast survival. Merged images of triplicate cultures show staining for live SF (green) using Calcein-AM and dead SF (red) using Ethidium homodimer-1 (left) with correlating SF survival graph (right). (B) Haematoxylin and Eosin staining carried out on Naïve and CIA SFs in the presence and absence of FN using an EVOS brightfield microscope at x20 magnification (scale: 275  $\mu$ m).

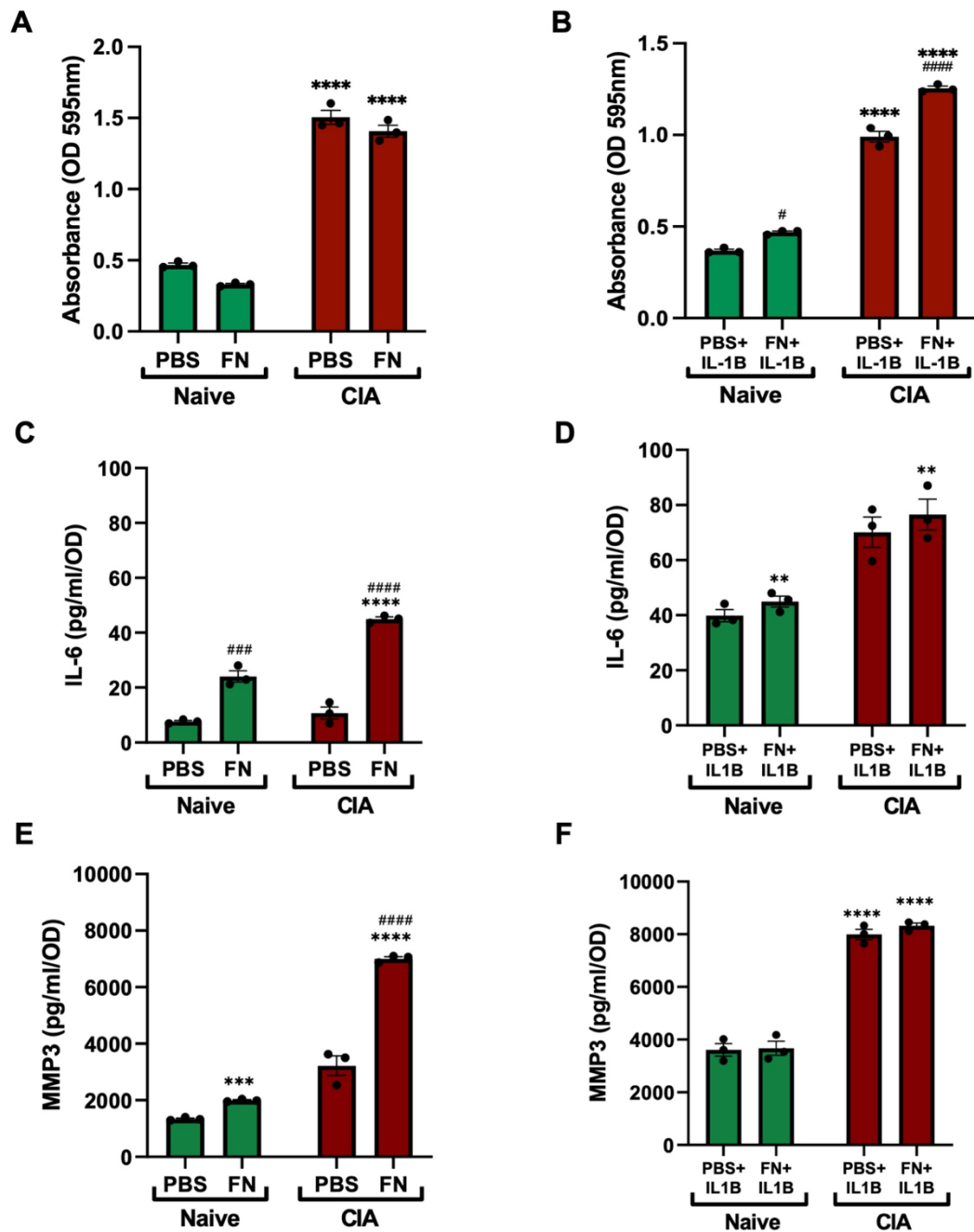
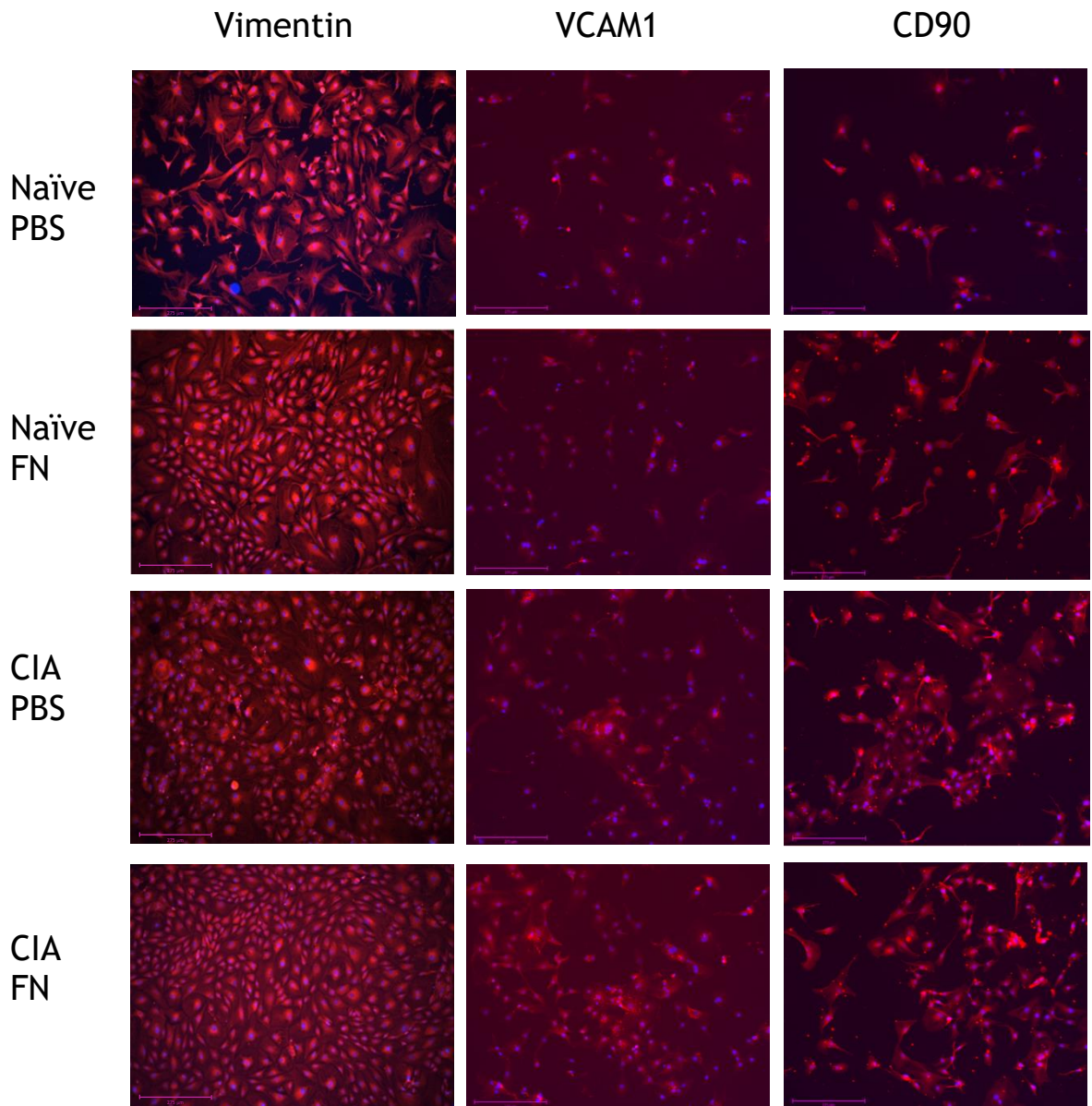


**Figure 3-4: Effect of FN on MMP3 and IL-6 secretion in SFs in 2D**

ELISA analysis of IL-6 and MMP3 released by Naïve and CIA murine cells cultured for 7 days in 2D in the presence and absence of both FN as well as  $\pm$  overnight IL-1 $\beta$  cytokine stimulation was carried out. The absorbance of SFs in the absence (A) and presence (B) of IL-1 $\beta$  stimulation was determined by crystal violet. The cytokine concentration was determined by ELISA and data were normalized with the crystal violet absorbance values. Cytokine expression of (C) IL-6 in the absence and (D) presence of IL-1 $\beta$  stimulation and (E) MMP3 expression in the absence and (F) presence of IL-1 $\beta$  stimulation (are shown. Data show means  $\pm$  SD, with each dot representing a biological replicate (in technical triplicate). Statistical significance was evaluated by ordinary one-way ANOVA and Tukey's test for multiple comparisons; Naïve PBS vs CIA PBS or Naïve FN vs CIA FN (\*\* $p < 0.001$  and \*\*\*\* $p < 0.0001$ ) and Naïve PBS vs Naïve FN or CIA PBS vs CIA FN (###  $p < 0.001$  and #####  $p < 0.0001$ ).



### Vimentin/VCAM1/CD9

**Figure 3-5: Expression of SF subset markers - VCAM1 and CD90 - in the presence and absence of FN.**

Immunofluorescence staining on Naïve and CIA murine cells. Column 1 shows stromal cell staining; Vimentin (red) and DAPI (blue); Column 2 shows SF lining marker VCAM1 (red) and DAPI (blue); Column 3 shows SF sublining marker CD90 (red), DAPI (blue). Images were taken on a fluorescent microscope at x10 magnification (scale: 500  $\mu$ m)

# Chapter 4 Characterisation of explant Naïve- and CIA-SF responses following transfer to 3D polystyrene scaffolds

## 4.1 Introduction

The investigation of the pathophysiological mechanisms underpinning disease has benefitted from the development of relevant animal models and their validation in genetically-modified strains but has been limited, when exploring the role of adherent cells by the *in vitro* molecular and cellular analysis provided by monolayer (2D) cell culture systems (Kapałczyńska et al., 2016) such as those described in Chapter 3, as the 2D monolayer environment can cause the functional phenotype of cells to diverge considerably from that observed *in vivo* (Duval et al., 2017).

For example, adherent cells grown in a monolayer adopt a flattened morphology, exposing their surface to the surrounding environment in a manner that does not mimic their natural 3D structures *in vivo* and this can result in them losing their differentiated phenotype (Maltman and Przyborski, 2010; Von Der Mark, Gauss, Von Der Mark and Muller, 1977). Notably, this difference in cell morphology can influence their function (Kilian, Bugarija, Lahn and Mrksich, 2010), structural organisation within the cell, cell signalling as well as their secretion of molecules like cytokines (Nelson and Bissell, 2006) resulting in profound differences in their behaviour *ex vivo* (Petersen, Ronnov-Jessen, Howlett and Bissell, 1992). In particular, the cell-cell and cell-ECM interactions responsible for cell proliferation, survival, migration, differentiation, protein and gene expression and responsiveness to stimuli (Cukierman, Pankov, Stevens and Yamada, 2001; Pampaloni, Reynaud and Stelzer, 2007; Mseka, Bamburg and Cramer, 2007) do not appear to be fully recapitulated in 2D cultures and hence, may provide misleading data (Edmondson, Broglie, Adcock and Yang, 2014) as in such cultures, many cell types develop functional genotypes distinct from their phenotype *in vivo* (Abbott, 2003; Pampaloni, Reynaud and Stelzer, 2007). This clearly could have drastic implications for experimental drug discovery in terms of prediction of drug

efficacy and off-target effects (Edmondson, Broglie, Adcock and Yang, 2014; Jensen and Teng, 2020).

In terms of this thesis, such phenotypic plasticity needs to be considered in the context of the aberrant migration of SFs in RA, with studies showing that the characteristic clinical sign of destructive arthritis spreading between joints is mediated, at least in part, by the transmigration of activated RA-SFs (Lefèvre et al., 2009), characteristics that are potentially lost in classical explant monolayer cultures. However, as 3D culture systems form a more lattice-like structure that allows for a more “physiological” cellular architecture, some cell types appear able to maintain/recover their physiological phenotype and function in these systems. For example, chondrocytes undergo transcriptional programming back towards their lost “native” phenotype when cultured in agarose gels, indicating the combined use of 2D and 3D platforms may provide a reversible culture system to investigate “physiological” regulation of their gene expression (Benya, 1982). Although 3D culture systems also have their limitations and cannot completely recapitulate the *in vivo* microenvironment, the optimisation of such 3D culture systems may allow a better understanding of the cellular biology involved in disease mechanisms. Certainly, the maintenance of tissue homeostasis is dependent on direct cues for the tissue microenvironment which need to be factored in when developing/optimising models in the future. For example, internal ‘warning’ signals are immunologically muted in healthy tissues, however upon cellular stress or tissue injury, pro-inflammatory responses provide “danger” flags for tissue repair. These signals include alarmins (intracellular molecules that are secreted into the ECM environment concurrent with cell activation or death) as well as ECM molecules that are upregulated or modulated at the time of tissue injury or that are subjected to post-translation modification (Buckley, Ospelt, Gay and Midwood, 2021). Thus, better understanding of how the tissue microenvironment impacts on their function within the synovium should clarify the role of SFs within the joint in health and disease as it is widely established that the synovium is essential for tissue homeostasis and any disruptions to the latter are destructive and can be pathogenic in RA (Kemble and Croft, 2021).

#### **4.1.1 Alvetex<sup>®</sup>: Three-dimensional polystyrene scaffold**

Increasingly, therefore, non-traditional methods of culturing and analysing cells are being developed to try to eradicate the altered responses resulting from growth of cells on a 2D surface, such as changes in gene expression and remodelling of the cytoskeleton, by generating a 3D environment that promotes optimal cellular growth, function and differentiation. One approach has been to exploit polystyrene scaffolds, such as those now commercially produced like Alvetex<sup>®</sup>, that have been designed specifically to enable cells to maintain a 3D ellipsoidal organisation and structure, potentially mimicking the *in vivo* situation where cells detect membrane proteins or extracellular matrix components and react to environmental changes (Maltman and Przyborski, 2010) (Figure 4-1).

Alvetex<sup>®</sup> is a synthetic, non-degradable and rigid (with a stiffness value of 77 kPa, analogous to that of bone) scaffold that is made of highly porous (90%) cross-linked polystyrene, which can be seen under electron microscopic analysis (Figure 4-2) to have a ‘sponge-like’ appearance (Costello et al., 2021). Typically, it is engineered to a thickness of 200  $\mu\text{m}$  with pores (36-40  $\mu\text{m}$ ) of sufficient size to allow cells to migrate through as well as receive nutrients and treatments. Electron microscope analysis also identifies “voids” (40  $\mu\text{m}$  diameter) that are interconnected via such pores, that further contribute to the porosity of the material. Cells are able to attach to the Alvetex<sup>®</sup> scaffold membrane and grow but such porosity promotes contact between cells, rather than between cells and the membrane, resulting in more *in vivo*-like morphologies when compared to cells grown in monolayer cells (Maltman and Przyborski, 2010) as the scaffold provides space into which cells can invade, proliferate and grow. Critically, the scaffold enables additional layers of cells to form complex 3D interactions with adjacent cells, at least in part, simulating the structure of tissue.

#### **4.1.2 Culture environment impacts on cell behaviour**

Physiological cellular morphology therefore appears to be more effectively maintained within the scaffold environment, with cells undergoing cellular interactions more resembling those seen *in vivo*. Moreover, the 3D nature of cellular interactions within the scaffold can promote expression of functionally important proteins and hence lead to our better understanding of cell-cell

signalling (Kim et al., 2017; Wood, Pajevic and Gooi, 2017) as well as reducing the cellular and nuclear flattening characteristic of cells in conventional *in vitro* monolayer culture systems (Florczyk et al., 2017).

Critically, when cells are seeded in monolayers, cellular stress appears to be far greater than on a scaffold in which they are able to move and organise themselves (Amith, Wilkinson and Fliegel, 2016) and this is evidenced by the greater changes in gene and protein expression observed *ex vivo* in a 2D, relative to a 3D, environment (Edmondson, Broglie, Adcock and Yang, 2014; Jensen and Teng, 2020). Moreover, as cells are free to move within the porous Alvetex® scaffold this allows them to better reproduce their behaviours within tissue microenvironments, such as secreting ECM components. Thus, preserving the structure and morphology of cells potentially allows greater interactions between them, in turn allowing a better understanding the function and role of these cells *in vivo*. Such maintenance of cell morphology and organisation also potentially results in improved cell function and responsiveness. For example, HepG2 cells not only showed increased viability when cultured on the Alvetex® scaffold compared to conventional plates but also exhibited increased albumin secretion, suggesting that the cells exhibited differential functional capacity in such 3D cultures (Schutte et al., 2011). To further promote cell-cell communication, migration and tissue interaction, scaffolds can also be readily coated with ECM components, with collagen, fibronectin and laminin being the most commonly used (Nicolas et al., 2020; Sackett et al., 2018).

Although various other models that have been developed that also create a 3D structural environment such as organotypic raft cultures designed to recapitulate epithelial differentiation (Anacker and Moody, 2012), they are generally technically demanding to reproduce consistently. Thus, polystyrene culture systems provide a generic *in vitro* organ model system for studies ranging from the growth of epithelial cells such as keratinocytes in skin models to those investigating cellular senescence. (Martinez Guimera et al., 2017). Such utility dictates that Alvetex® culture models can be used to better predict cellular responses to therapeutic candidates before pre-clinical and clinical *in vivo*

testing, leading to further understanding of human health and disease (Gomez-Roman et al., 2016).

## 4.2 Aims and Objectives

Pilot studies with the commercial 3D polystyrene scaffold, Alvetex<sup>®</sup> suggested that SFs were able to exhibit fibroblast subset (lining and sublining) differentiation as well as the aggressive physiological responses observed *in vivo* (Pineda, M.A. , *personal communication*). Thus, it was proposed to characterise the functional responses of Naïve and CIA SFs, following their transfer from 2D cultures to Alvetex<sup>®</sup> scaffolds, to explore whether any of the characteristics lost during conventional culture (as highlighted in Chapter 3) can be recovered, resulting in (re)differentiation of phenotypes more comparable to those of SFs freshly isolated *ex vivo*.

The specific objectives of this Chapter are to:

- to establish the morphology of SFs cultured in Alvetex<sup>®</sup>
- to investigate whether there is differential expression of pro-inflammatory cytokines in SFs cultured in 2D and 3D microenvironments
- to compare the impact of SFs-FN interactions on the pro-inflammatory mediator and morphological responses of SFs grown in 2D and Alvetex<sup>®</sup> cultures
- to investigate the ability of activated SFs to proliferate, migrate and organise interactions throughout the Alvetex<sup>®</sup> scaffold
- to determine, by analysis of SF subset marker expression whether the 3D growth interactions allowed by Alvetex<sup>®</sup> scaffolds can recover features lost in 2D, including differentiation of lining and sublining SF subpopulations.

## 4.3 Results

### ***4.3.1 Microenvironment and fibronectin effect morphology and pro-inflammatory gene expression in Naïve SFs***

To visualise the morphology of SFs in the Alvetex® scaffold, immunofluorescence analysis of phalloidin binding to cell actin filaments was carried out (Figure 4-3). Following conventional culture, SFs from Naïve mice (Naïve SFs) were cultured in the scaffold for 7 days in the presence and absence of FN and then sections were treated with phalloidin in order to stain for the cell actin filaments and counterstained with the nuclear stain, DAPI. The samples were then imaged using a confocal microscope and deconvolved to provide 3D visual representations of the staining using IMARIS cell biologist software. This revealed that the scaffold promoted the cells exhibiting a more 3D ellipsoidal structure and organisation, presumably due to the pores within the scaffold that allow the cells to signal each other from multiple directions as the SFs are exposed (rather than attached to plastic) in various regions. The latter also allows the samples cultured with FN (Figure 4-3B) to interact physiologically with this ECM component surrounding them and this was reflected by the SFs in these cultures appearing to exhibit more physiologically relevant morphology. This is important as the ECM is a dynamic structure that is constantly remodelled to control tissue homeostasis and thus, changes in ECM components regulate cell proliferation, differentiation, migration, survival, adhesion, as well as cytoskeletal organization and cell signalling in normal physiology and development and in RA (Bonnans, Chou and Werb, 2014; Mouw, Ou and Weaver, 2014).

After observing the morphology and environmental interactions of the SFs grown in Alvetex®, SF expression of pro-inflammatory mediators and matrix proteases implicated in RA pathogenesis were investigated. Cells were following culture in monolayers or following their transfer to Alvetex®, the latter in the presence and absence of FN, to determine any functional differences driven by the culture microenvironment.

For example, the chemokine CCL2 is a major regulator of monocyte infiltration in RA joints that has been found to be expressed at aberrant levels in RA-SFs,

potentially providing a diagnostic marker for RA and therapeutic target (Liao et al., 2021). Consistent with this CIA-SFs were shown to release higher steady-state and IL-17-stimulated levels of CCL2 than their Naïve counterparts (Chapter 3; Figure 3-2A). Rather unexpectedly, given that it was predicted that 3D cultures would promote SF responsiveness, the Ccl2 mRNA levels in Alvetex® SFs were reduced relative to those grown in conventional cultures irrespective of whether or not they had been grown on FN (Figure 4-4A). Likewise, TGF- $\beta$ 1 production, which contributes to the inflammation and destruction of joints in RA by increasing expression of pro-inflammatory cytokines in SFs (Cheon et al., 2002) was also reduced by growth in the 3D cultures (Figure 4-4D). By contrast, Mmp9 expression (Figure 4-4B) was found to be significantly elevated in the SFs transferred to 3D Alvetex® cultures compared to those maintained on 2D alone, and such expression was further increased by coating of the scaffold with FN presumably reflecting that FN is proteolytically processed by MMP9 and that FN induces the production of activated forms of MMP9 (Esparza et al., 1999). Whilst Mmp13 (Figure 4-4C) also showed an increased in expression in SFs grown on the 3D scaffold, this was not further elevated but rather decreased by the presence of FN. This could be explained as MMP13 has been shown to target collagens during cartilage degradation (Hu and Ecker, 2021; Cathcart, Pulkoski-Gross and Cao, 2015). These MMPs are considered to play a critical role in the degradation of cartilage in RA joints, with MMP9, and MMP13 expression upregulated in RA-SFs and contributing to RA-SF survival, proliferation, migration and invasion (Xue et al., 2014). Indeed, production and activity of MMP13 has been found to be significantly increased in the synovial fluid and serum of RA patients by SFs and is therefore considered a useful marker for the activity of diseases characterised by ECM remodelling (Asano et al., 2005). Thus, given the effects on MMP9 expression, it appears that transfer to a porous, FN-expressing 3D environment may mimic some of the early events promoting SF migration in disease. Finally, ST6Gal1 is an enzyme that regulates  $\alpha$ 2-6 sialylation, a lack of which promotes the transformation of synovial fibroblasts to RA-SFs (Wang et al., 2021). Interestingly therefore, and perhaps consistent with the hypothesis that an MMP-producing, environment facilitates migration promotes SF transformation, mRNA levels of ST6Gal1 (Figure 4-4E) were decreased when the SFs were cultured on Alvetex®.

Two additional genes, IL-6 and MMP3, important to SF pathogenesis in RA (Ogata, Kato, Higa and Yoshizaki, 2019; Zeisel, Druet, Wachsmann and Sibia, 2005) were also investigated in terms of determining the effects of FN interactions on their expression by SFs grown in Alvetex® scaffolds. This was because expression of IL-6 was found to correlate with that of promatrix MMP3 (proMMP3) in early RA suggesting a link between proteinase activity and IL-6 (Roux-Lombard, 2001) and consistent with this, IL-6 has been reported to induce enhancement of MMP production from chondrocytes and SFs resulting in the degradation of the cartilage (Yoshida and Tanaka, 2014; Hashizume and Mihara, 2011). Since we were primarily interested in genes that could contribute to the aggressive, invasive behaviour of RA FLSs, the reported marked up-regulation of the MMP3 gene, which plays a major role in cartilage degradation, prompted us to further study its expression in SFs. Certainly, in RA, MMP3 is locally produced in the inflamed joint and released into the blood stream and, as its serum levels are found to correspond to those within the synovium, it can act as a biomarker for severity of rheumatoid synovitis (Fadda, Abolkheir, Afifi and Gamal, 2016). Moreover, it plays an important role in bone erosion and cartilage degradation in RA due to imbalance between MMPs and their specific tissue inhibitors (TIMPs) (Prodanovic et al., 2018).

It can be seen in Figure 4-5 that the presence of FN increases the expression of Mmp3 (Figure 4-5A), perhaps due to it, like MMP9, providing a cue for the SF-mediated breakdown of the ECM in normal physiological processes such as tissue remodelling (as well as in diseases such as RA). Certainly, as MMP3 degrades FN, laminin, collagens as well as cartilage proteoglycans (O'Brien et al., 2007), this could explain the differential responses observed. Indeed, in normal cartilage, FN is localised mainly in the matrix of the surface zone and an increase in its expression is associated with tissue remodelling and repair (Barilla and Carsons, 2000; Homandberg et al., 1997). Moreover, the 29-kDa amino-terminal FN fragment was shown to stimulate proteoglycan breakdown, enhancing nitric oxide production and increasing expression of MMP3, MMP1 and MMP13. The latter could provide an explanation as to why FN could induce hyper-responsiveness of Naïve SFs cultured in a 3D microenvironment although by contrast, the expression of IL-6 (Figure 4-5B) is greater in the absence of FN, which was not as expected.

To further investigate differential functional responses of SFs grown in monolayers, relative those subsequently transferred to a 3D microenvironment, chemokine (CCL2), cytokine (IL-6) and ECM remodelling (MMP3) responses in monolayer and scaffold cultures were directly compared over 7 days from the same seeding population of Naïve cells (Figure 4-6), with the experiment carried out in the absence of FN. This revealed that production of all mediators (Figure 4-6A-C) peaked at day 1, irrespective of 2D or 3D microenvironment, declining profoundly thereafter in terms of IL-6 and CCL2 release whilst MMP3 production was relatively stable up to at least day 3. However, and in contrast to what was observed with the Ccl2 mRNA data (Figure 4-4A), cytokine release was enhanced by culture on Alvetex®, although as indicated in Figure 4-6C, this is marginal with respect to MMP3.

As the 3D culture systems appear to enhance at least some of the steady-state cytokine and ECM-remodelling responses of Naïve SFs, the impact of the Alvetex® 3D microenvironment on the differential functional responses of Naïve- and CIA-SFs was next investigated.

#### ***4.3.2 Organisation, migration, proliferation and pro-inflammatory phenotype of Naïve- and CIA-SFs cultured on 3D polystyrene scaffolds***

Having established that the microenvironment plays a role in determining morphology and gene expression of Naïve SFs, the capacity of 3D scaffolds and ECM components to impact on the organisation and migration of Naïve and CIA SFs was investigated. Thus, histological (H&E staining) analysis of SFs cultured in the scaffold for 7 days was carried out to identify the location of cells within the scaffold, with cells in specific regions of the scaffold quantified using ImageJ. Specifically, the polystyrene Alvetex® disc was divided into 3 main sections as shown in the schematic (Figure 4-7A), with the seeding area referred to as the ‘upper’ section, the centre referred to as the ‘middle’ section and bottom region referred to as the ‘lower’ section. The scaffold was split in this manner to understand whether the cells were able to disperse evenly through the scaffold or

simply remained in the seeding area and to determine whether exposure to FN impacted on this.

The images in Figure 4-7B show that both Naïve and CIA SFs cultured on Alvetex® tend to congregate and remain mainly within the seeding area, as indicated by the data showing over 50% of the cells to be retained in the ‘upper’ region as opposed dispersing freely to the ‘middle’ and ‘lower’ regions (Figure 4-7C). Contrarily, both Naïve and CIA SFs cultured in the presence of FN can be seen to have dispersed more evenly throughout the scaffold (Figure 4-7B & C) and organise themselves throughout the scaffold. This differential behaviour likely reflects that FN plays a role in fibroblast migration and organisation (Briggs, 2005; Shelef, Bennin, Mosher and Huttenlocher, 2012; Konttinen et al., 2000) and suggests that FN promotes migration of both Naïve and CIA SFs.

The Naïve and CIA SFs essentially demonstrated comparable migratory potential: thus, as aberrant proliferation of resident SFs is characteristic of RA and the accretion of SFs directly contributes to joint destruction through enhanced production of MMPs and indirectly via excessive cytokine release that boost the immune system (Kramer I et al., 2003), the potential differential effect of FN on proliferation of these SFs within the experimental 3D scaffold was next investigated. To address this, immunofluorescence staining of Ki67, an antigen associated with proliferation (Figure 4-8A) was carried out on Alvetex® sections of Naïve and CIA SFs (counterstained with the nuclear dye, DAPI) and the percentage of Ki67 positive cells was quantified (Figure 4-8B), along with Ki67 staining intensity (Figure 4-8C) using ImageJ software. As predicted by the proposed “transformed” nature of the CIA SFs, Ki-67 staining was brightest in CIA SFs, with this group exhibiting a higher percentage, and brighter staining, of Ki67 positive cells relative to Naïve SFs. However, when the SFs were grown on FN scaffolds there was a significant increase in the proliferation for both SF populations (Figure 4-8B & 4-8C). That CIA-SFs grown on FN scaffolds exhibited the highest levels of proliferation may reflect that these cells will adhere to, and respond most strongly to, FN because of their increased expression levels of  $\alpha 5\beta 1$  integrins which are involved in adherence and migration (Rinaldi et al., 1997; Ospelt, 2017). The data

could also suggest that the increased “cell migration” observed *in vivo* could be due, at least in part, to the increased number of SFs resulting from hyperplasia.

To further investigate the SF hyperplasia associated with CIA, crystal violet staining was carried out to determine the levels of cell proliferation when Naïve and CIA SFs are cultured on Alvetex® scaffolds. As cells lose their adherence during cell death, the impact of FN, as well as that of a pro-inflammatory signal (IL-1 $\beta$ ) associated with RA pathogenesis, was assessed (Figure 4-9A & B). Reflecting the ‘aggressive’ proliferative nature of CIA SFs, these cells showed higher staining than Naïve SFs but this was not increased by incorporation of FN into the scaffolds: rather, Naïve SFs showed a decrease in crystal violet staining when grown on FN perhaps suggesting that FN-Naïve SFs interactions keep hyperplasia in check whereas CIA-SFs lose this control and consequent restriction of hyperplasia and migration indicating that interactions with this ECM component may have differential functional outcomes in Naïve and CIA SFs.

The data presented in Chapter 3 (Figure 3-5) confirmed that CIA-SFs maintain a hyper-responsive phenotype, in terms of pro-inflammatory mediator production, even when grown *ex vivo* as conventional monolayer cultures for 4 passages. In addition, it was established that growth on FN-coated plates increased responsiveness of both Naïve and CIA SFs. Thus, it was proposed to examine whether this was also the case when cells from such explant cultures were transferred to, and grown for 7 days on, 3D scaffolds and in particular, how FN interactions in this microenvironment impacted on their responses to fresh pro-inflammatory cues, such as challenge (on day 6) with IL-1 $\beta$ . Analysis of the key pathogenic mediators, IL-6 and MMP3 showed that both were released at increased levels by CIA-SFs, compared to Naïve SFs (Figure 3-5 E & F), although in this case of the 3D scaffolds the IL-6 hyper-responsiveness was more obvious than that of MMP3, an inverse situation to that seen with monolayer cultures. There was also an increase in IL-6 and MMP3 release by both Naïve and CIA SFs when grown on FN, with the responses of CIA-SFs more strongly upregulated: as this enhancement was also observed in monolayer cultures, these data suggest that the FN-integrin interactions contributing to the induction of the pro-inflammatory cytokine (IL-6) and cartilage degrading enzyme (MMP3) are not qualitatively affected by the

change in microenvironment. Likewise, the enhanced release in response to IL-1 $\beta$  stimulation of Naïve and CIA SFs was observed in this scaffold model and again, this was not further increased by FN interactions (Figure 4-9C-F). Thus again, CIA-SFs appeared to be rewired in their responses to FN, presumably as a consequence of their transformation from their Naïve state during CIA.

#### ***4.3.3 The effect of FN and 3D microenvironment on SF subset differentiation in Naïve and CIA-SFs***

It was previously established in section 3.3.4 that lining and sublining SF subsets cannot be discriminated in cells cultured in 2D. Rather, the lining and sublining markers were both expressed by all Naïve and CIA SFs suggesting loss of the *in vivo* phenotype and induction of a homogeneous population of cells. It was therefore investigated whether the distinct subpopulations can be recovered from a mixed population of cells by transfer to a 3D microenvironment and also whether this is impacted by FN-SF interactions on Alvetex® scaffolds.

Specifically, immunofluorescence staining was carried out targeting vimentin as a stromal cell marker and exploiting differential VCAM1 (lining marker) and CD90 (sublining marker) expression to address whether SF subsets are recovered (Figure 4-10), as well as to assess the impact of ECM interactions on subset development. In all conditions, the cells express vimentin confirming they are of stromal origin, whilst staining for lining and sub-lining SF markers showed positive staining of both markers in both Naïve and CIA conditions, with the cells expressing VCAM1 and CD90 appearing brighter when cultured in the presence of FN, which could be due to the fact that FN is rich within the synovial joint, being generated inside the joint cavity and may be a source of activation and acquisitions of invasiveness of SFs (Sanchez-Pernaute, 2003). Interestingly therefore, it appears from Figure 4-10A that SFs expressing VCAM1 (regardless of whether they are Naïve and CIA-SFs, grown on FN or not) tend to organise themselves towards the middle of the scaffold, whilst those expressing CD90 are found more towards the outer edges of the scaffold. This could perhaps suggest that the 3D scaffold allows for the organisation of subsets in a manner similar to their anatomical location within the synovial joint, with VCAM1 positive cells representing lining SFs and CD90 positive

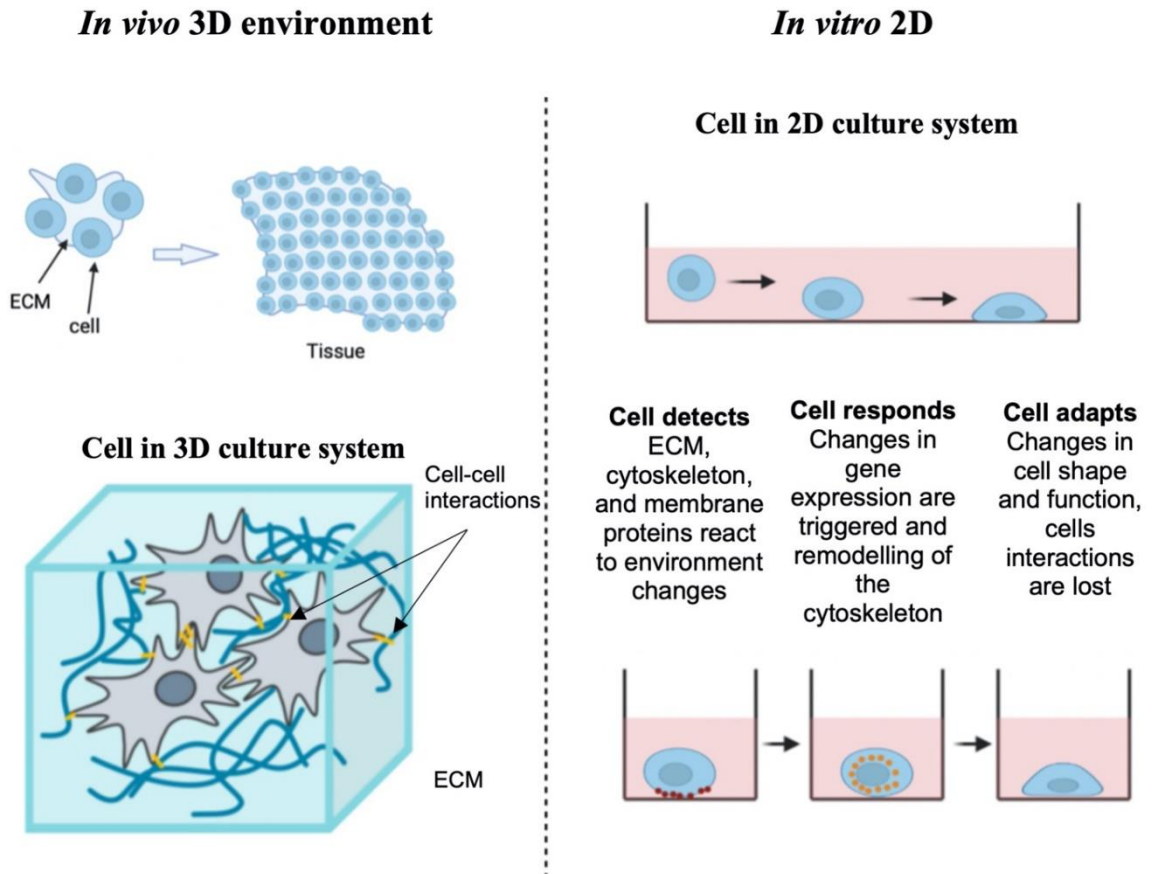
cells, sublining SFs (Croft et al., 2019). Moreover, and corroborating the ‘aggressive’ phenotype of CIA SFs, there appears to be a greater number of these SFs in the cultures, despite Naïve and CIA SFs being seeded at the same levels.

To further explore whether Alvetex® promoted subset differentiation and organisation, dual staining of the sections was carried out and analysis showed subsequent culture of 2D-grown SFs on Alvetex® scaffold potentially supported the differentiation of SF subsets as the cells (as indicated by the DAPI nuclear staining) did not appear to be a homogenous population expressing both SF markers but rather seemed to differentially exhibit expression of VCAM1 and CD90, regardless of whether they are grown on FN or not (Figure 4-10B and Figure 4-10C). The latter suggest that culture in a 3D microenvironment allows the recovery of SF responses and signals lost when cultured in 2D. Interestingly however, unlike the predominance of the sublining, relative to the lining, SF population when the cells were analysed immediately following *ex vivo* isolation, under these conditions both subtypes were able to be detected and whilst this balance was not consistently modulated by growth on FN, the CIA-SFs showed less of a sublining bias.

#### 4.4 Concluding remarks

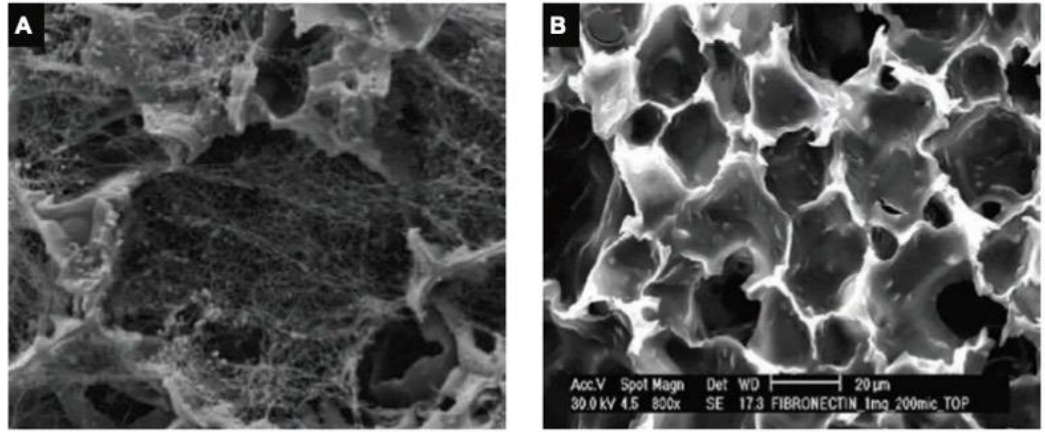
The data presented above provides evidence that 3D cell morphology (or tissue architecture) has an impact on relevant aspects of SF pathophysiology, such as their proliferation, migration and organisational properties that cannot be recapitulated in conventional 2D cultures. Differences observed between 2D and Alvetex® suggest that the use of 3D cell culture could potentially recover some SF functionality lost in 2D and hence presumably rewire gene expression as suggested by the (re)differentiation of SF subsets observed. This is in addition to the maintenance, and perhaps even enhancement, of the ‘aggressive’ CIA-SF phenotype also recapitulated in monolayers, at least in terms pro-inflammatory cytokine and MMP secretion (as observed in Chapter 3). Many of these responses can be further enhanced when SFs are grown on FN-coated scaffolds, which likely reflect FN-integrin signalling in SFs during their aberrant migration and pro-inflammatory, joint destroying activities in the arthritic synovium.

However, although Alvetex<sup>®</sup> scaffolds provide supporting structures that perhaps allow better modelling of the SF interactions of the 3D microarchitecture of the synovium, the scaffold itself is made from plastic and is rigid. Indeed, it has a stiffness of 77kPa, which is more akin to that of bone rather than the synovium which has a stiffness of ~7-10 kPa under conditions of inflammatory arthritis and therefore may, like 2D platforms, induce inappropriate synovial cell responses. Thus, in the next chapter, the responses of the re-differentiated, homogenous population of SFs arising in conventional cultures will be characterised following their transfer to hydrogels pegylated with FN, particularly with respect to their functional pro-inflammatory and migratory responses, in the context of CIA-SF hyper-responsiveness. In addition, the use of such hydrogels will allow investigation of the effect of changes in gel stiffness to address the impact of the increased physiological stiffness of the arthritic joint on SF function.

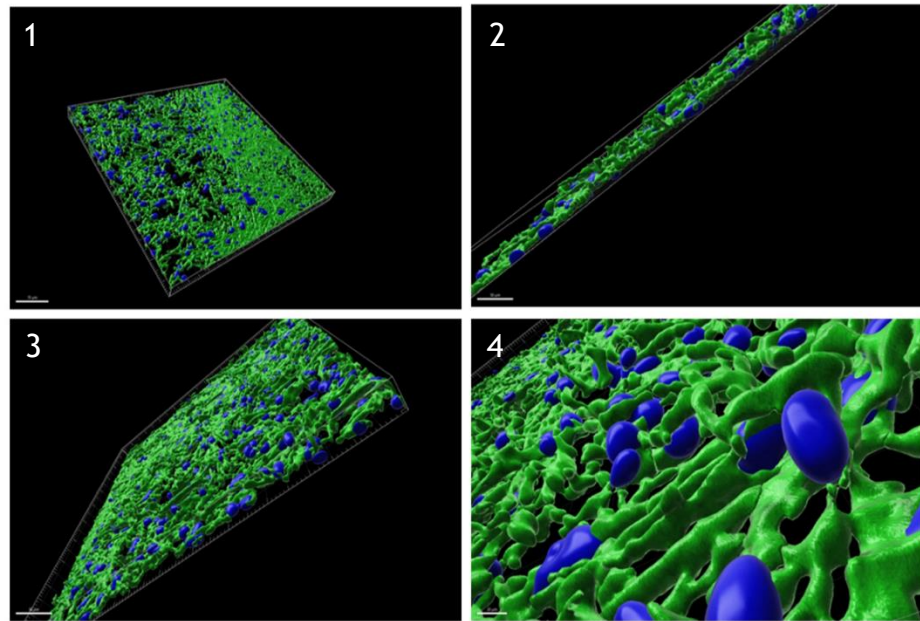
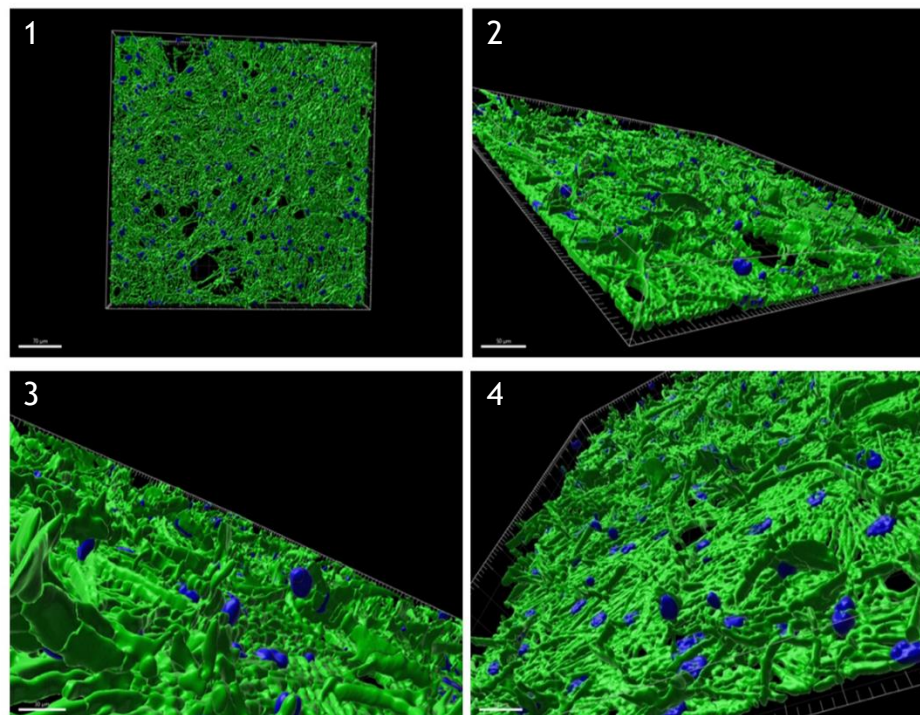


**Figure 4-1: Cell morphology in *in vivo* environments and in 2D *in vitro* environments.**

In 3D *in vivo* environments, cells typically maintain a 3D ellipsoidal structure and organisation and in 2D *in vitro* environments cells form a monolayer of a flattened morphology (adapted from Przyborski, 2017 and boku.ac.at and created with Biorender.com).



**Figure 4-2: Alvetex® can be treated with differing ECM components.** Electron microscope images of **A)** Scaffold pre-loaded with Collagen IV. **(B)** Coating scaffold with fibronectin. The ECM proteins form a web of fibres spanning voids into which cells can grow and migrate in 3D (reprocell.com).

**A****B**

**Figure 4-3: Morphology of Naïve SF in a 3D polystyrene scaffold.**

Naïve SFs were cultured for 4 passages in 2D before being cultured for 7 days in 3D scaffolds in the presence and absence of FN. Sections were cut prior to staining with an antibody specific for phalloidin in order to stain for the cell actin filaments (and counterstained with the nuclear stain, DAPI). The samples were then imaged using a confocal microscope and made into 3D visual representations of the staining using IMARIS cell biologist software. Scaffold with Naïve cells treated with (A) media alone (PBS) and (B) with FN. Images show different orientations of the 3D image (x10 magnification, PBS scale: 1-70  $\mu\text{m}$ , 2-30  $\mu\text{m}$ , 3-30  $\mu\text{m}$ , 4-20  $\mu\text{m}$ ; FN scale: 1-70  $\mu\text{m}$ , 2-50  $\mu\text{m}$ , 3-50  $\mu\text{m}$ , 4-30  $\mu\text{m}$ )

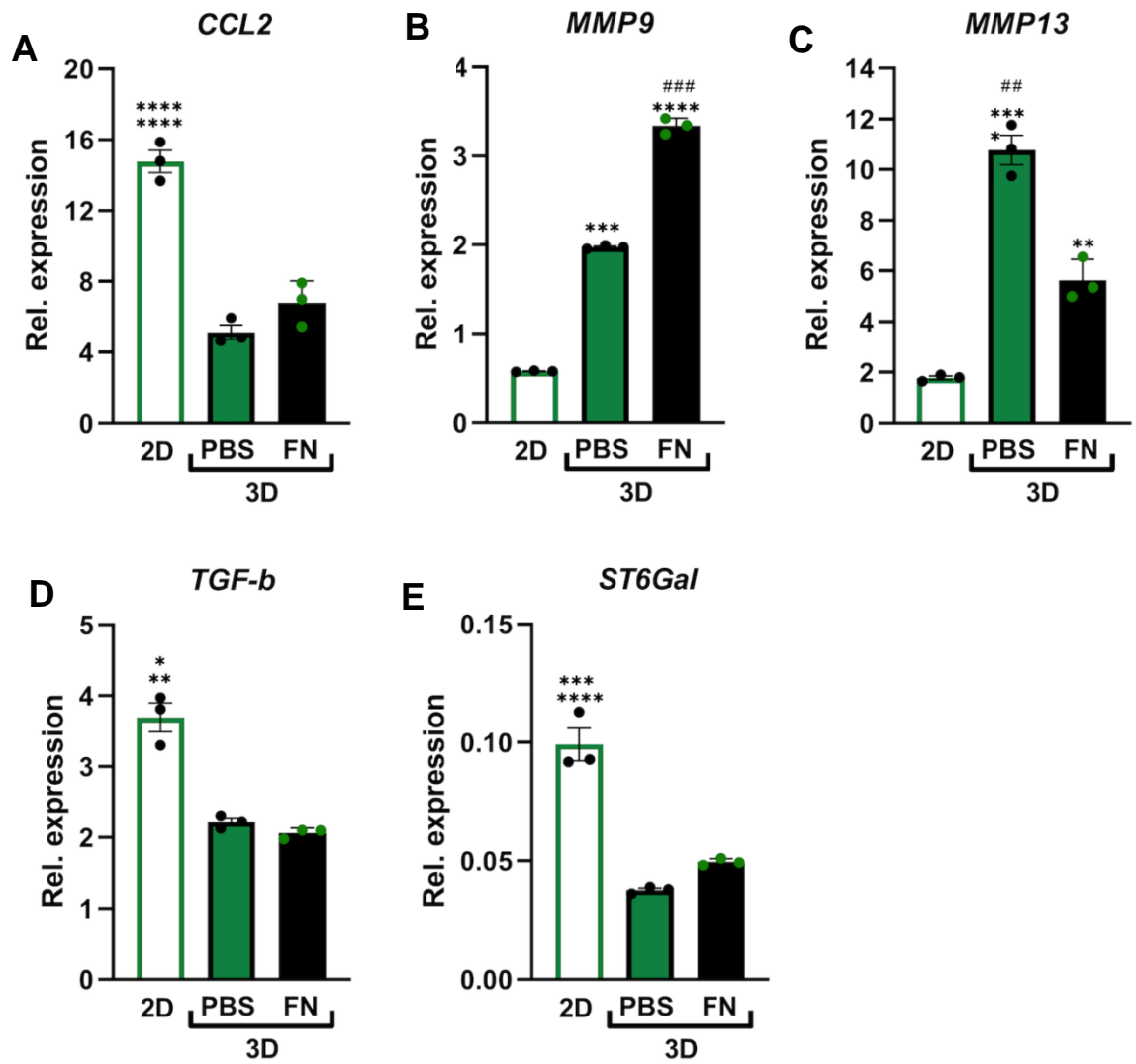


**Figure 4-4: Differential expression of Ccl2, Mmp9, Mmp13, Mmp13, Tgf-b1 and ST6Gal in SFs cultured in 2D and Alvetex® and the effect of the presence of FN.** Naïve SFs were expanded in 2D until passage 4 after which a portion were transferred to Alvetex® to be further cultured for 7 days, whilst the rest were further expanded in 2D for 10 days. Both were cultured in the presence and absence of FN. Following this, RT-PCR was carried out to quantify the expression of (A) Ccl2 (B) Mmp9 (C) Mmp13 (D) Tgfb1 (E) and ST6Gal. Expression of genes were relative to Actin and are presented as means  $\pm$  SD, where each dot represents a biological replicate (mean of technical triplicates). Statistical significance was determined using One-way ANOVA and Tukey's test for multiple comparisons; Naïve PBS vs Naïve FN or CIA PBS vs CIA FN (\* $p < 0.05$ , \*\* $p < 0.001$ , \*\*\* $p < 0.001$  and \*\*\*\* $p < 0.0001$ ) and Naïve PBS vs CIA PBS or Naïve FN vs CIA FN ( #  $p < 0.001$  and ###  $p < 0.001$ ).

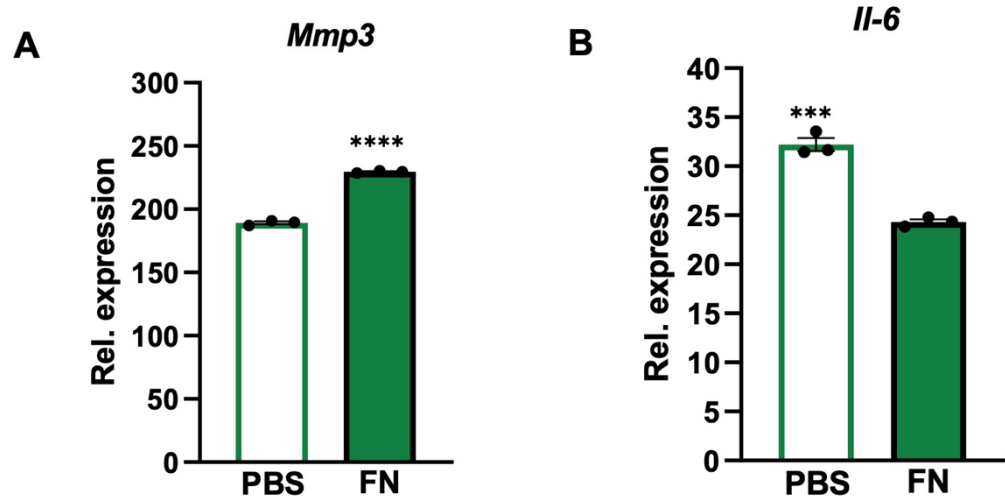


**Figure 4-5: Effect of the presence of FN on expression of *Mmp3* and *Il-6* in SFs cultured in a 3D polystyrene scaffold.**

Naïve SFs were cultured in Alvetex® in the presence and absence of FN, after which qRT-PCR was carried out to determine quantification of (A) *Mmp3* and (B) *Il-6* expression. Results show relative expression to Actin, showing mean ± SD. Each dot represents a biological replicate (in technical triplicate). Statistical significance was determined using t test for multiple comparisons; \*\* $p < 0.001$ , \*\*\* $p < 0.001$  and \*\*\*\* $p < 0.0001$

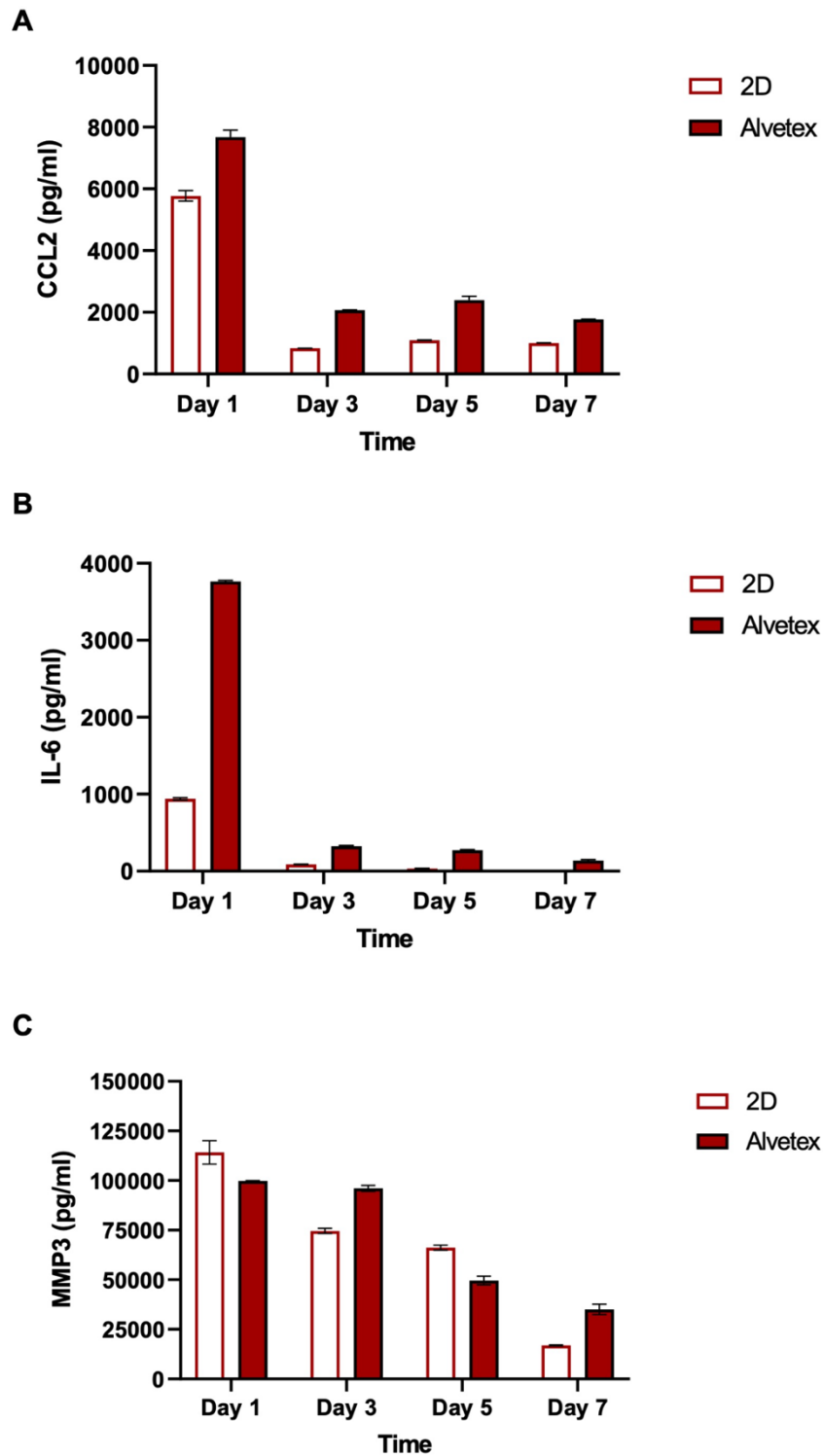


**Figure 4-6: Expression of inflammatory cytokines in Naïve SFs released by cells cultured in 2D and 3D culture systems.**

Naïve SFs were expanded in 2D and then either further cultured in 2D or Alvetex<sup>®</sup>. The cytokine expression for A) CCL2 (B) IL-6 (C) and MMP3 was determined at days 1, 3, 5 and 7. For each time point the supernatant was collected for ELISA analysis and the SFs immediately treated with fresh media for supernatant collection of the next time point. Data show means  $\pm$  SD, with each bar representing one biological replicate (in technical triplicate).

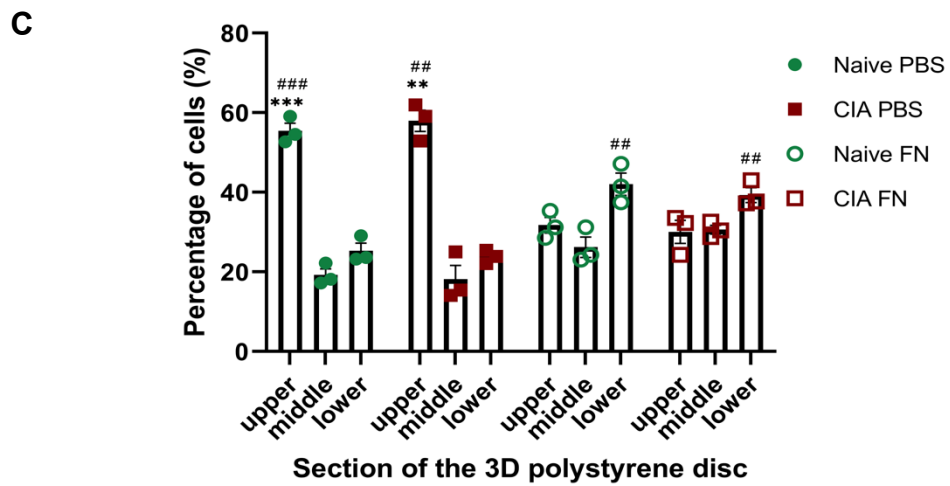
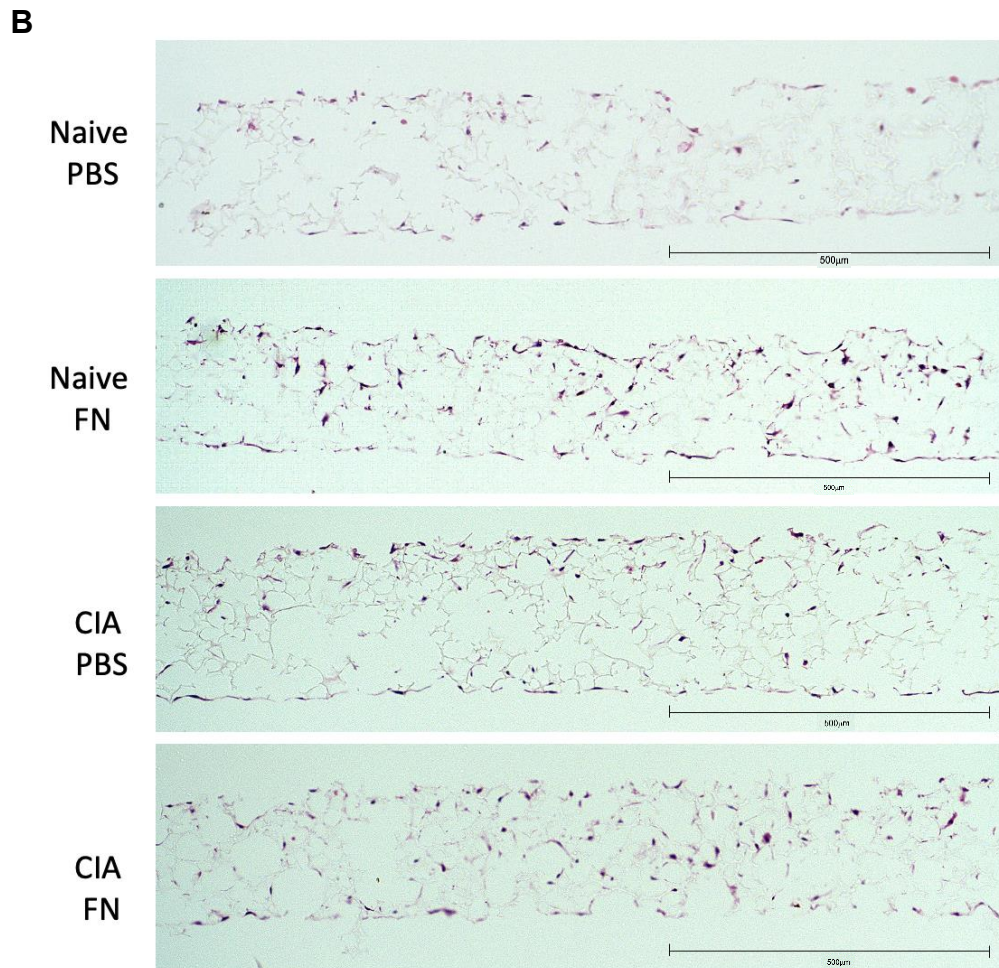
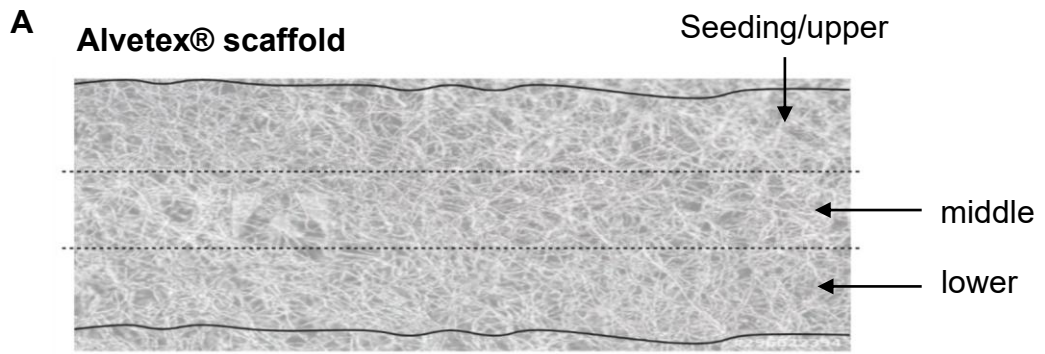


**Figure 4-7: Migration and organisation of SFs in Alvetex®.**

(A) Diagram of 3D polystyrene (Alvetex®) scaffold sectioning and seeding. Cells were expanded in 2D before being cultured for 7 days in Alvetex®. (B) Haemotoxylin and Eosin staining on Naïve and CIA SFs cultured in Alvetex® alone (PBS) or with the addition of fibronectin (FN). Images were taken on a EVOS brightfield microscope at x10 magnification (scale: 500  $\mu$ m). (C) Quantification of the number of SF (by nuclei) in the presence and absence of FN was carried out using ImageJ. The percentage of nuclei in each of the three sections, the upper section in which cells were deposited (seeding), the middle of the disc and the lower section. Data show means  $\pm$  SD where each dot represents a biological replicate (mean of technical triplicates). Statistical significance was evaluated by ordinary two-way ANOVA between conditions. Statistics shows inter condition comparison; upper vs lower (\*\*p<0.001 and \*\*\*p<0.001) and middle vs lower (##p<0.001 and ###p<0.001).

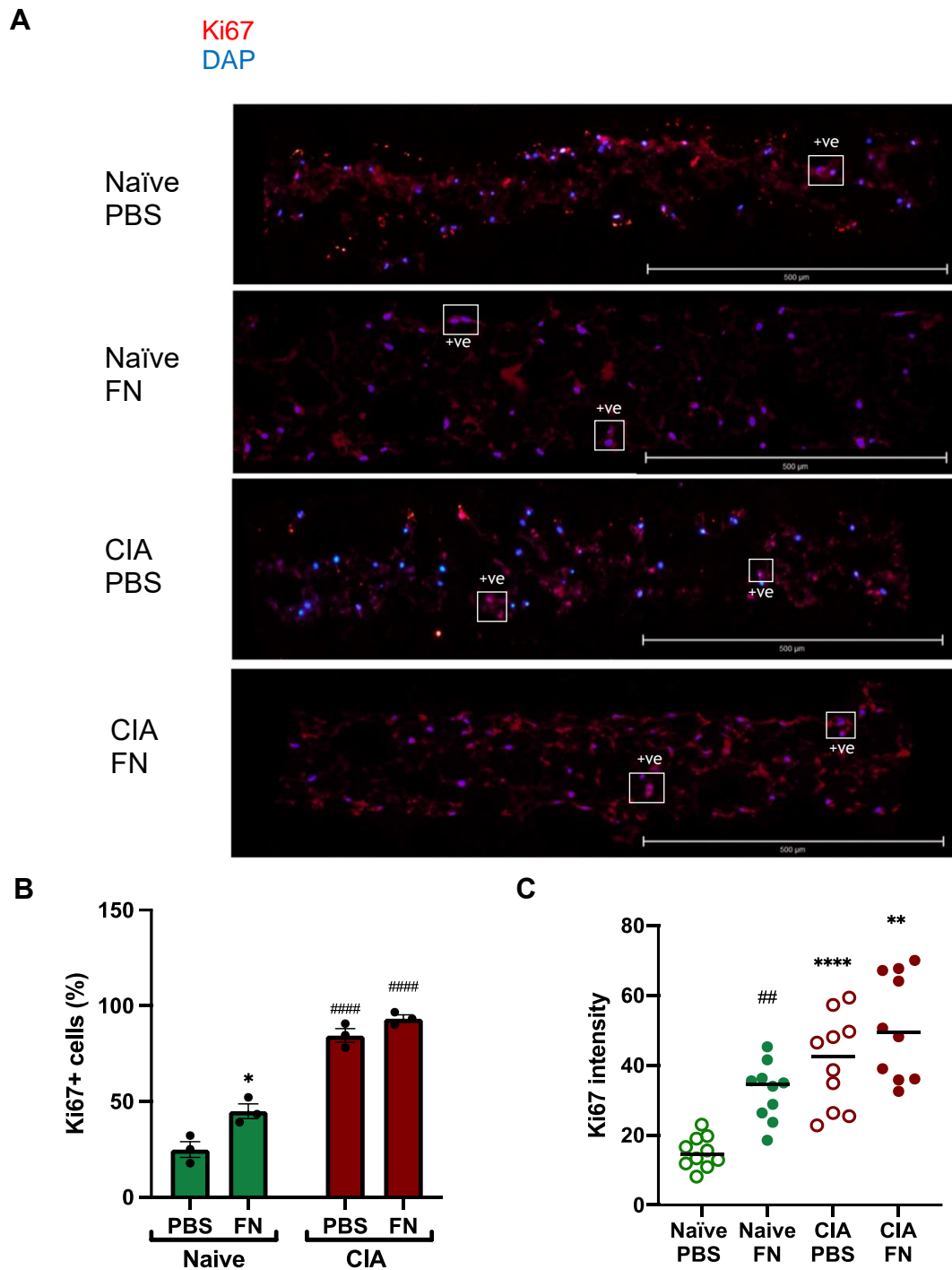


**Figure 4-8: The effect of FN on the proliferation of SFs.**

(A) Naïve and CIA SFs were cultured in Alvetex® for 7 days in the presence and absence of FN, after which immunofluorescence was carried out to stain for Ki67 (red) and counterstained with DAPI (blue). Images were taken on a EVOS brightfield microscope at x10 magnification (scale: 500  $\mu$ m). Ki67+ cells highlighted in white boxes. (B) The percentage of Ki67+ cells in each condition, showing means  $\pm$  SEM, where each dot represents a biological replicate (mean of technical triplicates), bar shows the mean. (C) Intensity of ki67+ cells, where each dot represents the intensity of an individual cell, bar shows the mean. Statistical significance was evaluated by ordinary one-way ANOVA and Tukey's test for multiple comparisons; Naïve PBS vs CIA PBS or Naïve FN vs CIA FN (\* $p$ <0.05, \*\* $p$ <0.0001, \*\*\*\* $p$ <0.0001) and the Naïve PBS vs Naïve FN or CIA PBS vs CIA FN (## $p$ <0.01, #### $p$ <0.0001).

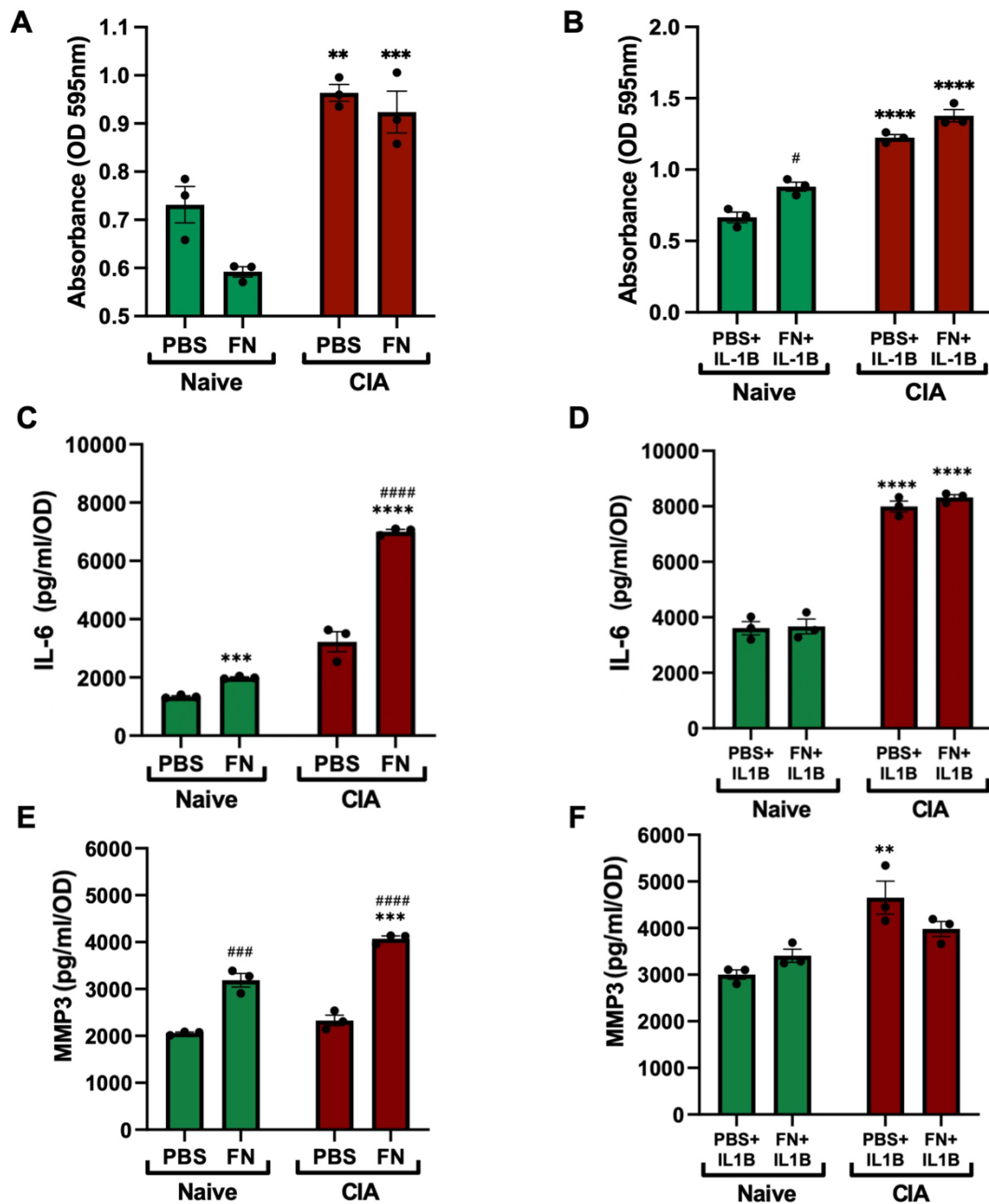
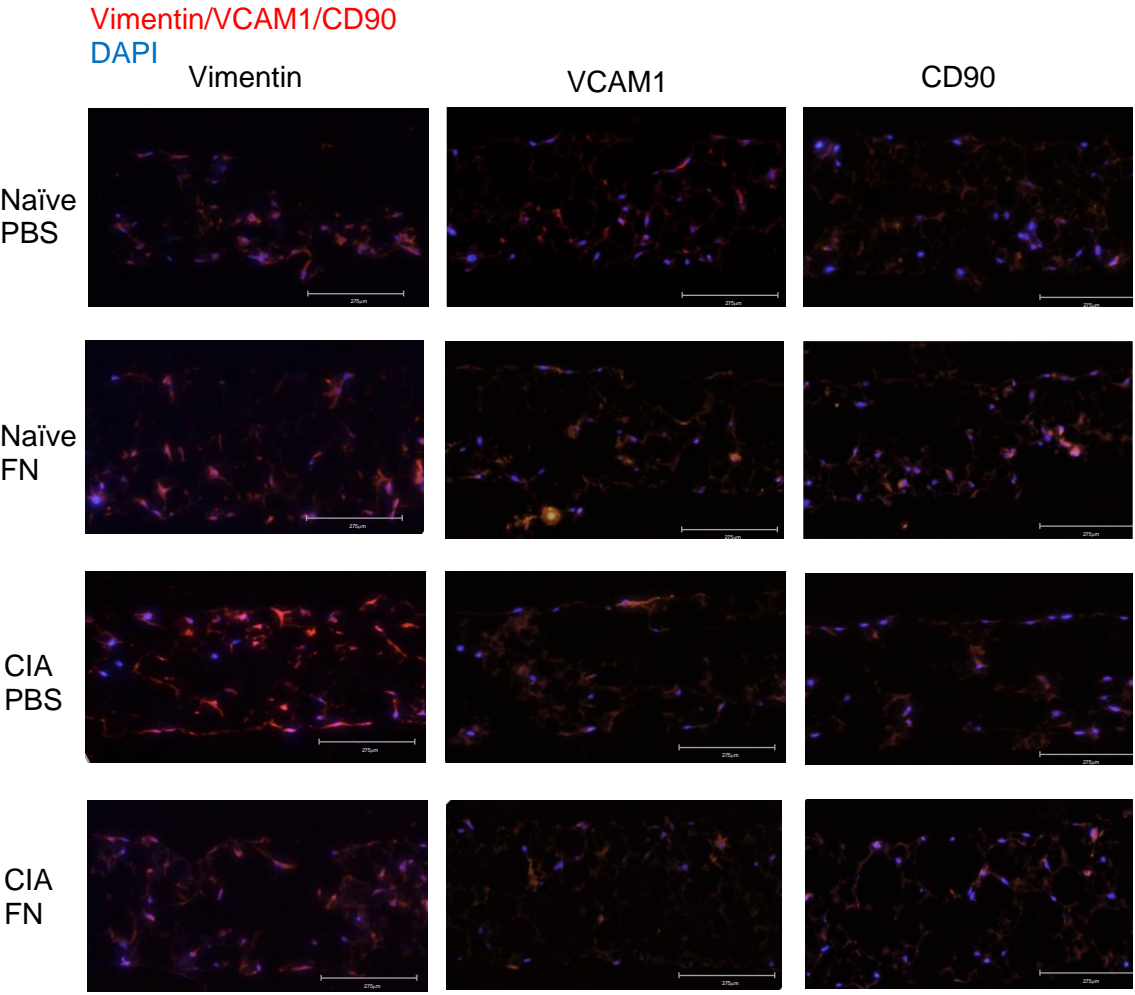


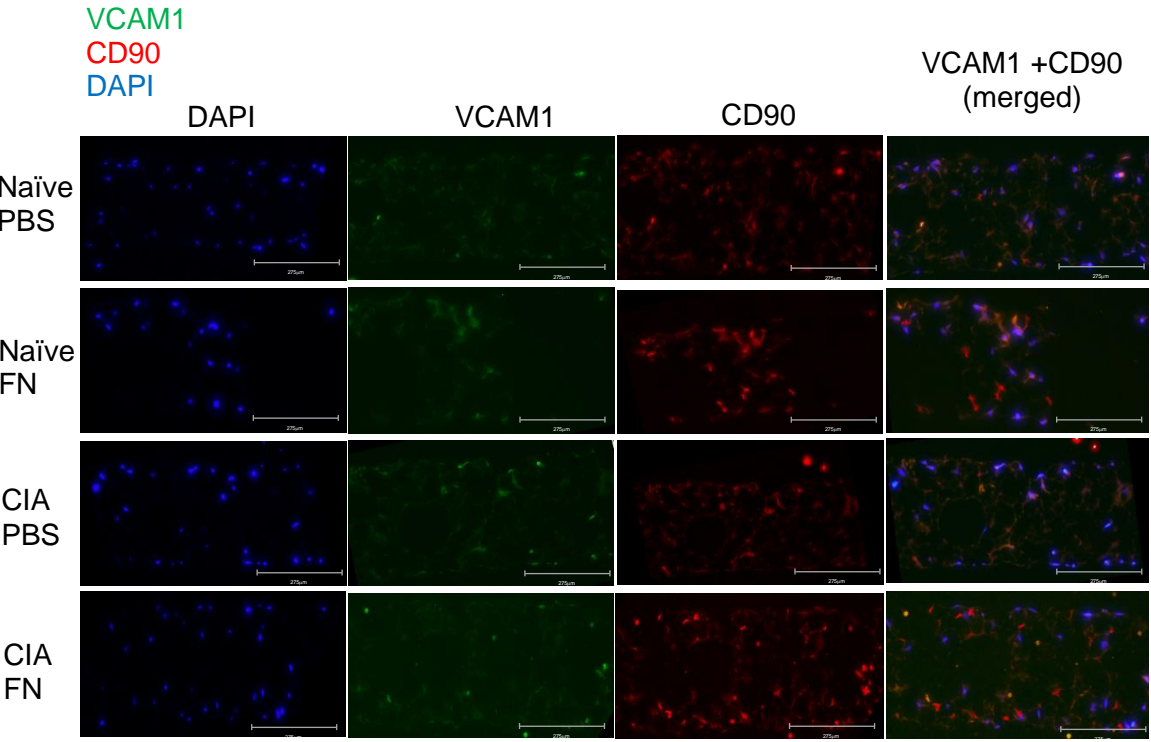
**Figure 4-9: Effects of FN and IL-1 $\beta$  stimulation on MMP3 and IL-6 secretion in SFs in Alvetex®.**

ELISA analysis of IL-6 and MMP3 released by Naïve and CIA murine cells expanded in 2D and cultured for 7 days in Alvetex® in the presence and absence of both FN as well as  $\pm$  overnight IL-1 $\beta$  cytokine stimulation was carried out. The staining of crystal violet was measured by absorbance (A) in the absence (B) and presence of IL-1 $\beta$  stimulation. The cytokine concentration was determined by ELISA and data were normalized with the crystal violet absorbance values. Cytokine expression of (C) IL-6 in the absence and (D) presence of IL-1 $\beta$  stimulation and (E) MMP3 expression in the absence and (F) presence of IL-1 $\beta$  stimulation (are shown. Data show means  $\pm$  SD, with each dot representing a biological replicate (in technical triplicate). Statistical significance was evaluated by ordinary one-way ANOVA and Tukey's test for multiple comparisons; Naïve PBS vs CIA PBS or Naïve FN vs CIA FN (\*\* $p < 0.001$  and \*\*\*\* $p < 0.0001$ ) and Naïve PBS vs Naïve FN or CIA PBS vs CIA FN (### $p < 0.001$  and #### $p < 0.0001$ ).

**A**



**B**



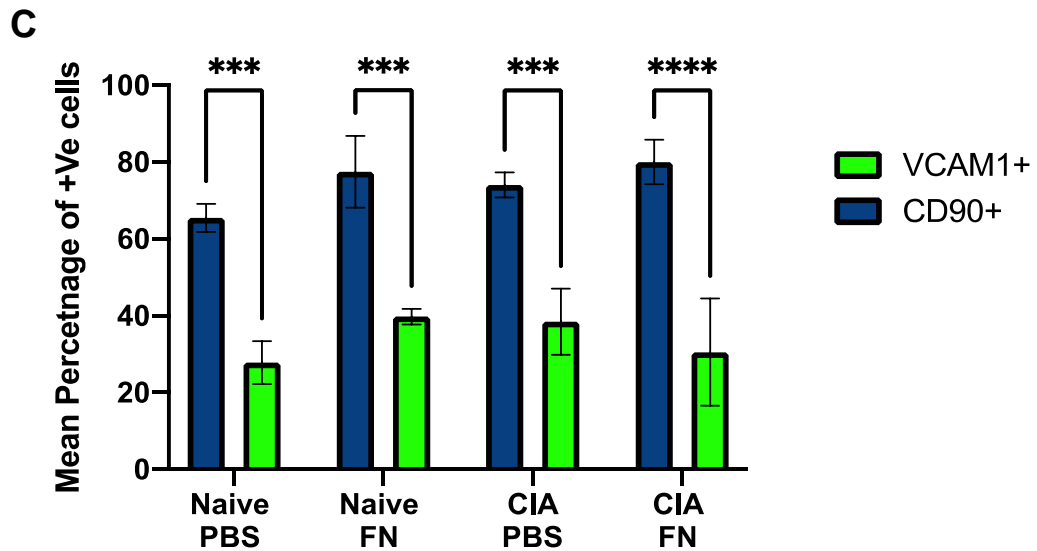


**Figure 4-10: Expression of stromal marker vimentin and by SF subset markers - VCAM1 and CD90 - in the presence and absence of FN.**

A-B Prior to staining, Naïve and CIA SFs were cultured in Alvetex® in the presence and absence of FN after which immunofluorescent staining was carried out for lining SF subset VCAM1 (green) and sub-lining SF subset CD90 (red) (A) and both subsets combined VCAM1 (green) and CD90 (red) and merged (B) Images were taken on a fluorescent microscope at x20 magnification (scale: 275  $\mu$ m). (C) Mean percentage of VCAM1+ and CD90+ SFs from 3 sections of Alvetex® (merged staining) in triplicate. Identification and cell counting of staining was carried out using ImageJ. Data show means  $\pm$  SD. Statistical significance was evaluated by two-way ANOVA and Tukey's test for multiple comparisons between each individual condition (\*\* $p < 0.001$  and \*\*\*\* $p < 0.0001$ ), no significance was found between VCAM1 or CD90 conditions.

# Chapter 5 Use of fibronectin pegylated hydrogels to study the responses of Naïve and CIA-SFs to determine if this platform supports recovery of functional specialization

## 5.1 Introduction

The Alvetex® scaffolds employed for studying SF responses in Chapter 4 were shown to be potentially beneficial for studying SF biology in inflammatory arthritis as in terms of some parameters they appear to provide a more *in vivo* like environment. As useful as these polystyrene scaffolds may be in studying SF cell biology, they have their own limitations, specifically their fixed rigidity. Thus, to more fully understand their cell physiology and the cues interpreted by SFs in the synovium during disease development, culture systems exhibiting less restricted movement/interactions of cells could prove more advantageous in terms of studying cell migration and consequently, their anatomical distribution.

Unique 3D culture systems are constantly being developed and improved to recreate particular *in vivo* environments. Hydrogels provide experimental models that have become increasingly popular because of their properties such as softness, flexibility, biocompatibility and high-water content that allow them to be used in a wide range of research areas, specifically because they offer the ability to accurately control mechanical properties of the material. Hydrogels are often used as mimics of the ECM as they can be synthesized to provide precise control over physical properties such as stiffness, and chemically modified to present ECM components, particularly biologically active peptides (Blache, Stevens and Gentleman, 2020). The latter allows a great deal of flexibility when investigating individual parameters, for example the stiffness can be altered depending on the rigidity of the tissue being investigated. Structurally, they comprise three-dimensional crosslinked networks of hydrophilic polymer chains involving covalent and/or non-covalent interactions (M. Trinadha et al., 2021). The hydrophilic nature of the hydrogels permits expansion and allows for the uptake of cells, growth factors and intervention reagents (Kim et al., 2015; Sun et al., 2016; Ahmed, 2015), whilst maintaining their structural integrity. Their

high-water content and viscoelastic polymeric networks also allow maintenance, to a certain extent, of flexibility comparable to that of natural tissue. (Chai, Jiao and Yu, 2017; Yu, Chen, Chai and Ayres, 2015). However, water retention in hydrogels is dependent on the precise structure, crosslinking density, composition of gel and method of synthesis. Therefore, given the malleable and adaptable nature of hydrogels with regards to their mechanical properties such as stiffness and size, they allow for understanding of cell behaviours that may not be seen in non-adaptable, solid or rigid, cultures (Daly, Riley, Segura and Burdick, 2019).

Hydrogels can be categorised depending on the materials (natural or synthetic polymers) used to synthesise them or the physical or chemical crosslinking techniques by which they are synthesised (Silva et al., 2008). Hydrogels created through physical crosslinking of polymers are converted from a liquid to a gel state via environmental changes such as in temperature, pH or ionic concentration, whereas those formed via chemical (covalent bonding) crosslinking offer mechanical integrity and resistance to degradation. Methods used for covalently crosslinking gels include grafting, enzyme reactions, thermo-gelation as well as radical polymerisation (Jabbari, Leijten, Xu and Khademhosseini, 2016).

Synthetic polymers have proved more useful than natural polymers due to their specific design, good mechanical properties and thermal stability. They can also be processed into a variety of shapes, opposed to the limited range of shapes able to be produced with natural polymers (Sionkowska, 2011). However, natural polymers are generally more biocompatible, as those that are synthetic can retain residual chemicals such reaction initiators as well as other impurities that could interfere with the growth of cells (Francis Suh and Matthew, 2000; Leclerc et al., 2004). Furthermore, natural polymers exhibit lower toxicity, biodegradability and are more accessible at a cheaper cost (Shogren and Bagley, 1999) promoting their use in a wide range of fields such as nano drug delivery, gene delivery, pharmaceuticals and cosmetics (Santander-Ortega et al., 2010; Roy, Mao, Huang and Leong, 1999; Shanmugam, Viswanathan and Varadarajan, 2005).

### **5.1.1 Fibronectin Pegylated hydrogels**

This chapter will investigate how hydrogel approaches, developed by Prof Manuel Salmeron-Sanchez in the School of Bioengineering to study cellular responses in cancer, could be used to find new material surfaces that can trigger physiological organisation of extracellular matrix components that mimic those in the RA joint. The hydrogels used are scaffold material constructed from synthetic polymers that combine poly(ethylene) glycol (PEG) and fibronectin into a composite polymeric hydrogel (Almany and Seliktar, 2005). These fibronectin pegylated (FNPEG) hydrogels offer the possibility of a model that allows a better understanding of the role of SFs and their sub-populations in RA as they are extremely biocompatible (Berri, Fares and Fares, 2018; Merrill and Salzman 1983) and display adaptable characteristics such as degradability and size, dependent on their molecular chain length, weight percentage and the density of crosslinking (Temenoff, Athanasiou, Lebaron and Mikos, 2001). Furthermore, PEG hydrogels are also able to undergo gelation, a controlled transition from liquid-to-solid state whilst in a cell suspension (Elbert and Hubbell, 2001) which can be achieved under harmless, non-toxic conditions by use of a photoinitiator (Elisseeff et al., 2000; Nguyen and West, 2002) and combining crosslinking components with a reactive solution of the functionalised PEG (Lutolf and Hubbell, 2003; Almany and Seliktar, 2005). This allows cells to be added to the gel, whilst it is still in a liquid state, ensuring their dispersal throughout.

The tissue and anatomical environment plays a major role in how cells function and morphology and reflecting this, the “stiffness” and mechanical properties of the ECM regulate cell behaviour (Yue, 2014; Urbanczyk, Layland and Schenke-Layland, 2020). Therefore, as hydrogel stiffness is easily adjustable through concentration changes of thiol linking crosslinkers, stiffness of the matrix is a key experimental parameter that can be examined in such *in vitro* cell cultures. This is particularly useful in SF research as in RA the synovium becomes “stiffer” - from ~5 kPa in a synovium to ~10 kPa - due to pannus formation and cell infiltration. Thus, the ability to change the stiffness of the hydrogel through a physiologically relevant kPa range, may allow for a better understanding of pathogenic changes in cell functions occurring in the arthritogenic environment of the joint. Another important property of hydrogels is swelling, which is the volume of water/buffer

absorbed into the hydrogel. This usually occurs a few days after incubating in media and resolves after a couple of days when the gel settles into the liquid environment (Trujillo et al., 2020). It is easily measured and an indicator of the polymer network hydrophilicity, as well as the relative crosslinking density, in which there is less swelling shown by stiffer gels. Degradation of hydrogels can result in differences in mechanics and swelling as time progresses, resulting in changes in cell behaviour such as motility, spreading and traction force generation (Khetan et al., 2013).

As mentioned previously in our ECM studies to this point, we had focused on FN, as it is found within the synovium and synovial fluid of RA patients an elevated level (Chang et al., 2005), making it a good ECM component to study SF interactions in inflammatory arthritis, due to its role in initiation of joint inflammation. Specifically, within the synovial lining FN impacts on the management of cellular interaction networks via attachment of SFs to their encompassing matrix environment. Moreover, the expression of this ECM molecule at the basal lamina as well as the endothelial surface of swollen and inflamed synovium has been found to act as a migration path for infiltrating lymphocytes, allowing cells to pass through the endothelial basement membrane in RA. Furthermore, displaced expression of FN in RA also facilitates aberrant cell adhesion with a considerable amount of FN being expressed in the pannus, resulting in the enhancement of SF adhesion to the cartilage and balancing invadopodia through the encouraging consistent regions of attachment that aid in invasion of the cartilage (Buckley, Ospelt, Gay and Midwood, 2021).

Importantly, FN can be adsorbed onto a varying range of surfaces, including synthetic PEG hydrogels (Missirlis and Spatz, 2013). In hydrogels, incorporation of FN has been shown to influence cell viability and the encouragement and advancement of adhesion properties in hydrophilic surfaces (Baugh and Vogel, 2004) as well as fibrillogenesis (Bieniek et al., 2019) and binding to various integrins (Keselowsky, Collard and García, 2003), underlining its adaptor role within the ECM (Pankov and Yamada, 2002). As FN contains binding sites (Leiss et al., 2008) for molecules such as collagen and fibrin, the use of full-length FN (as opposed to fragments) within synthetic hydrogels is therefore advantageous and desirable, allowing the recapitulation of the biological activity of FN in the ECM

(Trujillo et al., 2020). For example, such incorporation of FN within the hydrogel allows for a more physiological modelling of the reticular nature of ECM as opposed to that of 2D and polystyrene scaffold culture systems, where the ECM components can only coat the rigid surfaces and this can be studied under conditions where the chemical and mechanical properties can be manipulated and adapted to create a culture system best suited to the cell type (Almany and Seliktar, 2005).

Non-degradable hydrogels allow control over the polymer architecture, making them a favourable choice for experiments that do not focus on the structural integrity of the ECM-mimicking hydrogel (Trujillo et al., 2020). However, natural hydrogels generated by polymerisation of fibronectin and collagen have been shown to be degraded by cell-mediated proteases such as MMPs and this property allows for the study of how MMP-secreting SFs interact with the ECM. Thus, FN is of particular interest to our studies, as in addition to providing cell adherence, using FN as a backbone provides the hydrogels with inherent potential for degradation via through cell-mediated proteases (Elbert and Hubbell, 2001). Indeed, relevant to this, synthetic hydrogels are now being developed exploiting degradable peptide crosslinkers (Lutolf et al., 2003) that provide specificity in terms of investigating the differential roles of potential target proteases (Zheng et al., 2011). For example, the enzyme cleavable peptide sequence GCRDVPMSMRGGDRCG (VPM) can be incorporated into the hydrogel backbone to give synthetic hydrogels the capacity to be proteolytically degraded by cell secreted enzymes, with it shown to be degraded by proteases such as MMP1, MMP2, MMP9 and MMP13, as well as collagenase (Patterson and Hubbell, 2010; Foster et al., 2017).

## 5.2 Aims

The overall aim of this chapter is to investigate the responses of SFs transferred to FN-containing hydrogels in order to determine if this platform supports recovery of more “physiological” responses lost or non-detectable in classical 2D cultures. Specifically, it was planned to investigate the inflammatory and migratory responses of Naïve and CIA SFs and how these are impacted by FN and stiffness in hydrogels.

To achieve these aims, the synthetic hydrogels used in this study therefore contained full-length human FN protein that is functionalised with PEG-maleimide (PEGMAL), through PEGylation of FN (Figure 5-1) to covalently crosslink the protein to the synthetic hydrogel network. The latter network consists of 4-arm-PEG-maleimide (4-arm-PEG) crosslinked with PEG-dithiol (thiolated crosslinker). Hydrogels were generated both in non-degradable and degradable formats, using the same protocols with the exception of the addition of a protease-cleavable peptide crosslinker such as VPM (GCRDVPMSMRGGDRCG) (Ahmad et al., 2018) to the “degradable gels” to allow the breaking of the structural covalent bonds of the gel over time.

## 5.3 Results

### ***5.3.1 Fibronectin pegylated hydrogels provide a viable culture system for studying SF biology***

We have established that cues from the microenvironment shape the phenotype of cells and affect their cell signalling and responses. In the previous chapter we looked at the effect of a 3D microenvironment in the form of a polystyrene scaffold and incorporated the ECM component FN by coating the scaffold. Despite mitigating against the signalling artefacts induced in classical 2D cultures by incorporating 3D scaffolds such as Alvetex® for growth support, it was considered important to investigate whether SF responses would be further affected if the entire culture system was composed of FN. Thus, FNPEG hydrogels (Figure 5-2A) were exploited to study the response of SFs in a 3D microenvironment as they also allowed for determining the influence of stiffness on cellular responses, by generating such hydrogels with a range of stiffnesses (kPa) more akin to that of the healthy and arthritic synovium. The FNPEG hydrogels used were 5 wt % non-degradable, unless stated otherwise.

Firstly, the viability of the cells within the FNPEG gels was investigated to ensure the formulation of the gels were optimised for SF survival. As was the case with cells cultured in Alvetex®, the cells were expanded in 2D until passage 4, after which they were added to the FNPEG gels and cultured. The viability of Naïve SFs over 13 days was investigated using Live/Dead cell discriminating fluorochromes

and the cells were imaged using fluorescence microscopy (Figure 5-2B). SFs at day 1, 3 and 13 were all shown to have a survival rate of ~70-80%, indicating that the SFs survive well when introduced to the hydrogels from 2D cultures. This further suggests that these hydrogels may be used for longer periods of cell culture as the survival rate at day 13 is consistent with that at days 1 and 3, which could prove beneficial in future investigations.

Having established the SFs survive well in the FNPEG hydrogels, the morphology of the cells was then investigated, using immunofluorescence staining (Figure 5-2C) of actin in order to visualise the cell cytoskeleton, in conjunction with counterstaining of the nuclei. Widefield microscopy revealed the SFs to be ellipsoidal in shape, more akin to what would be seen *in vivo*. Also, the cells were found to have dispersed through the gel presumably as they have room to move and interact within the gel, due to the lack of a rigid structure adhering them in place (2D) or guiding their movement through pores (Alvetex®). The organisation of CIA-SFs within the FNPEG hydrogel was also investigated, in this case by H&E staining of gel sections (Figure 5-2D) which suggested that many of these SFs organise themselves towards the outer portions of the hydrogel. However, only a section of the entire gel could be analysed and imaged in this manner and to further explore this potentially polarised distribution of CIA, relative to Naïve, SFs, FNPEG gels were analysed and imaged by widefield microscopy to allow for a more accurate understanding of SF movement and organisation in this 3D culture system.

### **5.3.2 Organisation and properties of SFs in FNPEG hydrogels**

To visualise the morphology and distribution of Naïve and CIA SFs, the cells were stained for immunofluorescence analysis of their vimentin expression (Figure 5-3). The hydrogels were then imaged using a Leica widefield microscope and LAS X Life Science software, with pictures taken at z-steps of ~10 µm to ensure all cells were included. The tile-scan feature allowed the images to be taken in z-stacks and merged together to get a detailed representation of all the SFs throughout the 3D structure. Following this, the merged images were deconvoluted and processed using IMARIS software to obtain 3D reconstructions (Figure 5-3) of the hydrogels, ready for further IMARIS analysis of cell morphology. The FNPEG gels

were stained with vimentin to not only ensure that the cells within the gel were indeed stromal cells but also allow optimisation the imaging method. It allowed the recording of the position and protein expression of each single cell in the hydrogel in turn granting the generation of a unique and detailed method to map and quantify single SFs within a 3D microenvironment. This experimental method not only allowed for the visualisation of Naïve (Figure 5-3A) and CIA (Figure 5-3B) SFs and their location throughout the entire gel, but also granted analysis of morphological parameters such as volume, area, sphericity and staining intensity of every cell. Imaging using a widefield microscope in conjunction with IMARIS software therefore proved to be powerful tool in understanding SF properties and how they organise and move within FNPEG hydrogels.

To develop a better understanding of the (potentially distinct) morphology of Naïve and CIA SFs, a range of associated parameters were investigated (Figure 5-4). This revealed that the volume of cells (Figure 5-4A) is significantly greater in Naïve SFs as opposed to CIA-SFs, and consistent with this, this is also the case for the area of the individual cells (Figure 5-4C). However, there was no significant difference in the sphericity of cells between the groups (Figure 5-4B), indicating that despite differences in volume and area, SFs in both conditions still to an extent maintain their spherical appearance. The sum intensity of vimentin staining for every SF in each condition was then examined (Figure 5-4D), with a significant increase in the intensity in CIA- relative to Naïve-SFs, which could be due to the CIA-SFs perhaps exhibiting a more extensive cytoskeleton.

Having established that morphological parameters can be determined using IMARIS software and that Naïve and CIA present distinct morphological characteristics when cultured in hydrogels, potential differences in the organisation and location of Naïve and CIA SFs within the FNPEG hydrogel microenvironment were then investigated (Figure 5-5). The organisation and location of the SFs within the FNPEG hydrogels was established using IMARIS software that computed and pinpointed the location coordinates of every individual cell. Thus, the X, Y and Z positions of the cells were calculated in relation to the gel border (Figure 5-5A) by the IMARIS software. The cells were added to the gel in its liquid state prior to curing and thoroughly mixed to be dispersed throughout the gel, prior to the

analysis period. However, it can be seen from the percentage of positively stained DAPI (Figure 5-5B) and vimentin (Figure 5-5C) cells, that there are more CIA SFs located towards the edge of the hydrogel as opposed to Naïve SFs which appear to be more evenly distributed through the hydrogel. This is particularly interesting given that there are a greater number of CIA vimentin positive cells (Figure 5-5D) compared to Naïve and yet despite more cells the CIA-SFs locate towards the outer regions of the hydrogel.

### ***5.3.3 Organisation of SF subsets in FNPEG hydrogels***

The above analysis suggests that the organisation and movement of SFs within the culture system can be tracked, and we therefore exploited this methodology to investigate whether lining and sublining phenotypes can be detected to have differentiated within the gel and if so, whether they adopt distinct locations within the FNPEG hydrogel.

To achieve this, immunofluorescence staining of the differential markers of lining (VCAM1) and sublining (CD90) SFs (as well as nuclear counterstaining with DAPI) was carried out. Images were then taken on a widefield microscope after which 3D reconstruction of hydrogels containing Naïve (Figure 5-6A) and CIA SFs (Figure 5-6B) within the hydrogels was created and analysed using IMARIS software to quantify the intensity of both markers as well as the number and percentage of cells positively stained for each marker under both conditions (Figure 5-7). The intensity of staining of both VCAM1 and CD90 was significantly greater in Naïve compared to CIA SFs, which may be due to differences in cell volume (Figure 5-4A) and area (Figure 5-4C) observed previously with Naïve SFs presenting significantly higher for both. Therefore, the reason the intensity of each marker is greater in Naïve SFs may be based on the fact the cells appear to be larger, when staining for subset markers.

Interestingly, when investigating the number of positively stained cells for each marker (Figure 5-7B), we found that there was a greater number of CD90-positive, compared to VCAM1-positive Naïve SFs, whilst CIA-SFs displayed almost equally positive staining for each marker. This was further corroborated with the percentage SFs positively stained for each marker (Figure 5-7C), showing a similar

trend. The latter proportions are similar to what would be observed when extracting SFs immediately *ex vivo*.

This would suggest that in non-arthritic conditions the balance between subpopulations is tipped in favour of CD90 positive SFs - responsible for more pro-inflammatory responses when activated. However, in arthritic conditions there is more of balance between the subsets, with both bone and cartilage erosion and pro-inflammatory responses present. This could perhaps suggest that hydrogels may prove to be especially useful for studying sublining SFs, and their role in RA pathogenesis. That there were less CIA-SFs, compared to Naïve SFs, detected this is most likely due to differential seeding, rather than their ability to survive within the gel.

IMARIS software analysis was then carried out to determine the relative gel distributions of the SFs subsets from Naïve and CIA mice by determining the distance from the gel border of individual cells for each subset and treatment group to generate 3D scatter plots using Matlab (Figure 5-8). This confirmed the relative increased abundance of CD90+ relative to VCAM1+ SFs in the Naïve but not CIA group. Both subsets of Naïve SFs were found to be located throughout the entire gel, dispersed fairly evenly despite the difference in cell number (Figure 5-8A). The same can be said of the CIA-SF subsets (Figure 5-8B) as there does not seem to be any organisation of the subsets into anatomically relevant regions. Similarly, this is observed in Figure 5-8C as the percentage of VCAM1 and CD90 positive Naïve and CIA SFs correlates with those seen in Figure 5-8A and B, respectively.

#### ***5.3.4 Synovial fibroblast responses in degradable and non-degradable FNPEG hydrogels***

As mentioned in section 5.1.4 hydrogels were produced either to be degradable or non-degradable, both of which have their own technical advantages. For example, non-degradable hydrogels are best suited for studies related to imaging or immunofluorescence as they allow for the gel to maintain its shape, due to the stability of the covalent bonding, as well as allowing for cells to be studied over a longer period of time e.g., for conducting the time course experiments on cell

viability (Figure 5-2B). However, for analysis requiring harvesting of SF from the gels, for example, extracting the cells for RT-PCR analysis of inflammatory mediators proved difficult whereas the use of degradable hydrogels allows for the cells to be extracted easily and efficiently providing better and more pure yields of RNA. Initially, comparison of the CCL2, IL-6 and MMP3 responses of Naïve and CIA SFs cultured in non-degradable hydrogels for 7 days (Figure 5-9A) showed that there was a downregulation in MMP3, IL-6 and CCL2 cytokine secretion from Naïve to CIA, as opposed to the increase observed in Alvetex®. However, the non-degradable format may not be the best for cytokine studies as the majority of the protein remains within the gel itself. Therefore, the same experiment was repeated with degradable hydrogels (Figure 5-9B). Due to the addition of the VPM peptide that promotes the degradation of the gel, the experiment had to be carried out at day 3 as opposed to day 7 with non-degradable. It could be seen that the production of MMP3 in the degradable gels was significantly higher as was the production of IL-6. The secretion of CCL2 was also increased from Naïve to CIA. In order to investigate whether the latter was due to the time point in which it was carried out, the experiment was repeated using non-degradable hydrogels after 3 days of SF culture (Figure 5-9C). The results showed that there was an increase in the production of CCL2, whilst IL-6 production decreased when comparing Naïve and CIA cells. Interestingly, the MMP3 concentration was significantly elevated. However, as the degradable hydrogels are more responsive to the effects of MMP due to the presence of MMP sensitive VPM within the gel (Foster et al., 2017), the MMP3 secretion observed may have an effect on the integrity of the hydrogel. In the degradable hydrogels the upregulation of MMP3 and other MMPs are degrading the gel and therefore in turn there is greater release of MMP3 in this gel type. However, when the experiment was repeated in non-degradable gels at day 7, where the gels were not affected by the MMP activity, an upregulation of MMP3 by CIA-SFs is not observed. Furthermore, the significant upregulation of IL-6 seen in the degradable gels may not be due to the CIA-SFs producing more of the cytokine but because upregulated MMP production degrading the gel results in more IL-6 being released from by CIA-SFs compared to Naïve. Therefore, an artefactual result could be observed due to the quicker degradation of the gel with CIA-SFs.

Both degradable and non-degradable hydrogels appear to show differing results and whilst degradable hydrogels may be the best method to perform RNA studies, the MMP sensitivity that in turn affects the hydrogel integrity may make this conventional approach to measure cytokines secretion unsuitable for SFs, as the latter are designed to remodel the matrix. The above may provide rationale for the use of non-degradable hydrogels for cytokine secretion studies. However, in order to gain more clarity over these differing results, RNA-Seq would need to be carried out to get a full transcriptomic profile of the cells.

### ***5.3.5 The impact of cells and media on the stiffness of degradable FNPEG hydrogels over time***

To investigate the effect of joint swelling resulting from inflammation on SF responses, it was decided to monitor the behaviour of Naïve and CIA SFs in FNPEG hydrogels of differing stiffness. Firstly, it was necessary to optimise the composition of the FNPEG hydrogel, without the addition of cells or media, in order to obtain baseline stiffness values (Figure 5-10). This was achieved by synthesising degradable hydrogels (section 1.5.2), of 3 %, 5 % and 10 % FNPEG after which the elastic modulus (kPA) at multiple locations of each hydrogel at days 0, 3 and 7 were measured using nanoindentation (Figure 5-10A). As degradable hydrogels are required for RT-PCR analysis in order to extract the sufficient quality of RNA, these were used to allow a direct correlation between stiffness and functional responses. The range of FNPEG % was chosen to provide an understanding of the outcome of various pathophysiological levels of rigidity on SF responses. In the studies outlined above, analysis was carried out with 5% hydrogels as these exhibit the stiffness closest to the that of synovial fibroblasts in a healthy synovium (Xu et al., 2020). However, to mimic the effects of the infiltration of cells, thickening of the pannus and swelling, 10% gels were selected as this would provide a stiffness, comparable to the arthritic synovium. A set value of the stiffness of an arthritic synovium has yet to be established and so 10% hydrogels were used as this is double that of the healthy synovium. Thus, to characterise a spectrum of effects, hydrogels spanning 3-10% FNPEG were analysed. During the nanoindentation process, a calibrated indenter tip approaches the surface of the sample generating force-displacement data that is used to determine the point of contact. After the sample is contacted, the force

is linearly increased and the tip indents into the surface of the sample, providing the kPa value (Figure 5-10B). This showed that despite the addition of the VPM (peptide that encourages degradation of the hydrogels), the hydrogels remain relatively stable in the presence of PBS alone. Moreover, consistent with previous studies (Trujillo et al., 2020), it can be seen that these 3 % hydrogels were found to have a kPa of between 2 and 4, whilst the 5 % hydrogels presented kPa values of between 3 and 6 and kPa values of between 5 and 8 were observed with 10 % hydrogels (Figure 5-10C). The maintenance of kPa values was corroborated by the average curves determined for the elastic modulus of each FNPEG hydrogel at days 0, 3 and 7 (Figure 5-10D). The average elastic modulus of 3, 5 and 10 wt % FNPEG hydrogels measured at day 0, 3 and 7 showed that, whilst the stiffness remains relatively consistent for 3 %, 5 % and 10 % gels individually, the stiffness of the different FNPEG hydrogels can be clearly distinguished from one another over the 7-day period. Although during culture with PBS alone the stiffness remains relatively stable over the 7 days, there is, however, a significant difference between days 0 and 7 in 3 % and 5 % hydrogels and on day 3 of the 10% FNPEG hydrogels, most likely due to swelling of the gel overtime (Figure 5-10E).

Having established baseline kPa values, the impact of DMEM medium and Naïve SFs on gel stiffness was explored (Figure 5-11) because these cells likely secrete MMPs that target VPM and DMEM medium appears to promote some spontaneous hydrogel degradation (Valdes and Moussy, 2000). Visualisation of the SFs within the gels (using light microscopy) showed that the cells were dispersed within the gels at all three timepoints (Figure 5-11A). It was found that over time there was a decrease in the kPa values both in the presence of media alone as well as in the presence of cells. Nevertheless, at each time point the gels were “softer” with the presence of cells, as opposed to medium, which was as expected given the cells spontaneously release (basal levels) of enzymes that can degrade the hydrogels due to the presence of VPM (Figure 5-11 B-D). Similar findings (apart from with respect to the degree of the change) were observed in gels of all three “stiffnesses”, with the exception that in the 5% gels at day 3 the addition of cells resulted in a lower kPa than in day 7, which could be due to swelling of the hydrogels that has previously been shown to occur at day 3 (Trujillo et al., 2020) and results in ‘softer’ gels. The average elastic modulus of 3, 5 and 10 wt % FNPEG

hydrogels measured at day 0, 3 and 7 in media, with and without SFs can be seen in Figure 5-11E, and it can be concluded that the addition of media and/or cells impacts the stiffness of the degradable hydrogels as degradation occurs within a 7-day period, predominantly by day 3.

Following this characterisation of the effect of Naïve SFs, similar investigation of the impact of CIA-SFs and media was carried out (Figure 5-12) but focusing only on 3 % and 5 % FNPEG degradable hydrogels. Similarly, to that observed with Naïve SFs, CIA-SFs can be seen to be dispersed within both the 3 % and 5 % FNPEG gels (Figure 5-12A). The media can again be seen to have an impact on gel stiffness, exhibiting decreased kPa values for both the 3 % (Figure 5-12B) and 5 % (Figure 5-12C) gels over time. Also, as seen with the Naïve FNPEG hydrogels, the stiffness of the CIA-SFs FNPEG hydrogels also decreased, but unlike the gradual decrease over days 0, 3 and 7 observed with Naïve SFs, this was far greater and more sudden between days 0 and 3 for the 3% and 5% FNPEG hydrogels, with both showing significant decrease in stiffness. The average elastic modulus observed from the 3, and 5 wt % FNPEG hydrogels measured at day 0, 3 and 7 in media, with and without SFs (Figure 5-12D) clearly show this sudden decrease in the mean Young's Modulus at day 3, after which it remains somewhat constant at day 7. The reasoning for this could be the pro-inflammatory 'aggressive' phenotype of the CIA-SFs and their enhanced release of MMPs and cytokines (via paracrine and autocrine stimulation of CIA-SFs) that further promotes the VPM-targeted hydrogel degradation. Although the effects for media alone in terms of stiffness should be comparable to those seen in Figure 5-11, this did not appear to be the case: the reason for this is unknown but may reflect differences in batches of the media.

### ***5.3.6 Stiffness influences SF function in degradable FNPEG hydrogels***

Having established that the presence of SFs can influence the kPa of the hydrogels, it was investigated whether the microenvironmental stiffness impacts cell function (Figure 5-13). Specifically, the focus was on matrix remodelling capacity and thus in addition to the expression of matrix protease (Mmp3), the impact on the cell adhesion gene, Ctgf (also known as Ccn2), which appears to play a role in the regulation of the ECM in the inflammatory pathologies of RA (MacDonald et

al., 2021), was assessed. Likewise, expression of Sparc, which has been found to be involved in ECM synthesis and promotion of changes in cell shape was evaluated as overexpression of SPARC has also been associated with increased tumour invasion and metastasis through its effects on matrix composition and cell adhesion (Liu et al., 2019).

Expression of Mmp3, Ctgf and Sparc mRNA was determined in Naïve SFs cultured in conventional 2D plates or 3 %, 5 %, 10 % degradable FNPEG hydrogels to identify differences in their expression resulting from culture in 2D vs 3D systems and also changes in the “stiffnesses” of the microenvironment (as the hydrogels contained cells expanded in 2D, expression at day 0 in the hydrogels was not carried out). Mmp3 expression (Figure 5-13A) was found to be significantly elevated in 3 % gels at day 3 and to a lesser extent at day 7 (relative to that maintained in 2D cultures) but increased gel stiffness showed decreased expression, perhaps consistent with the low Mmp3 expression in the SFs cultured on rigid (~10,000 kPa) 2D plates (Skardal, Mack, Atala and Soker, 2013) at all three timepoints. Perhaps surprisingly, therefore, Ctgf expression (Figure 5-13B) in SFs grown on the 2D platform was significantly greater than those grown under any of the gel conditions, especially as those grown in the higher stiffness gels exhibited the lowest levels of expression. Finally, Sparc expression (Figure 5-13C) was found to be elevated in SFs grown in all three stiffnesses of hydrogels relative to those cultured in 2D, although there was a trend for the cells from the higher stiffness gels to show the lowest levels of expression within the hydrogel group. Collectively, these data indicate that the 2D vs 3D microenvironment as well as stiffness does indeed have an effect on cell function but to gain a deeper understanding of exactly how stiffness affects cell function, further investigations need to be carried out.

## 5.4 Concluding remarks

The data reported in this chapter suggest that hydrogels may prove to be a useful model for studying SF differentiation and function, particularly the sublining subset. This may reflect the capacity of hydrogels to allow free movement and organisation of SFs in a manner that is not influenced by a scaffold structure, and thus cannot be achieved in 2D or rigid 3D models such as Alvetex®. Hydrogels have

proved a particularly useful platform for imaging SFs and their cellular responses, the non-degradable formats, allowing for more ease of imaging and long-term culture whilst degradable hydrogels allowing, more efficient analysis of molecular responses which require cell harvesting/extraction.

In the next chapter, gene expression in Naïve and CIA SFs, not only from cells cultured in a 2D, Alvetex® and degradable FNPEG hydrogels but also from SFs extracted directly from the joint will be further investigated. The freshly isolated SFs will provide a baseline for the other models, allowing investigation into which culture systems are most effective at maintaining the *in vivo* transcriptional programming of SFs *in vitro* and hence, allowing analysis of the most pathophysiologically-relevant responses and promote our understanding of the mechanisms of SF pathogenesis found within the joint.

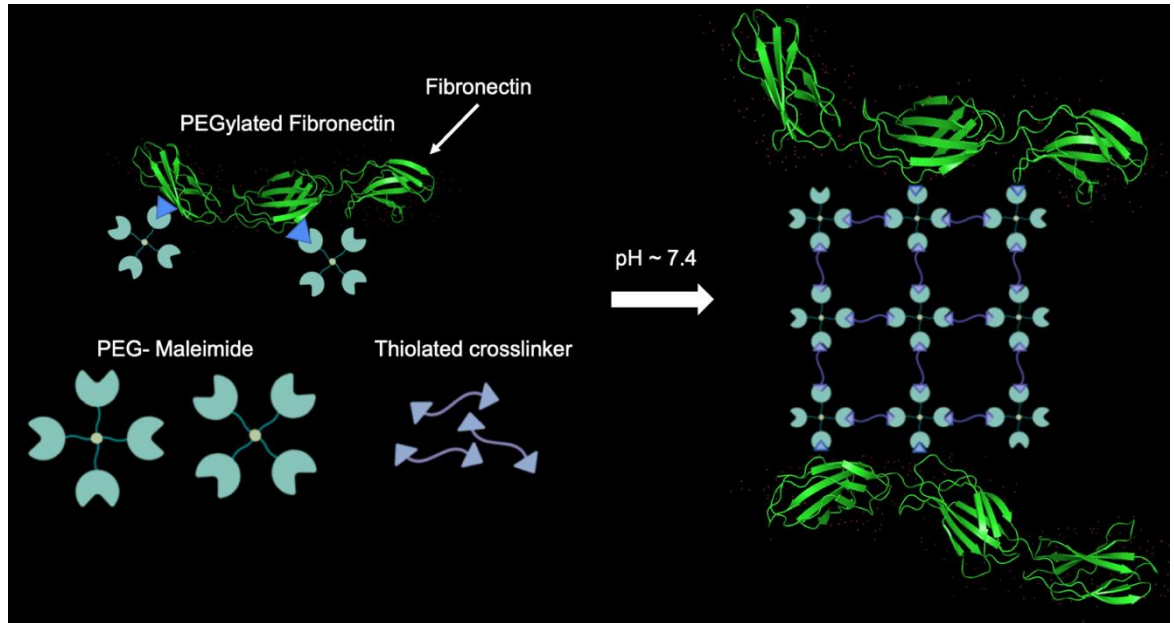
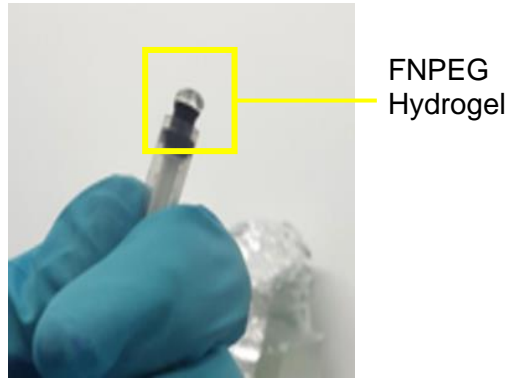


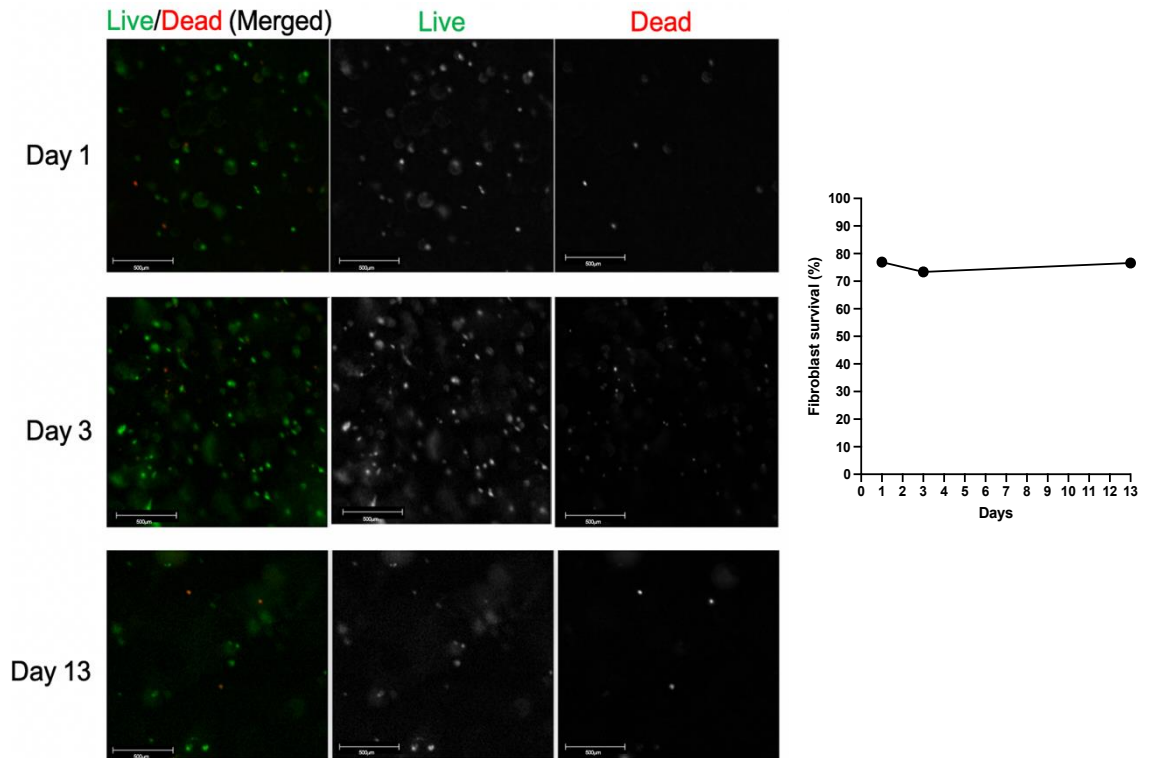
**Figure 5-1: Schematic diagram of hydrogel formation.**

PEG hydrogels were formed using Michael-type addition reaction under physiological pH and temperature. PEGylated FN was added to PEGMAL, then the thiolated crosslinker was added, at a molar ratio 1:1 maleimide:thiol to ensure full crosslinking. The crosslinkers used were either PEG-dithiol or mixtures of PEGSH and protease-degradable peptide, flanked by two cysteine residues (VPM) to create the hydrogel (adapted from Trujillo et al., 2020 and created with BioRender.com).

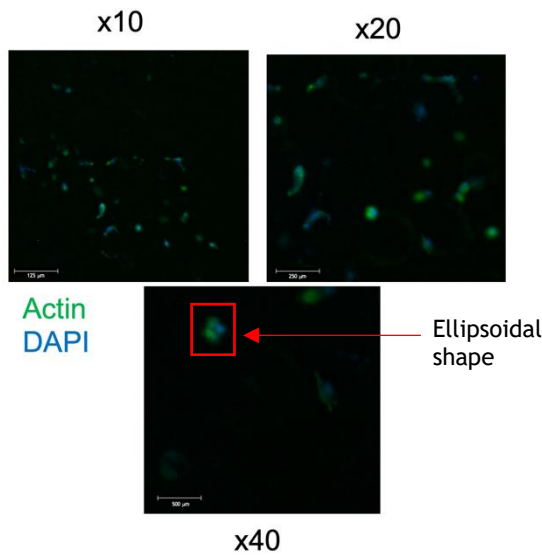
A



B



C



D

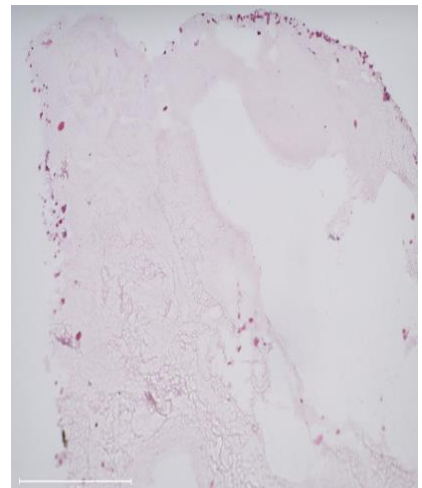


**Figure 5-2: Cell viability is not compromised by 3D culture in non-degradable 5 wt % FNPEG hydrogels.**

**(A)** Photographic image of FNPEG hydrogel. **(B)** Cellular viability of Naïve SFs expanded in 2D until passage 4 and then cultured in a FNPEG hydrogel. Representative microscope images of SFs stained with calcein AM (live) and ethidium homodimer (dead) viability staining kit at days 1, 3 and 7 in non-degradable FNPEG hydrogel using LIVE/DEAD<sup>®</sup> assay (Molecular Probes) (Life Technologies, Dublin, Ireland). The live cells were stained green, and the dead cells stained in red at x10 magnification (scale: 500  $\mu\text{m}$ ) using fluorescence microscopy (left). Survival of SFs at days 1, 3 and 13 represented graphically correlating with Live and Dead assay images (right). **(C)** Immunofluorescent staining was carried out of Naïve SDs to stain for Actin (green) and counterstained with DAPI (blue) in order to observe cell morphology. Images were taken using a widefield microscope at x10 (scale: 125  $\mu\text{m}$ ), x20 (scale: 250  $\mu\text{m}$ ) and x40 magnification (scale: 500  $\mu\text{m}$ ) **(D)** Haematoxylin and Eosin staining of CIA SFs was carried out on cryosections of FNPEG hydrogels after 7 days of culture and imaged using an EVOS brightfield microscope (scale: 500  $\mu\text{m}$ ), to visualise SFs within the gel.

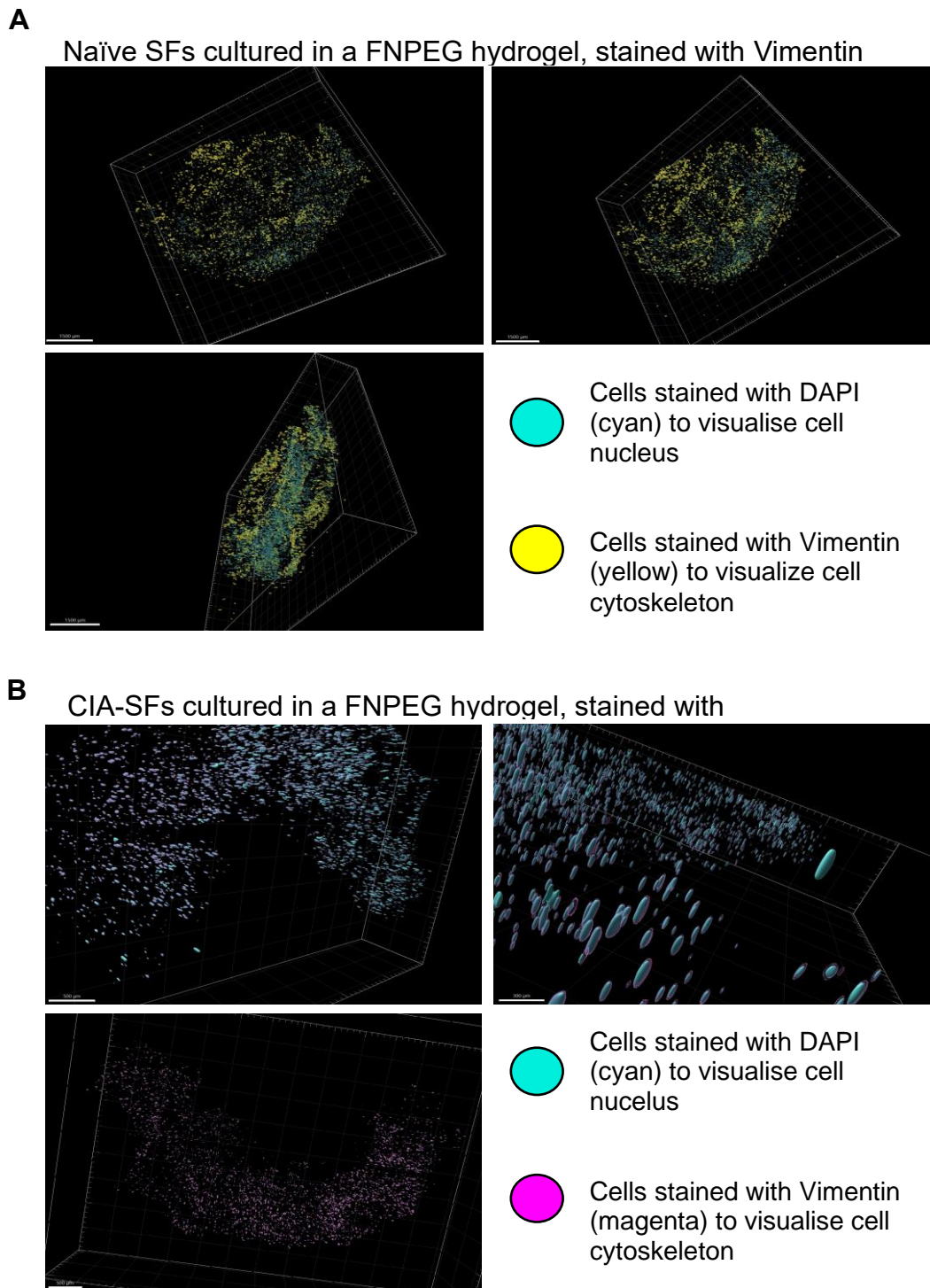


**Figure 5-3: 3D reconstruction of Naïve and CIA SFs cultured in non-degradable 5 wt % FNPEG hydrogels.**

Naïve and CIA SFs were expanded in 2D and cultured in non-degradable FNPEG hydrogels for 7 days, after which immunofluorescent staining was carried out to stain for vimentin (yellow - Naïve and pink - CIA) and counterstained with DAPI (blue). Images were taken using a widefield microscope in z steps of  $\sim 10 \mu\text{m}$  tile scanned, merged and deconvoluted to obtain a 3D image of the entire gel with SF staining. The 3D image was then processed using IMARIS software to generate a 3D reconstruction of the FNPEG hydrogels. Video stills of the 3D reconstructed hydrogels were created for gels containing (A) Naïve SFs (1-3: scale:  $1500 \mu\text{m}$ ) and (B) CIA SFs (Scale: 1-  $500 \mu\text{m}$ , 2-  $300 \mu\text{m}$ , 3-  $500 \mu\text{m}$ )

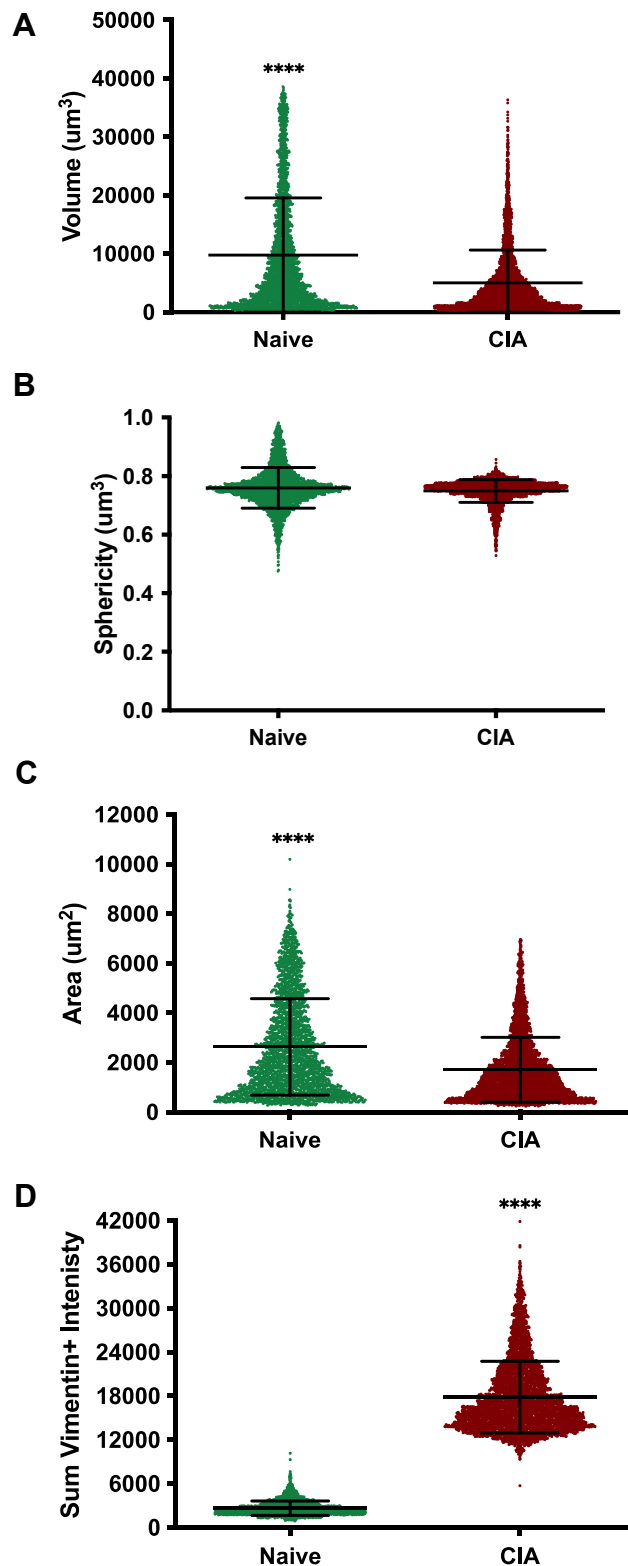


**Figure 5-4: Morphologies and physical cell properties of SFs in 5 wt % FNPEG hydrogels.**

IMARIS analysis of FNPEG hydrogel reconstructions (Figure 5-3) to observe differences in cell properties and morphologies between Naïve and CIA SFs in a 3D microenvironment. A-D Volume (A) Sphericity (B) Area (C) and Sum Vimentin Intensity (D) are shown comparing Naïve and CIA SFs. Data shown are representative of cells in an entire hydrogel. Data show means  $\pm$  SEM, with each dot representing a single cell. Statistics: two-tail unpaired  $t$ -test; \*\*\*\* $p < 0.0001$ .

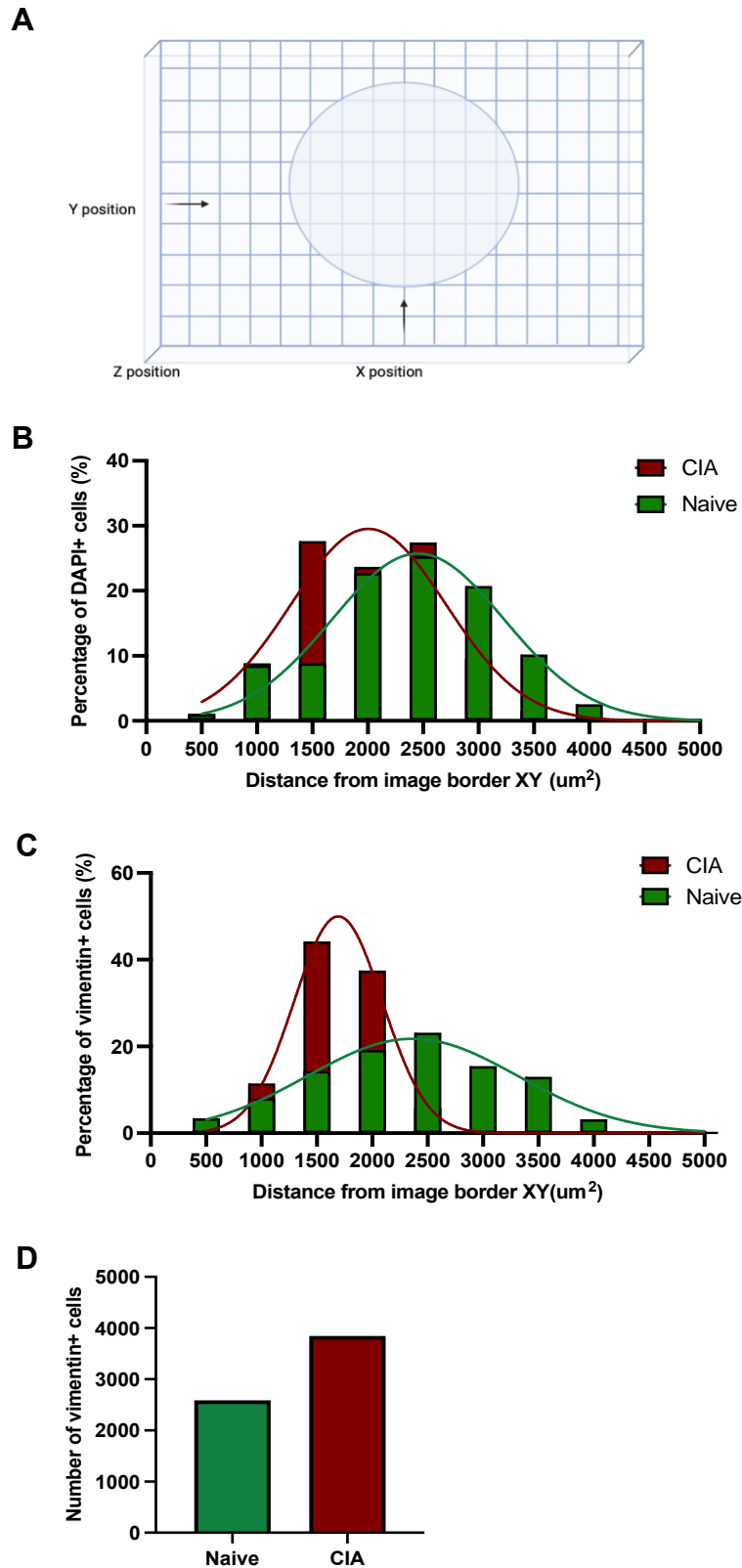
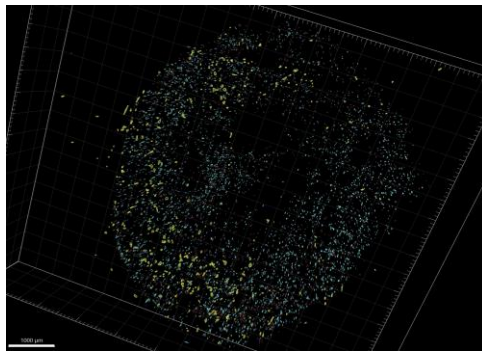
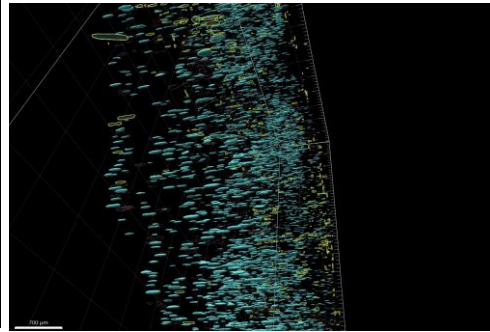
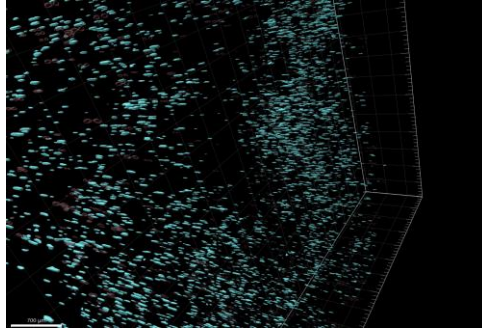


**Figure 5-5: Naïve and CIA SFs display a distinct distribution within 5 wt % FNPEG hydrogels.**

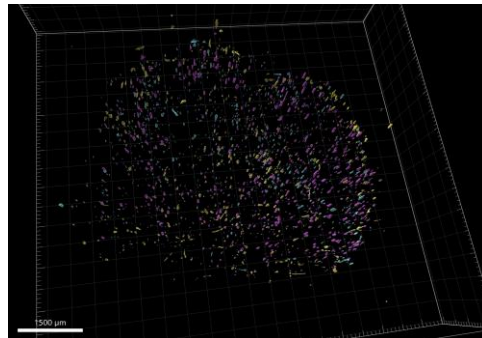
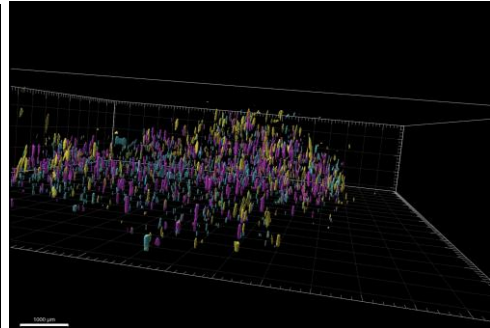
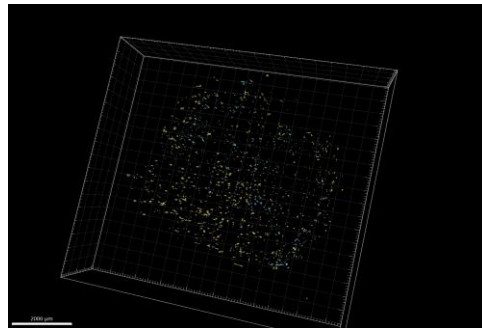
(A) Schematic of XY border graph from which graphs were constructed from IMARIS software. B-C The location from the distance from the image border was obtained using IMARIS and is represented as the percentage of cells stained positive for (B) DAPI and (C) vimentin within the gel for both Naïve and CIA SFs. (D) The total number of vimentin+ Naïve and CIA cells. Data are taken from individual cells within a hydrogel of each condition and analysed using IMARIS software to obtain number and location.

**A** Naïve SFs cultured in a FNPEG hydrogel, stained with VCAM1 (magenta) and CD90 (yellow)



-  Cells stained with DAPI (cyan) to visualise cell nucleus
-  Cells stained with CD90 (magenta) to visualize sublining SFs
-  Cells stained with VCAM1 (yellow) to visualize lining SFs

**B** CIA-SFs cultured in a FNPEG hydrogel, stained with VCAM1 (magenta) and CD90 (yellow)

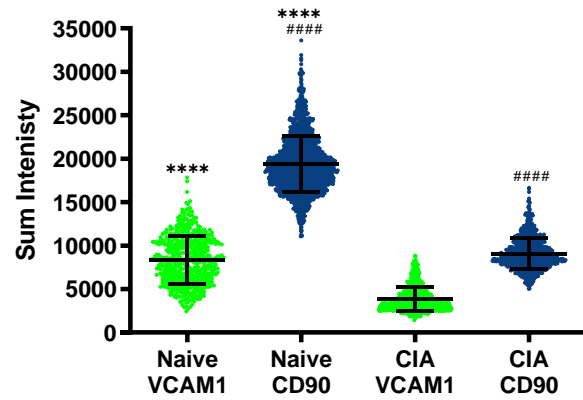


-  Cells stained with DAPI (cyan) to visualise cell nucleus
-  Cells stained with CD90 (magenta) to visualize sublining SFs
-  Cells stained with VCAM1

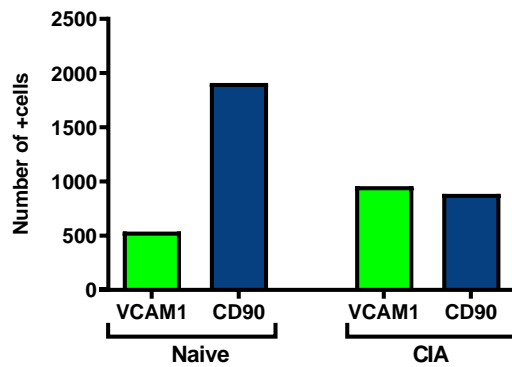
**Figure 5-6: 3D reconstruction of SFs subsets VCAM1 and CD90 cultured in non-degradable 5 wt % FNPEG hydrogels.**

Naïve and CIA SFs were expanded in 2D and cultured in non-degradable FNPEG hydrogels for 7 days, after which immunofluorescent staining was carried out to stain for VCAM1 (yellow), CD90 (magenta) and counterstained with DAPI (blue). Images were taken using a widefield microscope in z steps of  $\sim 10\ \mu\text{m}$  tile scanned, merged and deconvoluted to obtain a 3D image of the entire gel with SF staining. The 3D image was then processed using IMARIS software to generate a 3D reconstruction of the FNPEG hydrogels. Video stills of the 3D reconstructed hydrogels were created for gels containing **(A)** Naïve SFs (Scale: 1- 700  $\mu\text{m}$ , 2- 700  $\mu\text{m}$ , 3- 1000  $\mu\text{m}$ ) and **(B)** CIA SFs (Scale: 1- 2000  $\mu\text{m}$ , 2- 1000  $\mu\text{m}$ , 3- 1500  $\mu\text{m}$ ).

A



B



C

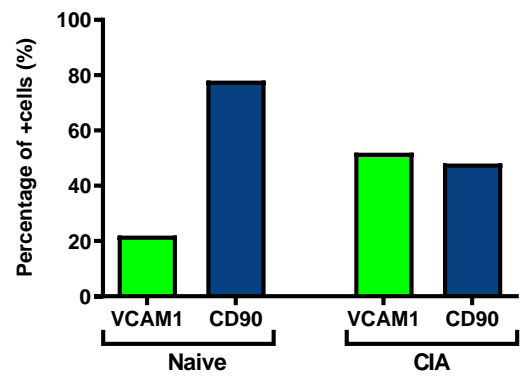


### Figure 5-7: Naïve and CIA SFs display differences in subset marker intensities.

Cells were prepared as mentioned in Figure 5-6 and IMARIS software was used to obtain the (A) intensity (B) number and (C) percentage for VCAM1+ and CD90+ SFs. Data shown are representative of cells in an entire hydrogel. Data show means  $\pm$  SD, with each dot representing a single cell. Statistical significance was evaluated by ordinary one-way ANOVA and Tukey's test for multiple comparisons. Naïve VCAM1 vs CIA VCAM1 or Naïve CD90 vs CIA CD90 (\*\*\*\* $p < 0.0001$ ), Naïve VCAM1 vs Naïve CD90 or CIA VCAM1 vs CIA CD90 (#### $p < 0.0001$ ).

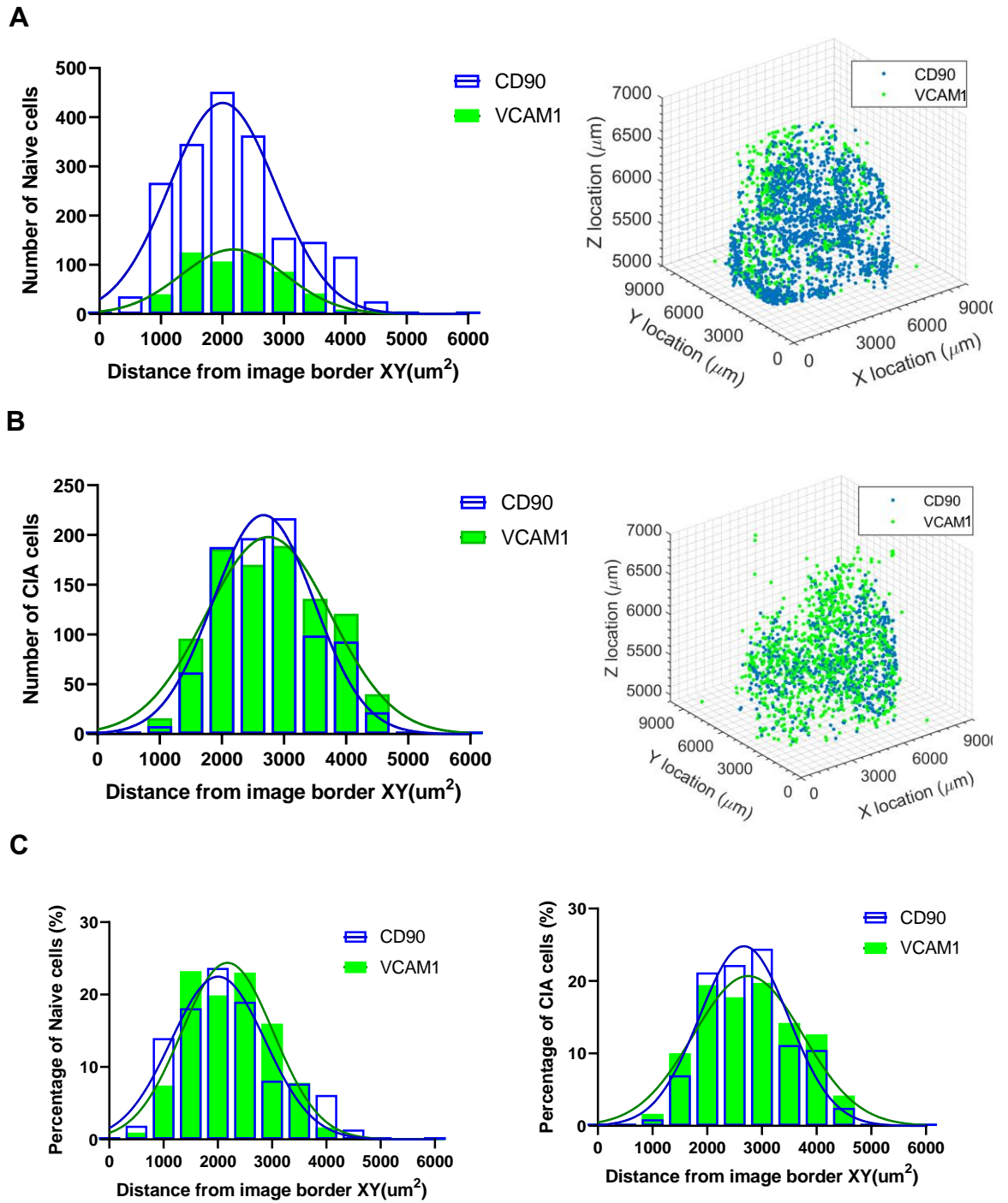


**Figure 5-8: An increase in SF lining subset (VCAM1) expression is observed when CIA-SFs are cultured in FNPEG hydrogels.**

Cells were prepared as mentioned in Figure 5-6 and IMARIS software was used to obtain the location of positively stained VCAM1 and CD90 (A) Naïve and (B) CIA SFs from the distance from the image border, with their corresponding 3D scatter plots created in Matlab using X,Y,Z positions of cells generated from. The percentage of VCAM1 and CD90 positive (C) Naïve and (D) CIA SFs and their distance from the image border.

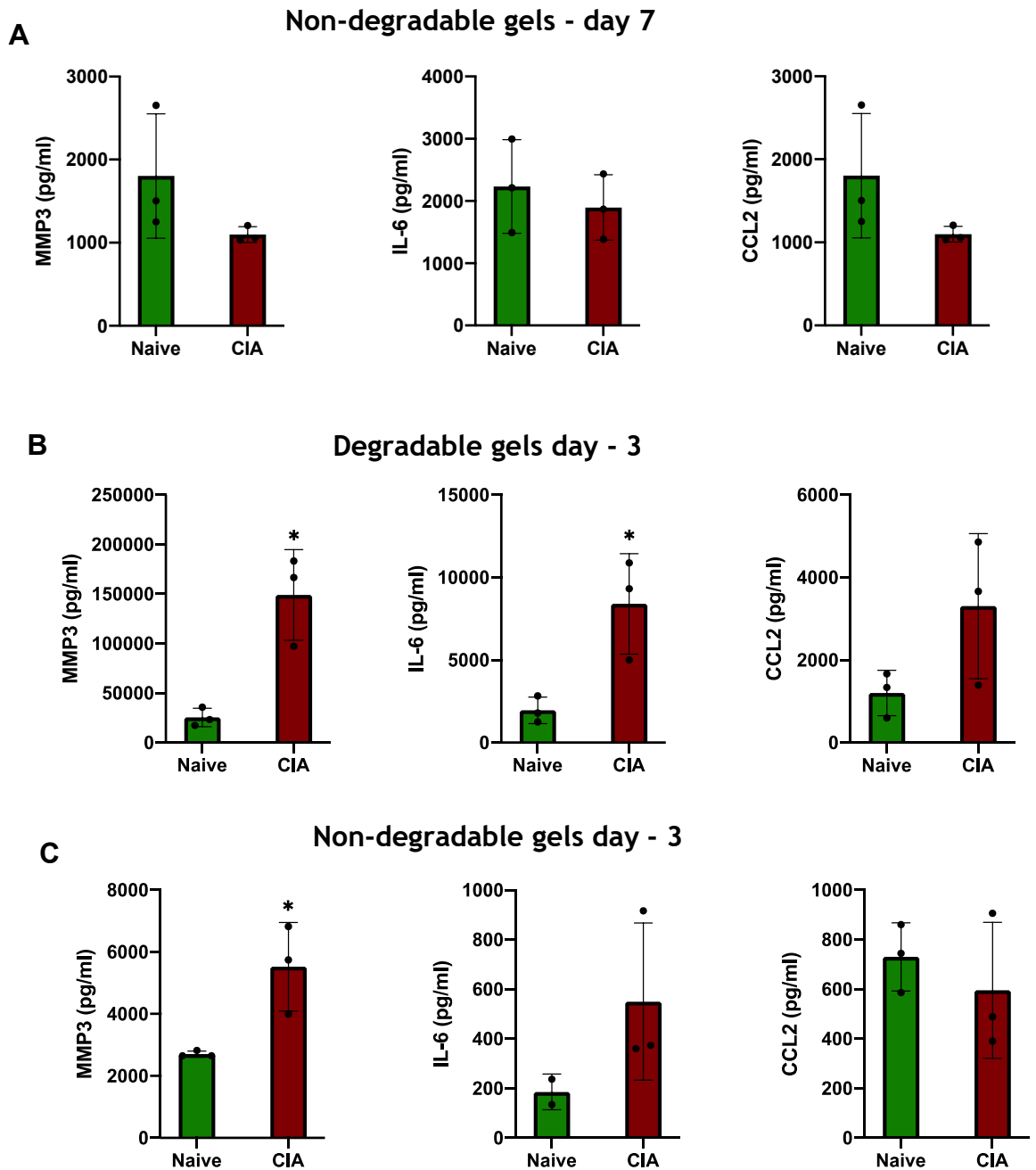


**Figure 5-9: SF cytokine expression of MMP3, CCL2 and IL-6 in degradable and non-degradable gels.**

Supernatant was collected from Naïve and CIA SFs cultured in degradable and non-degradable hydrogels and cytokine concentration was determined by ELISA. The concentration for MMP3, IL-6 and CCL2 in (A) non-degradable hydrogels (0% VPM) for 7 days (B) degradable FNPEG hydrogels (100% VPM) for 3 days (C) non-degradable hydrogels (0% VPM) for 3 days was obtained. Data show means  $\pm$  SD. Statistical significance was determined using unpaired *t*-test; \**p*<0.05.

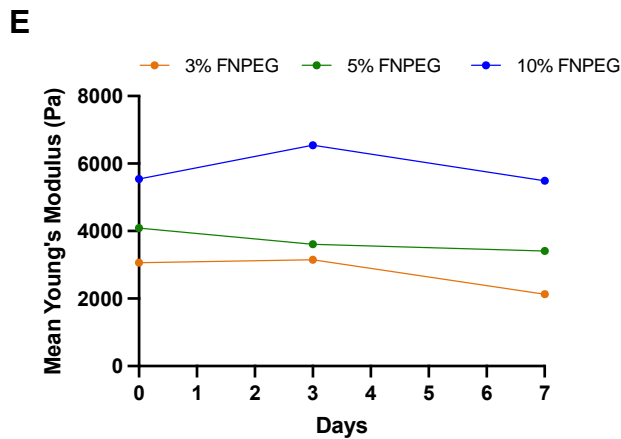
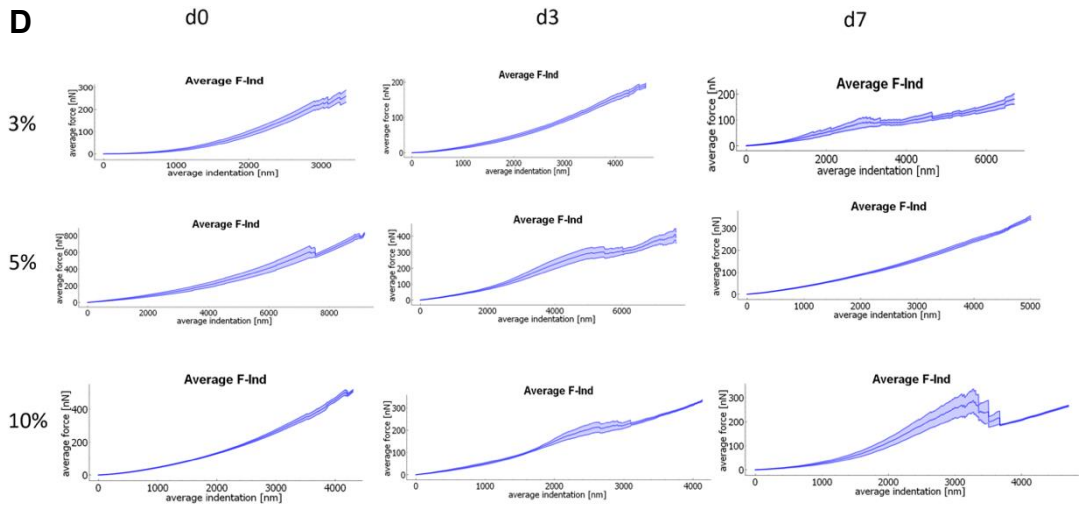
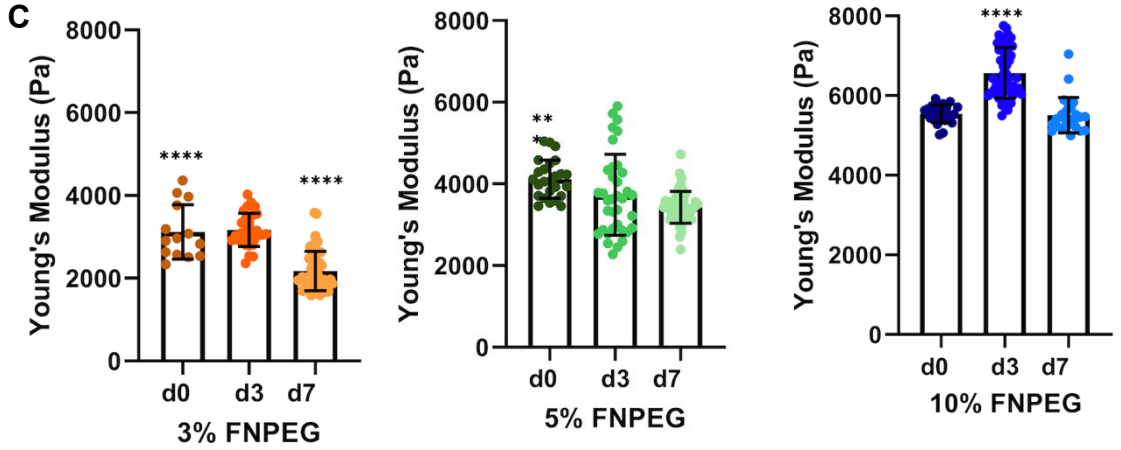
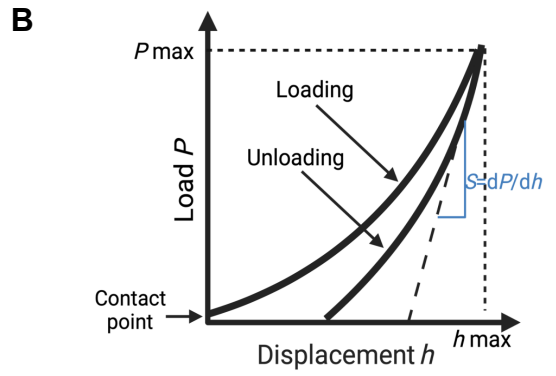
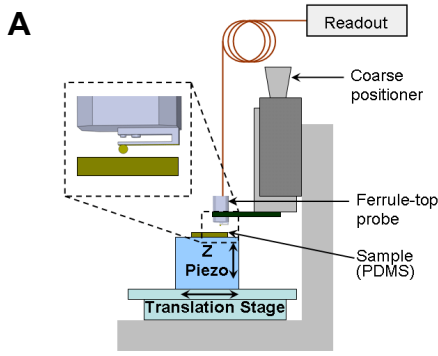
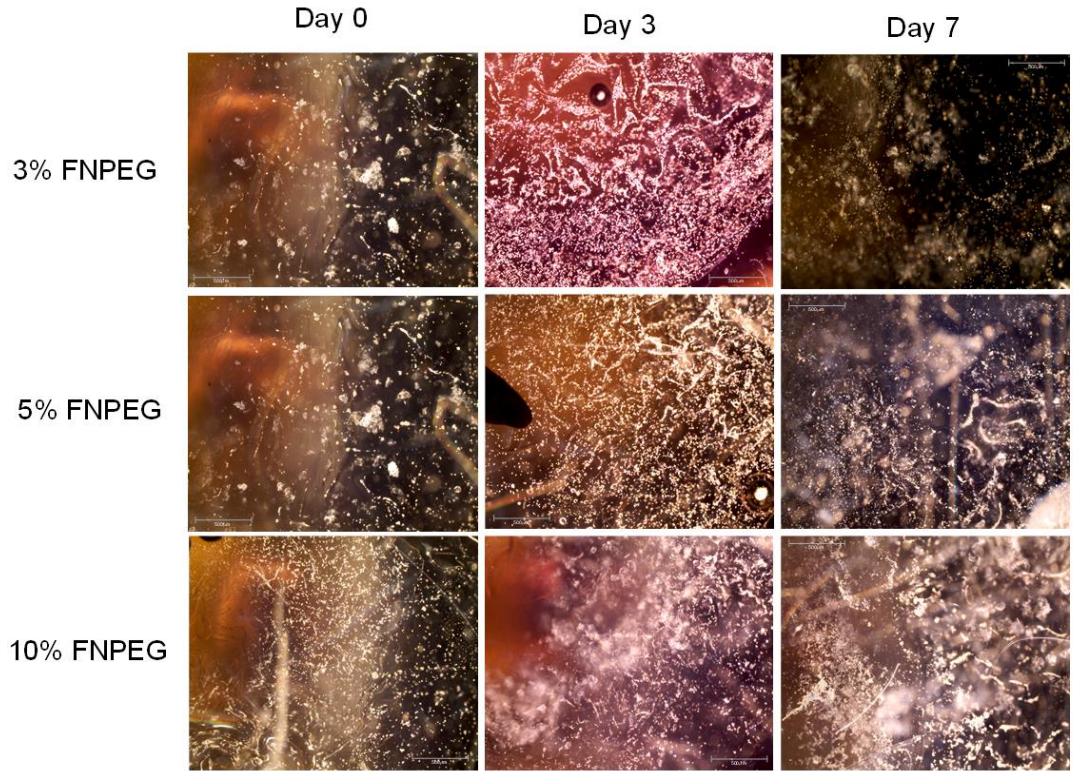


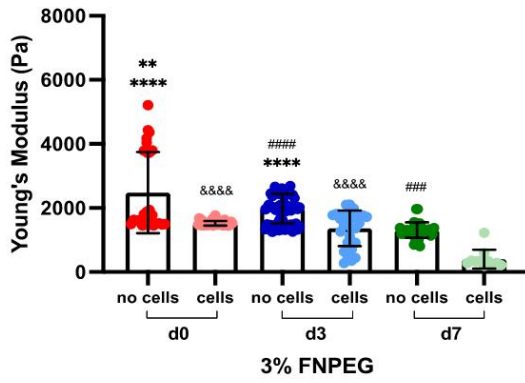
**Figure 5-10: Stiffness over time of different wt % degradable FNPEG hydrogels.**

(A) Schematic view of the ferrule-top nanoindenter setup (the same figure is shown in Figure 2-3) (B) Schematic representation of load vs depth graph from nanoindentation. Elastic modulus measured by AFM nanoindentation (the same figure is shown in Figure 2-4) of (C) 3 wt %, 5 wt % and 10 wt % degradable FNPEG hydrogels at day 0, 3 and 7 in PBS (mean  $\pm$  SD). (D) Average curved (n=3) and (E) Line graph of overall average elastic modulus for each FNPEG hydrogel at day 0, 3 and 7 in PBS. Data shown is representative of cells in an entire hydrogel, with each dot representing a single cell. Statistical significance was evaluated by ordinary one-way ANOVA and Tukey's test for multiple comparisons; \*\*\*p<0.001, \*\*\*\*p<0.0001.

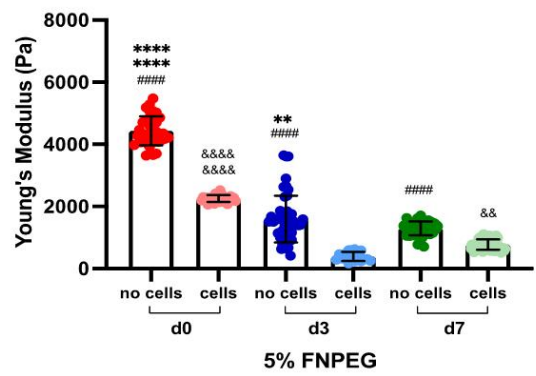
A



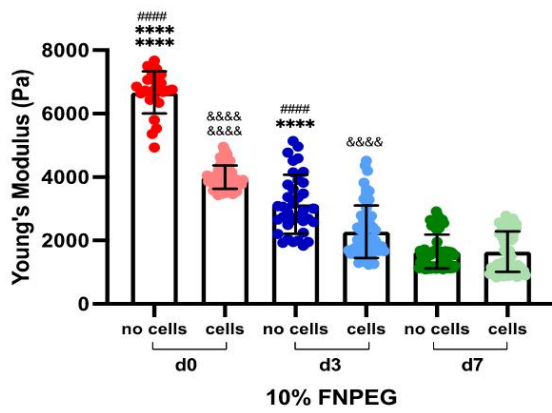
B



C



D



E

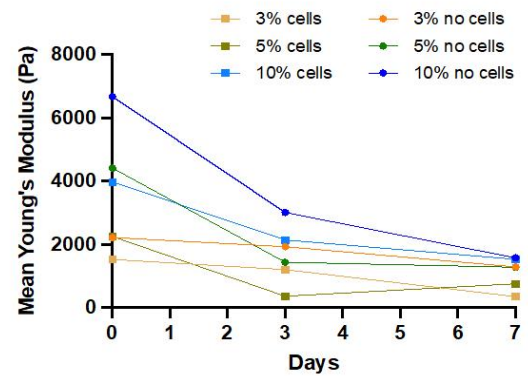


**Figure 5-11: The effect of Naïve SFs on the “stiffness” of different degradable wt % FNPEG hydrogels over 7 days.**

**(A)** Light microscope images of 3, 5 and 10 % wt % degradable FNPEG hydrogels containing Naïve cells at day 0, 3 and 7 at x10 magnification (scale: 500  $\mu\text{m}$ ). **B-D** Elastic modulus (kPA) measured by nanoindentation at day 0, 3 and 7 in media with and without Naïve cells (SFs) for **(B)** 3 wt % **(C)** 5 wt % and **(D)** 10 wt % FNPEG hydrogels. **(E)** Average elastic modulus of 3,5 and 10 wt % FNPEG hydrogels measured at day 0, 3 and 7 in media, with and without Naïve cells (SFs). Data shown are representative of cells in an entire hydrogel, with each dot representing a single cell. Statistical significance was evaluated by ordinary one-way ANOVA and Tukey’s test for multiple comparisons; No cells at different time points (\*\* $p < 0.001$ , \*\*\*\* $p < 0.0001$ ), no cells vs cell at the same time point (#### $p < 0.0001$ ), cells at different time points (<sup>##</sup> $p < 0.001$ , <sup>###</sup> $p < 0.0001$ ).

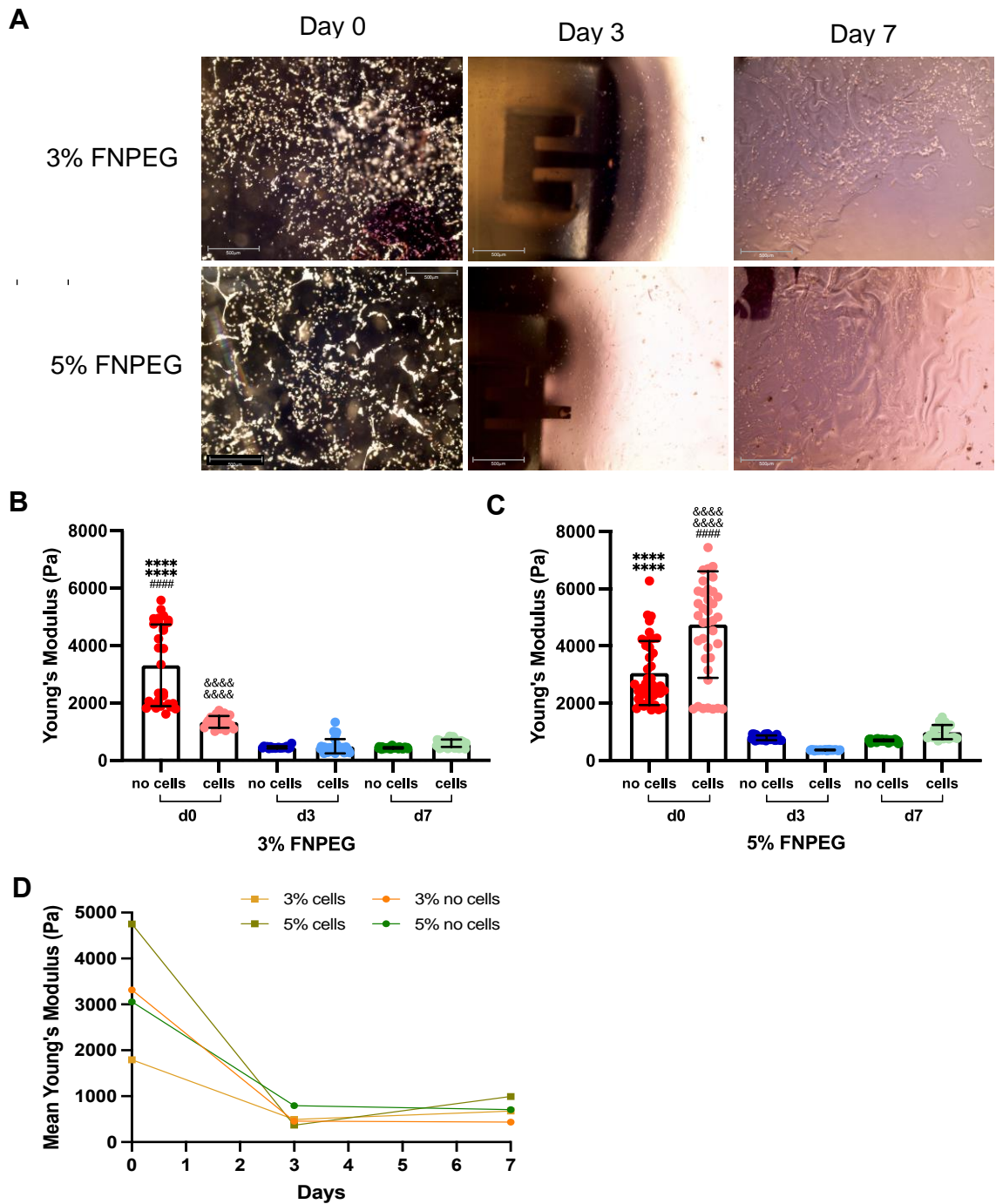


**Figure 5-12: The effect of different wt % FNPEG hydrogels containing CIA SFs on stiffness over 7 days.**

(A) Light microscope images of 3 and 5 wt % FNPEG hydrogels containing CIA cells at day 0, 3 and 7 at x10 magnification (scale: 500  $\mu$ m). B-C Elastic modulus measured by nanoindentation at day 0, 3 and 7 in media for with and without Naïve cells (SFs) for (B) 3 wt % and (C) 5 wt % FNPEG hydrogels. (D) Average elastic modulus of 3 and 5 wt % FNPEG hydrogels measured at day 0, 3 and 7 in media, with and without CIA cells (SFs). Data shown are representative of cells in an entire hydrogel, with each dot representing a single cell. Statistical significance was evaluated by ordinary one-way ANOVA and Tukey's test for multiple comparisons; No cells at different time points (\*\*\*\* $p < 0.0001$ ), no cells vs cell at the same time point (#### $p < 0.0001$ ), cells at different time points (##### $p < 0.0001$ ).

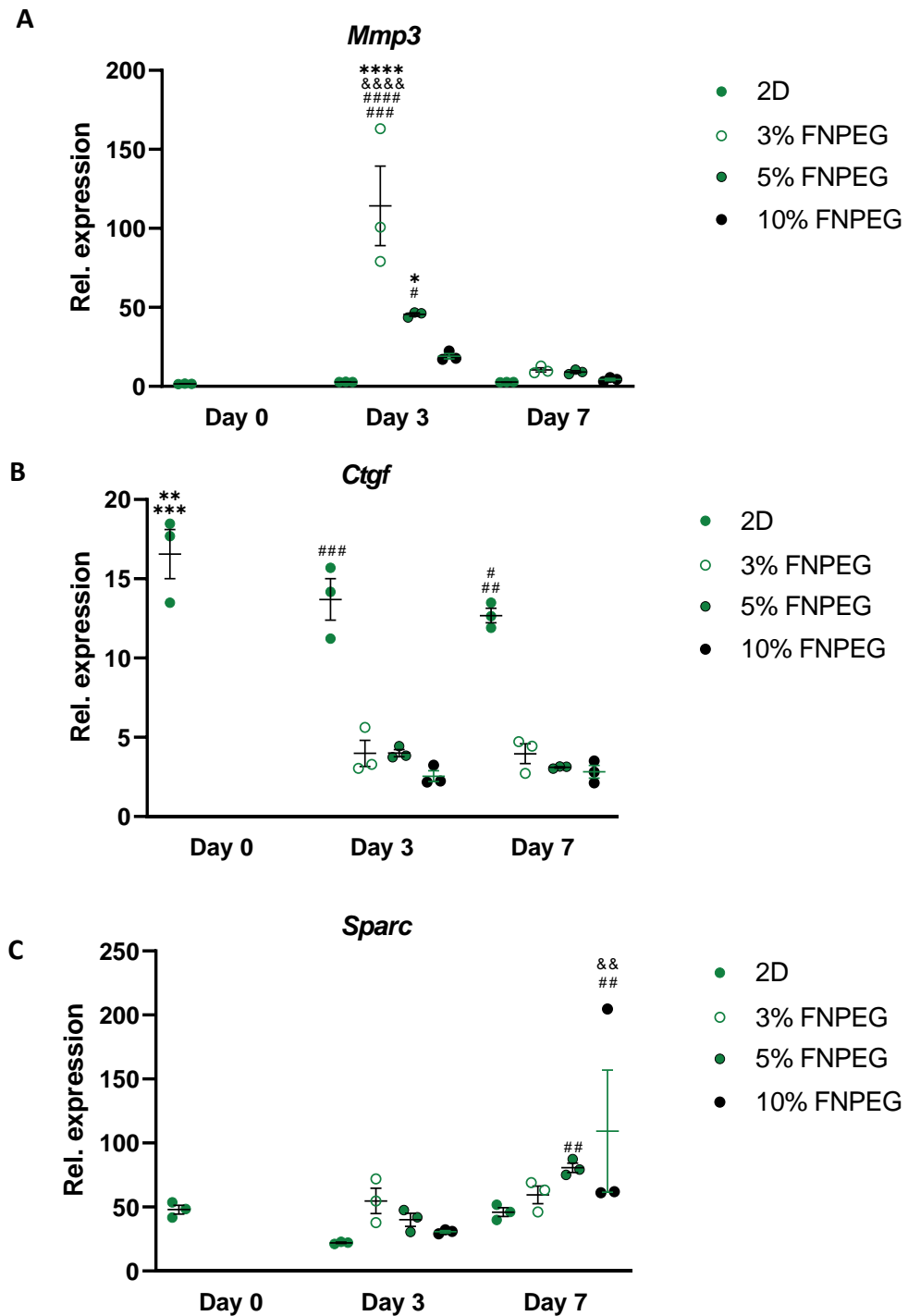


**Figure 5-13: Stiffness affects cell function.**

Naïve SFs were cultured in 2D at day 0, 3 and 7 in 3, 5 and 10 wt % FNPEG hydrogels for 3 and 7 days after which expression of genes was quantified using q-PCR. Genes quantified were (A) *Mmp3* (B) *Ctgf* and (C) *Sparc*. Results show relative expression to Actin, showing means  $\pm$  SEM, with each dot representing a biological replicate (in technical triplicate), bar shows the mean. Statistical significance was evaluated by ordinary one-way ANOVA and Tukey's test for multiple comparisons. 2D d0 vs 2D (d3 and d7) and 3%, 5% and 10% FNPEG gels at different time points (\* $p < 0.05$ , \*\* $p < 0.001$ , \*\*\* $p < 0.0001$ , \*\*\*\* $p < 0.00001$ ), different % FNPEG gel on the same day (# $p < 0.05$ , ## $p < 0.001$ , ### $p < 0.0001$ , #### $p < 0.00001$ ), same % FNPEG gel on the same day (†† $p < 0.001$ , †††† $p < 0.00001$ ).

## Chapter 6 SFs exhibit differential gene expression when cultured in different microenvironments

### 6.1 Introduction

The data presented in the Chapters 3-5 established that SFs cultured in 2D, and 3D (Alvetex® and hydrogel) culture systems not only exhibit differential morphology but also respond differently in terms of their pro-inflammatory and matrix remodelling responses, presumably due to the differences in their cellular interactions within the various microenvironments. As changes in these parameters occur during the transition of Naïve to aggressive SFs during arthritogenesis *in vivo*, by transcriptomic reprogramming as a result of remodelling of the epigenetic landscape, it was decided to investigate whether SFs, cultured in 2D and 3D platforms, display differential transcriptomic programmes (by RNA-Seq analysis). Specifically, it was planned to compare differentially expressed genes in SFs freshly extracted from the joint with those cultured in 2D alone or in the Alvetex® and hydrogels platforms to address determining how best to culture SFs *ex vivo* to mimic/recapitulate the *in vivo* functional responses of Naïve and CIA SFs, *in vitro*.

Due to its high resolution and sensitivity, RNA-Seq analysis has transformed our comprehension of the complexities of eukaryotic transcriptomes (Wang, Gerstein and Snyder, 2009). Although the use of PCR to investigate specific genes can be a useful tool to investigate already existing hypotheses, the ability to observe many thousands of genes can further gene expression analyses, allowing the latter to be more discovery based. RNA-Seq allows crucial benefits in comparison to microarrays when assessing gene expression as the genes targeted are not biased and thus, this tool can be used to understand fibroblast subpopulations and their varying functions, in turn leading to novel therapeutic interventions. In RA studies in particular, the use of RNA-Seq has provided novel insights and understanding of potential pathogenic mechanisms and roles of candidate genes involved in the disease (Yoshizawa et al., 2008; Kirkham, Kavanaugh and Reich, 2014; Kraan et al., 2001). For example, a study carried out by Orange et al, used bulk RNA-Seq to investigate the total synovial gene expression in conjunction with histology to subclassify RA subtypes. The technique allowed samples to be clustered as “high

or low inflammatory tissue” as well as identifying further mixed clusters. This showed that key histological variables within the synovial tissue samples concurred with sequencing data and indicated that the “high inflammatory” samples showed higher levels of immune system cell infiltration of tissue (Orange et al., 2018). Furthermore, single cell RNA-Seq has also helped reveal the presence of distinct fibroblast subpopulations, some of which we have investigated in this thesis, as well as the pathological significance of SF heterogeneity in RA (Croft et al., 2019). The latter only further shows how powerful RNA-Seq can be, not only for understanding the role of SFs in RA but perhaps also for signposting the best way in which they can be treated as a therapeutic target. This next section will utilise RNA-Seq to investigate and compare in detail, the differences the microenvironment makes to gene expression in Naïve and CIA SFs. All cells expanded *ex vivo* within the experiments in this section have been cultured with FN and the FNPEG hydrogels used were all of the 5% wt degradable format.

## 6.2 Aims and objectives

Thus, the core aim of this chapter is to determine the transcriptomic signatures of Naïve and CIA SFs grown solely in conventional 2D cultures to compare with those transferred to Alvetex® scaffolds or hydrogels (subsequent to their *ex vivo* expansion) in order to determine the impact of these 3D microenvironments on the transcriptomes of SFs. Specifically, it was planned to determine:

- the differentially expressed genes and, by subsequent pathway analysis, the signalling networks characteristic of freshly isolated SFs Naïve and CIA mice (sorted SFs) to provide transcriptomic signatures referencing their *in vivo* phenotypes.
- To compare the transcriptomic signatures of freshly isolated SFs with those of the corresponding SF groups grown, in the presence of FN, in classical 2D cultures and those subsequently transferred to the 3D environments provided by the Alvetex® or FNPEG hydrogel platforms.
- to investigate the ability of SFs to respond to inflammatory mediators in different culture systems. An IL-1 $\beta$  model was chosen as this cytokine is a known SF activator and a key driver of joint pathogenesis, as evidenced by it

being elevated in the synovium of RA patients and in various animal models including the CIA model. Moreover, it has been shown to be very effective at inducing transcriptional reprogramming of SFs *in vitro* (Corbet et al., 2021).

## 6.3 Results

### 6.3.1 RNA-Seq identifies that the microenvironment influences gene expression of inflammatory SFs

#### 6.3.1.1 Gene expression profiling of Naïve and CIA-SFs *in vivo*

To generate reference transcriptomic phenotypes exhibiting characteristics of Naïve and CIA SFs *in vivo*, cells extracted directly from the joint (Figure 6-1A) were sorted using Flow cytometry to isolate SFs (“sorted SFs”, purity >~97%) that were subjected to RNA-Seq and bioinformatic analysis (alignment of sequences using HiSat2, normalization and differential expression using DESeq2 and featurecounts) as outlined in section 2.10.4. Principal Component Analysis of the transcriptomic data confirmed the distinction between the phenotype of the freshly isolated Naïve and CIA SFs groups (Figure 6-1B). A list of differentially expressed (DE) SF genes was generated including 298 genes that were significantly upregulated (Full Table in Appendix A - [Sorted up-regulated list of differentially expressed genes](#)) and 88 genes that were downregulated (Full Table in Appendix A - [Sorted down-regulated list of differentially expressed genes](#)) [ $>2$ -fold,  $p_{\text{adj}} < 0.01$ ] in CIA, relative to Naïve, SFs and these are presented here both as a volcano plot and a heatmap (Figure 6-1C), the latter clearly illustrating the distinct transcriptomic signatures of healthy and pathogenic SFs *in vivo*. A list of the top 50 genes significantly up- and down-regulated in CIA, relative to Naïve, SFs is shown (Figure 6-1D). Following this, to understand the functional consequences of these transcriptomic changes, String Protein-Protein Interaction Networks Functional Enrichment Analysis was applied to genes upregulated in CIA compared to Naïve SFs (Figure 6-2), establishing pathogenic targeting of two main functional networks, one involved in cell cycle processes and the other regulating inflammatory and ECM responses (Figure 6-2A), reflecting the activation and hyperproliferation characteristic of CIA-SFs. By contrast, analysis of the genes downregulated in CIA, opposed to Naïve, SFs only showed focus on matrix-based pathways (Figure 6-2C). Corresponding KEGG pathway enrichment analysis was

performed showing “Rheumatoid Arthritis”, “IL-17 signalling”, and “TNF signalling” pathways to be significantly upregulated (Figure 6-2B) and “Cell adhesion molecules”, “ECM” and “Cellular process” pathways to be significantly down regulated (Figure 6-2D). These findings are consistent with the observed pathological activation of SFs in joint disease and the known cellular responses of SFs during disease.

### 6.3.1.2 Gene expression profiling of Naïve vs CIA-SFs cultured in 2D

Having established the transcriptomic profile of Naïve and CIA-SFs isolated from mouse joints, we next investigated the transcriptome profiles of Naïve and CIA-SFs expanded *ex vivo* in 2D conventional culture systems, using FN-coated plates (Figure 6-3A). We wanted to define gene expression of cells that were cultured *ex vivo*, to evaluate the changes undergoing cell growth in 2D surfaces. Cells were isolated from mouse joints as before from Naïve and CIA mice, and expanded *ex vivo* for 3-4 weeks, when RNA-Seq was conducted.

Principal Component Analysis of the transcriptomic data (Figure 6-3B) confirmed the functional data (Chapter 3) showing that even in a 2D microenvironment, CIA SFs stably maintain a distinct phenotype from healthy SFs even when expanded for several weeks *in vitro* and that this is reflected at the transcriptomic level. Here, analysis of the significantly differentially expressed (DE) genes indicated that only 112 genes were upregulated (Full Table in Appendix A - [2D up-regulated list of differentially expressed genes](#)), and 12 genes downregulated (Full Table in Appendix A - [2D down-regulated list of differentially expressed genes](#)) [ $>2$ -fold,  $p_{\text{adj}} < 0.01$ ] in CIA, relative to Naïve, SFs (Figure 6-3D) and again, these data are presented here, both as a volcano plot and a heatmap (Figure 6-3C). Thus, the number of differentially expressed genes was far lower in Naïve and CIA SFs cultured in 2D compared to their sorted freshly isolated counterparts, suggesting that some transcriptomic remodelling has taken place in response to their new microenvironment. Subsequent String Protein-Protein Interaction Networks Functional Enrichment Analysis of the upregulated genes showed significant enrichment in ECM, adhesion and migration pathways (Figure 6-4A & B). Moreover, analysis of the downregulated DE genes included networks involved in FN type III domains, immunoglobulins, serine proteases/trypsin-like peptidases (Figure 6-

4C), again processes likely involved in matrix remodelling and migration. Nevertheless, most of the differentially upregulated genes exhibited by sorted CIA-SFs are not regulated in SFs cultured in 2D, indicating that this conventional culture system microenvironment results in changes in gene expression in SFs, further confirming that 2D systems are not optimal models for the study of SF biology, despite them maintaining differential phenotypes that focus on ECM-based processes. The key loss appears to relate to the upregulation of cell cycle/proliferative signalling associated with the hyperplasia associated with the freshly isolated CIA-SFs. To corroborate that the main changes were related to ECM remodelling RT-PCR analysis was performed on selected genes, chosen for their roles in ECM remodelling and cell interactions (Figure 6-5). Thus, *Tinagl1* is an ECM protein involved in cell adhesion and consistent with this, has been implicated in the modulating of cell proliferation, migration, and differentiation (Sun et al., 2019), *Tnc* is an ECM protein associated with spatially and temporally restricted tissue distribution (like that of pannus formation) (Gremlich et al., 2020), *Timp1* is involved in ECM degradation (Song et al., 2016), *Sparc* is involved in ECM synthesis and promotion of changes to cell shape (Peixoto et al., 2014), *Fn1* encodes FN (Aslam, Singh, Cortese and Riegert-Johnson, 2019) and *Thbs4* is an adhesive glycoprotein that mediates cell-to-cell and cell-to-matrix interactions (Förster et al., 2011). The expression of *Tinagl1* was shown to be increased in CIA-SFs (Figure 6-5A), as was *Timp1* (Figure 6-5C) and *Sparc* (Figure 6-5D), albeit in the case of the latter genes this was not significant. However, interestingly the expression of *Thbs4* (Figure 6-5F), *Tnc* (Figure 6-5A) as well as *Fn1* (Figure 6-5E) trended towards being greater in Naïve SFs. The data for all the genes was then presented as a heatmap (Figure 6-9G) alongside the heatmap of the selected genes from the RNA-seq analysis (Figure 6-9H). The signatures were broadly similar, but with some inconsistencies which could be due to the sensitivity of the RNA-seq experiment or the fact that different mice and so different RNA was used for the RNA-seq and RT-PCR experiments.

### 6.3.1.3 Gene expression profiling of Naïve vs CIA-SFs cultured in Alvetex®

Next, a similar approach was used to study the transcriptomic activation of CIA-SFs cultured in Alvetex® (Figure 6-6A). We hypothesised that the 3D structure of this rigid scaffold could provide the appropriate signals to (re)induce expression

of the inflammatory gene profile that was partially lost when the cells were cultured in plastic 2D plates. Thus, expanded cells from Naïve and CIA mice, (as in Figure 6-3, 6-4) were seeded into Alvetex® discs and cultured for additional 9 days, when RNA was purified to conduct RNA-Seq studies. Principal Component Analysis of the transcriptomic data again illustrated the stable nature of distinct Naïve and CIA phenotypes (Figure 6-6B) even following their extended culture *ex vivo*. Interestingly, in contrast to the low numbers of differentially expressed genes observed in CIA, relative to Naïve, SFs grown under 2D conditions, the DE genes detected in SFs switched to Alvetex® scaffolds showed 548 genes to be upregulated (Full table in Appendix A - [Alvetex up-regulated list of differentially expressed genes](#)) and 203 genes downregulated (Full Table in Appendix A - [Alvetex down-regulated list of differentially expressed genes](#)) [ $>2$ -fold,  $p_{\text{adj}} < 0.01$ ] in CIA relative to Naïve SFs (Figure 6-6C). A list of the top 50 genes significantly up- and down-regulated in CIA, relative to Naïve were generated (Figure 6-6D). To investigate whether this reflected (partial) recovery of the *in vivo* CIA-SF phenotype, functional consequences of all differentially expressed genes were assessed String Protein-Protein Interaction Networks Functional Enrichment analysis (Figure 6-7). Essentially, the two main functional networks identified as being associated with the upregulated genes in freshly isolated SFs, one involved in cell cycle processes and the other involved in inflammatory responses were again represented in the Alvetex® grown SFs (Figure 6-7A) and consistent with this, corresponding KEGG pathway enrichment analysis showed “Rheumatoid Arthritis”, “IL-17 signalling”, and “TNF signalling” pathways to be significantly upregulated (Figure 6-7B). As these functional predictions were similar to those observed with the SFs purified from the joint prior to any cell culture, these data suggest that some of the pathways lost as a result of culture under 2D conditions were recovered when SFs were transferred to Alvetex®. Likewise, analysis of the downregulated DE genes in CIA showed enriched pathways for cellular processes, cell adhesion as well as calcium signalling pathways (Figure 6-7C). The RNA-Seq data was again validated using RT-PCR on selected genes mentioned previously. Sparc (Figure 6-13D) and Thbs4 (Figure 6-13F) expression was shown to be elevated in CIA-SFs compared to Naïve SFs, whilst the opposite was observed in Tnc (Figure 6-13A), Tinagl1 (Figure 6-13B), Timp1 (Figure 6-13C) and Fn1 (Figure 6-13E). The latter showing significant upregulations in the gene expression in Naïve SFs. Data

for all the genes was then presented as a heatmap (Figure 6-13G) alongside the heatmap of the selected genes from the RNA-Seq analysis (Figure 6-13H). The heatmaps for RNA-Seq and RT-PCR were similar for *Thbs4* and *Sparc*, however not for the rest of the genes. Again, this could be due to different RNA used for both experiments.

Collectively, these data could suggest that the epigenetic changes that occur in SFs grown on 2D platforms can be (at least partially) reversed when they are transferred to a 3D environment that provides more physiologically relevant matrix cues.

#### **6.3.1.4 Gene expression profiling of Naïve vs CIA-SFs cultured in FNPEG hydrogels**

Having observed these changes in gene expression which suggest a plasticity that confers the ability for SFs to at least partially recover some of their “lost” transcriptional programming and functional outcomes consequent to culture on 2D platforms, we also investigated whether this similarly occurs on transfer of “2D” SFs to 3D FNPEG hydrogels (Figure 6-9A). Principal Component Analysis again confirmed maintenance of separate Naïve and CIA phenotypes (Figure 6-9B). However, analysis of the DE genes showed only 112 genes upregulated (Full Table in Appendix A - [FNPEG hydrogels up-regulated list of differentially expressed genes](#)) and 67 downregulated (Full Table in Appendix A - [FNPEG hydrogels down-regulated list of differentially expressed genes](#)) [ $>2$ -fold,  $p_{\text{adj}} < 0.01$ ] (Figure 6-9), numbers lower than those seen with SFs grown on Alvetex® (Figure 6-6C) and more akin to those observed following culture in 2D plates alone. To further address whether this reflected the SFs remaining “fixed” in a “2D phenotype” the top 50 genes significantly upregulated and (all of those) downregulated in CIA-, relative to Naïve SFs were identified (Figure 6-9D) and the functional consequences of all differentially expressed genes was investigated by pathway analysis (Figures 6-10). String Protein-Protein Interaction Networks Functional Enrichment Analysis suggested a functional network concerned with ECM degradation, proteoglycans, interactions, organisation as well as focal and cell adhesion (Figure 6-10A) and KEGG pathway enrichment analysis identified “ECM receptor interaction”, “Focal adhesion”, “Cytokine-cytokine interactions” and “NK-Kappa B signalling”

pathways (Figure 6-10B). By contrast, the downregulated genes are implicated in the regulation of the immune system, cell cycle and MAPK cascade as well as microRNAs in cancer (Figure 6-10C), predictions supported by KEGG analysis identifying their involvement in “Rheumatoid Arthritis”, “Cytokine-cytokine receptor interactions”, “Cell cycle” and “MAPK signalling” pathways were found to be significantly down regulated (Figure 6-10D).

These data therefore suggest that FNPEG hydrogel SFs differ from each of freshly purified SFs, SFs expanded in 2D cultures and those subsequently transferred into the Alvetex® 3D microenvironment. Thus, hydrogels do not simply restore some of the gene expression changes between Naïve and CIA SFs that were lost following culture on 2D plates but rather induce a new phenotype which, as the gel acts as surrogate matrix having been pegylated with FN, focuses on matrix remodelling rather than inflammatory responses. Interestingly, the MMPs appear to be upregulated, whilst inflammatory cytokines/pathways are downregulated suggesting that the results from section 5.3.5 are not due to cytokine production but due to MMPs further degrading the gel affecting the integrity and the resultant upregulation of pro-inflammatory cytokines as a response to the structural degradation of the gels. Again, the RNA-Seq data were validated by RT-PCR analysis of our panel of selected genes associated with the ECM (Figure 6-11). Thus, the expression of Tnc (Figure 6-11A), Timp1 (Figure 6-11C), Sparc (Figure 6-11C), Fn1 (Figure 6-11D) and Thbs4 (Figure 6-11E) were all shown to be upregulated in Naïve SFs compared to CIA, whilst the opposite was seen with Tinagl1 expression (Figure 6-11B). Data for all the genes was then presented as a heatmap (Figure 6-11G) alongside the heatmap of the selected genes from the RNA-Seq analysis (Figure 6-11H). The heatmaps for each showed similar results only for Tinagl1 which again could be due to the RNA-Seq sensitivity, human error during the RT-PCR or different RNA used. Perhaps a repeat of this experiment with different batches of mice would provide more clarity.

#### **6.3.1.5 Comparison of Naïve and CIA-SFs cultured in 2D and 3D microenvironments**

To further address identifying which of the *in vitro* culture systems best supported maintenance of *in vivo* SF phenotypes, as evidenced by the *ex vivo* transcriptional

profiles of freshly isolated SFs, the differentially upregulated genes from SFs directly extracted from the joints as well as those cultured in 2D, Alvetex® and FNPEG hydrogels were compared and assessed using g:Profiler for statistical gene enrichment analysis (Figure 6-12). This revealed that the genes found to be upregulated as a result of CIA pathogenesis were involved in inflammatory responses, ECM and cytokine interactions, findings consistent with the pro-inflammatory nature of CIA-SFs (Figure 6-12A). The genes significantly upregulated in CIA-, relative to Naïve SFs when cultured in 2D were found to be involved in inflammatory, ECM and developmental processes (Figure 6-12B). Whilst upregulated genes from SFs cultured in Alvetex® were found to be involved in cytokine and inflammatory responses, cell division and regulation as well as IL-17 signalling (Figure 6-12C). Interestingly the upregulated genes and pathways observed when SFs were cultured in FNPEG hydrogels were associated with ECM processes, such as organisation, chain trimerization and degradation (Figure 6-12D).

Having established differences in transcriptomic profiling between Naïve and CIA SFs in freshly isolated SFs and those subsequently cultured in 2D and 3D culture systems, how the gene expression profiles of Naïve and CIA SFs were modulated under these differing conditions was investigated (Figure 6-13). Principal Component Analysis of the transcriptomic data for Naïve SFs (Figure 6-13A) showed that cells cultured in 2D alone and those subsequently transferred Alvetex® appear to exhibit a more similar phenotype to each other than either do with freshly isolated (sorted) SFs. Perhaps unexpectedly, the hydrogel group appear distinct from all the other SF groups. On the other hand, despite these differences the Naïve SFs cultured in the FNPEG hydrogels are observed to be similar to that of the sorted SFs from the joint, as opposed to those cultured in 2D or Alvetex®. This is interesting as when comparing the DE profiles of Naïve and CIA hydrogel SFs, they were shown to be significantly different when compared with the other systems, whereas the Naïve hydrogel SFs appear more akin to “*in vivo*” Naïve SFs than those associated with Naïve SFs, at least with respect to certain gene groups, from the other *in vitro* systems. This is further corroborated with the corresponding heatmap (Figure 6-13A) in which the cells cultured in 2D and 2D-Alvetex® appear most similar, whilst certain gene signatures in the Naïve

hydrogel SF cohort are more similar to those of the cells freshly from the joint. Similarly, interrogation of the CIA-SFs groups by Principal Component and Heatmap Analysis of the transcriptomic data (Figure 6-13B) again shows the 2D and 2D-Alvetex® group to be phenotypically related but distinct from the FNPEG hydrogel and freshly isolated SFs, although they do appear to share some signature subgroups with the latter. However, whilst like their Naïve SF counterparts, the hydrogel CIA-SFs share some partial signatures with the freshly isolated CIA-SFs, they also show some limited commonality with those from the 2D and 2D-Alvetex® groups.

### ***6.3.2 Stimulation with IL-1 $\beta$ influences differential gene expression in inflammatory SFs in different microenvironments***

Perhaps unexpectedly, transfer of the explant SFs from 2D cultures to the distinct 3D microenvironments differentially affected the gene expression of CIA-SFs, with culture on rigid scaffolds and hydrogels inducing quite distinct transcriptomes. Moreover, since culture in hydrogels did not (re)induce the inflammatory profile associated with arthritic fibroblasts, it was important to confirm that cells were still able to respond to inflammatory mediators and hence rule out the possibility that they had lost the ability of inducing inflammatory responses and/or had (terminally) differentiated to an alternative (pathogenic) phenotype perhaps associated with a particular maturation stage or SF subtype. Thus, we compared how *in vitro* stimulation of Naïve SFs with the pro-inflammatory cytokine IL-1 $\beta$ , affects the transcriptional reprogramming in 2D and following transfer, both the Alvetex® and FNPEG hydrogel 3D platforms. Thus, SFs were expanded in 2D until passage 4 as before and then cultured in their relevant microenvironments for 7 days (or 3 in the case of FNPEG hydrogels) in the presence of FN. Prior to RNA extraction the relevant SFs from each culture system were treated for 6 hours with IL-1 $\beta$  prior (Figure 6-14A). This cytokine was chosen because it is a key driver of SF pathogenesis and chronic exposure to this cytokine drives epigenetic changes in Naïve SFs (Jeong et al., 2004; Corbet et al). Firstly, to model the effect of acute inflammation implicated in the initiation of the transformation of Naïve to CIA-SFs, IL-1 $\beta$ -mediated downstream effector mechanisms were assessed by RNA-Seq in the cells expanded in 2D-cultures. Principal Component Analysis (Figure 6-14B)

showed the treated SFs to be transcriptionally distinct from control Naïve SFs with analysis of the significantly DE genes revealing 273 genes to upregulated (Full Table in Appendix B - [2D up-regulated list of differentially expressed genes](#)) and 179 downregulated (Full Table in Appendix B - [2D down-regulated list of differentially expressed genes](#)) [ $>2$ -fold,  $p_{\text{adj}} < 0.01$ ] in response to IL-1 $\beta$  and these are represented both as a volcano plot and in a heatmap (Figure 6-14C), with the top 50 genes significantly upregulated and downregulated listed (Figure 6-14D). As expected, when analysing all differentially expressed genes using KEGG pathway analysis, the upregulated genes were found to be involved in the inflammatory response, interleukin and IL-6 signalling as well as MMP and chemokine signalling, findings consistent with IL-1 $\beta$  being a potent stimulator of RA (Dayer, Oliviero and Punzi, 2017) whilst interestingly, those downregulated were involved in developmental processes and ossification.

Next, we similarly investigated the effect of IL-1 $\beta$  stimulation on the transcriptomic profile of Naïve SFs cultured in Alvetex<sup>®</sup> (Figure 6-15A) and again detected two phenotypically distinct cell populations using Principal Component Analysis (Figure 6-15B). Under these culture conditions, 791 genes were significantly upregulated (Full Table in Appendix B - [Alvetex up-regulated list of differentially expressed genes](#)) and 706 downregulated (Full Table in Appendix B - [Alvetex down-regulated list of differentially expressed genes](#)) [ $>2$ -fold,  $p_{\text{adj}} < 0.01$ ] as shown in the volcano plot and heatmap (Figure 6-15C) of which the top 50 genes significantly upregulated and downregulated in response to IL-1 $\beta$  SFs are listed (Figure 6-15D). As with the cells cultured under conventional 2D conditions, KEGG pathway analysis showed that the upregulated genes were involved in the inflammatory response, whilst those downregulated were associated with Wnt signalling, TGF-beta signalling, Hippo signalling, PI3K-Akt signalling as well as Rap1 signalling.

Finally, the effect of IL-1 $\beta$  on transcriptomic profile of SFs cultured in FNPEG hydrogels was also investigated (Figure 6-16A) and this again showed that exposure to the cytokine drove development of a new distinct population of SF (Figure 6-16B) which exhibited significant upregulation of 706 genes (Full Table in Appendix B - [FNPEG hydrogels up-regulated list of differentially expressed genes](#))

and downregulation of 21 genes (Full Table in Appendix B - FNPEG hydrogels down-regulated list of differentially expressed genes) [ $>2$ -fold,  $p_{\text{adj}} < 0.01$ ], as indicated in the accompanying volcano and heatmap plots (Figure 6-16C) and lists of the top 50 genes significantly upregulated and all downregulated (Figure 6-16D). Similarly, to all the conditions investigated above, the upregulated genes were involved in the inflammatory response. By contrast, the downregulated genes were implicated in regulation of fluid shear stress and atherosclerosis, MAPK and NF-Kappa B signalling, osteoclast and Th17 cell differentiation, as well as inflammatory mediator regulation of transient receptor potential (TRP) channels, which maintain intracellular calcium homeostasis to regulate various functions in cells such as production and release of inflammatory mediators, phagocytosis, and cell migration.

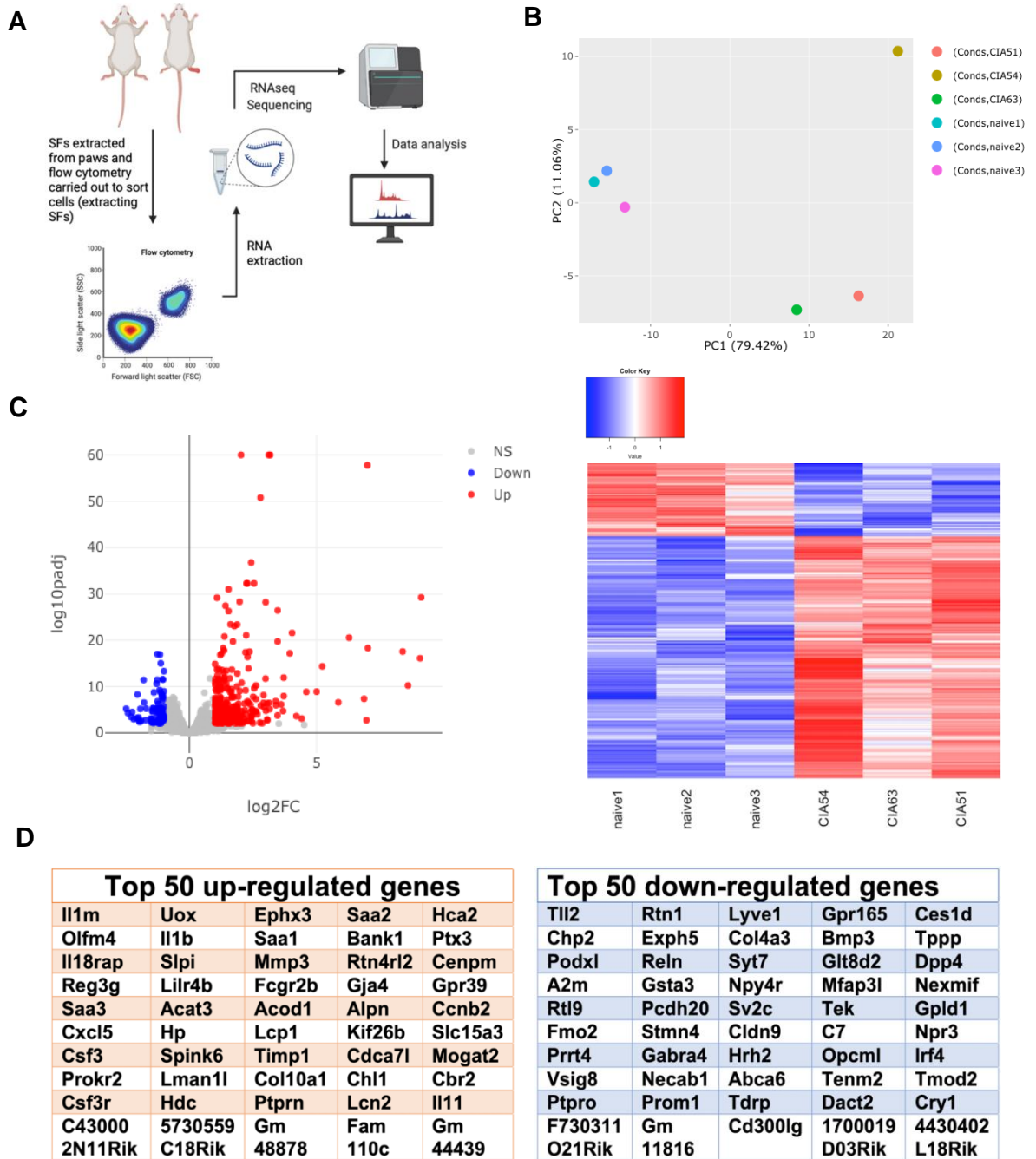
The above KEGG pathway data are presented as Venn diagrams to allow comparison of the commonality and differences between the IL-1 $\beta$  upregulated genes in each culture system (Figure 6-17). Consistent with these Naïve + IL-1 $\beta$  SFs reflecting initiation of a transcriptional programme towards that of CIA-SFs, KEGG pathway enrichment analysis showed that for all three culture systems, there was upregulation of the same pathways namely; “Rheumatoid Arthritis”, “IL-17 signalling”, “TNF signalling”, “Chemokine signalling” and “Cytokine-cytokine signalling”. The genes involved in the pathways for each system do however differ, but it can be concluded that regardless of the system in which the SFs are cultured, IL-1 $\beta$  induces transcriptional reprogramming of Naïve SFs towards that of a more CIA-like phenotype. This in turn suggest that SFs retained the capacity to respond to inflammatory mediators, showing that the non-inflammatory phenotype observed in CIA-SFs cultured in FN hydrogels is a reversible phenotype, since cells are still highly responsive to IL-1 $\beta$ , similarly to those grown in 2D or Alvetex®.

## 6.4 Concluding remarks

RNA-Seq analysis, as evidenced by the PCA plots, confirmed that irregardless of the culture system that the Naïve and CIA SFs exhibited distinct transcriptional profiles, suggesting that all of the systems allow for maintenance of distinct phenotypes associated with healthy and arthritic SFs. Furthermore, it revealed

that SFs cultured in 2D exhibit a modulated DE (CIA versus Naïve SFs) profile from the freshly isolated SFs but that this can be partially recovered when the SFs are cultured in Alvetex®, further establishing that the 3D environment provided by Alvetex® better recapitulates the *in vivo* environment better than conventional 2D cultures. However, when the SFs were subsequently cultured in FNPEG hydrogels, the CIA-SFs displayed a quite distinct phenotype, exhibiting a less pro-inflammatory transcriptional programming, actively downregulating inflammatory pathways and upregulating those associated with the ECM. This could be due to SFs from a 2D culture system simply coated with FN adapting to a microenvironment entirely comprised of FN.

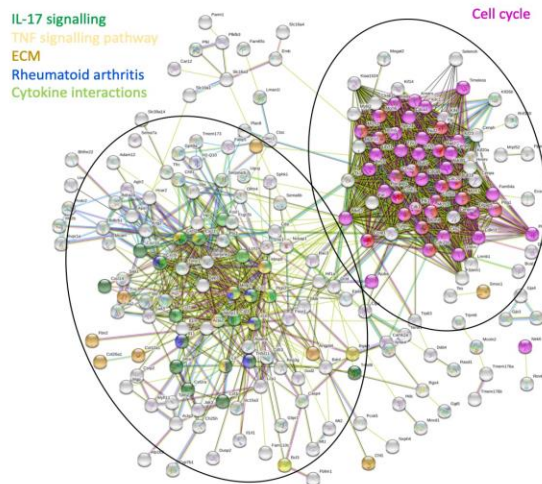
Regarding the transcriptomic profiling observed in the Naïve SFs, it could be seen that pro-inflammatory pathways were upregulated in response to acute stimulation with IL-1 $\beta$ . This was true for SFs cultured in 2D, Alvetex® and FNPEG hydrogels, suggesting that not only do SFs respond to inflammatory mediators such as IL-1 $\beta$  in all models resulting in transcriptional programming of Naïve SFs to more CIA-like, but also that the SFs are able to become similarly activated *in vitro* as observed *in vivo*. Moreover, interestingly despite the CIA-SFs displaying more Naïve-like features in FNPEG hydrogels, when stimulated with IL-1 $\beta$  they exhibit the capacity to become more pro-inflammatory. This suggests that the FNPEG hydrogels still have the potential to maintain the ‘arthritic’ and pro-inflammatory phenotype of SFs upon stimulation.

**Naïve vs CIA:****Figure 6-1: RNA-Seq analysis of sorted SFs.**

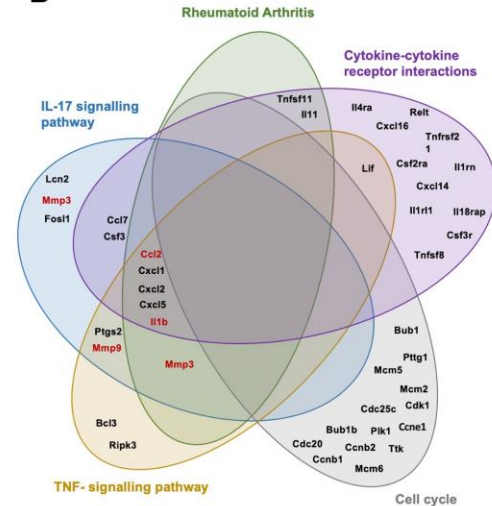
(A) Bulk RNA-Seq setup. RNA was isolated from healthy ( $n = 3$ ) and arthritic CIA ( $n = 3$ , scores of 9, 10, and 11) mice and subjected to bulk RNA-Seq (75 bp paired-end, 30 M reads). (B) Principal component analysis (PCA) confirmed distinction between Naïve and CIA groups (conds = conditions). (C) Differential expression (DE) of genes are shown. All detected genes are plotted as a volcano plot (left) where  $x =$  gene expression healthy,  $y =$  gene expression arthritic. Genes that pass a threshold of  $p_{adj} < 0.01$  and  $|\log_2\text{foldChange}| > 2$  in DE analysis are shown in blue when they are downregulated and red when upregulated in the CIA mice. Heatmap (right) shows up and downregulated genes; [unsupervised clustering in rows and columns based on Euclidean distances]. (D) Top 50 up and down-regulated differentially expressed (DE) genes in CIA.

## Up-regulated

A

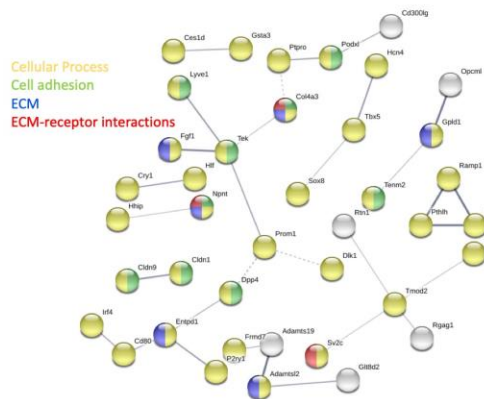


B



## Down-regulated

C



D

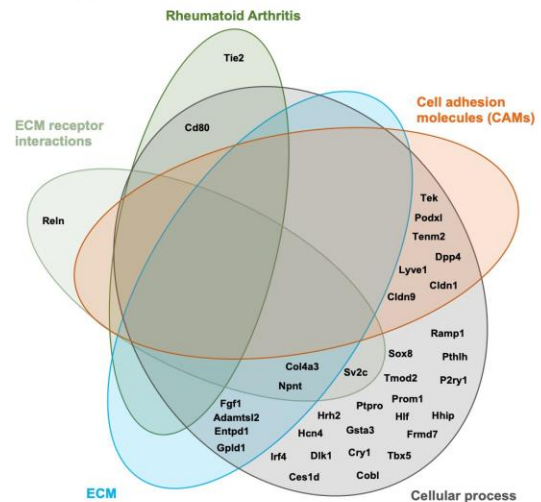


**Figure 6-2: Up and downregulated pathways in CIA sorted SFs compared to Naïve.** Function enrichment and network analysis regulated by synovial inflammation. STRING protein-protein interaction network (<https://string-db.org>) was performed on DE genes from the previous figure. Significantly (A) upregulated and (C) down regulated modulated pathways and cellular components associated with DE genes in arthritic mice are shown on the diagram. [PPI enrichment  $p$ -value:  $< 1.0e-16$ ]. Colour code for nodes in upregulated pathways is, dark green: IL-17 signalling, yellow: TNF signalling pathway, khaki: ECM, blue: Rheumatoid arthritis, light green: cytokine interactions, pink: cell cycle: pink. Colour code for nodes in downregulated pathways is yellow: cellular process, blue: ECM, light green: cell adhesion, red: ECM-receptor interactions. Venn diagram of prominent top 50 (B) up-regulated and (D) downregulated KEGG pathways. Colour code for each KEGG pathway is dark green: Rheumatoid arthritis, purple: cytokine-cytokine receptor interactions, light grey: cell cycle, yellow: TNF signalling pathway, blue: IL-17 signalling pathway, light green: ECM receptor interactions, cyan: ECM, dark grey: cellular process and orange: cell adhesion molecules (CAMs).

## Naïve vs CIA: 2D

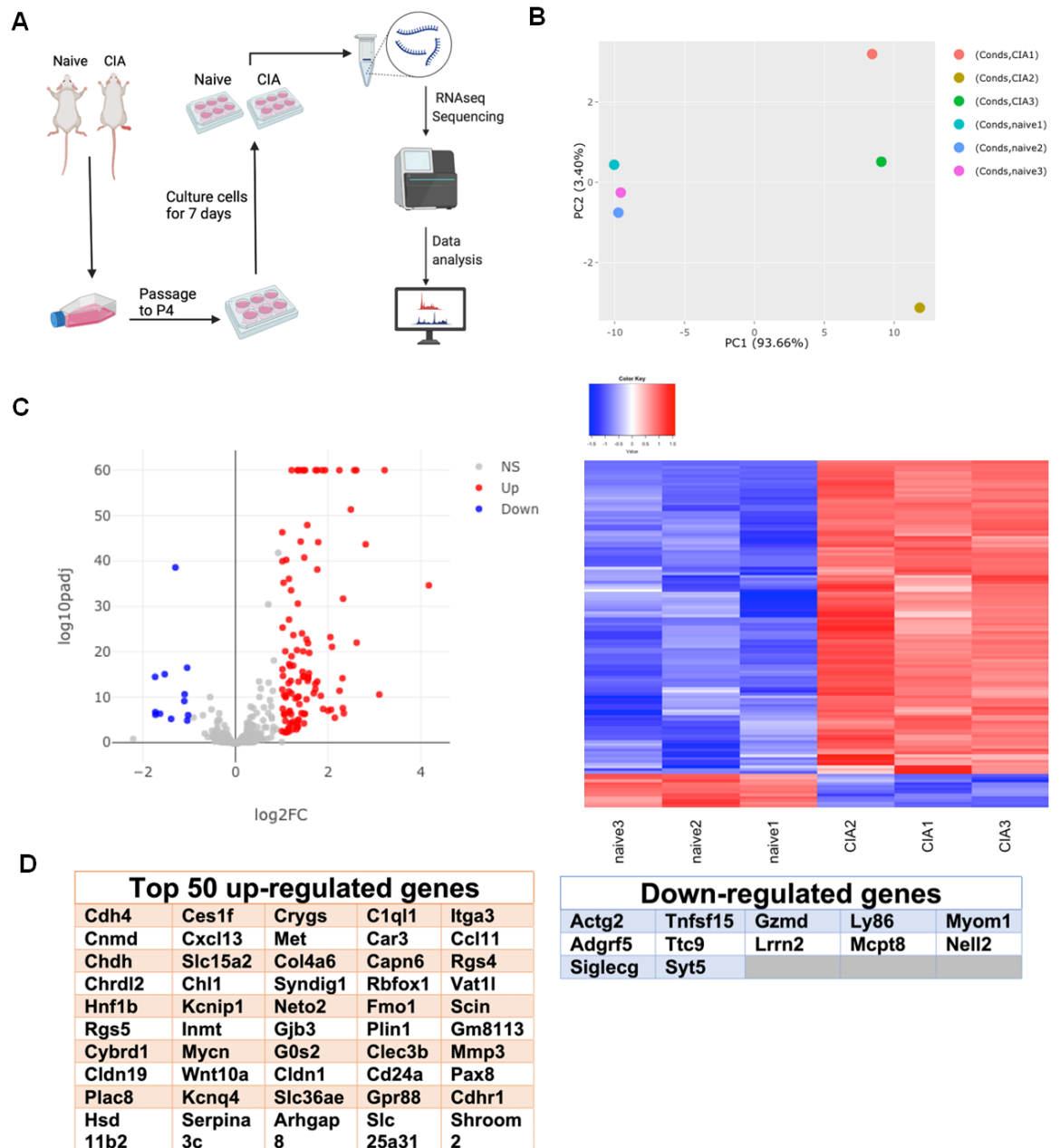


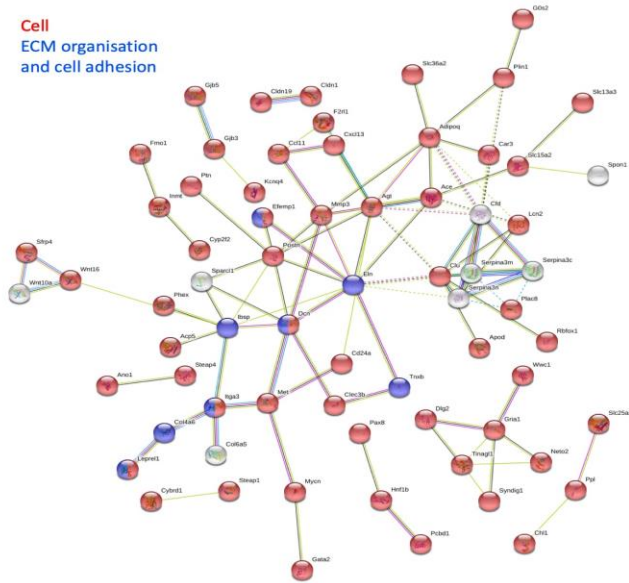
**Figure 6-3: RNA-Seq analysis of SFs cultured in 2D.**

(A) Bulk RNA-Seq setup. RNA was isolated from healthy and arthritic CIA murine SFs and cultured in 2D with FN for 7 days and then subjected to bulk RNA-Seq (75 bp paired-end, 30 M reads). (B) Principal component analysis (PCA) confirmed distinction between Naïve and CIA groups (conds = conditions). (C) Differential expression (DE) of genes are shown. All detected genes are plotted as a volcano plot (left) where  $x$  = gene expression healthy,  $y$  = gene expression arthritic. Genes that pass a threshold of  $p_{adj} < 0.01$  and  $|\log_2\text{foldChange}| > 2$  in DE analysis are shown in blue when they are downregulated and red when upregulated in the CIA mice. Heatmap (right) shows up and downregulated genes; [unsupervised clustering in rows and columns based on Euclidean distances]. (D) Top 50 upregulated and all down-regulated differentially expressed (DE) genes in CIA.

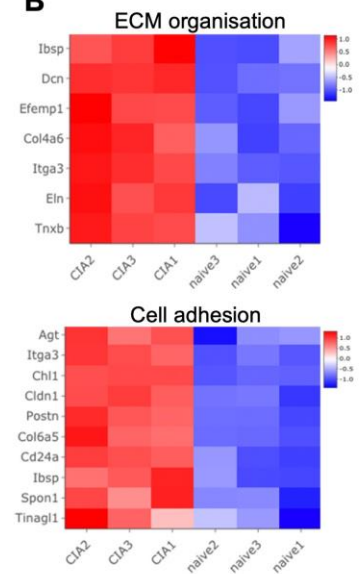
## Up-regulated

A

Cell  
ECM organisation  
and cell adhesion



B



## Down-regulated

C

Fibronectin type III domain  
Immunoglobulins  
Serine proteases / trypsin like  
peptidase

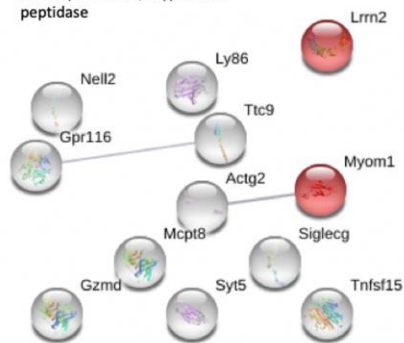


**Figure 6-4: Up and downregulated gene expression in Naïve and CIA SFs cultured in 2D with FN for 7 days.**

Function enrichment and network analysis regulated by synovial inflammation. STRING protein-protein interaction network (<https://string-db.org>) was performed on DE genes from the previous figure. Significantly (A) upregulated and (C) down regulated modulated pathways and cellular components associated with DE genes in arthritic mice are shown on the diagram. [PPI enrichment  $p$ -value:  $< 1.0e-16$ ]. Colour code for nodes in upregulated pathways is, red: cell, blue: ECM organisation and cell adhesion. Colour code for nodes in downregulated pathways is red: fibronectin type 3 domain, black: Immunoglobulins and serine proteases/trypsin like peptidase. (B) Heatmaps of genes involved in ECM organisation and cell adhesion in top 50 up-regulated genes.

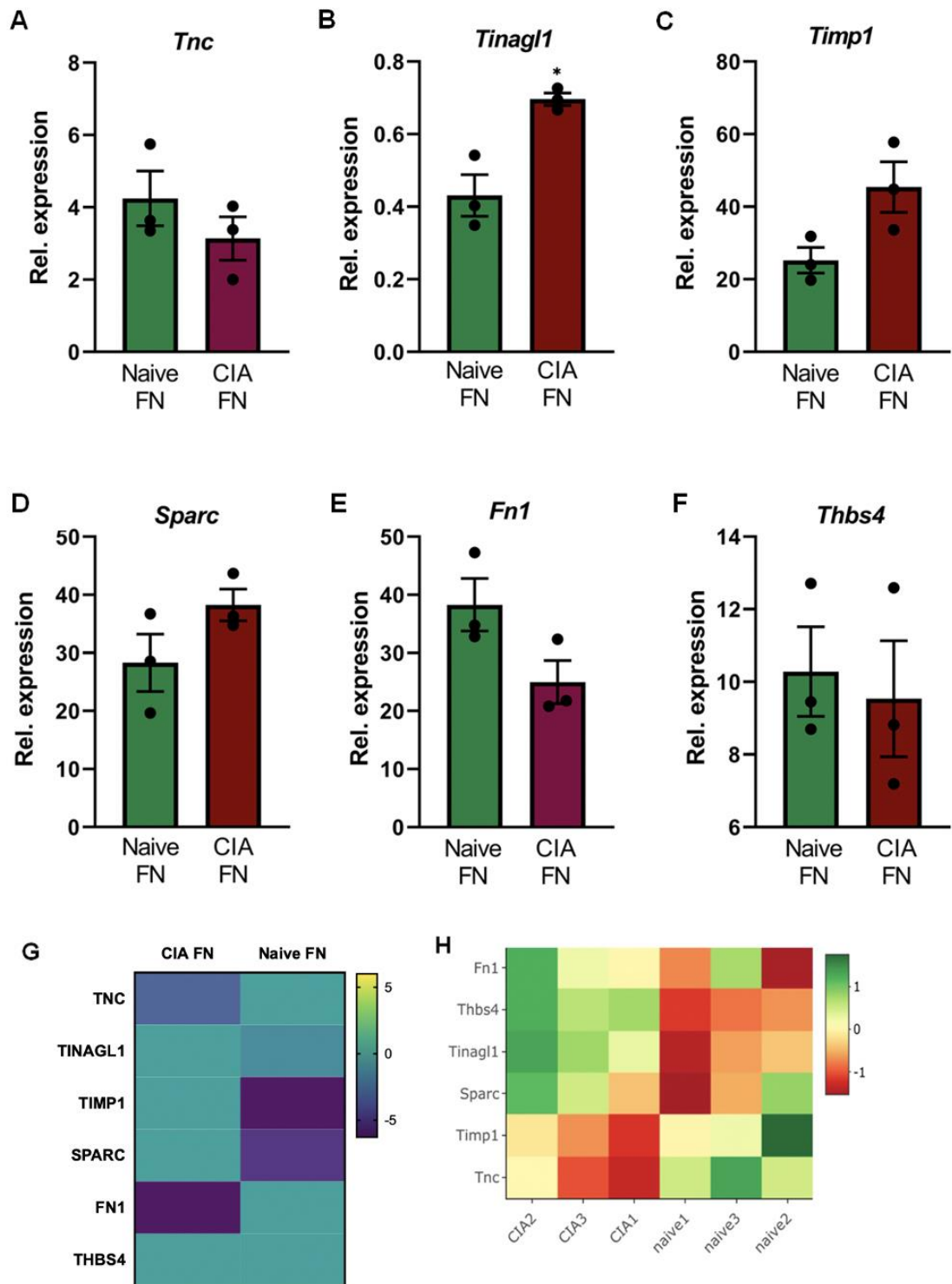


**Figure 6-5: 2D RNA-Seq validation.**

Naïve and CIA SFs were expanded and cultured in 2D plates coated with FN for 7 days after which q-PCR was carried out to determine quantification of (A) *Tnc* (B) *Tinagl1* (C) *Timp1* (D) *Sparc* (E) *Fn1* and (F) *Thbs4* expression. Naïve vs CIA gene heatmap for (G) above experiments and (H) corresponding RNA-Seq experiment. Results show relative expression to Actin, showing mean  $\pm$  SD. Each dot represents a biological replicate (in technical triplicate). Statistical significance was determined using unpaired *t*-test; \*\* $p < 0.01$

## Naïve vs CIA: Alvetex®

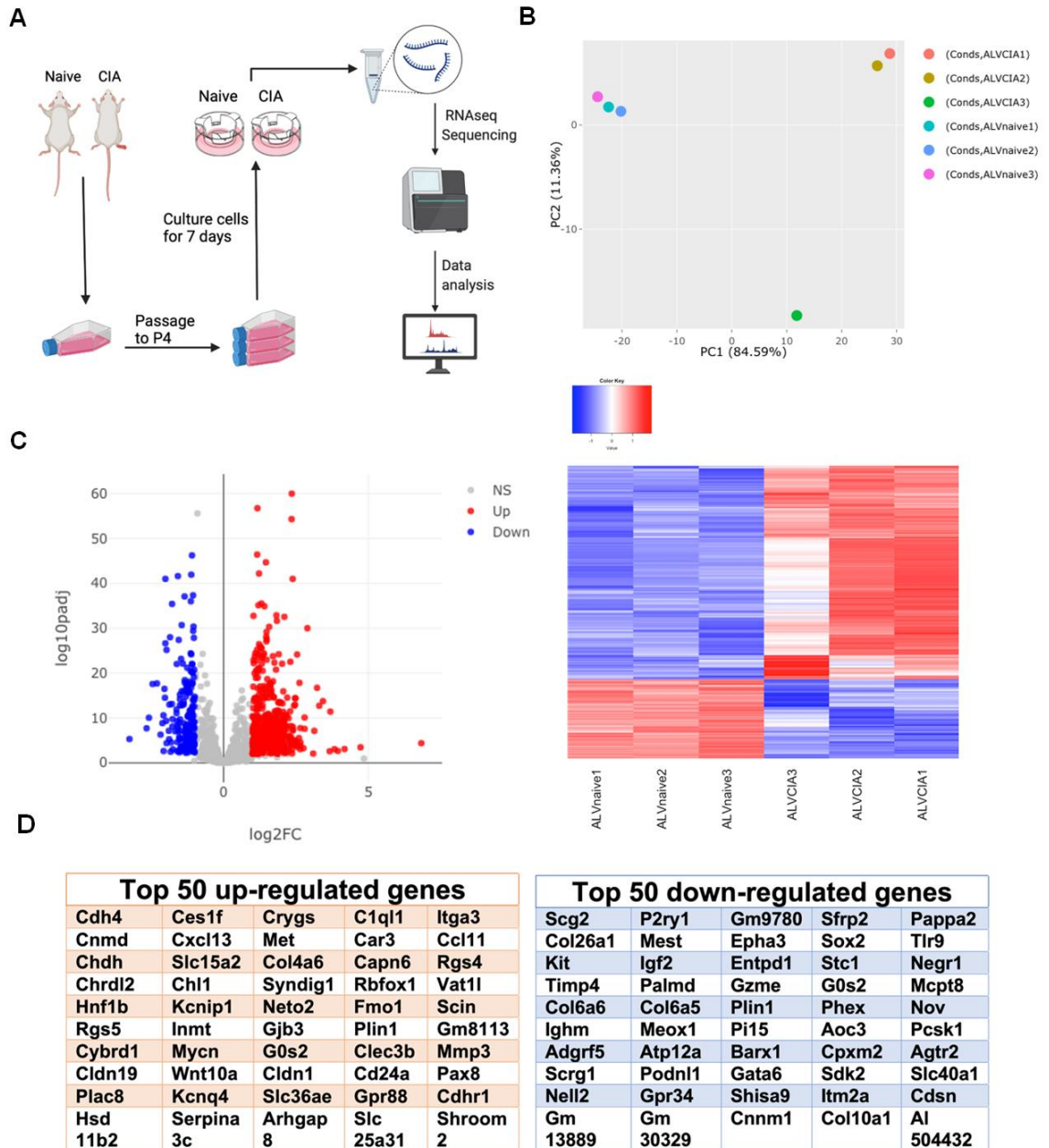


**Figure 6-6: RNA-Seq analysis of SFs cultured in Alvetex®.**

(A) Bulk RNA-Seq setup. RNA was isolated from healthy and arthritic CIA murine SFs expanded in 2D cultured in Alvetex® with FN for 7 days and then subjected to bulk RNA-Seq (75 bp paired-end, 30 M reads). (B) Principal component analysis (PCA) confirmed distinction between Naïve and CIA groups (conds = conditions). (C) Differential expression (DE) of genes are shown. All detected genes are plotted as a volcano plot (left) where  $x$  = gene expression healthy,  $y$  = gene expression arthritic. Genes that pass a threshold of  $p_{adj} < 0.01$  and  $|\log_2\text{foldChange}| > 2$  in DE analysis are shown in blue when they are downregulated and red when upregulated in the CIA mice. Heatmap (right) shows up and downregulated genes; [unsupervised clustering in rows and columns based on Euclidean distances]. (D) Top 50 up and down-regulated differentially expressed (DE) genes in CIA.



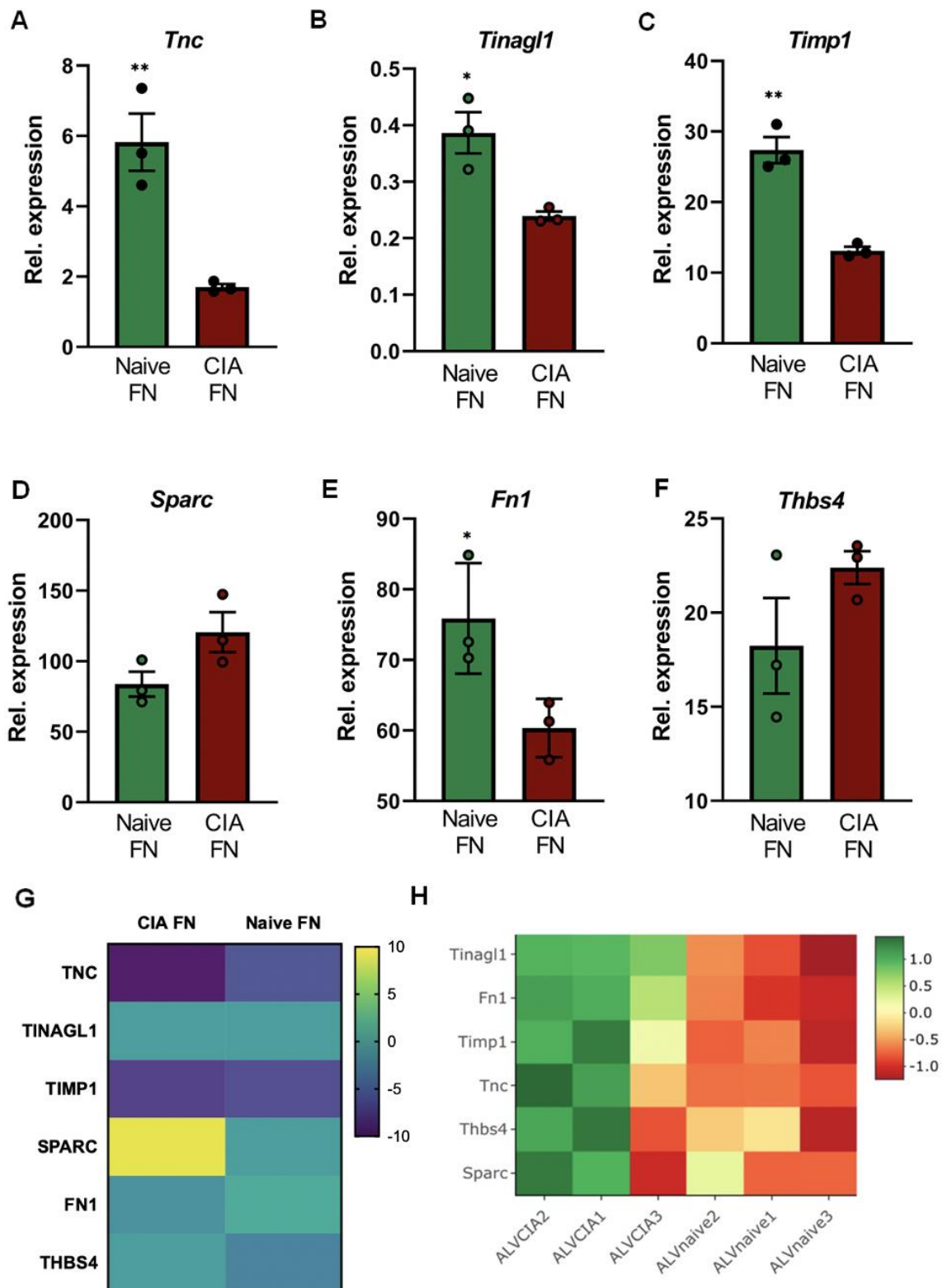


**Figure 6-8: Alvetex® RNA-Seq validation.**

Naïve and CIA SFs were expanded in 2D then cultured in Alvetex® in FN for 7 days after which q-PCR was carried out to determine quantification of (A) *Tnc* (B) *Tinagl1* (C) *Timp1* (D) *Sparc* (E) *Fn1* and (F) *Thbs4* expression. Naïve vs CIA gene heatmap for (G) above experiments and (H) corresponding RNA-Seq experiment. Results show relative expression to Actin, showing mean  $\pm$  SD. Each dot represents a biological replicate (in technical triplicate). Statistical significance was determined using unpaired *t*-test; \* $p < 0.05$ , \*\* $p < 0.01$

## Naïve vs CIA: FNPEG Hydrogel

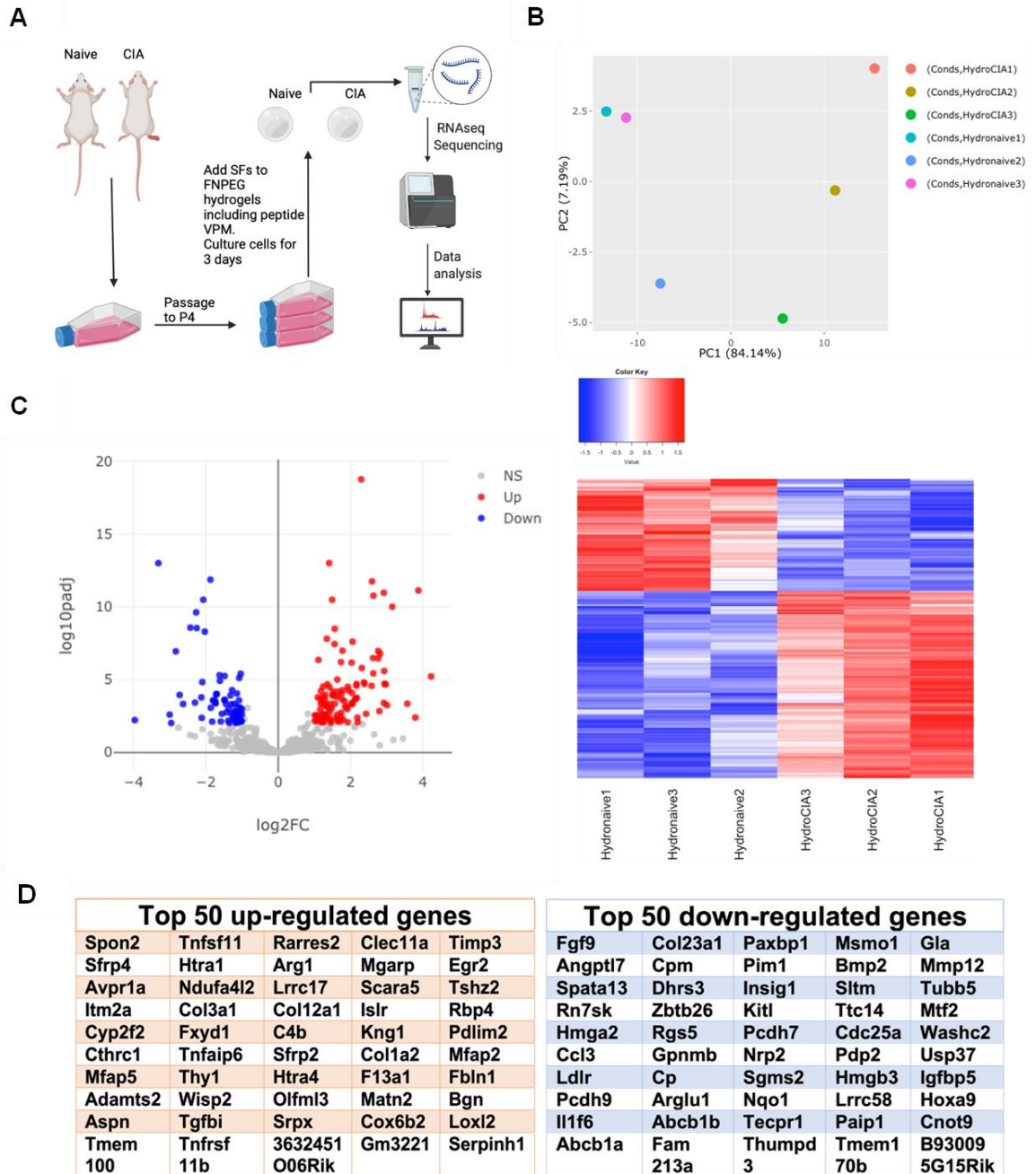
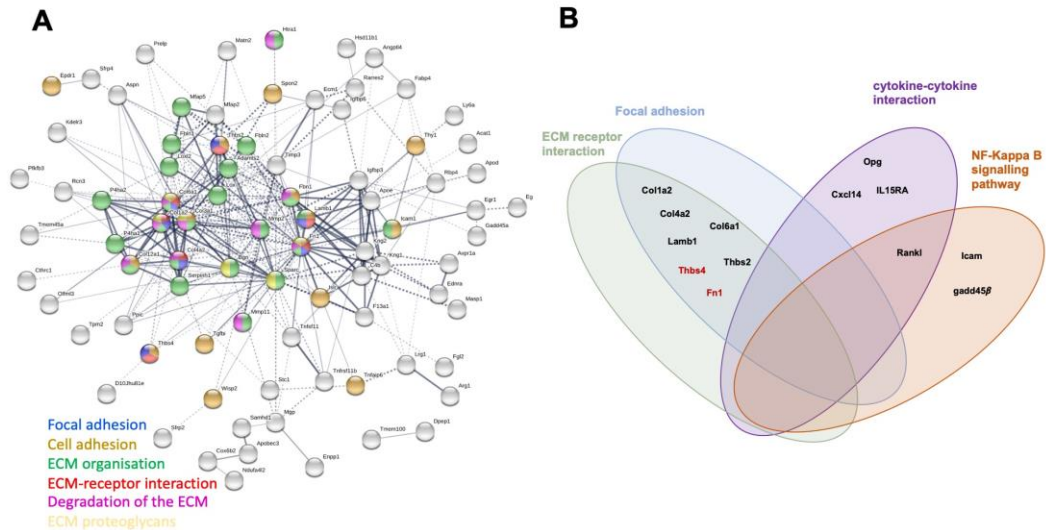


**Figure 6-9: RNA-Seq analysis of SFs cultured in FNPEG hydrogels.**

(A) Bulk RNA-Seq setup. RNA was isolated from healthy and arthritic CIA murine SFs expanded in 2D cultured in Alvetex<sup>®</sup> with FN for 3 days and then subjected to bulk RNA-Seq (75 bp paired-end, 30 M reads). (B) Principal component analysis (PCA) confirmed distinction between Naïve and CIA groups (conds = conditions). (C) Differential expression (DE) of genes are shown. All detected genes are plotted as a volcano plot (left) where  $x$  = gene expression healthy,  $y$  = gene expression arthritic. Genes that pass a threshold of  $p_{adj} < 0.01$  and  $|\log_2\text{foldChange}| > 2$  in DE analysis are shown in blue when they are downregulated and red when upregulated in the CIA mice. Heatmap (right) shows up and downregulated genes; [unsupervised clustering in rows and columns based on Euclidean distances]. (D) Top 50 up and down-regulated differentially expressed

## Up-regulated



## Down-regulated

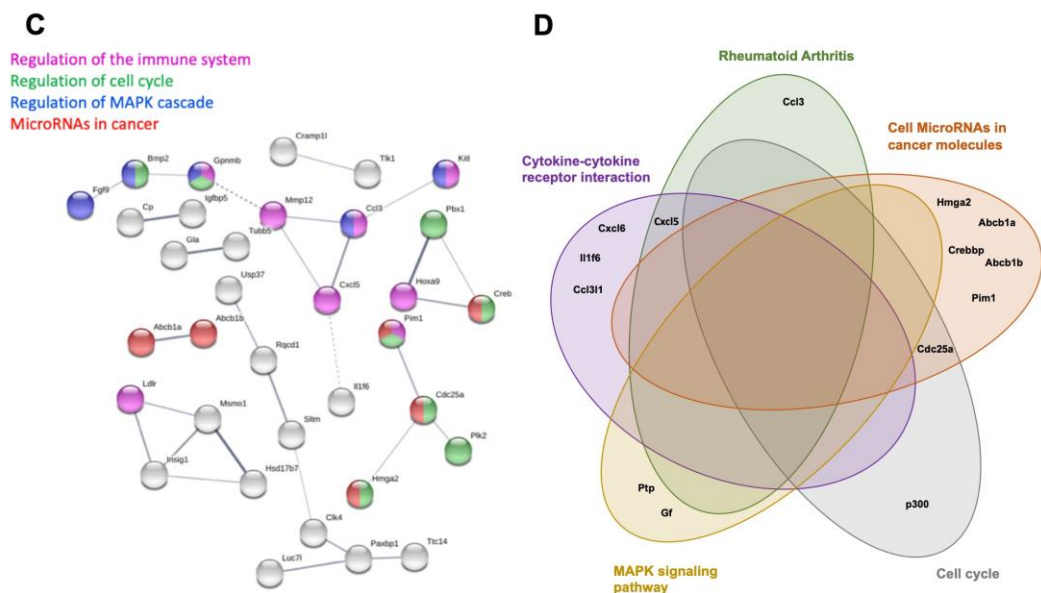


**Figure 6-10: Up and downregulated gene expression in Naïve and CIA SFs cultured in FNPEG hydrogels for 3 days.**

Function enrichment and network analysis regulated by synovial inflammation. STRING protein-protein interaction network (<https://string-db.org>) was performed on DE genes from the previous figure. Significantly (A) upregulated and (C) down regulated modulated pathways and cellular components associated with DE genes in arthritic mice are shown on the diagram. [PPI enrichment  $p$ -value:  $< 1.0e-16$ ]. Colour code for nodes in upregulated pathways is, green: ECM organisation, yellow: ECM proteoglycans, khaki: cell adhesion blue: focal adhesion, pink: Degradation of the ECM, red: ECM-receptor interaction. Colour code for nodes in downregulated pathways is blue: Regulation of MAPK cascade, green: Regulation of cell cycle, red: MicroRNAs in cancer and pink Regulation of immune system. Venn diagram of prominent top 50 (B) up-regulated and (D) downregulated KEGG pathways. Colour code for each KEGG pathway is dark green: Rheumatoid arthritis, purple: cytokine-cytokine receptor interactions, light grey: cell cycle, yellow: MAPK signalling pathway, orange: cell microRNAs in cancer molecules, light green: ECM receptor interactions, light blue: focal adhesion, dark orange: NK-kappa B signalling pathway.

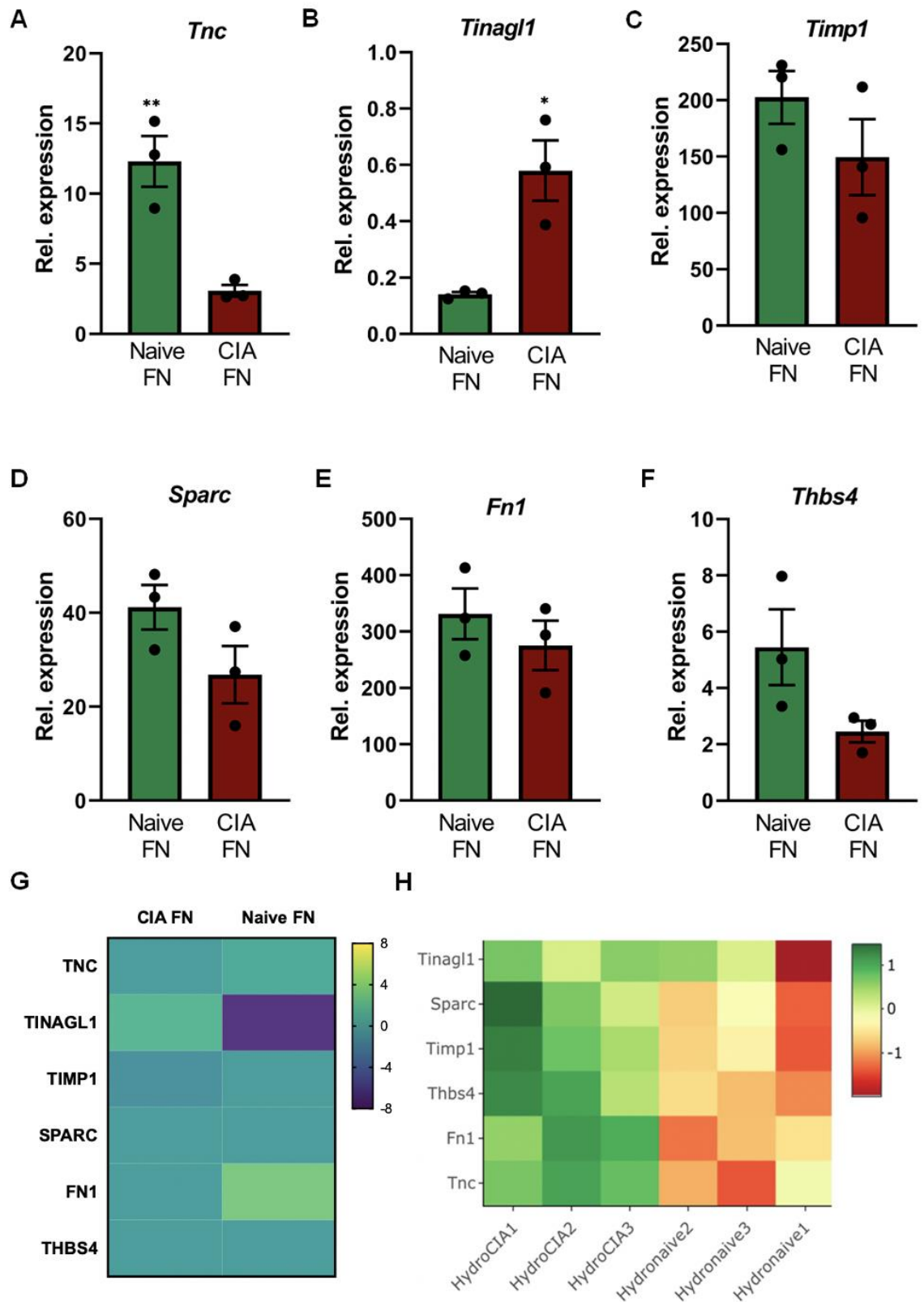
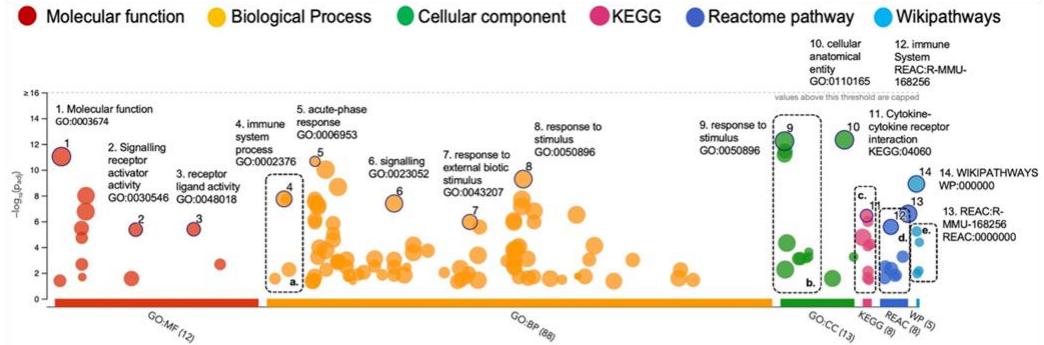


**Figure 6-11: FNPEG RNA-Seq validation.**

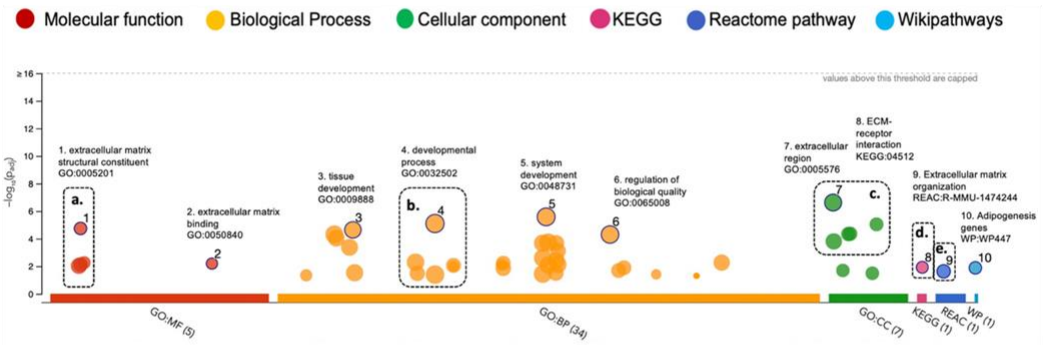
Naïve and CIA SFs were cultured in degradable FNPEG hydrogels for 3 days after which q-PCR was carried out to determine quantification of (A) *Tnc* (B) *Tinagl1* (C) *Timp1* (D) *Sparc* (E) *Fn1* and F *Thbs4* expression. Naïve vs CIA gene heatmap for (G) above experiments and (H) corresponding RNA-Seq experiment. Results show relative expression to Actin, showing mean  $\pm$  SD. Each dot represents a biological replicate (in technical triplicate). Statistical significance was determined using unpaired *t*-test; \* $p < 0.05$ , \*\* $p < 0.01$

A



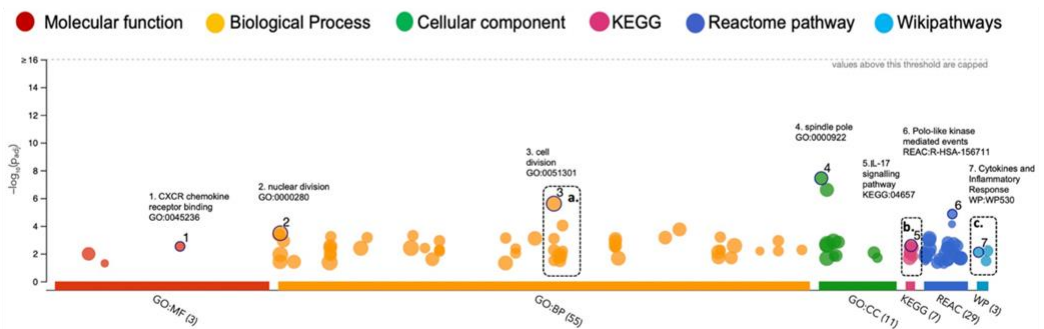
- a. Immune system: regulation, process, inflammatory response
- b. ECM: ECM space, ECM region, external encapsulating structure
- c. Cytokine- cytokine receptor interaction: IL-17, TNF and JAK-STAT signaling, RA
- d. Immune system (IS): Innate IS, cytokine signalling, signalling by interleukins
- e. Wikipathways: cytokines and inflammatory response, MMPs, IL-1 signalling pathway

B



- a. ECM structural constituent, glycosaminoglycan binding, structural molecule activity
- b. Developmental process: cell differentiation, migration, cell junction organisation
- c. Extracellular region, extracellular space, ECM, collagen-containing ECM
- d. KEGG: ECM receptor interaction
- e. Reactome: ECM organisation

C



- a. Cell division and regulation
- b. KEGG: IL-17 signalling pathway, cytokine-cytokine receptor interactions, viral protein interaction, cell cycle
- c. WP: cytokines and inflammatory response, fibrin complement receptor 3 signalling pathway, SARS-CoV-2 Innate Immunity Evasion and Cell-specific immune response

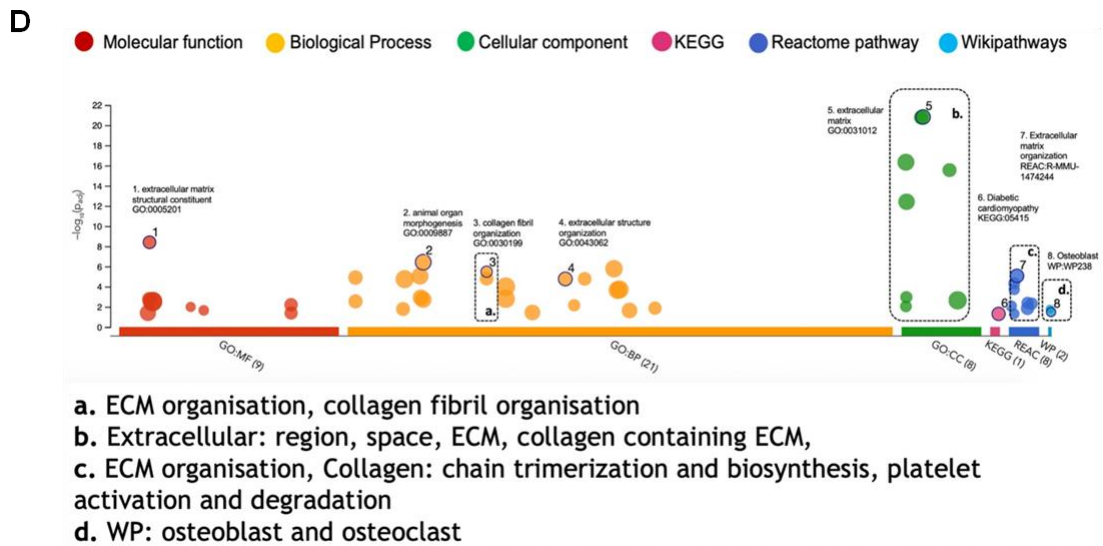


**Figure 6-12: The functional consequences of SFs cultured in differing culture systems.**

Differentially up-regulated genes (A) from sorted joint SFs and SFs cultured in (B) 2D (C) Alvetex® and (D) FNPEG hydrogels. Data was assessed by the publicly available server g:Profiler using the databases KEGG, Gene Ontology (GO) and Reactome to detect significantly enriched biological processes, pathways and protein complexes visualized with a Manhattan-like-plot.

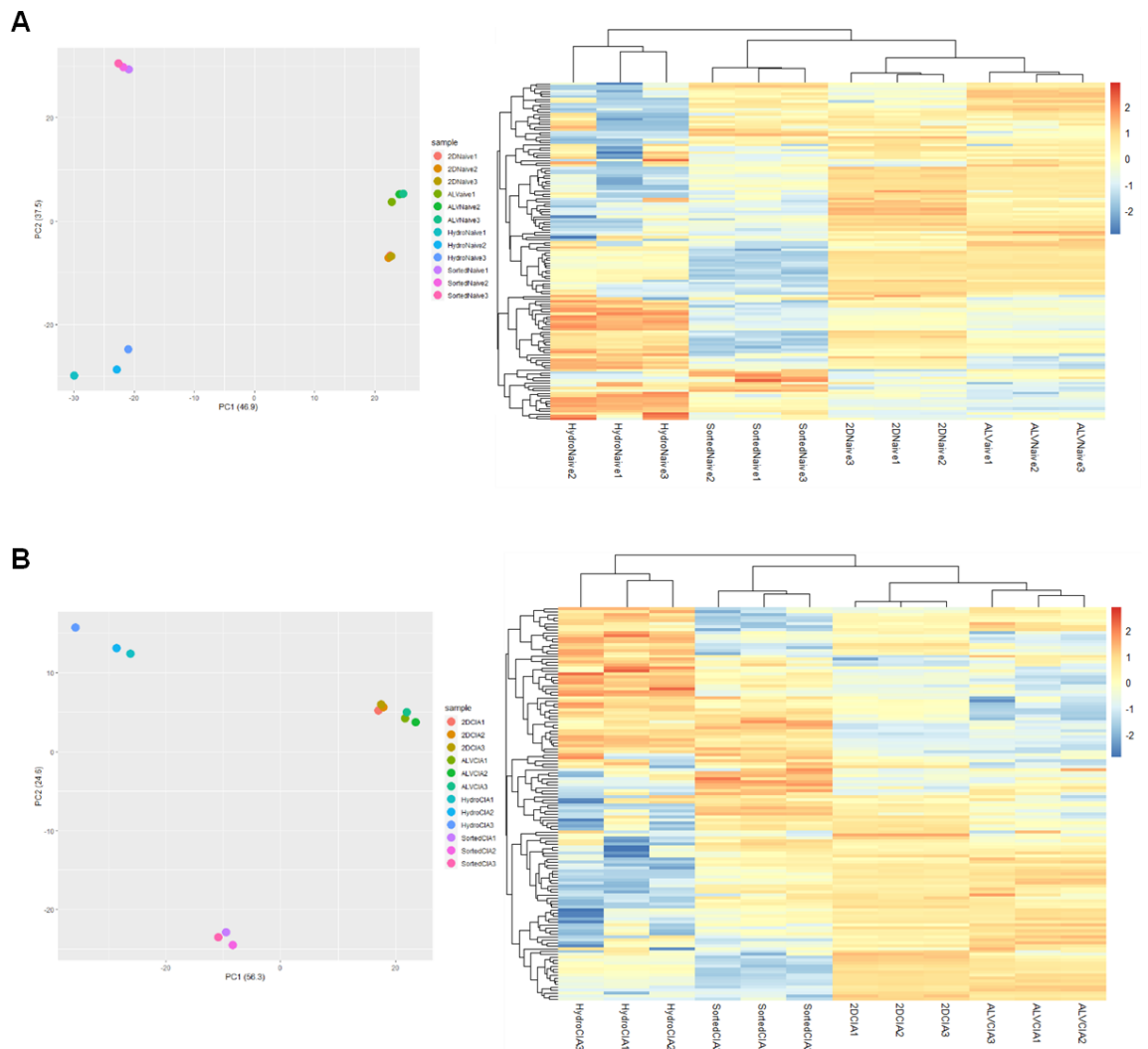


**Figure 6-13: PCA and differential gene expression comparison of SFs cultured in different microenvironments.**

RNA was isolated from healthy ( $n = 3$ ) and arthritic CIA ( $n = 3$ , scores of 9, 10, and 11) mice as well as SFs expanded in 2D and cultured with FN in 2D, Alvetex® and FNPEG hydrogels for 7 days after which they were subjected to bulk RNA-Seq (75 bp paired-end, 30 M reads). Principal component analysis (PCA) and differential expression (DE) are shown for all (A) Naïve and (B) CIA SFs, clearly showing distinct differences between systems. Genes that pass a threshold of  $p_{adj} < 0.01$  and  $|\log_2\text{foldChange}| > 2$  in DE analysis are coloured in blue when they are downregulated and red when they are upregulated in the arthritic (CIA) mice. Corresponding heatmaps for (A) Naïve and (B) CIA SFs show upregulated and downregulated genes; [unsupervised clustering in rows and columns based on Euclidean distances].

## Naïve vs Naïve + IL-1 $\beta$ : 2D

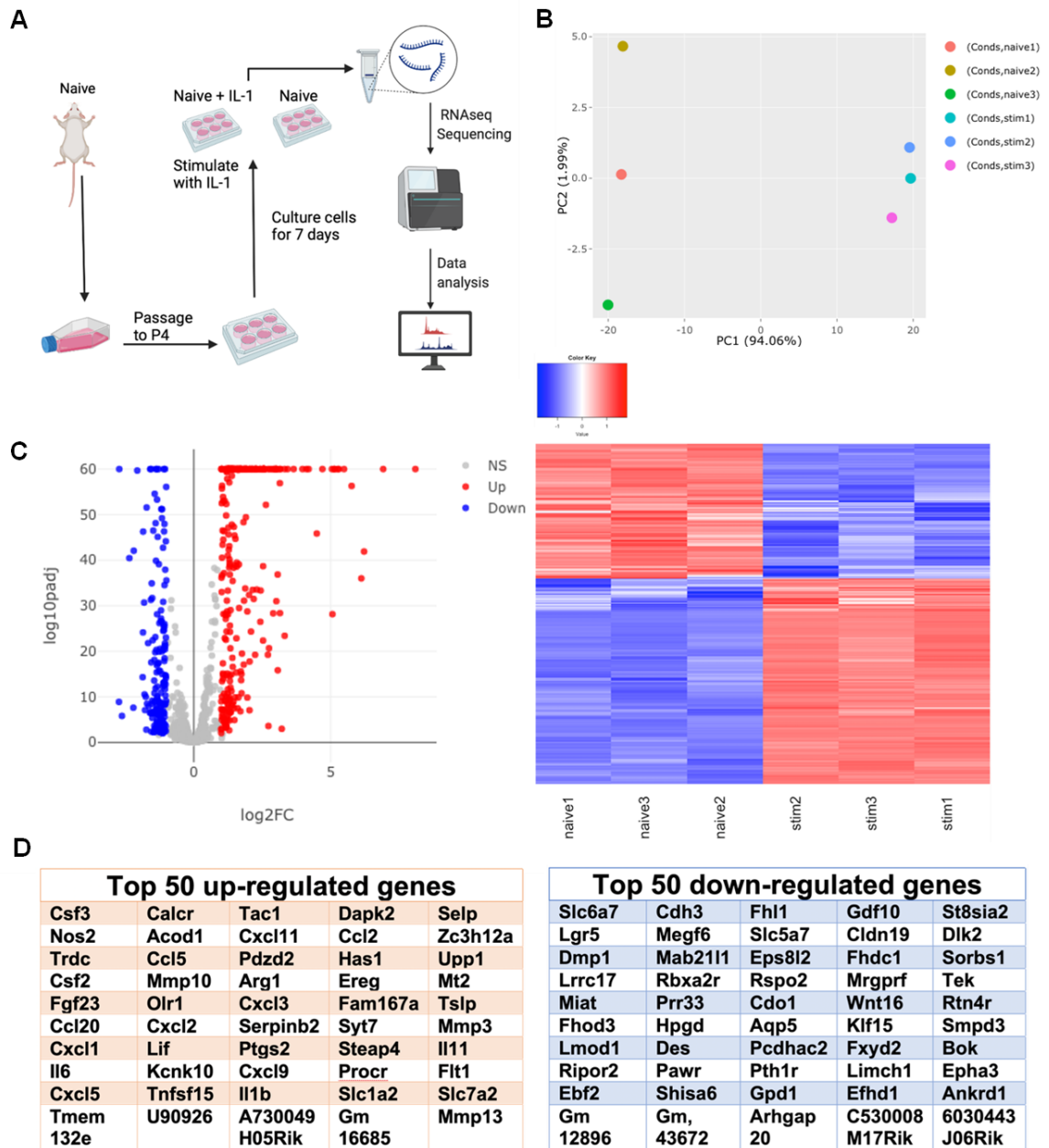


**Figure 6-14: RNAseq analysis of SFs Naïve cultured in 2D with FN in the presence and absence of IL-1 $\beta$ : stimulation.**

(A) Bulk RNAseq setup. RNA was isolated from Naïve SFs, in the presence and absence of overnight IL-1 $\beta$  stimulation cultured in 2D with FN for 7 days and subjected to bulk RNA-Seq (75 bp paired-end, 30 M reads). (B) Principal component analysis (PCA) confirmed distinction between Naïve stimulated and unstimulated groups (conds = conditions). (C) Differential expression (DE) of genes are shown. All detected genes are plotted as a volcano plot (left) where  $x$  = gene expression healthy,  $y$  = gene expression arthritic. Genes that pass a threshold of  $p_{adj} < 0.01$  and  $|\log_2\text{foldChange}| > 2$  in DE analysis are shown in blue when they are downregulated and red when upregulated in the stimulated mice. Heatmap (right) shows up and downregulated genes; [unsupervised clustering in rows and columns based on Euclidean distances]. (D) Top 50 up and down-regulated differentially expressed (DE) genes.

## Naïve vs Naïve + IL-1 $\beta$ : Alvetex®

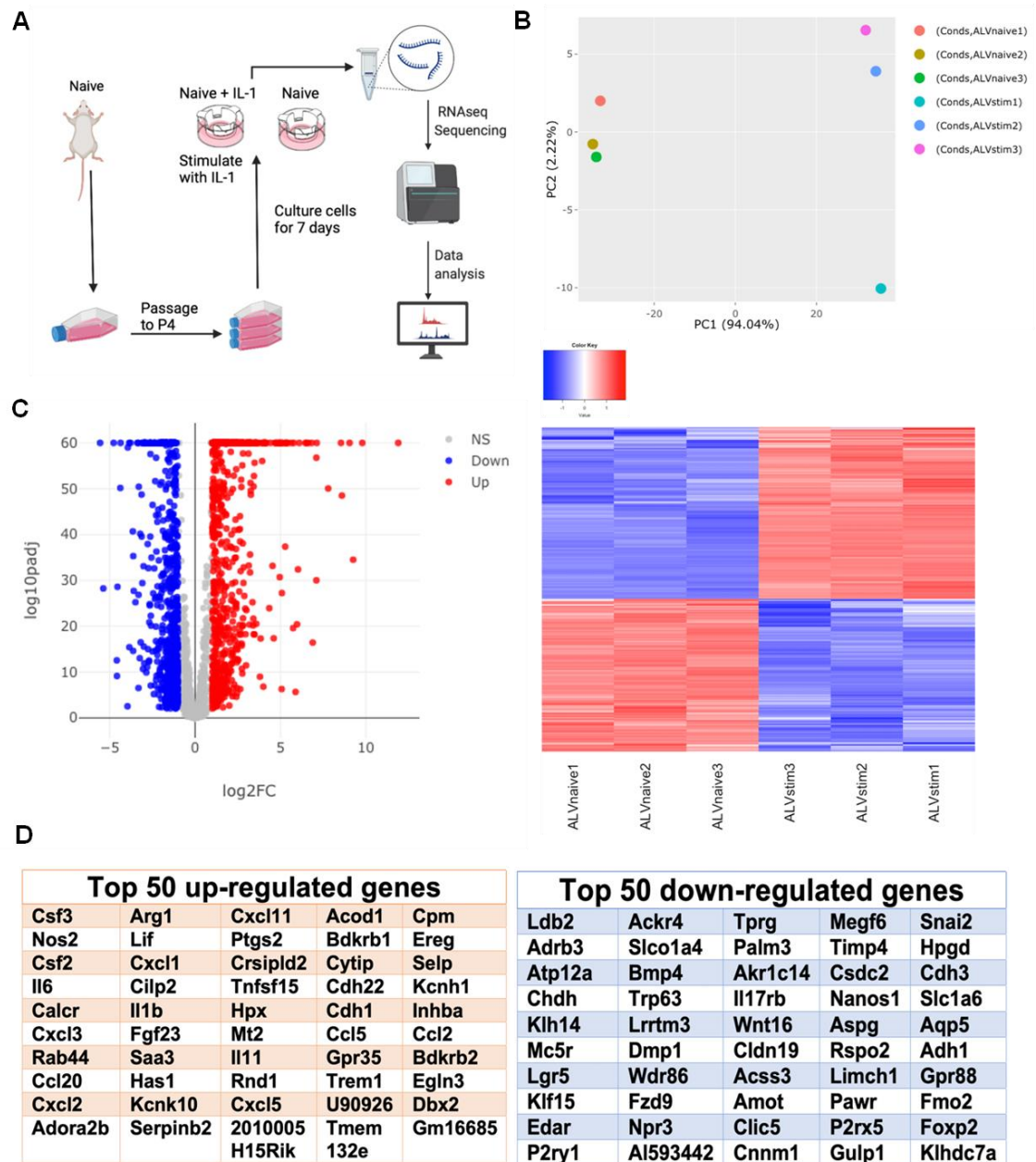


**Figure 6-15: RNA-Seq analysis of SFs Naïve cultured in Alvetex® with FN in the presence and absence of IL-1 $\beta$ : stimulation.**

(A) Bulk RNA-Seq setup. RNA was isolated from Naïve SFs, in the presence and absence of IL-1 $\beta$  stimulation cultured in Alvetex® with FN and subjected to bulk RNA-Seq (75 bp paired-end, 30M reads). (B) Principal component analysis (PCA) confirmed distinction between Naïve stimulated and unstimulated groups (conds = conditions). (C) Differential expression (DE) of genes are shown. All detected genes are plotted as a volcano plot (left) where x = gene expression healthy, y = gene expression arthritic. Genes that pass a threshold of  $p_{adj} < 0.01$  and  $|\log_2\text{foldChange}| > 2$  in DE analysis are shown in blue when they are downregulated and red when upregulated in the stimulated mice. Heatmap (right) shows up and downregulated genes; [unsupervised clustering in rows and columns based on Euclidean distances]. (D) Top 50 up and down-regulated differentially expressed (DE) genes.

## Naïve vs Naïve + IL-1 $\beta$ : FNPEG Hydrogels

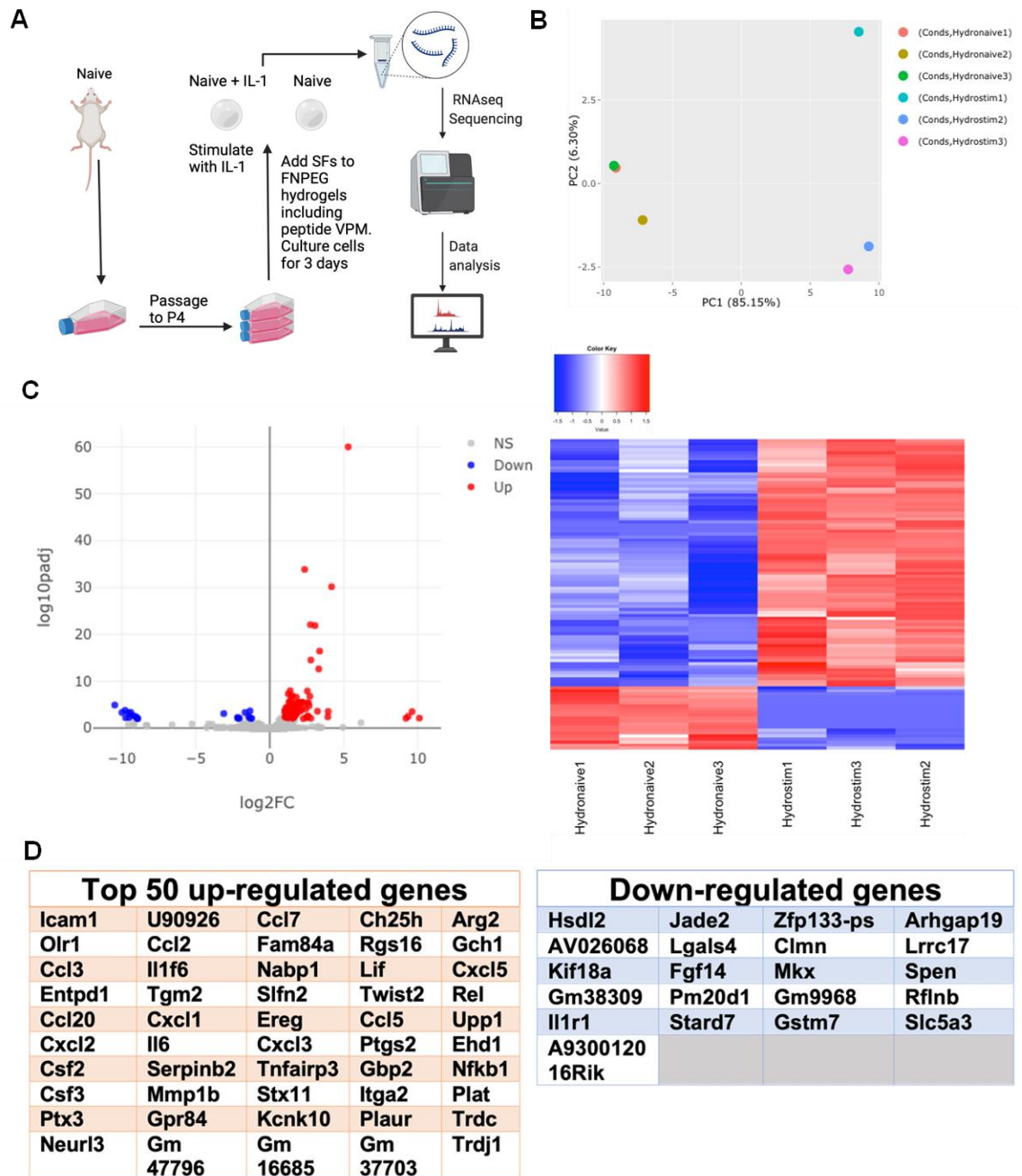


**Figure 6-16: RNA-Seq analysis of SFs Naïve cultured in FNPEG hydrogels with FN in the presence and absence of IL-1 $\beta$ : stimulation.**

(A) Bulk RNA-Seq setup. RNA was isolated from Naïve SFs, in the presence and absence of IL-1 $\beta$  stimulation cultured in FNPEG hydrogels and subjected to bulk RNA-Seq (75 bp paired-end, 30 M reads). (B) Principal component analysis (PCA) confirmed distinction between Naïve stimulated and unstimulated groups (conds = conditions). (C) Differential expression (DE) of genes are shown. All detected genes are plotted as a volcano plot (left) where x = gene expression healthy, y = gene expression arthritic. Genes that pass a threshold of  $p_{adj} < 0.01$  and  $|\log_2\text{foldChange}| > 2$  in DE analysis are shown in blue when they are downregulated and red when upregulated in the stimulated mice. Heatmap (right) shows up and downregulated genes; [unsupervised clustering in rows and columns based on Euclidean distances]. (D) Top 50 up and down-regulated differentially expressed (DE) genes.

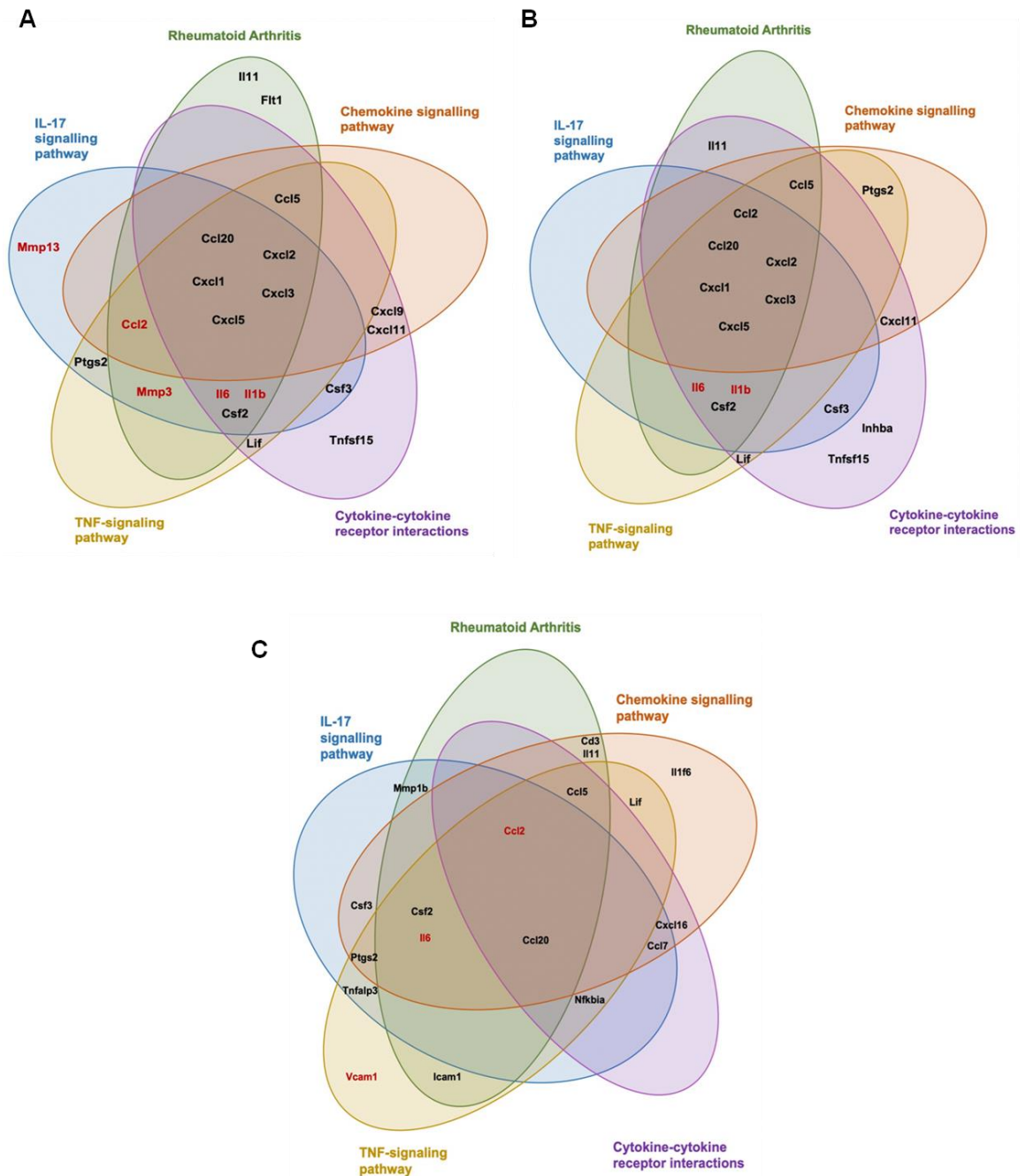


**Figure 6-17: Up regulated gene expression in Naïve SFs in the presence of overnight IL-1 $\beta$  stimulation cultured with FN for 7 days (2D and Alvetex®) or 3 days (FNPEG hydrogels), in differing culture systems.**

Function enrichment and network analysis regulated by synovial inflammation. STRING protein-protein interaction network (<https://string-db.org>) was performed on DE genes from the previous figure. Top 50 significantly upregulated modulated KEGG pathways associated with DE genes are shown in (A) 2D (B) Alvetex® and (C) FNPEG hydrogels. Colour code for each upregulated KEGG pathway is dark green: Rheumatoid arthritis, purple: cytokine-cytokine receptor interactions, yellow: TNF signalling pathway, blue: IL-17 signalling pathway, orange: chemokine signalling pathway.

## Chapter 7 Discussion

### 7.1 Summary

The overall aims and objectives of this project were to investigate and characterise the inflammatory responses of both Naïve and CIA SFs when cultured in 2D and 3D microenvironments as well as define whether SF subsets could be identified and maintained within each culture system. Despite the Naïve and CIA SF responses in 2D proving to be consistent with that of literature involving animal models and *in vivo* studies, the culture system does not allow for the identification of the lining and sublining SF subpopulations. On the other hand, when cultured in the 3D polystyrene scaffold Alvetex®, there was shown to be a differentiation of subsets, at least partially, resulting in an increase of lining SFs which could be due to the very high rigidity of the scaffold. As the latter is more akin to that of bone it could provide an explanation as to why the bone eroding lining SFs increase when grown in this culture system. Moreover, the FNPEG hydrogels also were found to allow identification of the differential subsets, specifically the sublining SFs, which were shown to be increased likely because of the ability for the cells to move freely within the gel.

Next the impact of 2D and 3D culture systems on the pro-inflammatory gene expression of Naïve and CIA-SF in the presence of FN was investigated using RNA-Seq. The transcriptomic profiling of Naïve and CIA SFs was initially carried out using SFs extracted directly from the joint (sorted) to use as a reference for differentially expressed genes *in vivo*. It could be seen that SFs cultured in 2D appear to lose expression of certain genes, which is then partially recovered when the cells are subsequently cultured in Alvetex®. On the other hand, when observing the transcriptomic profile of the CIA-SFs subsequently cultured in FNPEG hydrogels there is downregulation of pro-inflammatory pathways and genes that were shown to be upregulated in sorted SFs from the joints and those cultured on Alvetex®. However interestingly, when Naïve hydrogel SFs were stimulated with IL-1 $\beta$ , there was an upregulation of pro-inflammatory pathways and genes, similarly to that observed in all the other culture conditions. This suggests that Naïve hydrogel SFs have the potential to become an arthritic, proinflammatory cells despite this phenotype not apparently being maintained by the

(unstimulated) CIA-SFs grown in this platform. Furthermore, comparing the systems alone with the same cell type it could be seen that despite their differences when comparing Naïve and CIA, 2D and Alvetex® show similar responses whilst SFs cultured in FNPEG hydrogels are more similar to *in vivo* than to the responses observed in 2D and Alvetex®.

Finally, the migration and organisation of SF through the 3D culture systems - Alvetex® and FNPEG hydrogels - was explored and this showed that Alvetex® scaffolds allowed a certain degree of SF subset polarisation that was enhanced by the addition of FN to the scaffold, albeit this appeared to be limited by the rigidity of the scaffold and its structure. On the other hand, within FN integrated hydrogels, the SFs were able to distribute themselves throughout the scaffold, with an increase observed in the lining SFs, almost equal to that of the sublining. Although differential distribution between subsets was not observed within the gels, when looking at the transcriptomic profile, the SFs presented unlike that of traditional lining or sublining SFs.

## **7.2 Towards developing platforms for more effective pre-clinical testing of therapies for RA**

Major advances in developing treatments for RA have been made over the last decade, however, as the therapies available for RA patients all target immune system cells and inflammation, they are subject to potentially serious side-effects. Despite increasing knowledge of the important role SFs play in the perpetuation of disease, to date this information has not been successfully translated to the development of therapies targeting SFs, from the pre-clinical to clinical stage. Although there are no approved drugs that target SFs to treat RA, there have been significant advances made in the past few years that have allowed investigators to begin targeting stromal cells such as SFs in inflammatory diseases, with a number of compounds being shown to inhibit SF activity. For example, the pre-clinical drug (5z)-7-oxozeaenol (5ZO), developed to target transforming growth factor  $\beta$ -associated kinase 1 (TAK1) has been shown to be effective in inhibiting SF activation as the ability of drugs to block SF activation is strongly dependent on the identity of the activating cytokine and thus, similar molecules

to 5ZO are being used to generate RA therapeutics (Jones et al., 2016). Another approach has focused on reports that RA-SFs have increased glycolytic activity and thus of potential relevance, Shikonin, a component of the comfrey shrub used in traditional Chinese medicine, has been shown to inhibit the activity of Pyruvate Kinase M2 (PKM2) by regulating glycolysis and ATP production (Li et al., 2021). Moreover, a newly developed drug in the early trial phase, Seliciclib (R-roscovitine) is an orally available cyclin-dependent kinase inhibitor that suppresses fibroblast proliferation *in vitro* and *in vivo* by not only inhibiting cyclin-dependent kinase 2 (CDK2), but also by inducing expression of the endogenous CDK inhibitor p21, which is otherwise downregulated in SFs in RA patients. It has been shown efficacious in preclinical arthritis models (Pratt et al., 2021; Siebert et al., 2020).

One reason for the lack of success to date could be that the *in vitro* assays used in such studies do not accurately recapitulate SFs *in vivo*, preventing identification of disease relevant target. Perhaps consistent with this, the data in this thesis have established that the particular culture microenvironment impacts substantially on the transcriptomic and functional phenotype of SFs and thus it is essential to more closely mimic the microenvironment of the joint to fully address understanding of SF function in pathogenesis.

Nevertheless, conventional 2D culture systems have been useful in developing our understanding of the mechanisms and pathways underpinning RA pathogenesis. They are simple, easy to use and cost effective and have shown to be capable of maintaining (at least some of) the hyper responses characteristic of SFs in CIA and RA *in vivo* (Figure 3-2 & Figure 3-4). However, these platforms do not appear to be effective in the study of SF subpopulations, as when stained with markers for lining and sublining SFs, only a homogeneous SF population was observed (Figure 3-5). The ability to target a particular subset would be useful as the lining SFs have been shown to associated with more bone erosion and cartilage degradation, whilst sublining SFs have been found to be involved with the pro-inflammatory signalling/pathways associated with diseases such as RA. Therefore, more specific therapeutics dependent on need could potentially be developed when individual subsets can be better identified and studied. For example, our RNA-Seq data

clearly showed substantial loss of the differential gene expression observed between Naïve and CIA SFs freshly isolated *ex vivo* following culture of these cells under 2D conditions, with an apparent loss/reversal of the transcriptomic remodelling associated with some pathogenic pathways (Figure 6-4 & Figure 6-7) activated in aggressive SFs *in vivo* (Figure 6-2). Thus, our findings that SFs can partially recover lost features when transferred to a 3D microenvironment may have important implications for drug development particularly with respect to target identification. Indeed, our pathway analysis (Figure 6-12) suggested that the differential expression (upregulated), particularly those relating to the hyperplasia, witnessed *in vivo* but lost following expansion of the SFs in 2D cultures, are recovered by their subsequent transfer to Alvetex® scaffolds. However, perhaps surprisingly, there were a greater number of differentially expressed genes observed in CIA-, relative to Naïve-SFs grown on Alvetex® (Figure 6-6C), compared to the profile of freshly isolated SFs (Figure 6-1C), suggesting that despite Alvetex® perhaps providing a better platform to mimic SF responses in RA (when compared with 2D cultures), it does not precisely recapitulate the pathophysiological microenvironment of the joint synovium. This could be due to the bone-like stiffness of the scaffold differentially inducing/repressing additional genes in the epigenetically remodelled CIA-SFs. Nevertheless, the Alvetex® system appears to allow a better understanding of various aspects of SF biology, specifically in distinguishing the roles of SF subpopulations (lining and sublining SFs) (Figure 4-10), particularly in terms of their differential migration and clustering (within the limits of scaffold), physiological parameters that are not possible to investigate in 2D models. Certainly, the loss of subset differentiation to the observed heterogenous SF population (Figure 3-5) could provide a reason as to why no SF specific RA therapeutics have been fully developed/passed clinical trials as of yet. Moreover, our data have shown that the incorporation of ECM components like FN can further modulate *ex vivo* SF responses (Figure 4-4) and this presumably reflects mimicking of the FN-integrin signalling in SFs occurring during their aberrant migration and pro-inflammatory mediator production that is characteristic of their pathogenic role in RA.

### 7.3 Hydrogels - culture systems to study SF biology and/or therapeutic delivery tools for RA

Although, culture on Alvetex<sup>®</sup> scaffolds appeared to be better, than that on 2D platforms, at modelling the organisation and movement of SFs and allowed “recovery” of the differential gene expression in Naïve and CIA SFs associated with “pathogenic” pathways observed *in vivo*, the scaffold itself is made from plastic and has a rigidity more akin to bone (~77 kPa), perhaps explaining their increased differential gene expression relative to that seen in SFs freshly isolated from the joint. We therefore decided to study SF responses using FNPEG hydrogels, as an alternative 3D culture system, since their mechanical properties are more easily manipulated and may therefore be able to better mimic the synovial environment. For example, previous research has shown that the stiffness of, and associated mechanical strain on, the microenvironment impacts on cell function, in particular with respect to continuous passive motion, decreasing SF production of inflammatory mediators, including prostaglandin E(2) (PGE(2)) and proteinases, in the temporomandibular joint (Sambajon, Cillo, Gassner and Buckley, 2003). Moreover, another study carried out by Xu et al, showed that SFs exposed *in vivo* to metal-on-metal (MoM) total hip arthroplasty (THA) implants, that release cobalt chromium-wear debris, exhibited dramatic alterations in phenotype and functional changes (Xu et al., 2020). We therefore exploited the hydrogel platform to investigate the effects of stiffness more akin to that of the healthy and arthritic synovium (kPA of ~5-7) and concluded that even changes within this range of “stiffness” impact on SF function (Figure 5-13). For example, the SF expression of Mmp3 and ctgf decreased with greater stiffness, whilst that of sparc increased, suggesting that environmental stiffness affects the transcriptomic profiling. These preliminary experiments need to be extended, first examining pro-inflammatory genes, such as Il-6 and Ccl2, in order to more fully understand the impact of changing stiffness of the joint during arthritogenesis on SF pathogenesis.

As mentioned previously CIA-SFs cultured in FNPEG hydrogels showed a downregulation in pro-inflammatory pathways, displaying a more Naïve-like phenotype. This could be due to various reasons, one of which being that the CIA-SFs adopt a “remission”-like phenotype. It could also be due to epigenetic changes

induced in response to a decreased stiffness following their transfer from conventional 2D plates, as this Naïve-like phenotype was not observed in the rigid Alvetex® scaffold. Moreover, as the hydrogel is pegylated with FN, this ubiquitous exposure to FN could also have an effect on the observed phenotype, as it has shown that FN interaction with integrins are affected by stiffness as cells sense and respond to the mechanical properties of their microenvironment. For example, after exposure to breast cancer cell-secreted factors, adipose stromal cells initially deposit high volumes of stiff and unfolded FN with an altered topology, shown to deregulate the behaviour of neighbouring cells through cell-matrix interaction modifications and indeed, tumour induced FN matrix deregulation activated integrin switches in neighbouring cells (Wang et al., 2015). Moreover, a study by Carraher et al, showed that rigidity-dependent FN matrix assembly is determined by extracellular events, mainly the engagement of FN by cells (Carraher and Schwarzbauer, 2013), suggesting that the rigidity of the microenvironment coupled with the FN-matrix interactions with the SFs could have played a role in the phenotype presented in the CIA-SF transcriptomic profile.

Another interesting feature of the hydrogel platform was its relative promotion of lining SFs and thus, the finding that there are less sub-lining CIA-SFs present may provide a rationale for the skewing towards a less pro-inflammatory transcriptomic profile in this platform. Indeed, as there are more VCAM1+ SFs for every CD90+ SFs (Figure 5-7B & C ), this could perhaps support the hypothesis that sublining CIA-SFs dedifferentiate and/or lining CIA-SFs differentiate/proliferate more allowing generation of a more remission-like phenotype in this platform. In any case, this skewing of SF populations indicates a potential beneficial feature to using FNPEG hydrogels in studies pertaining to sublining SFs and their role in RA pathogenesis.

Importantly, widefield imaging of the FNPEG hydrogels allowed the investigation of SF organisation and migration (Figure 5-3) that is not possible with cells grown in 2D models. It appears the SFs congregate towards the outer portion of the hydrogel (Figure 5-5), which may suggest they are mimicking their migration and organisation within the joint. A future experiment to investigate whether SFs

organise themselves in an anatomical manner similar to within a joint would be to create a hydrogel that contains an inner portion composed of FN and surrounded by an outer gel composed of laminin (LN), as LN has been shown to be present in the hyperplastic sublining layer of active rheumatoid synovitis (Ospelt, 2017; Schneider et al., 1994), whilst FN has been shown to be present in the lining region of the synovial joint (Tamer, 2013). Also, hydrogels pegylated with Tenascin (TNC) could also be investigated as TNC levels have been found to be elevated in diseased cartilage synovium and synovial fluid of RA patients and has also been detected in the blood of individuals with RA making it a potential biomarker for the disease. (Page et al., 2012; Hasegawa, Yoshida and Sudo, 2020). TNC is a multimeric protein known to express in adult tissues mainly during tissue injury or remodelling and so studies have been carried out to use and apply TNC in gels to support viability and proliferation. It has been shown that these gels can potentially be used as designer injectable matrices (Sharma, Kaur and Roy, 2019). Therefore, further investigations into how they can be used as possible drug delivery systems in RA could be carried out.

In contrast to commercially available matrigels, which are limited in their applicability to cellular biology, drug discovery and therapeutic manufacturing of cells due their complex nature, components can be added individually to our customised hydrogels, allowing more control of the microenvironment created. This allows certain factors to be investigated in detail before adding further components into the mix. Indeed, matrigels are not supportive of manipulation both physically and biochemically, thus making it more demanding to make the matrix promote the planned cell behaviours and attain certain biological outcomes, specific to the research carried out (Aisenbrey and Murphy, 2020). For example, as mentioned above, live imaging of hydrogels using a widefield microscope, followed by analysis using IMARIS would allow the observation of the organisation of the SFs within the hydrogel and whether the subpopulations favour a FN or LN enriched region connected to their anatomical location within the joint. However, in addition, as hydrogels are easily adaptable, the addition of growth factors known to be present within the joint and the effect this would have of the SF migration and organisation could also be investigated.

Certainly, experiments carried out by Trujillo et al, have shown that the FNPEG hydrogels provide a synthetic microenvironment for 3D culture that integrates growth factors to achieve functional myoblast cell responses, alter cell behaviour and support the idea that hydrogels provide a useful tool for the study of the role of SF and their subsets in perpetuation of inflammation in RA. Additional research by the Salmeron-Sanchez lab has developed laminin-pegylated hydrogels, which allow the incorporation of isoforms for efficient presentation of growth factors. Thus, a study carried out by Dobre *et al.*, 2021 showed that various laminin isoforms were able to effectively bind to growth factors, in turn allowing presentation of small doses to specific tissues (Dobre et al., 2021). As mentioned previously laminin is a crucial structural protein of the ECM that has specific roles within tissues and reflecting this, it's ability to bind to growth factors can be used to control differentiation of stem cells, indicating the potential that these Matrigel-inspired hydrogels have in differentiation of stem cells to osteogenic lineages and stimulation of neural cells growth. Thus, using these already established hydrogels, further investigations with SF subsets could therefore determine whether an environment can be created where subsets move towards more anatomical locations and exploited to determine their differential functional roles and therapeutic targets.

Finally, hydrogels have been shown to be used not only as a research tool but also as a therapeutic, acting as a drug delivery system. An example of this being hydrogels loaded with triamcinolone acetonide, which is released when the hydrogels are exposed to synovial fluid/enzymes from RA patients. Importantly, the hydrogels allow control of drug release and in arthritic mice the hydrogels encapsulated with a fluorescent dye showed flare dependent disassembly assessed as a loss of fluorescence. Moreover, a unique dose of these gels showed a decrease in arthritic manifested in injured paws after 14 days. As such hydrogels do not affect the metabolic process of living organisms and metabolites can easily pass through their pores, this non-foreign ECM is likely to provide models with rational indications for diagnostic and therapeutic investigations (Oliveira et al., 2021).

Some hydrogels used for the delivery of drugs or bioactive agents used in the treatment of RA include fibrin gels used to administer bone marrow mesenchymal

stem cells in AIA, resulting in a reduction of inflammatory cytokine levels as well as improved joint swelling. Preservation of the adjacent cartilage and enhanced cartilage repair were also observed (Liu et al., 2016). Also, nano-structured lipid carriers (NLCs) formulated by lipid mixture and chemical permeation enhancer-based hydrogels used to transdermally deliver methotrexate (MTX) showed decreased inflammation in animal models (Garg et al., 2016). Another interesting concept could be to transfer “remission”-like SFs, like those observed in the FNPEG hydrogels into the joint which could potentially modulate the behaviour of the endogenous pathogenic SFs. Moreover, from cytokine and RNA-Seq studies, it appears that SFs are plastic cells that are able to be reprogrammed towards inflammatory or anti-inflammatory pathways opening up the possibility of manipulating SFs from arthritic patients to remodel the whole inflammatory network of the joint. It could lead to restoration of SF subsets, as well as change the gene expression. The SFs cultured in the FNPEG hydrogels don't present as conventional lining or sublining SFs and show them to be almost “remission”-like. SFs have been found to have a high degree of plasticity which is well known in immune system cells however, not so well known in this particular cell type.

Thus, in conclusion, the data shown in this thesis support the idea that hydrogels could be potentially used both as an experimental tool and also as therapeutics to treat RA through targeting SFs. The challenge remains to more fully understand the mechanisms of SF transformation in order to recognise specific targets to manage the process. Furthermore, gaining a deeper understanding of the influence of differing SF subsets on joint inflammation can enhance our knowledge of RA pathogenesis, models best used to investigate them as well as develop targeted therapies for the influencing RA-SFs.

## List of References

- Abbott, A., 2003. Biology's new dimension. *Nature*, 424(6951), pp.870-872.
- Abuwarwar, M., Knoblich, K. and Fletcher, A., 2018. A pathogenic hierarchy for synovial fibroblasts in rheumatoid arthritis. *Annals of Translational Medicine*, 6(S1), pp.S75-S75.
- Aggarwal, B., Danda, D., Gupta, S. and Gehlot, P., 2009. Models for prevention and treatment of cancer: Problems vs promises. *Biochemical Pharmacology*, 78(9), pp.1083-1094.
- Ahmad, N., Colak, B., Gibbs, M., Zhang, D., Becer, C., Watkinson, M., Gautrot, J. and Krause, S., 2018. Collagenase Biosensor Based on the Degradation of Peptide Cross-Linked Poly(Ethylene Glycol) Hydrogel Films. *Proceedings*, 2(13), p.961.
- Ahmed, E., 2015. Hydrogel: Preparation, characterization, and applications: A review. *Journal of Advanced Research*, 6(2), pp.105-121.
- Aisenbrey, E. and Murphy, W., 2020. Synthetic alternatives to Matrigel. *Nature Reviews Materials*, 5(7), pp.539-551.
- Akram, M., Pery, N., Butler, L., Shafiq, M., Batool, N., Rehman, M., Grahame-Dunn, L. and Yetisen, A., 2021. *Challenges for biosimilars: focus on rheumatoid arthritis*.
- Alghamdi, M., Alasmari, D., Assiri, A., Mattar, E., Aljaddawi, A., Alattas, S. and Redwan, E., 2019. An Overview of the Intrinsic Role of Citrullination in Autoimmune Disorders. *Journal of Immunology Research*, 2019, pp.1-39.
- Almany, L. and Seliktar, D., 2005. Biosynthetic hydrogel scaffolds made from fibrinogen and polyethylene glycol for 3D cell cultures. *Biomaterials*, 26(15), pp.2467-2477.
- Amith, S., Wilkinson, J. and Fliegel, L., 2016. Assessing Na<sup>+</sup>/H<sup>+</sup> exchange and cell effector functionality in metastatic breast cancer. *Biochimie Open*, 2, pp.16-23.
- Anacker, D. and Moody, C., 2012. Generation of Organotypic Raft Cultures from Primary Human Keratinocytes. *Journal of Visualized Experiments*, (60).
- Arend, W., Malyak, M., Guthridge, C. and Gabay, C., 1998. Interleukin-1 Receptor Antagonist: Role in Biology. *Annual Review of Immunology*, 16(1), pp.27-55.
- Armaka, M., Gkretsi, V., Kontoyiannis, D. and Kollias, G., 2009. A standardized protocol for the isolation and culture of normal and arthritogenic murine synovial fibroblasts. *Protocol Exchange*
- Asano, Y., Ihn, H., Kubo, M., Jinnin, M., Mimura, Y., Ashida, R. and Tamaki, K., 2005. Clinical significance of serum levels of matrix metalloproteinase-13 in patients with systemic sclerosis. *Rheumatology*, 45(3), pp.303-307.

- Aslam, N., Singh, A., Cortese, C. and Riegert-Johnson, D., 2019. A novel variant in FN1 in a family with fibronectin glomerulopathy. *Human Genome Variation*, 6(1).
- Asquith, D., Miller, A., McInnes, I. and Liew, F., 2009. Animal models of rheumatoid arthritis. *European Journal of Immunology*, 39(8), pp.2040-2044.
- Bachman, H., Nicosia, J., Dysart, M. and Barker, T., 2015. Utilizing Fibronectin Integrin-Binding Specificity to Control Cellular Responses. *Advances in Wound Care*, 4(8), pp.501-511.
- Barilla, M. and Carsons, S., 2000. Fibronectin fragments and their role in inflammatory arthritis. *Seminars in Arthritis and Rheumatism*, 29(4), pp.252-265.
- Bartok, B. and Firestein, G., 2010. Fibroblast-like synoviocytes: key effector cells in rheumatoid arthritis. *Immunological Reviews*, 233(1), pp.233-255.
- Bauer, S., Jendro, M., Wadle, A., Kleber, S., Stenner, F., Dinser, R., Reich, A., Faccin, E., Gödde, S., Dinges, H., Müller-Ladner, U. and Renner, C., 2006. *Arthritis Research & Therapy*, 8(6), p.R171.
- Baugh, L. and Vogel, V., 2004. Structural changes of fibronectin adsorbed to model surfaces probed by fluorescence resonance energy transfer. *Journal of Biomedical Materials Research*, 69A(3), pp.525-534.
- Benjamin O, Bansal P, Goyal A, Lappin SL. Disease Modifying Anti-Rheumatic Drugs (DMARD). 2021 Jul 6. In: StatPearls [Internet]. Treasure Island (FL): StatPearls Publishing; 2021 Jan-. PMID: 29939640.
- Benya, P., 1982. Dedifferentiated chondrocytes reexpress the differentiated collagen phenotype when cultured in agarose gels. *Cell*, 30(1), pp.215-224.
- Berri, N., Fares, J. and Fares, Y., 2018. Polyethylene Oxide and Silicon-Substituted Hydroxyapatite Composite: A Biomaterial for Hard Tissue Engineering in Orthopedic and Spine Surgery. *Advanced Biomedical Research*, 7(1), p.117.
- Bieniek, M., Llopis-Hernandez, V., Douglas, K., Salmeron-Sanchez, M. and Lorenz, C., 2019. Minor Chemistry Changes Alter Surface Hydration to Control Fibronectin Adsorption and Assembly into Nanofibrils. *Advanced Theory and Simulations*, 2(12), p.1900169.
- Biotrend.com. 2021. *Polystyrene 12-well inserts for 3D culture - Alvetex Strata Biotrend*. [online] Available at: <<https://www.biotrend.com/en/buy/cat-polystyrene-12-well-inserts-for-4076.html>> [Accessed 4 August 2021].
- Bird, A., 2007. Perceptions of epigenetics. *Nature*, 447(7143), pp.396-398.
- Blache, U., Stevens, M. and Gentleman, E., 2020. Harnessing the secreted extracellular matrix to engineer tissues. *Nature Biomedical Engineering*, 4(4), pp.357-363.

- Bonnans, C., Chou, J. and Werb, Z., 2014. Remodelling the extracellular matrix in development and disease. *Nature Reviews Molecular Cell Biology*, 15(12), pp.786-801.
- Bottini, N. and Firestein, G., 2012. Duality of fibroblast-like synoviocytes in RA: passive responders and imprinted aggressors. *Nature Reviews Rheumatology*, 9(1), pp.24-33.
- Brand, D., Latham, K. and Rosloniec, E., 2007. Collagen-induced arthritis. *Nature Protocols*, 2(5), pp.1269-1275.
- Briggs, S., 2005. The role of fibronectin in fibroblast migration during tissue repair. *Journal of Wound Care*, 14(6), pp.284-287.
- Buckley, C., Ospelt, C., Gay, S. and Midwood, K., 2021. Author Correction: Location, location, location: how the tissue microenvironment affects inflammation in RA. *Nature Reviews Rheumatology*, 17(4), pp.246-246.
- Bullock, J., Rizvi, S., Saleh, A., Ahmed, S., Do, D., Ansari, R. and Ahmed, J., 2018. Rheumatoid Arthritis: A Brief Overview of the Treatment. *Medical Principles and Practice*, 27(6), pp.501-507.
- Burger, D., Rezzonico, R., Li, J., Modoux, C., Pierce, R., Welgus, H. and Dayer, J., 1998. Imbalance between interstitial collagenase and tissue inhibitor of metalloproteinases 1 in synoviocytes and fibroblasts upon direct contact with stimulated T lymphocytes: Involvement of membrane-associated cytokines. *Arthritis & Rheumatism*, 41(10), pp.1748-1759.
- Bustamante, M., Garcia-Carbonell, R., Whisenant, K. and Guma, M., 2017. Fibroblast-like synoviocyte metabolism in the pathogenesis of rheumatoid arthritis. *Arthritis Research & Therapy*, 19(1).
- Caiello, I., Minnone, G., Holzinger, D., Vogl, T., Prencipe, G., Manzo, A., De Benedetti, F. and Strippoli, R., 2014. IL-6 Amplifies TLR Mediated Cytokine and Chemokine Production: Implications for the Pathogenesis of Rheumatic Inflammatory Diseases. *PLoS ONE*, 9(10), p.e107886.
- Caplazi, P., Baca, M., Barck, K., Carano, R., DeVoss, J., Lee, W., Bolon, B. and Diehl, L., 2015. Mouse Models of Rheumatoid Arthritis. *Veterinary Pathology*, 52(5), pp.819-826.
- Carraher, C. and Schwarzbauer, J., 2013. Regulation of Matrix Assembly through Rigidity-dependent Fibronectin Conformational Changes. *Journal of Biological Chemistry*, 288(21), pp.14805-14814.
- Carter, R. and Wicks, I., 2001. Vascular cell adhesion molecule 1 (CD106): A multifaceted regulator of joint inflammation. *Arthritis & Rheumatism*, 44(5), pp.985-994.
- Chabaud, M., Garnero, P., Dayer, J., Guerne, P., Fossiez, F. and Miossec, P., 2000. CONTRIBUTION OF INTERLEUKIN 17 TO SYNOVIUM MATRIX DESTRUCTION IN RHEUMATOID ARTHRITIS. *Cytokine*, 12(7), pp.1092-1099.

- Chabaud, M., Lubberts, E., Joosten, L., van den Berg, W. and Miossec, P., 2001. *Arthritis Research*, 3(3), p.168.
- Chai, Q., Jiao, Y. and Yu, X., 2017. Hydrogels for Biomedical Applications: Their Characteristics and the Mechanisms behind Them. *Gels*, 3(1), p.6.
- Chang, X., Yamada, R., Suzuki, A., Kochi, Y., Sawada, T. and Yamamoto, K., 2005. Citrullination of fibronectin in rheumatoid arthritis synovial tissue. *Rheumatology*, 44(11), pp.1374-1382.
- Chavan, D., van de Watering, T., Gruca, G., Rector, J., Heeck, K., Slaman, M. and Iannuzzi, D., 2012. Ferrule-top nanoindenter: An optomechanical fiber sensor for nanoindentation. *Review of Scientific Instruments*, 83(11), p.115110.
- Cheon, H., Yu, S., Yoo, D., Chae, I., Song, G. and Sohn, J., 2002. Increased expression of pro-inflammatory cytokines and metalloproteinase-1 by TGF- $\beta$ 1 in synovial fibroblasts from rheumatoid arthritis and normal individuals. *Clinical & Experimental Immunology*, 127(3), pp.547-552.
- Choi, I., Karpus, O., Turner, J., Hardie, D., Marshall, J., de Hair, M., Maijer, K., Tak, P., Raza, K., Hamann, J., Buckley, C., Gerlag, D. and Filer, A., 2017. Stromal cell markers are differentially expressed in the synovial tissue of patients with early arthritis. *PLOS ONE*, 12(8), p.e0182751.
- Choy, E., 2012. Understanding the dynamics: pathways involved in the pathogenesis of rheumatoid arthritis. *Rheumatology*, 51(suppl 5), pp.v3-v11.
- Clark, R., An, J., Greiling, D., Khan, A. and Schwarzbauer, J., 2003. Fibroblast Migration on Fibronectin Requires Three Distinct Functional Domains. *Journal of Investigative Dermatology*, 121(4), pp.695-705.
- Cooke, M., Phillips, S., Shah, D., Athey, D., Lakey, J. and Przyborski, S., 2008. Enhanced cell attachment using a novel cell culture surface presenting functional domains from extracellular matrix proteins. *Cytotechnology*, 56(2), pp.71-79.
- Corbet, M., Pineda, M., Yang, K., Tarafdar, A., McGrath, S., Nakagawa, R., Lumb, F., Harnett, W. and Harnett, M., 2020. ES-62 suppression of arthritis reflects epigenetic rewiring of synovial fibroblasts to a joint-protective phenotype.
- Costello, L., Darling, N., Freer, M., Bradbury, S., Mobbs, C. and Przyborski, S., 2021. Use of Porous Polystyrene Scaffolds to Bioengineer Human Epithelial Tissues In Vitro. *Methods in Molecular Biology*, pp.279-296.
- Crofford, L., 2013. Use of NSAIDs in treating patients with arthritis. *Arthritis Research & Therapy*, 15(S3).
- Croft, A., Campos, J., Jansen, K., Turner, J., Marshall, J., Attar, M., Savary, L., Wehmeyer, C., Naylor, A., Kemble, S., Begum, J., Dürholz, K., Perlman, H., Barone, F., McGettrick, H., Fearon, D., Wei, K., Raychaudhuri, S., Korsunsky, I., Brenner, M., Coles, M., Sansom, S., Filer, A. and Buckley, C., 2019. Distinct

- fibroblast subsets drive inflammation and damage in arthritis. *Nature*, 570(7760), pp.246-251.
- Croft, A., Naylor, A., Filer, A. and Buckley, C., 2014. Effect of cartilage implantation on synovial fibroblasts from patients with rheumatoid arthritis. *The Lancet*, 383, p.S38.
- Croft, A., Naylor, A., Marshall, J., Hardie, D., Zimmermann, B., Turner, J., Desanti, G., Adams, H., Yemm, A., Müller-Ladner, U., Dayer, J., Neumann, E., Filer, A. and Buckley, C., 2016. Rheumatoid synovial fibroblasts differentiate into distinct subsets in the presence of cytokines and cartilage. *Arthritis Research & Therapy*, 18(1).
- Croft, A., Naylor, A., Zimmermann, B., Jaurez, M., Hardie, D., Desanti, G., Filer, A., Ulf Muller-Ladner, U., Neuman, E. and Buckley, C., 2013. FRI0042 Synovial fibroblasts from patients with rheumatoid arthritis differentiate into distinct fibroblast subsets in the presence of cartilage. *Annals of the Rheumatic Diseases*, 72(Suppl 3), pp.A382.1-A382.
- Croft, D., McIntyre, P., Wibulswas, A. and Kramer, I., 1999. Sustained Elevated Levels of VCAM-1 in Cultured Fibroblast-like Synoviocytes Can Be Achieved by TNF- $\alpha$  in Combination with Either IL-4 or IL-13 through Increased mRNA Stability. *The American Journal of Pathology*, 154(4), pp.1149-1158.
- Croft, D., McIntyre, P., Wibulswas, A. and Kramer, I., 1999. Sustained Elevated Levels of VCAM-1 in Cultured Fibroblast-like Synoviocytes Can Be Achieved by TNF- $\alpha$  in Combination with Either IL-4 or IL-13 through Increased mRNA Stability. *The American Journal of Pathology*, 154(4), pp.1149-1158.
- Cukierman, E., Pankov, R., Stevens, D. and Yamada, K., 2001. Taking Cell-Matrix Adhesions to the Third Dimension. *Science*, 294(5547), pp.1708-1712.
- Curtis, J. and Singh, J., 2011. Use of Biologics in Rheumatoid Arthritis: Current and Emerging Paradigms of Care. *Clinical Therapeutics*, 33(6), pp.679-707.
- Cutolo, M., 2011. IL-1Ra: its role in rheumatoid arthritis. *Reumatismo*, 56(1s).
- Daly, A., Riley, L., Segura, T. and Burdick, J., 2019. Hydrogel microparticles for biomedical applications. *Nature Reviews Materials*, 5(1), pp.20-43.
- Damjanov, N., 2018. Matrix Metalloproteinases-3 Baseline Serum Levels in Early Rheumatoid Arthritis Patients without Initial Radiographic Changes: A Two-Year Ultrasonographic Study. *Medical Principles and Practice*, 27(4), pp.378-386.
- Danielson, J., Perez, N., Romano, J. and Coppens, I., 2018. Modelling Toxoplasma gondii infection in a 3D cell culture system In Vitro: Comparison with infection in 2D cell monolayers. *PLOS ONE*, 13(12), p.e0208558.
- Danks, L., Komatsu, N., Guerrini, M., Sawa, S., Armaka, M., Kollias, G., Nakashima, T. and Takayanagi, H., 2015. RANKL expressed on synovial fibroblasts is primarily responsible for bone erosions during joint inflammation. *Annals of the Rheumatic Diseases*, 75(6), pp.1187-1195.
- Dayer, J., Oliviero, F. and Punzi, L., 2017. A Brief History of IL-1 and IL-1 Ra in Rheumatology. *Frontiers in Pharmacology*, 8.

Demoruelle, M. and Deane, K., 2011. Antibodies to Citrullinated Protein Antigens (ACPAs): Clinical and Pathophysiologic Significance. *Current Rheumatology Reports*, 13(5), pp.421-430.

Dinareello, C., Simon, A. and van der Meer, J., 2012. Treating inflammation by blocking interleukin-1 in a broad spectrum of diseases. *Nature Reviews Drug Discovery*, 11(8), pp.633-652.

Dobre, O., Oliva, M., Ciccone, G., Trujillo, S., Rodrigo-Navarro, A., Venters, D., Llopis-Hernandez, V., Vassalli, M., Gonzalez-Garcia, C., Dalby, M. and Salmeron-Sanchez, M., 2021. A Hydrogel Platform that Incorporates Laminin Isoforms for Efficient Presentation of Growth Factors - Neural Growth and Osteogenesis. *Advanced Functional Materials*, 31(21), p.2010225.

Doody, K., Bottini, N. and Firestein, G., 2017. Epigenetic alterations in rheumatoid arthritis fibroblast-like synoviocytes. *Epigenomics*, 9(4), pp.479-492.

Edmondson, R., Broglie, J., Adcock, A. and Yang, L., 2014. Three-Dimensional Cell Culture Systems and Their Applications in Drug Discovery and Cell-Based Biosensors. *ASSAY and Drug Development Technologies*, 12(4), pp.207-218.

Edwards, C. and Cooper, C., 2006. Early environmental exposure and the development of lupus. *Lupus*, 15(11), pp.814-819.

Elbert, D. and Hubbell, J., 2001. Conjugate Addition Reactions Combined with Free-Radical Cross-Linking for the Design of Materials for Tissue Engineering. *Biomacromolecules*, 2(2), pp.430-441.

Elisseeff, J., McIntosh, W., Anseth, K., Riley, S., Ragan, P. and Langer, R., 2000. Photoencapsulation of chondrocytes in poly(ethylene oxide)-based semi-interpenetrating networks. *Journal of Biomedical Materials Research*, 51(2), pp.164-171.

Esparza, J., Vilardell, C., Calvo, J., Juan, M., Vives, J., Urbano-Márquez, A., Yaguë, J. and Cid, M., 1999. Fibronectin Upregulates Gelatinase B (MMP-9) and Induces Coordinated Expression of Gelatinase A (MMP-2) and Its Activator MT1-MMP (MMP-14) by Human T Lymphocyte Cell Lines. A Process Repressed Through RAS/MAP Kinase Signaling Pathways. *Blood*, 94(8), pp.2754-2766.

Fadda, S., Abolkheir, E., Afifi, R. and Gamal, M., 2016. Serum matrix metalloproteinase-3 in rheumatoid arthritis patients: Correlation with disease activity and joint destruction. *The Egyptian Rheumatologist*, 38(3), pp.153-159.

Farrugia, M. and Baron, B., 2016. The role of TNF- $\alpha$  in rheumatoid arthritis: a focus on regulatory T cells. *Journal of Clinical and Translational Research*, 2(3).

Fassbender, H. and Simmling-Annefeld, M., 1983. The potential aggressiveness of synovial tissue in rheumatoid arthritis. *The Journal of Pathology*, 139(3), pp.399-406.

Ferraccioli, G., Bracci-Laudiero, L., Alivernini, S., Gremese, E., Toluoso, B. and De Benedetti, F., 2010. Interleukin-1 $\beta$  and Interleukin-6 in Arthritis Animal Models: Roles in the Early Phase of Transition from Acute to Chronic Inflammation

- and Relevance for Human Rheumatoid Arthritis. *Molecular Medicine*, 16(11-12), pp.552-557.
- Filer, A., 2013. The fibroblast as a therapeutic target in rheumatoid arthritis. *Current Opinion in Pharmacology*, 13(3), pp.413-419.
- Firestein, G. and McInnes, I., 2017. Immunopathogenesis of Rheumatoid Arthritis. *Immunity*, 46(2), pp.183-196.
- Firestein, G., 2003. Evolving concepts of rheumatoid arthritis. *Nature*, 423(6937), pp.356-361.
- Firestein, G., Gabriel, S., McInnes, I. and O'Dell, J., 2017. *Kelley and Firestein's textbook of rheumatology Volumes I and II*. 10th ed. Philadelphia, PA: Elsevier, pp.20-22.
- Florczyk, S., Simon, M., Juba, D., Pine, P., Sarkar, S., Chen, D., Baker, P., Bodhak, S., Cardone, A., Brady, M., Bajcsy, P. and Simon, C., 2017. A Bioinformatics 3D Cellular Morphotyping Strategy for Assessing Biomaterial Scaffold Niches. *ACS Biomaterials Science & Engineering*, 3(10), pp.2302-2313.
- Förster, S., Gretschel, S., Jöns, T., Yashiro, M. and Kemmner, W., 2011. THBS4, a novel stromal molecule of diffuse-type gastric adenocarcinomas, identified by transcriptome-wide expression profiling. *Modern Pathology*, 24(10), pp.1390-1403.
- Foster, G., Headen, D., González-García, C., Salmerón-Sánchez, M., Shirwan, H. and García, A., 2017. Protease-degradable microgels for protein delivery for vascularization. *Biomaterials*, 113, pp.170-175.
- Frangogiannis, N., 2016. Fibroblast–Extracellular Matrix Interactions in Tissue Fibrosis. *Current Pathobiology Reports*, 4(1), pp.11-18.
- Frank-Bertoncelj, M., Trenkmann, M., Klein, K., Karouzakis, E., Rehrauer, H., Bratus, A., Kolling, C., Armaka, M., Filer, A., Michel, B., Gay, R., Buckley, C., Kollias, G., Gay, S. and Ospelt, C., 2017. Epigenetically-driven anatomical diversity of synovial fibroblasts guides joint-specific fibroblast functions. *Nature Communications*, 8(1).
- Frisbie, D., 2012. Synovial Joint Biology and Pathobiology. *Equine Surgery*, pp.1096-1114.
- Garg, N., Tyagi, R., Singh, B., Sharma, G., Nirbhavane, P., Kushwah, V., Jain, S. and Katare, O., 2016. Nanostructured lipid carrier mediates effective delivery of methotrexate to induce apoptosis of rheumatoid arthritis via NF- $\kappa$ B and FOXO1. *International Journal of Pharmaceutics*, 499(1-2), pp.301-320.
- Gomez-Roman, N., Stevenson, K., Gilmour, L., Hamilton, G. and Chalmers, A., 2016. A novel 3D human glioblastoma cell culture system for modeling drug and radiation responses. *Neuro-Oncology*, p.164.
- Greenman, C., Stephens, P., Smith, R., Dalgliesh, G., Hunter, C., Bignell, G., Davies, H., Teague, J., Butler, A., Stevens, C., Edkins, S., O'Meara, S., Vastrik, I., Schmidt, E., Avis, T., Barthorpe, S., Bhamra, G., Buck, G., Choudhury, B.,

Clements, J., Cole, J., Dicks, E., Forbes, S., Gray, K., Halliday, K., Harrison, R., Hills, K., Hinton, J., Jenkinson, A., Jones, D., Menzies, A., Mironenko, T., Perry, J., Raine, K., Richardson, D., Shepherd, R., Small, A., Tofts, C., Varian, J., Webb, T., West, S., Widaa, S., Yates, A., Cahill, D., Louis, D., Goldstraw, P., Nicholson, A., Brasseur, F., Looijenga, L., Weber, B., Chiew, Y., deFazio, A., Greaves, M., Green, A., Campbell, P., Birney, E., Easton, D., Chenevix-Trench, G., Tan, M., Khoo, S., Teh, B., Yuen, S., Leung, S., Wooster, R., Futreal, P. and Stratton, M., 2007. Patterns of somatic mutation in human cancer genomes. *Nature*, 446(7132), pp.153-158.

Gremlich, S., Roth-Kleiner, M., Equey, L., Fytianos, K., Schittny, J. and Cremona, T., 2020. Tenascin-C inactivation impacts lung structure and function beyond lung development. *Scientific Reports*, 10(1).

Griffith, L. and Swartz, M., 2006. Capturing complex 3D tissue physiology in vitro. *Nature Reviews Molecular Cell Biology*, 7(3), pp.211-224.

Guo, Q., Wang, Y., Xu, D., Nossent, J., Pavlos, N. and Xu, J., 2018. Rheumatoid arthritis: pathological mechanisms and modern pharmacologic therapies. *Bone Research*, 6(1).

Gwon, S., Rhee, K. and Sung, H., 2018. Gene and Protein Expression Profiles in a Mouse Model of Collagen-Induced Arthritis. *International Journal of Medical Sciences*, 15(1), pp.77-85.

Han, S., Kwon, S. and Kim, K., 2021. Challenges of applying multicellular tumor spheroids in preclinical phase. *Cancer Cell International*, 21(1).

Haniffa, M., Collin, M., Buckley, C. and Dazzi, F., 2008. Mesenchymal stem cells: the fibroblasts' new clothes?. *Haematologica*, 94(2), pp.258-263.

Hasegawa, M., Yoshida, T. and Sudo, A., 2020. Tenascin-C in Osteoarthritis and Rheumatoid Arthritis. *Frontiers in Immunology*, 11.

Hashizume, M. and Mihara, M., 2011. The Roles of Interleukin-6 in the Pathogenesis of Rheumatoid Arthritis. *Arthritis*, 2011, pp.1-8.

Homandberg, G., Hui, F., Wen, C., Purple, C., Bewsey, K., Koepp, H., Huch, K. and Harris, A., 1997. Fibronectin-fragment-induced cartilage chondrolysis is associated with release of catabolic cytokines. *Biochemical Journal*, 321(3), pp.751-757.

Hopkins, S J et al. "Cytokines in synovial fluid. I. The presence of biologically active and immunoreactive IL-1." *Clinical and experimental immunology* vol. 72,3 (1988): 422-7.

Hu, Z., Farahikia, M. and Delfanian, F., 2014. Fiber bias effect on characterization of carbon fiber-reinforced polymer composites by nanoindentation testing and modeling. *Journal of Composite Materials*, 49(27), pp.3359-3372.

Huber, L., Distler, O., Tarner, I., Gay, R., Gay, S. and Pap, T., 2006. Synovial fibroblasts: key players in rheumatoid arthritis. *Rheumatology*, 45(6), pp.669-675.  
Hudson, A. and Whittum-Hudson, J., 2009. Rheumatoid arthritis: Disease or syndrome?. *Open Access Rheumatology: Research and Reviews*, p.179.

- Hwang, S., Kim, J., Kim, K., Park, M., Moon, Y., Kim, W. and Kim, H., 2004. *Arthritis Research & Therapy*, 6(2), p.R120.
- Hwang, S., Kim, J., Kim, K., Park, M., Moon, Y., Kim, W. and Kim, H., 2004. *Arthritis Research & Therapy*, 6(2), p.R120.
- I, C. and A.K.T, W., 2020. Regulation of the Extracellular Matrix by Ciliary Machinery. *Cells*, 9(2), p.278.
- Ingegnoli, F., Castelli, R. and Gualtierotti, R., 2013. Rheumatoid Factors: Clinical Applications. *Disease Markers*, 35, pp.727-734.
- Inglis, J., Criado, G., Medghalchi, M., Andrews, M., Sandison, A., Feldmann, M. and Williams, R., 2007. Collagen-induced arthritis in C57BL/6 mice is associated with a robust and sustained T-cell response to type II collagen. *Arthritis Research & Therapy*, 9(5), p.R113.
- Ishchenko, A. and Lories, R., 2016. Safety and Efficacy of Biological Disease-Modifying Antirheumatic Drugs in Older Rheumatoid Arthritis Patients: Staying the Distance. *Drugs & Aging*, 33(6), pp.387-398.
- Jabbari, E., Leijten, J., Xu, Q. and Khademhosseini, A., 2016. The matrix reloaded: the evolution of regenerative hydrogels. *Materials Today*, 19(4), pp.190-196.
- Jacoby W, Pasten I. *Methods in Enzymology: Cell Culture*. Vol. 58. New York: Academic Press; 1979.
- Jensen, C. and Teng, Y., 2020. Is It Time to Start Transitioning From 2D to 3D Cell Culture?. *Frontiers in Molecular Biosciences*, 7.
- Jeong, J., Kim, J., Cho, H., Hahn, W., Yu, S. and Kim, S., 2004. Effects of IL-1B on gene expression in human rheumatoid synovial fibroblasts. *Biochemical and Biophysical Research Communications*, 324(1), pp.3-7.
- Jin, T., Xu, X. and Hereld, D., 2008. Chemotaxis, chemokine receptors and human disease. *Cytokine*, 44(1), pp.1-8.
- Jones, D., Jenney, A., Swantek, J., Burke, J., Lauffenburger, D. and Sorger, P., 2016. Profiling drugs for rheumatoid arthritis that inhibit synovial fibroblast activation. *Nature Chemical Biology*, 13(1), pp.38-45.
- Joshi, N., Yan, J., Levy, S., Bhagchandani, S., Slaughter, K., Sherman, N., Amirault, J., Wang, Y., Riegel, L., He, X., Rui, T., Valic, M., Vemula, P., Miranda, O., Levy, O., Gravallesse, E., Aliprantis, A., Ermann, J. and Karp, J., 2018. Towards an arthritis flare-responsive drug delivery system. *Nature Communications*, 9(1).
- Juarez, M., Filer, A. and Buckley, C., 2012. Fibroblasts as therapeutic targets in rheumatoid arthritis and cancer. *Swiss Medical Weekly*, p142
- Kannan, K., Ortmann, R. and Kimpel, D., 2005. Animal models of rheumatoid arthritis and their relevance to human disease. *Pathophysiology*, 12(3), pp.167-181.

Kapałczyńska, M., Kolenda, T., Przybyła, W., Zajązkowska, M., Teresiak, A., Filas, V., Ibbs, M., Bliźniak, R., Łuczewski, Ł. and Lamperska, K., 2016. 2D and 3D cell cultures - a comparison of different types of cancer cell cultures. *Archives of Medical Science*,

Kapasa, E., Giannoudis, P., Jia, X., Hatton, P. and Yang, X., 2017. The Effect of RANKL/OPG Balance on Reducing Implant Complications. *Journal of Functional Biomaterials*, 8(4), p.42.

Karami, J., Aslani, S., Tahmasebi, M., Mousavi, M., Sharafat Vaziri, A., Jamshidi, A., Farhadi, E. and Mahmoudi, M., 2020. Epigenetics in rheumatoid arthritis; fibroblast-like synoviocytes as an emerging paradigm in the pathogenesis of the disease. *Immunology & Cell Biology*, 98(3), pp.171-186.

Karouzakis, E., Gay, R., Michel, B., Gay, S. and Neidhart, M., 2009. DNA hypomethylation in rheumatoid arthritis synovial fibroblasts. *Arthritis & Rheumatism*, 60(12), pp.3613-3622.

Kay, J., 2004. The role of interleukin-1 in the pathogenesis of rheumatoid arthritis. *Rheumatology*, 43(suppl\_3), pp.iii2-iii9.

Kemble, S. and Croft, A., 2021. Critical Role of Synovial Tissue-Resident Macrophage and Fibroblast Subsets in the Persistence of Joint Inflammation. *Frontiers in Immunology*, 12.

Kerlan-Candon, S., Combe, B., Vincent, R., Clot, J., Pinet, V. and Eliaou, J., 2001. HLA-DRB1 gene transcripts in rheumatoid arthritis. *Clinical & Experimental Immunology*, 124(1), pp.142-149.

Keselowsky, B., Collard, D. and García, A., 2003. Surface chemistry modulates fibronectin conformation and directs integrin binding and specificity to control cell adhesion. *Journal of Biomedical Materials Research Part A*, 66A(2), pp.247-259.

Khetan, S., Guvendiren, M., Legant, W., Cohen, D., Chen, C. and Burdick, J., 2013. Degradation-mediated cellular traction directs stem cell fate in covalently crosslinked three-dimensional hydrogels. *Nature Materials*, 12(5), pp.458-465.

Kilian, K., Bugarija, B., Lahn, B. and Mrksich, M., 2010. Geometric cues for directing the differentiation of mesenchymal stem cells. *Proceedings of the National Academy of Sciences*, 107(11), pp.4872-4877.

Kim, K., Park, S., Yang, J., Jeon, J., Bhang, S., Kim, B. and Hahn, S., 2011. Injectable hyaluronic acid-tyramine hydrogels for the treatment of rheumatoid arthritis. *Acta Biomaterialia*, 7(2), pp.666-674.

Kim, M., Wu, W., Choi, J., Kim, J., Jun, J., Ko, Y. and Lee, J., 2017. Galectin-1 from conditioned medium of three-dimensional culture of adipose-derived stem cells accelerates migration and proliferation of human keratinocytes and fibroblasts. *Wound Repair and Regeneration*, 26, pp.S9-S18.

Kim, Y., Liu, M., Ishida, Y., Ebina, Y., Osada, M., Sasaki, T., Hikima, T., Takata, M. and Aida, T., 2015. Thermoresponsive actuation enabled by permittivity

- switching in an electrostatically anisotropic hydrogel. *Nature Materials*, 14(10), pp.1002-1007.
- Kingsley, G. and Scott, D., 2015. Assessing the effectiveness of synthetic and biologic disease-modifying antirheumatic drugs in psoriatic arthritis &ndash; a systematic review. *Psoriasis: Targets and Therapy*, p.71.
- Kirkham, B., Kavanaugh, A. and Reich, K., 2014. Interleukin-17A: a unique pathway in immune-mediated diseases: psoriasis, psoriatic arthritis and rheumatoid arthritis. *Immunology*, 141(2), pp.133-142.
- Klimiuk, P., Sierakowski, S., Latosiewicz, R., Cylwik, B., Skowronski, J. and Chwiecko, J., 2002. Serum matrix metalloproteinases and tissue inhibitors of metalloproteinases in different histological variants of rheumatoid synovitis. *Rheumatology*, 41(1), pp.78-87.
- Kong, Y., Yoshida, H., Sarosi, I., Tan, H., Timms, E., Capparelli, C., Morony, S., Oliveira-dos-Santos, A., Van, G., Itie, A., Khoo, W., Wakeham, A., Dunstan, C., Lacey, D., Mak, T., Boyle, W. and Penninger, J., 1999. OPGL is a key regulator of osteoclastogenesis, lymphocyte development and lymph-node organogenesis. *Nature*, 397(6717), pp.315-323.
- Konttinen, Y., Li, T., Hukkanen, M., Ma, J., Xu, J. and Virtanen, I., 2000. *Arthritis Research*, 2(5), p.348.
- Kotake, S., Udagawa, N., Takahashi, N., Matsuzaki, K., Itoh, K., Ishiyama, S., Saito, S., Inoue, K., Kamatani, N., Gillespie, M., Martin, T. and Suda, T., 1999. IL-17 in synovial fluids from patients with rheumatoid arthritis is a potent stimulator of osteoclastogenesis. *Journal of Clinical Investigation*, 103(9), pp.1345-1352.
- Kraan, M., Patel, D., Haringman, J., Smith, M., Weedon, H., Ahern, M., Breedveld, F. and Tak, P., 2001. *Arthritis Research*, 3(1), p.65.
- Kramer I, Wibulswas A, Croft D, Genot E. Rheumatoid arthritis: targeting the proliferative fibroblasts. *Prog Cell Cycle Res.* 2003;5:59-70.
- Kucukural, A., Yukselen, O., Ozata, D., Moore, M. and Garber, M., 2019. DEBrowser: interactive differential expression analysis and visualization tool for count data. *BMC Genomics*, 20(1).
- Kurkó, J., Besenyeyi, T., Laki, J., Glant, T., Mikecz, K. and Szekanecz, Z., 2013. Genetics of Rheumatoid Arthritis – A Comprehensive Review. *Clinical Reviews in Allergy & Immunology*, 45(2), pp.170-179.
- Kukurba, K. and Montgomery, S., 2015. RNA Sequencing and Analysis. *Cold Spring Harbor Protocols*, 2015(11), p.pdb.top084970.
- Kurowska, W., Kuca-Warnawin, E., Radzikowska, A. and Maśliński, W., 2017. The role of anti-citrullinated protein antibodies (ACPA) in the pathogenesis of rheumatoid arthritis. *Central European Journal of Immunology*, 42(4), pp.390-398.
- Leclerc, Isabelle et al. “Metformin, but not leptin, regulates AMP-activated protein kinase in pancreatic islets: impact on glucose-stimulated insulin

secretion." *American journal of physiology. Endocrinology and metabolism* vol. 286,6 (2004): E1023-31.

Lee, D., Kiener, H., Agarwal, S., Noss, E., Watts, G., Chisaka, O., Takeichi, M. and Brenner, M., 2007. Cadherin-11 in Synovial Lining Formation and Pathology in Arthritis. *Science*, 315(5814), pp.1006-1010.

Lefèvre, S., Kneda, A., Tennie, C., Kampmann, A., Wunrau, C., Dinser, R., Korb, A., Schnäker, E., Tarner, I., Robbins, P., Evans, C., Stürz, H., Steinmeyer, J., Gay, S., Schölmerich, J., Pap, T., Müller-Ladner, U. and Neumann, E., 2009. Synovial fibroblasts spread rheumatoid arthritis to unaffected joints. *Nature Medicine*, 15(12), pp.1414-1420.

Lefevre, S., Meier, F., Neumann, E. and Muller-Ladner, U., 2014. Role of Synovial Fibroblasts in Rheumatoid Arthritis. *Current Pharmaceutical Design*, 21(2), pp.130-141.

Leiss, M., Beckmann, K., Girós, A., Costell, M. and Fässler, R., 2008. The role of integrin binding sites in fibronectin matrix assembly in vivo. *Current Opinion in Cell Biology*, 20(5), pp.502-507.

Lerman, M., Lembong, J., Muramoto, S., Gillen, G. and Fisher, J., 2018. The Evolution of Polystyrene as a Cell Culture Material. *Tissue Engineering Part B: Reviews*, 24(5), pp.359-372.

Levick, J., 1987. FLOW THROUGH INTERSTITIUM AND OTHER FIBROUS MATRICES. *Quarterly Journal of Experimental Physiology*, 72(4), pp.409-437.

Li, F., Tang, Y., Song, B., Yu, M., Li, Q., Zhang, C., Hou, J. and Yang, R., 2019. Nomenclature clarification: synovial fibroblasts and synovial mesenchymal stem cells. *Stem Cell Research & Therapy*, 10(1).

Li, J., Pang, J., Liu, Z., Ge, X., Zhen, Y., Jiang, C., Liu, Y., Huo, Q., Sun, Y. and Liu, H., 2021. Shikonin induces programmed death of fibroblast synovial cells in rheumatoid arthritis by inhibiting energy pathways. *Scientific Reports*, 11(1).

Liao, L., Liang, K., Lan, L., Wang, J. and Guo, J., 2021. Marker Genes Change of Synovial Fibroblasts in Rheumatoid Arthritis Patients. *BioMed Research International*, 2021, pp.1-17.

Liu, H., Ding, J., Li, C., Wang, C., Wang, Y., Wang, J. and Chang, F., 2016. Hydrogel is Superior to Fibrin Gel as Matrix of Stem Cells in Alleviating Antigen-Induced Arthritis. *Polymers*, 8(5), p.182.

Liu, Y., Li, L., Chen, X., Wang, Y., Liu, M., Yan, J., Cao, L., Wang, L. and Wang, Z., 2019. Atomic force acoustic microscopy reveals the influence of substrate stiffness and topography on cell behavior. *Beilstein Journal of Nanotechnology*, 10, pp.2329-2337.

Lowin, T. and Straub, R., 2011. Integrins and their ligands in rheumatoid arthritis. *Arthritis Research & Therapy*, 13(5), p.244.

Lowin, T., Straub, R., Neumann, E., Bosserhoff, A., Vogel, C., Moissl, C., Anders, S., Müller-Ladner, U. and Schedel, J., 2009. Glucocorticoids increase  $\alpha 5$  integrin

expression and adhesion of synovial fibroblasts but inhibit ERK signaling, migration, and cartilage invasion. *Arthritis & Rheumatism*, 60(12), pp.3623-3632.

Lubberts, E. and van den Berg, W., 2003. Cytokines in the Pathogenesis of Rheumatoid Arthritis and Collagen-Induced Arthritis. *Advances in Experimental Medicine and Biology*, pp.194-202.

Luross, J. and Williams, N., 2001. The genetic and immunopathological processes underlying collagen-induced arthritis. *Immunology*, 103(4), pp.407-416.

Lutolf, M. and Hubbell, J., 2003. Synthesis and Physicochemical Characterization of End-Linked Poly(ethylene glycol)-co-peptide Hydrogels Formed by Michael-Type Addition. *Biomacromolecules*, 4(3), pp.713-722.

M, Trinadha., CHVS, Phanindra., M, Yamino. and C. H., Prasad., 2021. HYDROGELS THE THREE DIMENSIONAL NETWORKS: A REVIEW. *International Journal of Current Pharmaceutical Research*, pp.12-17.

MA, X. and XU, S., 2012. TNF inhibitor therapy for rheumatoid arthritis. *Biomedical Reports*, 1(2), pp.177-184.

MacDonald, I., Huang, C., Liu, S., Lin, Y. and Tang, C., 2021. Targeting CCN Proteins in Rheumatoid Arthritis and Osteoarthritis. *International Journal of Molecular Sciences*, 22(9), p.4340.

Maia, M., de Vriese, A., Janssens, T., Moons, M., van Landuyt, K., Tavernier, J., Lories, R. and Conway, E., 2010. CD248 and its cytoplasmic domain: A therapeutic target for arthritis. *Arthritis & Rheumatism*, 62(12), pp.3595-3606

Maltman, D. and Przyborski, S., 2010. Developments in three-dimensional cell culture technology aimed at improving the accuracy of in vitro analyses. *Biochemical Society Transactions*, 38(4), pp.1072-1075.

Martinez Guimera, A., Welsh, C., Dalle Pezze, P., Fullard, N., Nelson, G., Roger, M., Przyborski, S. and Shanley, D., 2017. Systems modelling ageing: from single senescent cells to simple multi-cellular models. *Essays in Biochemistry*, 61(3), pp.369-377.

Mathiessen, A. and Conaghan, P., 2017. Synovitis in osteoarthritis: current understanding with therapeutic implications. *Arthritis Research & Therapy*, 19(1).

Matsuno, H., Yudoh, K., Katayama, R., Nakazawa, F., Uzuki, M., Sawai, T., Yonezawa, T., Saeki, Y., Panayi, G., Pitzalis, C. and Kimura, T., 2002. The role of TNF- $\alpha$  in the pathogenesis of inflammation and joint destruction in rheumatoid arthritis (RA): a study using a human RA/SCID mouse chimera. *Rheumatology*, 41(3), pp.329-337.

McHugh, J., 2019. Functionally distinct fibroblast subsets in RA. *Nature Reviews Rheumatology*, 15(8), pp.449-449.

McInnes, I. and Schett, G., 2007. Cytokines in the pathogenesis of rheumatoid arthritis. *Nature Reviews Immunology*, 7(6), pp.429-442.

McInnes, I. and Schett, G., 2017. Pathogenetic insights from the treatment of rheumatoid arthritis. *The Lancet*, 389(10086), pp.2328-2337.

Mehta, S., Akhtar, S., Porter, R., Önnarfjord, P. and Bajpayee, A., 2019. Interleukin-1 receptor antagonist (IL-1Ra) is more effective in suppressing cytokine-induced catabolism in cartilage-synovium co-culture than in cartilage monoculture. *Arthritis Research & Therapy*, 21(1).

Merrill, Edward W. and Edwin W. Salzman. "Polyethylene oxide as a biomaterial." *Asaio Journal* 6 (1983): 60-64.

Missirlis, D. and Spatz, J., 2013. Combined Effects of PEG Hydrogel Elasticity and Cell-Adhesive Coating on Fibroblast Adhesion and Persistent Migration. *Biomacromolecules*, 15(1), pp.195-205.

Miyazaki, Y., Nakayamada, S., Kubo, S., Nakano, K., Iwata, S., Miyagawa, I., Ma, X., Trimova, G., Sakata, K. and Tanaka, Y., 2018. Th22 Cells Promote Osteoclast Differentiation via Production of IL-22 in Rheumatoid Arthritis. *Frontiers in Immunology*, 9.

Mizoguchi, F., Slowikowski, K., Wei, K., Marshall, J., Rao, D., Chang, S., Nguyen, H., Noss, E., Turner, J., Earp, B., Blazar, P., Wright, J., Simmons, B., Donlin, L., Kalliolias, G., Goodman, S., Bykerk, V., Ivashkiv, L., Lederer, J., Hacohen, N., Nigrovic, P., Filer, A., Buckley, C., Raychaudhuri, S. and Brenner, M., 2018. Functionally distinct disease-associated fibroblast subsets in rheumatoid arthritis. *Nature Communications*, 9(1).

Mousavi, M., Karami, J., Aslani, S., Tahmasebi, M., Vaziri, A., Jamshidi, A., Farhadi, E. and Mahmoudi, M., 2021. Transformation of fibroblast-like synoviocytes in rheumatoid arthritis; from a friend to foe. *Autoimmunity Highlights*, 12(1).

Mouw, J., Ou, G. and Weaver, V., 2014. Extracellular matrix assembly: a multiscale deconstruction. *Nature Reviews Molecular Cell Biology*, 15(12), pp.771-785.

Mseka, T., Bamburg, J. and Cramer, L., 2007. ADF/cofilin family proteins control formation of oriented actin-filament bundles in the cell body to trigger fibroblast polarization. *Journal of Cell Science*, 120(24), pp.4332-4344.

Müller-Ladner, U et al. "Synovial fibroblasts of patients with rheumatoid arthritis attach to and invade normal human cartilage when engrafted into SCID mice." *The American journal of pathology* vol. 149,5 (1996): 1607-15.

Müller-Ladner, U., Ospelt, C., Gay, S., Distler, O. and Pap, T., 2007. Cells of the synovium in rheumatoid arthritis. Synovial fibroblasts. *Arthritis Research & Therapy*, 9(6), p.223.

Nakahara, H., Song, J., Sugimoto, M., Hagihara, K., Kishimoto, T., Yoshizaki, K. and Nishimoto, N., 2003. Anti-interleukin-6 receptor antibody therapy reduces vascular endothelial growth factor production in rheumatoid arthritis. *Arthritis & Rheumatism*, 48(6), pp.1521-1529.

Nakano, K., Whitaker, J., Boyle, D., Wang, W. and Firestein, G., 2012. DNA methylome signature in rheumatoid arthritis. *Annals of the Rheumatic Diseases*, 72(1), pp.110-117.

- Nelson, C. and Bissell, M., 2006. Of Extracellular Matrix, Scaffolds, and Signaling: Tissue Architecture Regulates Development, Homeostasis, and Cancer. *Annual Review of Cell and Developmental Biology*, 22(1), pp.287-309.
- Nguyen, K. and West, J., 2002. Photopolymerizable hydrogels for tissue engineering applications. *Biomaterials*, 23(22), pp.4307-4314.
- Nicolas, J., Magli, S., Rabbachin, L., Sampaolesi, S., Nicotra, F. and Russo, L., 2020. 3D Extracellular Matrix Mimics: Fundamental Concepts and Role of Materials Chemistry to Influence Stem Cell Fate. *Biomacromolecules*, 21(6), pp.1968-1994.
- Noack, M., Ndongo-Thiam, N. and Miossec, P., 2016. Interaction among activated lymphocytes and mesenchymal cells through podoplanin is critical for a high IL-17 secretion. *Arthritis Research & Therapy*, 18(1). A
- Noack, M., Ndongo-Thiam, N. and Miossec, P., 2016. Role of podoplanin in the high interleukin-17A secretion resulting from interactions between activated lymphocytes and psoriatic skin-derived mesenchymal cells. *Clinical and Experimental Immunology*, 186(1), pp.64-74. B
- NRAS. 2022. NRAS | Rheumatoid arthritis charity. [online] Available at: <<https://nras.org.uk>> [Accessed 6 January 2022].
- Nuttelman, C., Mortisen, D., Henry, S. and Anseth, K., 2001. Attachment of fibronectin to poly(vinyl alcohol) hydrogels promotes NIH3T3 cell adhesion, proliferation, and migration. *Journal of Biomedical Materials Research*, 57(2), pp.217-223.
- Nygaard, G. and Firestein, G., 2020. Restoring synovial homeostasis in rheumatoid arthritis by targeting fibroblast-like synoviocytes. *Nature Reviews Rheumatology*, 16(6), pp.316-333.
- O'Brien, M., O'Shaughnessy, D., Ahamide, E., Morrison, J. and Smith, T., 2007. Differential expression of the metalloproteinase MMP3 and the  $\alpha 5$  integrin subunit in human myometrium at labour. *Molecular Human Reproduction*, 13(9), pp.655-661.
- Ogata, A., Kato, Y., Higa, S. and Yoshizaki, K., 2019. IL-6 inhibitor for the treatment of rheumatoid arthritis: A comprehensive review. *Modern Rheumatology*, 29(2), pp.258-267.
- Ohshima, S., Saeki, Y., Mima, T., Sasai, M., Nishioka, K., Nomura, S., Kopf, M., Katada, Y., Tanaka, T., Suemura, M. and Kishimoto, T., 1998. Interleukin 6 plays a key role in the development of antigen-induced arthritis. *Proceedings of the National Academy of Sciences*, 95(14), pp.8222-8226.
- Oliveira, I., Fernandes, D., Cengiz, I., Reis, R. and Oliveira, J., 2021. Hydrogels in the treatment of rheumatoid arthritis: drug delivery systems and artificial matrices for dynamic in vitro models. *Journal of Materials Science: Materials in Medicine*, 32(7).
- Onuora, S., 2018. RA synovium harbours distinct fibroblast subsets. *Nature Reviews Rheumatology*, 14(5), pp.250-250.

Orange, D., Agius, P., DiCarlo, E., Robine, N., Geiger, H., Szymonifka, J., McNamara, M., Cummings, R., Andersen, K., Mirza, S., Figgie, M., Ivashkiv, L., Pernis, A., Jiang, C., Frank, M., Darnell, R., Lingampali, N., Robinson, W., Gravallesse, E., Bykerk, V., Goodman, S. and Donlin, L., 2018. Identification of Three Rheumatoid Arthritis Disease Subtypes by Machine Learning Integration of Synovial Histologic Features and RNA Sequencing Data. *Arthritis & Rheumatology*, 70(5), pp.690-701.

Ospelt, C., 2017. Synovial fibroblasts in 2017. *RMD Open*, 3(2), p.e000471.

Ospelt, C., Brentano, F., Jüngel, A., Rengel, Y., Kolling, C., Michel, B., Gay, R. and Gay, S., 2009. Expression, regulation, and signaling of the pattern-recognition receptor nucleotide-binding oligomerization domain 2 in rheumatoid arthritis synovial fibroblasts. *Arthritis & Rheumatism*, 60(2), pp.355-363.

Ospelt, C., Mertens, J., Jüngel, A., Brentano, F., Maciejewska-Rodriguez, H., Huber, L., Hemmatazad, H., Wüest, T., Knuth, A., Gay, R., Michel, B., Gay, S., Renner, C. and Bauer, S., 2010. Inhibition of fibroblast activation protein and dipeptidylpeptidase 4 increases cartilage invasion by rheumatoid arthritis synovial fibroblasts. *Arthritis & Rheumatism*, 62(5), pp.1224-1235.

Page, T., Charles, P., Piccinini, A., Nicolaidou, V., Taylor, P. and Midwood, K., 2012. Raised circulating tenascin-C in rheumatoid arthritis. *Arthritis Research & Therapy*, 14(6), p.R260.

Pampaloni, F., Reynaud, E. and Stelzer, E., 2007. The third dimension bridges the gap between cell culture and live tissue. *Nature Reviews Molecular Cell Biology*, 8(10), pp.839-845.

Pankov, R. and Yamada, K., 2002. Fibronectin at a glance. *Journal of Cell Science*, 115(20), pp.3861-3863.

Pap, T., 2005. Are fibroblasts involved in joint destruction?. *Annals of the Rheumatic Diseases*, 64(suppl\_4), pp.iv52-iv54.

Pap, T., Franz, J., Hummel, K., Jeisy, E., Gay, R. and Gay, S., 2000. *Arthritis Research*, 2(1), p.59.

Pap, T., Müller-Ladner, U., Gay, R. and Gay, S., 2000. *Arthritis Research*, 2(5), p.361.

Parisi, L., 2007. Biotech. *Theory, Culture & Society*, 24(6), pp.29-52.

Patterson, J. and Hubbell, J., 2010. Enhanced proteolytic degradation of molecularly engineered PEG hydrogels in response to MMP-1 and MMP-2. *Biomaterials*, 31(30), pp.7836-7845.

Pearson, B., Klebe, R., Boyan, B. and Moskowicz, D., 1988. Comments on the Clinical Application of Fibronectin in Dentistry. *Journal of Dental Research*, 67(2), pp.515-517.

Peixoto, E., Atorrasagasti, C., Aquino, J., Militello, R., Bayo, J., Fiore, E., Piccioni, F., Salvatierra, E., Alaniz, L., García, M., Bataller, R., Corrales, F.,

- Gidekel, M., Podhajcer, O., Colombo, M. and Mazzolini, G., 2014. SPARC (secreted protein acidic and rich in cysteine) knockdown protects mice from acute liver injury by reducing vascular endothelial cell damage. *Gene Therapy*, 22(1), pp.9-19.
- Petersen, O., Ronnov-Jessen, L., Howlett, A. and Bissell, M., 1992. Interaction with basement membrane serves to rapidly distinguish growth and differentiation pattern of normal and malignant human breast epithelial cells. *Proceedings of the National Academy of Sciences*, 89(19), pp.9064-9068.
- Pineda, M., Rodgers, D., Al-Riyami, L., Harnett, W. and Harnett, M., 2014. ES-62 Protects Against Collagen-Induced Arthritis by Resetting Interleukin-22 Toward Resolution of Inflammation in the Joints. *Arthritis & Rheumatology*, 66(6), pp.1492-1503.
- Pratt, A., Siebert, S., Cole, M., Stocken, D., Yap, C., Kelly, S., Shaikh, M., Cranston, A., Morton, M., Walker, J., Frame, S., Ng, W., Buckley, C., McInnes, I., Filer, A. and Isaacs, J., 2021. Targeting synovial fibroblast proliferation in rheumatoid arthritis (TRAFIC): an open-label, dose-finding, phase 1b trial. *The Lancet Rheumatology*, 3(5), pp.e337-e346.
- Prodanovic, S., Radunovic, G., Babic, D., Ristic, B., Sefik-Bukilica, M., Zlatanovic, M., Simic-Pasalic, K., Seric, S., Vujasinovic-Stupar, N., Samardzic, J. and
- Przyborski, S., 2017. *Technology platforms for 3D cell culture*. John Wiley & Sons, pp.225-227.
- Qu, Z., Garcia, C., O'Rourke, L., Planck, S., Kohli, M. and Rosenbaum, J., 1994. Local Proliferation of Fibroblast-Like Synoviocytes Contributes to Synovial Hyperplasia. *Arthritis & Rheumatism*, 37(2), pp.212-220.
- Rajaiah, R. and Moudgil, K., 2009. Animal Models. *Rheumatoid Arthritis*, pp.218-224.
- Rengel, Y., Ospelt, C. and Gay, S., 2007. Proteinases in the joint: clinical relevance of proteinases in joint destruction. *Arthritis Research & Therapy*, 9(5), p.221.
- Rinaldi, N., Schwarz-Eywill, M., Weis, D., Leppelmann-Jansen, P., Lukoschek, M., Keilholz, U. and Barth, T., 1997. Increased expression of integrins on fibroblast-like synoviocytes from rheumatoid arthritis in vitro correlates with enhanced binding to extracellular matrix proteins. *Annals of the Rheumatic Diseases*, 56(1), pp.45-51.
- Robert, M. and Miossec, P., 2019. IL-17 in Rheumatoid Arthritis and Precision Medicine: From Synovitis Expression to Circulating Bioactive Levels. *Frontiers in Medicine*, 5.
- Roux-Lombard, P., 2001. Cytokines, metalloproteinases, their inhibitors and cartilage oligomeric matrix protein: relationship to radiological progression and inflammation in early rheumatoid arthritis. A prospective 5-year study. *Rheumatology*, 40(5), pp.544-551.

Roy, K., Mao, H., Huang, S. and Leong, K., 1999. Oral gene delivery with chitosan-DNA nanoparticles generates immunologic protection in a murine model of peanut allergy. *Nature Medicine*, 5(4), pp.387-391.

Ruelas D, Chen C, Truong H, *et al.*, DEVELOPMENT OF FIBROBLAST-LIKE SYNOVIOCYTE ASSAYS FOR TARGET DISCOVERY IN RHEUMATOID ARTHRITIS. *Annals of the Rheumatic Diseases* 2020;**79**:938.

Sabaratnam, S., Coleman, P., Mason, R. and Levick, J., 2006. Interstitial matrix proteins determine hyaluronan reflection and fluid retention in rabbit joints: effect of protease. *The Journal of Physiology*, 578(1), pp.291-299.

Sackett, S., Tremmel, D., Ma, F., Feeney, A., Maguire, R., Brown, M., Zhou, Y., Li, X., O'Brien, C., Li, L., Burlingham, W. and Odorico, J., 2018. Extracellular matrix scaffold and hydrogel derived from decellularized and delipidized human pancreas. *Scientific Reports*, 8(1).

Sambajon, V., Cillo, J., Gassner, R. and Buckley, M., 2003. The effects of mechanical strain on synovial fibroblasts. *Journal of Oral and Maxillofacial Surgery*, 61(6), pp.707-712.

Sanchez-Pernaute, O., 2003. Fibrin generated in the synovial fluid activates intimal cells from their apical surface: a sequential morphological study in antigen-induced arthritis. *Rheumatology*, 42(1), pp.19-25.

Santander-Ortega, M., Stauner, T., Loretz, B., Ortega-Vinuesa, J., Bastos-González, D., Wenz, G., Schaefer, U. and Lehr, C., 2010. Nanoparticles made from novel starch derivatives for transdermal drug delivery. *Journal of Controlled Release*, 141(1), pp.85-92.

Saxena, A., Chen, W., Su, Y., Rai, V., Uche, O., Li, N. and Frangogiannis, N., 2013. IL-1 Induces Proinflammatory Leukocyte Infiltration and Regulates Fibroblast Phenotype in the Infarcted Myocardium. *The Journal of Immunology*, 191(9), pp.4838-4848.

Schiff, M., 2000. Role of interleukin 1 and interleukin 1 receptor antagonist in the mediation of rheumatoid arthritis. *Annals of the Rheumatic Diseases*, 59(90001), pp.103i-108.

Schneider, M., Voss, B., Rauterberg, J., Menke, M., Pauly, T., Miehle, R., Friemann, J. and Gerlach, U., 1994. Basement membrane proteins in synovial membrane: Distribution in rheumatoid arthritis and synthesis by fibroblast-like cells. *Clinical Rheumatology*, 13(1), pp.90-97.

Schultz, C., 2018. Targeting the extracellular matrix for delivery of bioactive molecules to sites of arthritis. *British Journal of Pharmacology*, 176(1), pp.26-37.

Schutte, M., Fox, B., Baradez, M., Devonshire, A., Minguéz, J., Bokhari, M., Przyborski, S. and Marshall, D., 2011. Rat Primary Hepatocytes Show Enhanced Performance and Sensitivity to Acetaminophen During Three-Dimensional Culture on a Polystyrene Scaffold Designed for Routine Use. *ASSAY and Drug Development Technologies*, 9(5), pp.475-486.

Scott, D., Coleman, P., Abiona, A., Ashhurst, D., Mason, R. and Levick, J., 1998. Effect of depletion of glycosaminoglycans and non-collagenous proteins on interstitial hydraulic permeability in rabbit synovium. *The Journal of Physiology*, 511(2), pp.629-643.

Shanmugam, S., Viswanathan, B. and Varadarajan, T., 2005. Polyoxometalate based soft chemical route for preparation of Pt nanorods and self-assemblies. *Bulletin of Materials Science*, 28(6), pp.629-633.

Sharma, P., Kaur, H. and Roy, S., 2019. Designing a Tenascin-C-Inspired Short Bioactive Peptide Scaffold to Direct and Control Cellular Behavior. *ACS Biomaterials Science & Engineering*, 5(12), pp.6497-6510.

Shelef, M., Bennin, D., Mosher, D. and Huttenlocher, A., 2012. Citrullination of fibronectin modulates synovial fibroblast behavior. *Arthritis Research & Therapy*, 14(6), p.R240.

Shiozawa, K., Shiozawa, S., Shimizu, S. and Fujita, T., 1984. Fibronectin on the surface of articular cartilage in rheumatoid arthritis. *Arthritis & Rheumatism*, 27(6), pp.615-622.

Shogren, R. and Bagley, E., 1999. Natural Polymers as Advanced Materials: Some Research Needs and Directions. *Biopolymers*, pp.2-11.

Siebert, S., Pratt, A., Stocken, D., Morton, M., Cranston, A., Cole, M., Frame, S., Buckley, C., Ng, W., Filer, A., McInnes, I. and Isaacs, J., 2020. Targeting the rheumatoid arthritis synovial fibroblast via cyclin dependent kinase inhibition. *Medicine*, 99(26), p.e20458.

Silva, A., Richard, C., Bessodes, M., Scherman, D. and Merten, O., 2008. Growth Factor Delivery Approaches in Hydrogels. *Biomacromolecules*, 10(1), pp.9-18.

Sionkowska, A., 2011. Current research on the blends of natural and synthetic polymers as new biomaterials: Review. *Progress in Polymer Science*, 36(9), pp.1254-1276.

Sitt, J., Griffith, J. and Wong, P., 2016. Ultrasound-guided synovial biopsy. *The British Journal of Radiology*, 89(1057), p.20150363.

Skardal, A., Mack, D., Atala, A. and Soker, S., 2013. Substrate elasticity controls cell proliferation, surface marker expression and motile phenotype in amniotic fluid-derived stem cells. *Journal of the Mechanical Behavior of Biomedical Materials*, 17, pp.307-316.

Smeets, T J M et al. "Analysis of the cell infiltrate and expression of proinflammatory cytokines and matrix metalloproteinases in arthroscopic synovial biopsies: comparison with synovial samples from patients with end stage, destructive rheumatoid arthritis." *Annals of the rheumatic diseases* vol. 62,7 (2003): 635-8. doi:10.1136/ard.62.7.635

- Smith, M., 2003. Microarchitecture and protective mechanisms in synovial tissue from clinically and arthroscopically normal knee joints. *Annals of the Rheumatic Diseases*, 62(4), pp.303-307.
- Song, G., Xu, S., Zhang, H., Wang, Y., Xiao, C., Jiang, T., Wu, L., Zhang, T., Sun, X., Zhong, L., Zhou, C., Wang, Z., Peng, Z., Chen, J. and Wang, X., 2016. TIMP1 is a prognostic marker for the progression and metastasis of colon cancer through FAK-PI3K/AKT and MAPK pathway. *Journal of Experimental & Clinical Cancer Research*, 35(1).
- Srirangan, S. and Choy, E., 2010. The role of Interleukin 6 in the pathophysiology of rheumatoid arthritis. *Therapeutic Advances in Musculoskeletal Disease*, 2(5), pp.247-256.
- Srirangan, S. and Choy, E., 2010. The role of Interleukin 6 in the pathophysiology of rheumatoid arthritis. *Therapeutic Advances in Musculoskeletal Disease*, 2(5), pp.247-256.
- Stougaard, J., Lomholt, S., Ommen, P., Kelsen, J. and Kragstrup, T., 2018. The antifibrotic drug pirfenidone inhibits spondyloarthritis fibroblast-like synoviocytes and osteoblasts in vitro. *BMC Rheumatology*, 2(1).
- Strand, V., 1999. Treatment of Active Rheumatoid Arthritis With Leflunomide Compared With Placebo and Methotrexate. *Archives of Internal Medicine*, 159(21), p.2542.
- Sudoł-Szopińska, I., Kontny, E., Maśliński, W., Prochorec-Sobieszek, M., Kwiatkowska, B., Zaniewicz-Kaniewska, K. and Warczyńska, A., 2012. The pathogenesis of rheumatoid arthritis in radiological studies. Part I: Formation of inflammatory infiltrates within the synovial membrane. *Journal of Ultrasonography*, 12(49), pp.202-213.
- Suh, J K, and H W Matthew. "Application of chitosan-based polysaccharide biomaterials in cartilage tissue engineering: a review." *Biomaterials* vol. 21,24 (2000): 2589-98.
- Summers, L., Kielty, C. and Pinteaux, E., 2009. Adhesion to fibronectin regulates interleukin-1 beta expression in microglial cells. *Molecular and Cellular Neuroscience*, 41(2), pp.148-155.
- Sun, L., Dong, Z., Gu, H., Guo, Z. and Yu, Z., 2019. TINAGL1 promotes hepatocellular carcinogenesis through the activation of TGF- $\beta$ ; signaling-mediated VEGF expression. *Cancer Management and Research*, Volume 11, pp.767-775.
- Sun, S., Bay-Jensen, A., Karsdal, M., Siebuhr, A., Zheng, Q., Maksymowych, W., Christiansen, T. and Henriksen, K., 2014. The active form of MMP-3 is a marker of synovial inflammation and cartilage turnover in inflammatory joint diseases. *BMC Musculoskeletal Disorders*, 15(1).
- Sung, K., Su, X., Berthier, E., Pehlke, C., Friedl, A. and Beebe, D., 2013. Understanding the Impact of 2D and 3D Fibroblast Cultures on In Vitro Breast Cancer Models. *PLoS ONE*, 8(10), p.e76373.
- Suzuki, M., Hashizume, M., Yoshida, H. and Mihara, M., 2009. Anti-inflammatory mechanism of tocilizumab, a humanized anti-IL-6R antibody: effect on the

- expression of chemokine and adhesion molecule. *Rheumatology International*, 30(3), pp.309-315.
- Sweeney, S. and Firestein, G., 2004. Rheumatoid arthritis: regulation of synovial inflammation. *The International Journal of Biochemistry & Cell Biology*, 36(3), pp.372-378.
- Szekanecz, Z., Kim, J. and Koch, A., 2003. Chemokines and chemokine receptors in rheumatoid arthritis. *Seminars in Immunology*, 15(1), pp.15-21.
- Tamer, T., 2013. Hyaluronan and synovial joint: function, distribution and healing. *Interdisciplinary Toxicology*, 6(3), pp.111-125.
- Tanaka, T., Narazaki, M. and Kishimoto, T., 2014. IL-6 in Inflammation, Immunity, and Disease. *Cold Spring Harbor Perspectives in Biology*, 6(10), pp.a016295-a016295.
- Tarafder, S. and Lee, C., 2016. Synovial Joint. *In Situ Tissue Regeneration*, pp.253-273.
- Tchou, J., Zhang, P., Bi, Y., Satija, C., Marjumdar, R., Stephen, T., Lo, A., Chen, H., Mies, C., June, C., Conejo-Garcia, J. and Puré, E., 2013. Fibroblast activation protein expression by stromal cells and tumor-associated macrophages in human breast cancer. *Human Pathology*, 44(11), pp.2549-2557.
- Temenoff, J., Athanasiou, K., Lebaron, R. and Mikos, A., 2001. Effect of poly(ethylene glycol) molecular weight on tensile and swelling properties of oligo(poly(ethylene glycol) fumarate) hydrogels for cartilage tissue engineering. *Journal of Biomedical Materials Research*, 59(3), pp.429-437.
- Teves, M., Strauss, J., Sapao, P., Shi, B. and Varga, J., 2019. The Primary Cilium: Emerging Role as a Key Player in Fibrosis. *Current Rheumatology Reports*, 21(6).
- Toffoli, A., Parisi, L., Bianchi, M., Lumetti, S., Bussolati, O. and Macaluso, G., 2020. Thermal treatment to increase titanium wettability induces selective proteins adsorption from blood serum thus affecting osteoblasts adhesion. *Materials Science and Engineering: C*, 107, p.110250.
- Trujillo, S., Gonzalez-Garcia, C., Rico, P., Reid, A., Windmill, J., Dalby, M. and Salmeron-Sanchez, M., 2020. Engineered 3D hydrogels with full-length fibronectin that sequester and present growth factors. *Biomaterials*, 252, p.120104.
- Tu, J., Wang, X., Gong, X., Hong, W., Han, D., Fang, Y., Guo, Y. and Wei, W., 2020. Synovial Macrophages in Rheumatoid Arthritis: The Past, Present, and Future. *Mediators of Inflammation*, 2020, pp.1-8.
- Urbanczyk, M., Layland, S. and Schenke-Layland, K., 2020. The role of extracellular matrix in biomechanics and its impact on bioengineering of cells and 3D tissues. *Matrix Biology*, 85-86, pp.1-14.
- Valdes, T. and Moussy, F., 2000. In Vitro and In Vivo Degradation of Glucose Oxidase Enzyme Used for an Implantable Glucose Biosensor. *Diabetes Technology & Therapeutics*, 2(3), pp.367-376.

- Van Bezooijen, R., Papapoulos, S. and Löwik, C., 2001. Effect of interleukin-17 on nitric oxide production and osteoclastic bone resorption: is there dependency on nuclear factor- $\kappa$ B and receptor activator of nuclear factor  $\kappa$ B (RANK)/RANK ligand signaling?. *Bone*, 28(4), pp.378-386.
- Vasanthi, P., Nalini, G. and Rajasekhar, G., 2007. Role of tumor necrosis factor-alpha in rheumatoid arthritis: a review. *APLAR Journal of Rheumatology*, 10(4), pp.270-274.
- Vasko R, Streich JH, Blaschke S, Müller GA, Mai B, Kostrzewa M, Sparbier K, Korsten P, Bohr S, Dihazi H. Vimentin fragments are potential markers of rheumatoid synovial fibroblasts. *Clin Exp Rheumatol*. 2016 May-Jun;34(3):513-20. Epub 2016 Apr 6. PMID: 27049516.
- Vincenti, M. and Brinckerhoff, C., 2002. Transcriptional regulation of collagenase (MMP-1, MMP-13) genes in arthritis: integration of complex signaling pathways for the recruitment of gene-specific transcription factors. *Arthritis Research & Therapy*, 4(3).
- Von Der Mark, K., Gauss, V., Von Der Mark, H. and Muller, P., 1977. Relationship between cell shape and type of collagen synthesised as chondrocytes lose their cartilage phenotype in culture. *Nature*, 267(5611), pp.531-532.
- Walsh, A., Whitaker, J., Huang, C., Cherkas, Y., Lamberth, S., Brodmerkel, C., Curran, M. and Dobrin, R., 2016. Integrative genomic deconvolution of rheumatoid arthritis GWAS loci into gene and cell type associations. *Genome Biology*, 17(1).
- Wang, K., Andresen Eguiluz, R., Wu, F., Seo, B., Fischbach, C. and Gourdon, D., 2015. Stiffening and unfolding of early deposited-fibronectin increase proangiogenic factor secretion by breast cancer-associated stromal cells. *Biomaterials*, 54, pp.63-71.
- Wang, Y., Khan, A., Antonopoulos, A., Bouché, L., Buckley, C., Filer, A., Raza, K., Li, K., Tolusso, B., Gremese, E., Kurowska-Stolarska, M., Alivernini, S., Dell, A., Haslam, S. and Pineda, M., 2021. Loss of  $\alpha$ 2-6 sialylation promotes the transformation of synovial fibroblasts into a pro-inflammatory phenotype in arthritis. *Nature Communications*, 12(1).
- Wang, Z., Gerstein, M. and Snyder, M., 2009. RNA-Seq: a revolutionary tool for transcriptomics. *Nature Reviews Genetics*, 10(1), pp.57-63.
- Warde, N., 2011. Cadherin 11: a key mediator of fibroblast inflammation. *Nature Reviews Rheumatology*, 7(7), pp.374-374.
- Weyand, C. and Goronzy, J., 2020. The immunology of rheumatoid arthritis. *Nature Immunology*, 22(1), pp.10-18.
- Williams, R., 2004. Collagen-Induced Arthritis as a Model for Rheumatoid Arthritis. *Tumor Necrosis Factor*, 98(207), pp.207-216.
- Wilsdon, T. and Hill, C., 2017. Managing the drug treatment of rheumatoid arthritis. *Australian Prescriber*, 40(2), pp.51-58.

- Wood, C., Pajevic, P. and Gooi, J., 2017. Osteocyte secreted factors inhibit skeletal muscle differentiation. *Bone Reports*, 6, pp.74-80.
- Xu, J., Yang, J., Chen, J., Zhang, X., Wu, Y., Hart, A., Nyga, A. and Shelton, J., 2020. Activation of synovial fibroblasts from patients at revision of their metal-on-metal total hip arthroplasty. *Particle and Fibre Toxicology*, 17(1).
- Xue, M., McKelvey, K., Shen, K., Minhas, N., March, L., Park, S. and Jackson, C., 2014. Endogenous MMP-9 and not MMP-2 promotes rheumatoid synovial fibroblast survival, inflammation and cartilage degradation. *Rheumatology*, 53(12), pp.2270-2279.
- Yamada, K. and Cukierman, E., 2007. Modeling Tissue Morphogenesis and Cancer in 3D. *Cell*, 130(4), pp.601-610.
- Yap, H., Tee, S., Wong, M., Chow, S., Peh, S. and Teow, S., 2018. Pathogenic Role of Immune Cells in Rheumatoid Arthritis: Implications in Clinical Treatment and Biomarker Development. *Cells*, 7(10), p.161.
- Yoshida, Y. and Tanaka, T., 2014. Interleukin 6 and Rheumatoid Arthritis. *BioMed Research International*, 2014, pp.1-12.
- Yoshizawa, T., Hammaker, D., Sweeney, S., Boyle, D. and Firestein, G., 2008. Synoviocyte Innate Immune Responses: I. Differential Regulation of Interferon Responses and the JNK Pathway by MAPK Kinases. *The Journal of Immunology*, 181(5), pp.3252-3258.
- Yu, X., Chen, X., Chai, Q. and Ayres, N., 2015. Synthesis of polymer organogelators using hydrogen bonding as physical cross-links. *Colloid and Polymer Science*, 294(1), pp.59-68.
- Yuan, G., Tanaka, M., Masuko-Hongo, K., Shibakawa, A., Kato, T., Nishioka, K. and Nakamura, H., 2004. Characterization of cells from pannus-like tissue over articular cartilage of advanced osteoarthritis. *Osteoarthritis and Cartilage*, 12(1), pp.38-45.
- Yue, B., 2014. Biology of the Extracellular Matrix. *Journal of Glaucoma*, 23, pp.S20-S23.
- Zeisel, M., Druet, V., Wachsmann, D. and Sibilica, J., 2005. *Arthritis Research & Therapy*, 7(1), p.R118.
- Zheng, X., Cook, J., Watkinson, M., Yang, S., Douglas, I., Rawlinson, A. and Krause, S., 2011. Generic protease detection technology for monitoring periodontal disease. *Faraday Discuss.*, 149, pp.37-47.
- Zrioual, S., Lenief, V., Hot, A. and Miossec, P., 2012. IL-17 and TNF $\alpha$  combination induces a HIF-1 $\alpha$ -dependent invasive phenotype in synoviocytes. *Annals of the Rheumatic Diseases*, 71(Suppl 1), pp.A60.3-A61.
- Zvaifler, N., 2006. Relevance of the stroma and epithelial-mesenchymal transition (EMT) for the rheumatic diseases. *Arthritis Research & Therapy*, 8(3), p.210.

## Appendix

All supplementary data on differentially expressed genes from RNA-Seq for this project is accessible on OneDrive at:

[https://1drv.ms/u/s!AkQDlrZPiehqi3ma4QoGSBhg\\_4k?e=xyxvGj](https://1drv.ms/u/s!AkQDlrZPiehqi3ma4QoGSBhg_4k?e=xyxvGj)

Links for each component contained in the main Appendix folder is also included:

### Appendix A- Naïve vs CIA

- [Sorted up-regulated list of differentially expressed genes](#)
- [Sorted down-regulated list of differentially expressed genes](#)
- [2D up-regulated list of differentially expressed genes](#)
- [2D down-regulated list of differentially expressed genes](#)
- [Alvetex up-regulated list of differentially expressed genes](#)
- [Alvetex down-regulated list of differentially expressed genes](#)
- [FNPEG hydrogels up-regulated list of differentially expressed genes](#)
- [FNPEG hydrogels down-regulated list of differentially expressed genes](#)

### Appendix B- Naïve vs Naïve + IL-1 $\beta$

- [2D up-regulated list of differentially expressed genes](#)
- [2D down-regulated list of differentially expressed genes](#)
- [Alvetex up-regulated list of differentially expressed genes](#)
- [Alvetex down-regulated list of differentially expressed genes](#)
- [FNPEG hydrogels up-regulated list of differentially expressed genes](#)
- [FNPEG hydrogels down-regulated list of differentially expressed genes](#)